SAPIENZA
UNIVERSITÀ DI ROMA

Neural underpinnings of visuomotor functions:

Insights from brain connectivity

Faculty of Medicine and Psychology

Department of Psychology

PhD program in Behavioral Neuroscience - XXXVI

Federica Bencivenga

Matricola 1799111

Supervisor

Gaspare Galati

A.A. 2022/2023

"I devour my existence with an insatiable appetite.
How all this will end, I don't know."

Pier Paolo Pasolini

ACKNOWLEDGMENTS

Although doing a PhD is usually described as a rollercoaster, I wouldn't lie by saying that mine has covered the best time of my life. There hasn't been a day in these three years I didn't live as a new adventure. This is entirely thank to the colleagues that inspired me and cheered for me every single day.

Above all: my supervisor, prof. Gaspare Galati. He taught me everything he could, doing fMRI analyses together, coding with me (and every time he amazed me as the first one), and discussing of every neuropsychological topic I was asking for. While teaching me how to rigorously conduct research and being my personal Reviewer #2, he left me free of making my choices without being afraid of eventual mistakes.

To Maria Giulia Tullo, my first mentor and the most accurate researcher I've ever met, and Veronica di Palma, my incredible neuropsychologist: thank you for your friendship.

Thank to Maddalena Boccia for being a lighthouse during all the storms I faced.

My deepest gratitude to those who welcomed me in their labs for short-time internships: Alessandro Farnè, Claudio Brozzoli, and David Thura, for all the conversations we had in Lyon, and for having changed my career forever. Thank you to Caroline Catmur and Marco Davare, my supervisors in London. To Marco, for the hours spent with me welding cables and explaining even the most basic concepts of motor control and TMS.

To the Master's students I supervised: seeing you growing and gaining competence during your time with me has been the most incredible experience. Thank you for making me a better person and researcher.

To my friends all over the world who are my daily source of inspiration.

To my family, for supporting me despite my choices.

TABLE OF CONTENTS

ABSTRACT 8

CHAPTER 1 9

GENERAL INTRODUCTION 10
1.1 "THE ONLY WAY TO GO OUT IS THROUGH".. CONNECTIVITY 14
1.2 ONLINE MONITORING OF ACTION EXECUTION 16
1.2.1 Insights from motor imagery 16
1.2.2 Behavioral paradigms to test online motor control 17
1.2.3 Neural underpinnings of online motor control 18
1.2.4 Challenging current paradigms in the motor control research 20
1.2.5 From cortex to muscles and back: neurophysiologic correlates of motor control 22

CHAPTER 2 24

EFFECTOR-SELECTIVE MODULATION OF THE EFFECTIVE CONNECTIVITY WITHIN FRONTOPARIETAL CIRCUITS DURING VISUOMOTOR TASKS 25
ABSTRACT 26
2.1 INTRODUCTION 26
2.2 MATERIALS AND METHODS 29
2.2.1 Participants 29
2.2.2 Procedure and experimental design 30
2.2.3 Apparatus and preprocessing steps 31
2.2.4 Surface- and volume-based analyses 32
2.2.5 Regions of interest selection and timeseries extraction 34
2.2.6 Resting-state functional connectivity 35
2.2.7 DCM Model Specification 36
2.2.8 Estimation of DCM and Parametrical Empirical Bayes (PEB) 37
2.3 RESULTS 38
2.3.1 Volume- and surface-based group maps of dorsal fronto-parietal cortex during saccades and hand and foot pointing 38
2.3.2 Individual results and regions of interest selection 42
2.3.3 Resting-state functional connectivity 47
2.3.4 DCM analysis 49
2.4. DISCUSSION 55
2.4.1 Surface-based and Volume-based analyses 56
2.4.2 Resting state functional connectivity 58
2.4.3 Effective connectivity within the effector-specific parieto-frontal circuits 59
2.4.4 Merging activation- and connectivity-based approaches 63
2.5 CONCLUSIONS 64

CHAPTER 3 66

ASSESSING THE EFFECTIVE CONNECTIVITY OF PREMOTOR AREAS DURING REAL VS IMAGINED GRASPING: A DCM-PEB APPROACH 67

ABSTRACT 67
3.1 INTRODUCTION 68
3.2 METHODS 72
3.2.1 Participants 72
3.2.2 Procedure and experimental design 73
3.2.3 Apparatus 74
3.2.4 Preprocessing and surface reconstruction 75
3.2.5 Regions of interest selection and time series extraction 76
3.2.6 Dynamic Causal Modeling 78
3.2.7 Specification of the model: driving inputs and modulation of connectivity 79
3.2.8 Estimation of DCM and Parametrical Empirical Bayes (PEB) 80
3.3 RESULTS 82
3.3.1 Whole-brain analysis and ROIs selection 82
3.3.2 DCM analysis 85
3.4. DISCUSSION 87
3.4.1 Pantomimed grasping 88
3.4.2 Imagined vs Pantomimed grasping 91
3.4.3 Limitations 94
3.5 CONCLUSIONS 95

CHAPTER 4 97

INTERHEMISPHERIC INTERPLAY BETWEEN THE LEFT AND RIGHT PREMOTOR CORTEX DURING GRASPING AS ASSESSED BY DYNAMIC CAUSAL MODELLING 98
ABSTRACT
4.1 INTRODUCTION 99
4.2 METHODS 103
4.2.1 Participants and tasks 103
4.2.2 Image acquisition and analysis 104
4.2.3 Region definition 105
4.2.4 Dynamic Causal Modeling 106
4.2.5 Estimation of DCM and parametrical empirical Bayes (PEB) 108
4.3 RESULTS 109
4.3.1 Whole-brain and regional activations 109
4.3.2 Right-hemisphere DCM-PEB results 111
4.3.3 Interhemispheric DCM-PEB results 113
4.4 DISCUSSION 114
4.4.1 Pantomimed grasping 115
4.4.2 Grasping imagery 118
4.5 CONCLUSION 119

CHAPTER 5 121

BEHAVIORAL, KINEMATIC, AND PHYSIOLOGICAL EVIDENCE OF TARGET UPDATING DURING REACH-TO-GRASP ACTIONS IN A VIRTUAL ENVIRONMENT 122
ABSTRACT 122
5.1 INTRODUCTION 123

5.2 METHODS 126
5.2.1 Subjects 126
5.2.2 Experimental paradigm 127
5.2.3 Partner's movements and bottle's lighting 131
5.2.4 Physiological recordings 133
5.2.5 Data Analysis 134
5.3 RESULTS 135
5.3.1 Fixation analysis 136
5.3.2 Physiological results: HRV 137
5.3.3 Behavioral results 138
5.3.4 Kinematic results 144
5.4 DISCUSSION 149
5.4.1 Methodological considerations 149
5.4.2 Kinematic indices and their modulation by social interactions 151
5.4.3 Intra- and inter-trial effects of fast motor corrections 152
5.5 CONCLUSION 153

CHAPTER 6 155

MOTUM: A MOTION ONLINE TRACKING UNDER MRI SYSTEM 156
ABSTRACT 156
6.1 INTRODUCTION 157
6.2 METHODS 160
6.2.1 Camera system 161
6.2.2 Amagnetic glove 164
6.2.3 Virtual reality glasses 165
6.2.4 Acquisition procedure 165
6.2.5 Subjects and experimental paradigm 169
6.2.6 fMRI acquisition 172
6.2.7 fMRI data analysis 173
6.2.8 Behavioral and kinematic measures 174
6.3 RESULTS 174
6.3.1 Behavioral and kinematic measures 175
6.3.2 Movement artefacts 176
6.3.3 Task-evoked activations 177
6.4 DISCUSSION 182
6.4.1 Methodological considerations 183
6.4.2 Movement observation and execution 184
6.4.3 Joint actions 186
6.5 CONCLUSIONS 188

CHAPTER 7 189

UNRAVELLING THE CONTRIBUTION OF CORTICO-CORTICAL INPUTS TO M1 IN SENSORIMOTOR PROCESSING DURING SKILLED GRASP: A DIRECTIONAL TMS PROTOCOL 190
ABSTRACT 191
7.1 INTRODUCTION 192

7.2 METHODS 195
7.2.1 Participants 195
7.2.2 Grip Device 195
7.2.3 Experimental task 197
7.2.4 TMS procedure and EMG recording 197
7.2.5 Statistical Analyses 199
7.3 RESULTS 199
7.4 DISCUSSION 201
7.4.1 Cortical pathways triggered by AP and PA stimulation 201
7.4.2 Possible sources of late synaptic inputs to M1 during online update of sensorimotor memory 203
7.5 CONCLUSION 205

CHAPTER 8 **207**

GENERAL DISCUSSION **208**
EPILOGUE: THOUGHTS FROM REAL CONVERSATIONS 211
"Neuroscience needs evolution" 211
From the hand-as-tool to the tool-in-hand 212
"I act, therefore I am": lessons from movement control in climbing plants 214

SUPPLEMENTARY MATERIAL **218**

CHAPTER 2 **218**
CHAPTER 3 **222**
CHAPTER 4 **223**

REFERENCES **225**

ABSTRACT

Besides being essential for our survival, actions provide meaning to our exchanges with the external world. To successfully interact with the objects surrounding us, we need to extract their relevant visual features, turn them into motor possibilities, and perform movements while integrating visual, tactile, and motor information. In my work, I investigated how this different information is merged in the brain and nested in a process that is continuously updated as the action unfolds. I used neuroimaging techniques in humans to prove that such mechanisms lie in the connections between multiple brain areas. I provided evidence that parietal and frontal areas are bounded by feed-forward/feedback loops during the execution of reaching and grasping movements, showing their different interplay during motor imagery with implications for rehabilitation protocols of motor functions. To test the idea that such circuits are stressed under changing environmental contexts, using virtual reality I created ecological environments to expand the range of action possibilities to be investigated. I tested these paradigms under functional MRI by developing an MRI-compatible motion tracking system to study the neural underpinnings of the online update of motor plans. I have also investigated the neurophysiological correlates of mechanical and tactile hand-object interactions using transcranial magnetic stimulation and providing evidence of stronger cortico-cortical inputs to M1 under conditions of sensorimotor uncertainty during grasp-lift tasks. Overall, by combining multiple techniques and paradigms my work uniquely explored the neural correlates of multiple facets of human motor behavior.

CHAPTER 1

General Introduction

From an evolutionary perspective, the only way to ensure one own's survival is to act on the external environment, and action must be intended as the ultimate goal of each individual. The umbrella term "goal-directed behavior" covers a wide range of motor acts, such as walking, foraging, eating, running away from a predator, and using other elements in the environment. A massive part of individual-environment interactions is driven by hand movements, through which we explore the environment and eventually act on it, establishing or avoiding contact with the objects. During visually guided interactions with the objects, the motor output is ultimately a compounded behavior raising from the visual inspection of the environment, and requiring the extraction of the object affordances, the selection of the most appropriate movement to meet one own's goals, and its implementation. Where (and when) in the brain these processes occur remains an unfolded issue that has captured the fascination of neuroscientists since the late 20th century.

The posterior parietal cortex (PPC) has been identified as the candidate for the high-order level processes taking place during goal-directed movements. This region acts as a sensorimotor interface that receives perceptual information about environmental stimuli, combines and encodes them, and forms motor "intentions" (i.e., "high level cognitive plans for movement"; Andersen and Buneo 2002) for the planning of goal-directed movements. The peculiar anatomical features of the PPC explain its functions. This associative region is located at the crossroad of visual and somatosensory areas, at maximal distance from the primary sensorial and motor cortex dealing with perceiving and acting in the here and now (Valk et al., 2020). Macaque studies have provided the fundaments of the current knowledge on this region by describing it as a mosaic of small patches. Indeed, segregated areas with both unique and shared features across the neighboring regions (Luppino et al., 2001; Andersen and Bueno, 2006) and showing uni- or bi-modal responses can be detected. Within the intraparietal sulcus (IPS), distinct areas have been described as part of wider networks responsible for distinct ethologically relevant behaviors (Graziano 2009; Kaas et al., 2011) in specific reference frames: the

medial intraparietal (MIP), lateral intraparietal (LIP), anterior intraparietal (AIP), and ventral intraparietal (VIP) area. Reaching, saccadic, grasping, and defensive behaviors are respectively processed by area MIP in eye- and limb-centered coordinates, LIP in eye-centered coordinates, AIP in limb-centered coordinates, and VIP in head-centered coordinates. Conversely to this body of evidence in non-human primates, human literature on the topic is somewhat more inconclusive. Due to the differentiation of limb functions and the expansion and convolution of the PPC surface during evolutionary history, the comparison between humans and other primates is not straightforward. Although overlap in the structural and functional organization of movement domains can be found across primates, in humans the homologs of areas MIP, LIP, AIP, and VIP appear to be more spatially separated, likely to support human-specific and more complex functions (Konen et al., 2013). Furthermore, the willingness to shed light on the topic using different approaches and criteria (e.g., functional vs anatomical definition) has led to inconsistent results.

The attempts to identify segregated functional properties of subregions within the PPC are crucial to getting an understanding of its role in motor functions. However, bolding its segregation at the expense of its distributed features appears to be a mistake. On the contrary, the PPC can be described as a heterogenous region in which a set of continuous gradients spans along multiple directions: a) a visual-to-somatic gradient along the postero-anterior axis; b) an effector-specific (hand-eye-arm-foot) gradient along the lateral-medial axis; c) a broad abstract-to-concrete action encoding representation gradient (Turella et al., 2020). That is, functional boundaries appear to be smoothed rather than geometrically defined and anatomically delineated. After all, even in the apparently simple organization of M1 is hard to trace back topographically distinct boundaries, as the bidimensional space of the cerebral cortex does not univocally line up with the multidimensional nature of motor behaviors.

But what is the functional role of these continuums? An outstanding proposal is that these continuous representations merge both single- and cross-effectors frames of reference,

integrating visual, somatosensorial, proprioceptive, and vestibular input. The ultimate goal appears to be bridging external (environment-related) and internal (body-related) representations. In the "state estimator" framework, Medendorp and Heed (2019) allocate these two distinct sets of representations to the caudal and the rostral PPC. According to this view, the former projects the body onto the environment, mainly through visual perception, building up allocentric representations; the latter codes the environment relative to the body, relying on body-sensorial signals (including touch, proprioception, and vestibular cues) in an egocentric perspective.

Ultimately, the peculiar structural and functional organization of the PPC endows with the possibility to switch from one state to another one, or, in other words, supports a flexible behavior. It is essential to remind that the role of the PPC areas does not rule out when motor implementation arises. On the contrary, the most established theory on motor control, namely the Optimal Feedback Control (OFC; Todorov, 2004), describes the motor system as a feedback controller. In this view, building on top of previous experience the brain forms internal forward models, namely predictions of the consequences of motor behaviors. Such predictions on the future state of the body and the environment are then matched with the actual information (feedback) arising from sensory signals during movement. The PPC is an ideal candidate for the state estimation and the forward-feedback alignment, as it combines information related to the predictions (postulated by the cerebellum), the actual sensory feedback (from motor and sensorial cortex), and the goals of the action (selected by the basal ganglia and the prefrontal cortex) (see Figure 1.1).

During my 3 years of PhD studies, I have tried to tackle some of the abovementioned open issues in the human neuroscience research on motor control by performing behavioral (kinematics) and neuroimaging (functional magnetic resonance imaging (fMRI) and transcranial magnetic stimulation (TMS)) studies. In the following paragraphs, I will introduce four *leitmotifs* of my work: a) characterize the functional networks underlying different goal-directed behaviors using fMRI experiments; b) shift

the focus from the study of the static motor planning and execution to the more challenging aspects of the online monitoring and update of motor plans; c) adopting virtual reality (VR) as a tool to address real-life challenges for motor control functions, with the ultimate goal of developing new paradigms and tools to test more realistic and complex actions; d) investigate the neurophysiological correlates of the mechanical and tactile information raising from the contact with the objects.

Rather than driving conclusions on all these aspects of motor control, the present work renders open perspectives and draws future challenges for research in this field. It represents a journey in which experimental questions and hypotheses added on top of each other and progressed with each experiment I conducted, sometimes dragging my ideas and competencies far away from their starting point. All the experiences I undertook, and the techniques and methodologies I learned, have been propaedeutic to a single aim: contributing to the current theories on motor control.

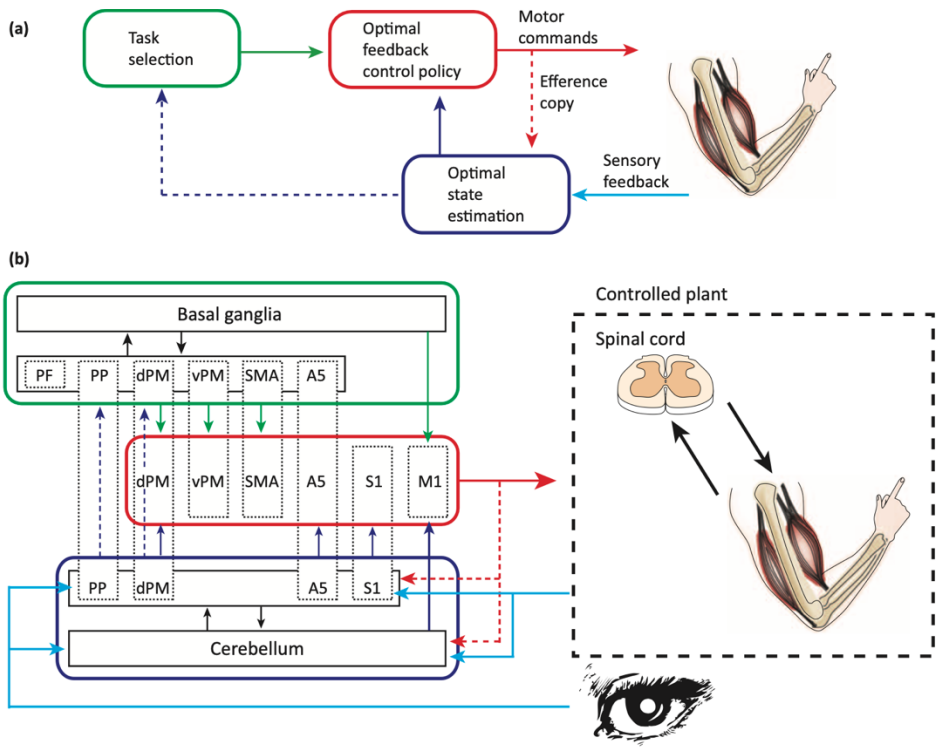

Figure 1.1. Schema of the core mechanisms of the Optimal Feedback Control theory and their neural circuitries: Task Selection (green squares), Optimal Feedback Control Policy (red squares), and Optimal State Estimation (blue squares). From Scott, 2012.

1.1 "The only way to go out is through".. connectivity

"The whole is greater than the sum of its parts", as the saying goes. I would rather say that the whole cannot exist without the sum of its parts. If a neuron loses its connection with the other neurons, it is fated to death.

It is therefore foregone to state that the PPC does not act alone. Rather, it interacts with visual, sensorial, and motor areas to extract environmental features and implement goal-directed movements. The contribution of premotor areas during motor planning and execution is synergic to - and to some extent dependent on- that of parietal areas. For instance, in monkeys the effect of electrical stimulation of frontal areas is partially altered by muscimol injections in parietal cortex, whereas movements supposedly to be evoked by stimulation of parietal areas are inhibited by muscimol inactivations of frontal areas (Stepniewska et al., 2005). TMS studies in humans (Davare et al., 2006, 2007) confirmed a serial contribution of parietal and premotor areas during grasping, whereby TMS-induced disruption of cortical areas impaired hand shaping when administered at different timings (270-220ms before touching the object when stimulating AIP, 50ms later in the case of PMv). The functional organization of prefrontal cortex is somewhat similar but partially mirrored to that of the PPC: it keeps consistency with the mediolateral effector-specific gradient described in the parietal cortex, but the abstract-to-concrete continuum is inverted to an antero-posterior direction. For instance, more rostral areas such as dlPFC and PMd are involved in the decision making related to action selection, whereas the more caudal part of the frontal lobe, including M1, deals with the concrete aspects of motor planning and execution. Intriguingly, the premotor cortex shows a similar multi-domain organization to that described in the parietal areas. Areas F2, FEF, and F5 control reaching, saccadic, and grasping movements in synergy with MIP, LIP, and AIP (Figure 1.2), respectively. Additionally, each of these subregions projects in a

somatotopic fashion to devoted portions of M1 (e.g., hand, eyes), wrapping up the action maps in the primary motor cortex.

While such organization of parietofrontal loops subserving visuomotor functions has been extensively described in macaques, part of my work was aimed to address effective (or causal) connectivity within these networks with fMRI. The underlying assumption is that the brain may be thought of as an orchestra: if one just focuses on one element within it (e.g., the piano), the meaning of the whole opera, whose essence lies in the way elements orchestrate each other, will be missed. In Chapter 2, I will present an attempt of segregating brain patches in the PPC using functional magnetic resonance imaging (fMRI) and applying connectivity approaches to describe their preferential connections with their frontal counterparts. In other words, I will show that "the only way to go out (the complexity of motor functions) is through (connectivity)" by providing evidence of parieto-frontal forward-feedback connections. The next step of my PhD studies was aimed to test the hypotheses that these connectivity estimates represent the hallmark of nested loops linking parietal and premotor areas, that continuously share information to refine the movements and update the forward models.

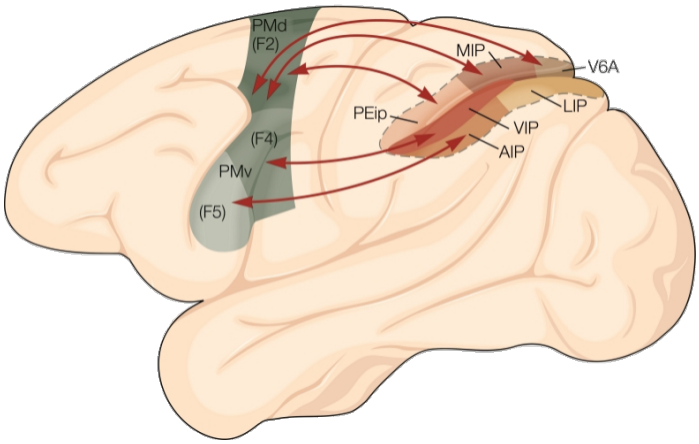

Figure 1.2. Main parietofrontal pathways. *Kandel et al. Principles of neural science, 4th ed.*

1.2 Online monitoring of action execution

1.2.1 Insights from motor imagery

Neuroscientists undertaking research in the motor field can't praise Marc Jeannerod enough for his pioneer and visionary contribution to our understanding of the basic principles of motor control. Among his works, one of the most acclaimed and still valid theories is the "simulation hypothesis", according to which imagined (covert) movements are an internal simulation of actual (overt) movements, as both share some principles (one example above all: the speed-accuracy trade off). The ultimate evidence that motor imagery and execution share overlapping brain networks (see Hètu et al., 2013 for a meta-analytic review) has paved the way for the usage of motor imagery in motor rehabilitation after neurological traumatic events affecting motor control areas and as a tool to control brain machine interfaces and prosthetic limbs.

As a (false) straightforward consequence, motor imagery has been often used as a surrogate of action planning. The comparison between motor imagery and execution has been often used as a glimpse into the distinct mechanisms subserving action planning and implementation. Such a paradigm has overall achieved the goal of easing the study of motor actions in settings where movements are limited due to mechanical and physical constraints.

With the same idea, I investigated effective connectivity using fMRI within parietofrontal frontal network in the contralateral (Chapter 3) and ipsilateral (Chapter 4) hemisphere during unilateral grasping execution and imagery. To anticipate the key result, during grasping execution I found evidence of a feedback inhibition from PMv to AIP, which was absent during grasping imagery. My hypothesis is that this connection hosts the transmission of the sensorimotor feedback to the parietal cortex, as part of the optimal feedback control. When performing, but not when imagining, actions we obtain feedback signals on the position of our hand in the space, the muscles engaged in the movement, and the overall estimate of the current state of our hand is compared with the predicted one to eventually correct and reshape the movement itself. In a nutshell, I came up with

the idea that such fronto-to-parietal feedback is a key hallmark of the online monitoring mechanism supporting the actual execution of the action.

But why did this idea trigger my curiosity so much? While the feedback control is scaffolded on the predictions of the consequences of our actions and continuously compared with them, it also deals with unpredictable externally- or internally-driven changes in our behavior that can challenge the predictions themselves. In this vein, The Optimal Feedback Control framework stresses the importance of using sensory feedback to guide and update behavior. To target this, we need to consider a highly distributed network whose role does not run out with planning but keeps being engaged while the movement unfolds.

1.2.2 Behavioral paradigms to test online motor control

Surprisingly, while most literature has focused on the planning and implementation of straightforward movements, little consideration has been given to flexible motor control.

Among the most classic paradigms to tackle adaptive motor control, visuomotor corrections are addressed using target or cursor jumps while participants are performing reaching movements. Other behavioral paradigms include task-dependent corrective responses due to external perturbation in mechanical or goal-related aspects of the ongoing movement. In the former case, the required adaptive movements can be acknowledged in the class of the "Reactive Adaptive Behaviors" (RABs), including online motor corrections caused by rapid perturbation of the movements and no or scarcely influenced by volition (Novembre & Iannetti, 2021). Spinal and supraspinal contributions to the non-voluntary aspects of movement corrections can be disambiguated by analyzing the short- (SLR) and the long- (LLR) latency responses in the targeted muscles. The earliest corrections (SLRs) occur between 20-45ms and are vehiculated by spinal networks using group I afferent input. Later responses (LLR) occur ~50-100ms and reflect signal conduction in both group I (spinal circuits) and group II afferents (supraspinal

circuits, including motor cortex and reticular formation). Voluntary reactions show a longer latency (>100ms) and involve a broader network, of which basal ganglia are a crucial hub (see Pruszynski and Scott, 2012 for a review).

Within this line of research, Nashed et al. (2014) administered a mechanical perturbation to the arm while participants were performing a reaching movement and making decisions to avoid obstacles in the environment. According to the OFC, motor commands are selected to minimize the cost-to-go, namely the mechanical cost to accumulate until attaining the movement goal. In line with this tenet, the Authors showed that the current position of the hand at the time of the perturbation (more shifted to the left, or the right) influences the decision to avoid the obstacle, shifting towards its left or right. The change in the electromyography activity (EMG) of the hand muscle occurred at ~60ms from the perturbation onset, namely within the window of the LLR. Whenever multiple targets were presented, the perturbation led to a change in the selected goal at ~75ms after perturbation onset, likely engaging motor decision making processes. Another study (Selen et al., 2012) pointed out that decisional processes play a key role in determining the onset of LLRs, as it depends on the accumulated sensory evidence. In this case, subjects viewed a dynamic random dot motion and were asked to identify the preferred movement direction. The onset of LLRs depended on the coherence of the moving dots and the duration of viewing.

Overall, these studies show that even simple movement corrections are mediated by sophisticated mechanisms at the bridge between reflexes and voluntary responses.

1.2.3 Neural underpinnings of online motor control

The neural correlates of online motor correction are still largely unknown. As anticipated above, RABs have been linked to both spinal and supraspinal contributions. LLRs are supposed to be mediated by a transcortical pathway spanning from area 3a of the primary somatosensory cortex to the primary motor cortex, which then projects to spinal

motoneurons. However, the contribution of other cortical areas and the cerebellum appear to play a key role, e.g., LLRs are also modulated by the task instructions (Tanji and Evarts, 1976; Evarts and Tanji, 1976) which are unlikely to be processed in somatomotor areas. On top of this evidence, other insights were raised by the studies conducted at the beginning of this century on the Optic Ataxia (OA). This neurological deficit generally prompts as a difficulty in reaching visually guided targets in peripheral vision. Nevertheless, it is also characterized by the inability or slowness to correct the hand's trajectory in central vision in "target jump" paradigms, therefore suggesting a disruption of the online motor control processes (Blangero et al., 2008). Lesions underlying OA are mainly located in the posterior parietal cortex (Perenin, 1997; Karnath and Perenin, 2005), consistently with its associative visuomotor nature.

In the grasping domain, a bunch of human TMS studies have identified the role of AIP during online adjustments of grasping movements, whereby disruption of AIP activity impaired the change in hand configuration necessary to react to a change in the orientation of the object to be grasped (Tunik et al., 2005; Rice et al., 2006). These studies claim that when an online correction is necessary, AIP doesn't play a role in the error detection, but rather processes the motor features necessary to implement the error correction.

Studies aiming to use highly spatial-resolution neuroimaging techniques (e.g., MEG, fMRI) to investigate the neural correlates of online motor control in healthy individuals have faced several obstacles. For instance, in the case of fMRI the shape and the structure of the magnet constraint and limit the range of complex movements participants can perform. Participants lay down on the MRI table and cannot directly see their hands; body movements are discouraged because they can cause head movements, overall compromising the quality of the signal. As a consequence, fMRI studies on the topic have adopted simplified paradigms. In some cases, the brain activity evoked by the execution of a movement has been compared to that induced by the planning (without execution) of the same movement (Glover et al., 2012). This is an extremely simplified view as it

assumes that planning and execution are two dissociable aspects of motor control. In a recent study on grasping movements (Baltaretu et al., 2020), the coil was tilted in order for the participants to see their hands and the target, and an experimenter randomly modified the orientation of the target, requiring a change in the hand shaping to grasp it.

While contributing to our knowledge of online motor control, these paradigms represent a simplification of the complex situations we face in everyday life. In the next paragraph, I will propose a radical shift in our approach to the field of motor control.

1.2.4 Challenging current paradigms in the motor control research

For decades, simplification of reality has constituted the basis of neuropsychological research. This has dealt with the necessity of controlling variables and decomposing issues into sub-issues, easier to solve. Within the motor field, this resulted in testing small, decontextualized, and fractioned movements, often lacking a personally relevant goal. Whilst we have benefited a lot from such a reductionist approach, times are mature enough for real-life questions. How many times in real life do we point or reach toward dots in space? Or do we perform simple motor tasks, gaining a monetary reward? In the frame of motor control research, in most paradigms a target is provided, and participants are asked to execute movements towards it. In other words, such experiments can be rounded to stimulus/response paradigms. Theoretically, we are miles away from this view: the frameworks I introduced in the previous paragraphs, including the OFC theory, stress the relevance of an adaptive behavior that unfolds with the movement itself, which is dynamically changed and updated based on internal or external demands. Nevertheless, we still test brain functioning using the same, "stimulus-response" based, protocols.

What is more, in the vast majority of studies on motor control participants are active executors under passive circumstances: they are seated, and can perform only partial and constrained movements. How far is this from real life, where our actions in the external

world are much more intricated, and we can catch balls while running, grasp a cup of coffee while writing a dissertation, use our hands to shape the clay, or even hold a surfboard while the ocean waves challenge our balance? In real-world environments, the goals set by both the context and the individual himself are much more complex. Circumstances are variable and unpredictable, eventually demanding sudden changes in motor behaviors; individuals do not only react to external stimuli, but proactively search for stimuli and select between multiple options, and actively explore the environment. Again, we often neglect that the main and evolutionary-set goal of each organism is pursuing active behavior no matter how changing the circumstances are.

Still, if we wish to have a glimpse into the everyday challenges of movement control, we need to find a balance between naturalistic setups and neuroimaging "non-realistic" techniques. An intriguing option is to use virtual reality environments: if we can't take neuroimaging in the real life (yet), let's take real life within the labs.

Part of the last year of my PhD studies was devoted to planning a grasping paradigm that could test online motor control in a situation where task-dependent movement corrections were required to deal with competition between different cues, different cognitive loads, and social interactions. In Chapter 5, I will present behavioral and kinematic data related to this paradigm.

The next goal was to explore the neural correlates of such complex behavior. Here, I faced a methodological challenge: I wanted to combine online motion tracking and virtual reality inside the MRI scan, a methodology that no one has ever succeeded in before. We therefore developed MOTUM – a Motion Online Tracking Under MRI system (Chapter 6). Briefly, this system uses a set of cameras to track arm position and rotation, an amagnetic glove to track finger movements, and VR glasses to reproduce in real time participants' movements on a first-person virtual avatar. In a pilot study, we used MOTUM to reproduce under fMRI the online motor correction task paradigm introduced in Chapter 5. We will show data obtained by a small number of participants, which however prove the efficacy of our method, the possibility to clean the data from

movement artifacts, and provide a glimpse into the neural correlates of on-flight movement corrections.

1.2.5 From cortex to muscles and back: neurophysiologic correlates of motor control

So far, I have focused my attention on the visuomotor transformations, namely the process through which we turn visual inputs into action plans. But as soon as I approached the end of my PhD, I realized that my research on hand/object interactions was biased toward action planning and neurons rather than movement implementation and muscles. However, the way a motor plan is transformed into a suitable pattern of muscle activity and adjusted after the contact with the object is not less complex.

The primary motor cortex is the principal output through which the motor command is funneled to the spinal cord, finally reaching muscles. Once the motor plan is implemented and the contact with the object occurs, somatosensory feedback mainly driven by cutaneous mechanoreceptors provide the relevant information to acquire, maintain and update internal motor representations given the dynamics of our body and the object's features.

A key point is that while sensory feedback is for its intrinsic nature noisy and delayed, adjustments of motor plan can occur quickly. Let's consider the case of force control. When we hold an object, we must adjust our grip force to not let the object slip away nor generate excessive force. Our brain anticipates grip force adjustments based on both objects' features (e.g., weight and surface friction) but also on the body state (e.g., movement). For instance, if we walk while holding an object, we can anticipate the inertial forces exerted by our body motion on the object and counteract them. Once again, the optimal feedback control framework provides an explanation for such ability, whereby internal models and visual inputs are used to set grip forces *prior* movement execution. Sensory feedback-driven control is then charged of comparing the actual somatosensory input with the predicted one, detecting eventual mismatch, triggering

corrective responses, and ultimately updating the internal models. Visual feedback can somewhat support the feedback control, but probably in an effector- and action-specific manner, e.g., being more useful to adjust arm movement kinematics but useless to regulate grip forces. For instance, deafferented subjects fail to adjust force scaling being forced to rely only on visual feedback (Nowak et al., 2004).

The most common and intuitive methodology to non-invasively assess corticospinal pathways in humans is TMS. A single TMS pulse produces repetitive excitation of corticospinal neurons in M1 emerging as early (direct stimulation of corticospinal neurons through the axons of fast pyramidal tract neurons) and late (indirect stimulation of corticospinal neurons through interneurons) waves. In Chapter 7, I will introduce a TMS experiment in which we estimated corticospinal excitability and the extent to which this can be modulated by the processing load of incoming sensory inputs from S1. This was achieved using a grip-and-lift paradigm where we controlled the relative contribution of predictive vs online sensory feedback control.

Altogether, by combining multiple techniques and paradigms my work explored the neural correlates of multiple facets of human motor behavior.

CHAPTER 2

This chapter has been published in March 2023 as:

Bencivenga, F., Tullo, M. G., Maltempo, T., von Gal, A., Serra, C., Pitzalis, S., & Galati, G. (2023). Effector-selective modulation of the effective connectivity within frontoparietal circuits during visuomotor tasks. Cerebral Cortex, 33(6), 2517-2538.

https://doi.org/10.1093/cercor/bhac223

Effector-selective modulation of the effective connectivity within frontoparietal circuits during visuomotor tasks

Federica Bencivenga[1,2,3,†], Maria Giulia Tullo[1,2,4,†], Teresa Maltempo[3,5], Alessandro von Gal[1,2], Chiara Serra[5], Sabrina Pitzalis[3,5], and Gaspare Galati[1,3]

[1] Brain Imaging Laboratory, Department of Psychology, Sapienza University, Rome, Italy

[2] PhD program in Behavioral Neuroscience, Sapienza University of Rome, Rome, Italy

[3] Cognitive and Motor Rehabilitation and Neuroimaging Unit, Santa Lucia Foundation (IRCCS Fondazione Santa Lucia), Rome, Italy

[4] Department of Translational and Precision Medicine, "Sapienza" University of Rome, Rome, Italy

[5] Department of Movement, Human and Health Sciences, University of Rome "Foro Italico", Rome, Italy

† These authors contributed equally to this work

Abstract

Despite extensive research, the functional architecture of the subregions of the dorsal posterior parietal cortex (PPC) involved in sensorimotor processing is far from clear. Here, we draw a thorough picture of the large-scale functional organization of the PPC to disentangle the fronto-parietal networks mediating visuomotor functions. To this aim, we reanalyzed available human functional magnetic resonance imaging data collected during the execution of saccades, hand, and foot pointing, and we combined individual surface-based activation, resting-state functional connectivity, and effective connectivity analyses. We described a functional distinction between a more lateral region in the posterior intraparietal sulcus (lpIPS), preferring saccades over pointing and coupled with the frontal eye fields (FEF) at rest, and a more medial portion (mpIPS) intrinsically correlated to the dorsal premotor cortex (PMd). Dynamic causal modelling revealed feedforward-feedback loops linking lpIPS with FEF during saccades and mpIPS with PMd during pointing, with substantial differences between hand and foot. Despite an intrinsic specialization of the action-specific fronto-parietal networks, our study reveals that their functioning is finely regulated according to the effector to be used, being the dynamic interactions within those networks differently modulated when carrying out a similar movement (i.e., pointing) but with distinct effectors (i.e., hand and foot).

2.1 Introduction

Over two decades of research on the segregation between human brain areas in the posterior parietal cortex (PPC) have not disambiguated to what extent these regions share properties with their monkey homologues. Areas in the PPC of non-human primates have been studied based on their retinotopic organization, cyto- and myelo-architectonic, histological, anatomical, and functional properties, as well as by addressing their connectivity profiles with surrounding and distant areas (Orban 2016). Despite the richness of methods employed to segregate these regions, the distinction between adjacent areas has not always been easy to accomplish. From a functional perspective,

this is due to the multimodal nature of PPC neurons, for which single-cell neurophysiological analyses show mixed sensory, attentional, memory-, decision-, and action-related responses. This has been taken as evidence of the PPC involvement in combining different reference frames for sensorimotor transformations necessary for planning, executing, and monitoring actions. Within a continuous visual-to-somatic gradient (Burnod et al. 1999), specific cortical fields have been associated with preference for specific actions: the parietal reach region (PRR) (Snyder et al. 1998), an area encompassing both the medial intraparietal area (MIP) and V6A, is connected with the premotor cortex (F2) (Wise et al. 1997) and contains a majority of reaching-related neurons (Batista et al. 1999; Andersen and Buneo 2002; Buneo et al. 2002; Gail and Andersen 2006; Chang et al. 2008; Andersen and Cui 2009), while the lateral intraparietal area (LIP), connected with the frontal eye fields (FEF), contains a majority of saccade-related neurons (Blatt et al. 1990; Snyder et al. 1998; Paré and Wurtz 2001).

A comparable segregation of the human PPC has proved difficult to unequivocally demonstrate, due to several issues: a) areas in the superior parietal lobule (SPL) underwent substantial, evolutionary-driven modifications, being more medially displaced in humans (Hill et al. 2010; Chaplin et al. 2013; Gregory et al. 2017); b) there is a relative, rather than an absolute, preference of the subregions within the PPC for reaching or saccades (Snyder et al. 1997; Snyder et al. 2000; Calton et al. 2002; Andersen and Cui 2009); c) a wide set of studies using functional magnetic resonance imaging (fMRI) to explore the segregation of the human PPC detected overlapping activations in this territory during both saccades and reaching or pointing movements (Beurze et al. 2007; Levy et al. 2007; Beurze et al. 2009; Hinkley et al. 2009; Vesia and Crawford 2012), or reported that separate areas of the posterior intraparietal sulcus (pIPS) show similar preparatory activity across effectors (Gallivan et al. 2011b).

Despite that, human homologues of PRR and LIP have been proposed (Sereno et al. 2001; Connolly et al. 2003; Schluppeck et al. 2005; Beurze et al. 2007; Hagler et al. 2007; Tosoni et al. 2008; Galati et al. 2011), supporting a view of the human PPC as organized in an

action or effector-specific fashion (Cui and Andersen 2007; Andersen and Cui 2009; Hinkley et al. 2009). Evidence of an effector-specific gradient has been found in the anterior part of the SPL, where the human homologues of the somatotopic area PE and its caudal part (namely, the PEc) have been identified (Pitzalis et al. 2019). Differently, within the intraparietal sulcus (IPS), a functional (i.e., saccades vs pointing) rather than an effector (i.e., eye vs hand) specificity emerges (Heed et al. 2011, 2016) when comparing pointing movements carried out using lower and upper limbs. Several studies have accounted for this hypothesis by showing only a relative effector-specificity within PPC (Gallivan et al. 2013; Turella et al. 2020), also in dysplasic individuals (Liu et al. 2020), leading to the view that areas within the PPC represent dichotomies of effectors rather than a specific effector (Leoné et al. 2014). This trend, which suggests an apparent lack of specificity of the PPC, is in line with its integrative sensorimotor nature.

The PPC is a region with a complex anatomical configuration, located at the crossroad of visual and somatosensory areas; due to its anatomical location, it acts as a sensorimotor interface that receives perceptual information about environmental stimuli, encodes them, and forms motor 'intentions' (Andersen & Buneo, 2002) for the planning of goal-directed movements. If one aims univocally to segregate PPC subregions trying to identify if they are involved in some cognitive functions, the dynamic recruitment of this region would only be partially grasped. Indeed, the PPC appears to be composed of nodes whose involvement may not be univocal but dynamically adapted to the environmental demands through a variety of fronto-parietal networks (Galletti and Fattori 2018). To use a metaphor, if one focuses on an instrument in a symphonic orchestra, it would be hard to catch the overall meaning of the opera.

The current study aims at extending the pre-existing knowledge on the functional role of PPC subregions by considering their involvement in broader parieto-frontal networks. The dynamic couplings between frontal and parietal areas may be taken as a comprehensive neural signature reflecting the sensorimotor processing and the motor execution of saccades and movements with different effectors.

Here, we benefited from two different types of connectivity analyses, namely resting-state functional connectivity (rs-fc) and task-based effective connectivity, as tools to disentangle the neuronal fronto-parietal networks mediating distinct visuo-motor actions, performed with different effectors, drawing a thorough picture of the large-scale functional organization of the PPC. We reanalyzed BOLD data from the study of Pitzalis and colleagues (Pitzalis et al. 2019) on saccades and pointing performed with the foot or the hand, implementing three hierarchical steps.

As a first step, we used a surface-based analysis (SBA) and an individual analysis approach with the aim of detecting subtle differences among the areas in the PPC since the anatomical configuration in this brain region is complex due to the massive presence of sulci and gyri. Indeed, the SBA has been proposed as an alternative method to the canonical volume-based analysis of fMRI data (Van Essen et al. 1998; Bruce Fischl et al. 1999) and has emerged as a powerful approach to increase the spatial accuracy in the cortical activation pattern of adjacent areas (Oosterhof et al. 2011; Brodoehl et al. 2020).

Pending success of the first step, we aimed at defining the intrinsic neural architecture linking frontal and parietal areas through a seed-to-seed resting-state functional connectivity analysis.

Last, taking the results of the previous two steps into account, we used dynamic causal modelling (DCM; Friston et al. 2003) to yield an estimate of the dynamic couplings between the areas of the parieto-frontal circuits involved in hand pointing, foot pointing, and saccades. By combining the aforementioned analyses, our results provide a new perspective of the organizational principle of sensory-motor brain networks.

2.2 Materials and Methods

2.2.1 Participants

Here, we reanalyzed BOLD data from a subsample of 17 healthy subjects (8 males, mean age 25, range 22 – 28 years) who participated in a previous experiment held in our laboratory (Pitzalis et al. 2019). All participants were right-handed, as assessed by the

Edinburgh Handedness Inventory (Oldfield 1971), had normal or corrected-to-normal vision, and had no previous history of psychiatric or neurologic diseases. Participants gave their written informed consent to participate in the study. The study was approved by the local research ethics committee of the IRCCS Fondazione Santa Lucia in Rome, according to the Declaration of Helsinki.

2.2.2 Procedure and experimental design

Each subject performed three scans of a visuomotor task, alternating blocks of delayed visually guided hand pointing, foot pointing, and saccades, and two resting-state scans. A detailed description of the experimental setup and procedure is provided in Pitzalis and colleagues (Pitzalis et al. 2019). Briefly, in each visuomotor scan, 4 blocks for each condition (hand pointing, foot pointing, and saccade), each lasting 18s and composed of 4 trials, were interleaved with 11 fixation periods lasting 12, 14 or 16 s. Blocks were arranged in a pseudo-random sequence and were introduced by a written instruction (400 ms) to inform about the task to be performed. In the resting-state scans, subjects were lying at rest with eyes closed and no experimenter-imposed task.

In each visuomotor trial, subjects started from a rest position, fixating a central white cross, and pressing a button with their right finger and a pedal with their right foot. The trial started with a peripheral target (0.9° diameter, 4° eccentricity) shown for 300 ms at one of eight possible positions. After a variable interval (1.5, 2.5, 3.5 or 4.5 s), the fixation point turned green (go signal), and subjects moved their hand, foot, or eyes toward the remembered location of the target. During saccades, they were asked to stay still and move only the eyes; during hand and foot pointing, they had to keep their sight on the central fixation point. The hand pointing movement consisted in releasing the button, extending the right index, and moving the wrist to point to the remembered location of the target, whereas the foot pointing was performed by releasing the pedal, rotating the right ankle, and indicating the remembered location of the target with the extended right big toe. Once the movement was executed, the subject was asked to return to the rest position.

2.2.3 Apparatus and preprocessing steps

MR images were acquired at the Santa Lucia Foundation using a 3T Siemens Allegra MR scanner (Siemens Medical Systems, Erlangen, Germany) equipped for echo-planar imaging with a receiving/transmitting head coil. To minimize movements, each subject's head was stabilized with foam padding and with a chin rest mounted inside the head coil. We used blood-oxygenation level-dependent BOLD imaging (Kwong et al. 1992) and a gradient echo EPI sequence to acquire functional MR images (TR= 2s, TE=30 ms, flip angle= 70°, 64×64 image matrix, 3 × 3 mm in-plane resolution, 30 slices, 3.5 mm slice thickness with no gap, interleaved excitation order) in the AC–PC plane. For visuomotor and resting-state scans we acquired 201 and 128 volumes, respectively. Images were acquired starting from the superior convexity including the whole cerebral cortex but excluding the ventral portion of the cerebellum. Also, a three-dimensional, high-resolution T1-weighted image was acquired for each participant (Siemens MPRAGE sequence, TR= 2s, TE= 4.38ms, flip angle= 8°, 512×512 image matrix, 0.5 × 0.5 mm in-plane resolution, 176 contiguous 1 mm thick sagittal slices). For each scan, we discarded the first four volumes to achieve steady-state, and the experiment started at the beginning of the fifth volume.

A detailed description of the preprocessing steps is provided in our previous study (Pitzalis et al. 2019). Briefly, we used FreeSurfer 5.1 (http://surfer.nmr.mgh.harvard.edu/) to analyze structural images, obtaining a surface representation of each individual cortical hemisphere in a standard space. Then, we transformed the surface reconstruction to the symmetrical FS-LR space (Van Essen et al. 2012) using tools in the Connectome Workbench software (https://www.humanconnectome.org/software/get-connectome-workbench), resulting in surface meshes with approximately 74K nodes per hemisphere.

We analyzed functional images both in the volume and the surface space using SPM12 (Wellcome Department of Cognitive Neurology, London, UK). Specifically, we corrected the functional images of each participant for slice timing, using the middle slice acquired in time as a reference. Then, images were corrected for head movement, using a least-

squares approach and six parameter rigid body spatial transformations. Images of each participant were coregistered onto their T1 image. Then, in the voxel-based analysis (VBA), images were normalized using an automatic nonlinear stereotaxic normalization procedure and spatially smoothed using a three-dimensional Gaussian filter (6 mm full-width-half-maximum). Instead, in the surface-based analysis (SBA), functional data were resampled to the individual cortical surface using ribbon-constrained resampling as implemented in Connectome Workbench (Glasser et al. 2013) and finally smoothed along the surface with an iterative procedure emulating a Gaussian kernel with a 6mm full width at half-maximum (FWHM).

2.2.4 Surface- and volume-based analyses

The intrinsic topology of the cerebral cortex is that of a two-dimensional, highly convoluted sheet (Dale et al. 1999). However, volume-based analyses of fMRI data represent the curvature pattern of the cortical surface in a three-dimensional space, resulting in an underestimated computation of the true distance between points on the cortical surface (Fischl et al. 1999). For instance, regions displaced at the two opposite banks of the same sulcus (e.g., the primary motor cortex and somatosensory cortices) are geodetically distant in the unfolded surface but appear to be closer when using a Euclidean distance in a 3D space (Brodoehl et al. 2020). Consequently, volume-based analyses may result in the contamination of the signal time course of each area with that of its neighboring regions, leading to a lack of spatial accuracy in defining the activation boundaries of anatomically close areas (Oosterhof et al. 2011). This issue is of remarkable relevance in regions with complex sulcal anatomy (e.g., the PPC) and/or a strong individual variability in the folding of the cortex.

The introduction of surface-based visualization and analysis (Van Essen et al. 1998; Fischl et al. 1999) made it possible to deal with the complexity and the variability of the human cortical convolutions. Indeed, it aims at circumventing the issues in the segregation in the cortical activation pattern of adjacent areas by taking the individual folding pattern of the cortical sheet in a 2D space into account (Oosterhof et al. 2011; Brodoehl et al. 2020).

Furthermore, it has been reported that SBA avoids that the noise outside the gray matter influences the signal (Jo et al. 2007; Brodoehl et al. 2020).

Given this evidence, we performed both surface and volume-based analyses. Beyond performing both analyses at the group-level, we inspected individual activations obtained through SBA with the aim of distinguishing segregated regions involved in pointing and saccades, especially in cortical regions with complex sulcal anatomy as the pIPS.

We analyzed functional images for each participant on a voxel-by-voxel basis in the VBA, and on a vertex-by-vertex basis in the SBA, according to the General Linear Model (GLM), by modelling each "active" block (hand pointing, foot pointing, and saccade) as a box-car function, convolved with a canonical hemodynamic response function as implemented in SPM12. Fixation blocks were not explicitly modelled as GLM regressors and were thus treated as part of the residual variance. We also modelled the FD regressor. Note the quantity of head movement was in general very low, with the hand pointing and saccadic conditions not showing more head movement than the baseline; head movement was somewhat higher in the foot pointing condition, but only 12 time points with suspect motion artefacts (i.e., with FD > 0.9 mm, Siegel et al. 2014) were detected across the whole dataset (for a complete analysis, see paragraph 2.7 and Supplementary Figs. 1 and 2 of Pitzalis et al. 2019).

We obtained group-level statistical parametric maps by implementing one-sample t-tests, comparing signal in each condition to the baseline. Moreover, we performed paired t-tests to compare each pair of conditions (e.g., foot pointing > hand pointing). We further computed conjunction null analyses of the three conditions, i.e., (foot pointing > fixation) AND (hand pointing > fixation) AND (saccades > fixation), and comparing the pointing tasks with saccades, i.e., (hand pointing > saccades) AND (foot pointing > saccades), as well as (saccades > hand pointing) AND (saccades > foot pointing).

Results were obtained defining clusters of adjacent voxels or vertices surviving at least an uncorrected voxel-level threshold of $p < 0.001$; then, statistical maps were corrected for multiple comparisons at the cluster level ($p < 0.05$) through a topological false discovery rate procedure based on random field theory (Chumbley et al. 2010).

2.2.5 Regions of interest selection and timeseries extraction

We defined several regions on the cortical surface of each individual left hemisphere, selecting them by different, motivated contrasts that will be extensively described in the results section after the description of the group-level VBA and SBA findings. We defined the regions of interest by considering the activations evoked by saccades, hand pointing, and foot pointing in the territory of our interest, i.e., the superior parietal and premotor cortex.

The rationale behind the mapping procedure we implemented here was to use a data-driven approach to ROI definition, tailored to individual differences in gyral anatomy and structure-to-function mapping, but still generalizable across individuals, and as much observer-independent as possible. To reach this goal, we applied a watershed transform, a commonly used algorithm in image processing (adapted to surface meshes following Mangan & Whitaker, 1999), to activation maps. This procedure allows to split up activation maps into distinct "neighborhoods", by starting from all activation peaks (i.e., local maxima) in the map and following the descending gradient of activation around it in all directions until the whole cluster is "filled". As a result, neighborhoods are split along the relative local minima. This procedure has the advantage of being completely data-driven and threshold-independent, and results in multiple regions within the same cluster (i.e., not separated by voxels below threshold) when there are multiple peaks, unambiguously assigning each voxel to the "belonging" peak and generating regions with follow the activation gradient and have no predefined size or shape.

Next, from the individual data-driven regions detected by the watershed transform, we selected as individual ROIs the ones which mostly met the anatomical landmarks that

will be extensively described in the results section. Finally, the resulting region were limited when necessary to the most activated 300 cortical nodes. For each subject and region, we extracted "adjusted" time series from individual surface ROIs, having regressed out effects of no interest; we retained the first principal component (eigenvariate) of adjusted data to carry out both the rs-fc and the DCM analyses.

2.2.6 Resting-state functional connectivity

We analyzed BOLD data from a subset of subjects (N = 16, 7 males, mean age 25 years, range 22 – 28 years) who underwent the resting state scans, in addition to the experimental scans. Resting state data were band-pass filtered with a low-pass cut-off frequency of 0.1 Hz to include only slow BOLD fluctuations (Fox and Raichle 2007) and a high-pass cut-off frequency of 0.01 Hz. We then applied a GLM at each and every brain vertex modelling the global signal time course, the constant terms to model overall differences across scans, and some nuisance regressors to reduce noise due to physiological fluctuations, such as white matter (WM) and cerebrospinal fluid (CSF) regressors, computed as the first four eigenvariates of a singular value decomposition of the resting-state time courses of all voxels within the WM and CSF, respectively. We additionally controlled for subject motion by using the framewise displacement (FD) as an additional regressor: FD is an estimate of the amount of instantaneous head movement at each time point (Power et al., 2012).

We evaluated the functional connectivity between the selected ROIs during resting-state. The underlying assumption of this analysis is that correlated spontaneous fluctuations during resting state reveal functional networks linking our ROIs (van den Heuvel and Hulshoff Pol 2010). Based on the results of our GLM surface-based analysis, and the previous knowledge about the areas involved in pointing and saccades, we expected to find evidence of parieto-frontal connections similar to those observed in macaques during visuomotor tasks.

For each subject and pair of individually defined regions, we computed the seed-to-seed correlation coefficients between the first eigenvariates of each regional BOLD adjusted

time course as an index of the inter-regional temporal coupling between the regions. To assess whether the correlations were significantly higher than zero, we normalized the data by means of the Fisher transform and we performed one-sample one-tailed t-tests on the z values, separately for each pair of regions ($p < 0.05$ Bonferroni corrected for the number of connections included in the analysis).

2.2.7 DCM Model Specification

Crucially for the present study, we aimed at characterizing the connectivity pattern associated with each task, providing an estimate of the dynamic couplings among areas known to play a crucial role in hand pointing, foot pointing, or saccades. To this aim, we used the Dynamic Causal Modelling approach (Friston et al. 2003).

DCM analysis aims at establishing the direct influence of one region on another, i.e., effective connectivity. According to DCM, the following equation estimates the change in neural activity over time ($\dot{z}$) due to experimental conditions:

$$\dot{z} = \left(A + \sum_{j=1}^{M} u_j B^j \right) z + Cu$$

where parameters in matrix A specify the intrinsic connectivity between nodes (i.e., the regions) at the baseline; the parameters in matrices B represent the connectivity modulatory effect of one region on another due to each experimental condition (k = 1…n); u stands for each experimental input stimulus and C specifies a matrix where each parameter shows the sensitivity of a region to the driving input stimulus (Zeidman et al. 2019).

DCM parameters stand for the neural connectivity strength and have a useful interpretation: positive values of A-matrix parameters are interpreted as excitatory influence of one area on another while negative values are interpreted as inhibitory influence. Similarly, B-matrix parameters reflect the increase (positive value) or decrease

(negative value) of the coupling from one region to another due to the modulation by the experimental conditions. In both cases, the parameters are measured in the frequency domain (Hz) because they represent the rate of change of one region activity on another and the absolute parameter value defines the strength of the neural connection.

The architecture of the DCM model we implemented here will be extensively described in the results section given that we took into account both the literature relative to visuomotor tasks and the findings of our SBA and rs-fc analyses.

2.2.8 Estimation of DCM and Parametrical Empirical Bayes (PEB)

For each subject, we specified and inverted a DCM. We checked that each subject-specific DCM met the following criteria: (1) the variance explained by the model was at least 10%, as an index of the success of model inversion (Zeidman et al. 2019); (2) at least one connection had a connection strength greater than 1/8 Hz; (3) at least one parameter was effectively estimated (based on Kullback-Leibler divergence of posterior from prior distribution). All the subject DCMs encountered these criteria and were thus included in the group level analysis.

To estimate DCM parameters at the group level we performed a Parametric Empirical Bayes (PEB) analysis (Friston et al. 2016). Briefly, PEB is a hierarchical Bayesian model that uses both non-linear (at the first level) and linear (at the second level) analyses. The advantage of using PEB is to assess commonalities and differences among subjects in the effective connectivity domain. A comparison among the full and the reduced models, in which a combination of parameters are switched off, was performed and, thus, parameters not contributing to the model evidence were pruned out through Bayesian Model Reduction (BMR). We summarized parameters across models using Bayesian Model Average (BMA) selecting only parameters whose posterior probability of being present in the model was at least 90%.

Finally, we computed Bayesian contrasts (Dijkstra et al. 2017) to compare parameters of interest within or between conditions; then, we evaluated the posterior distribution over this contrast.

2.3 Results

The results section is organized into three parts, which reflect the three main steps of our analysis pipeline, aimed at characterizing the dynamic couplings between specific fields in the human posterior parietal and premotor cortex during the sensorimotor processing and execution of different visuo-motor actions.

First, we analyzed the activation evoked by the visuo-motor tasks in the cortical territories of our interest, both at the group level (using volume- and surface-based analysis) and on the individual hemispheric surfaces, with the aim of detecting distinct parietal and premotor fields to be used as the seed nodes of the subsequent connectivity analysis. Both the group and the individual analysis on the cortical surface allowed us to identify four parietal and three premotor fields, which are described in the first section. Second, we performed a seed-to-seed resting-state functional connectivity among these seven regions, to characterize the intrinsic neural architecture of the parieto-frontal system involved in visuo-motor control. This analysis contributed the necessary evidence for building an informed model of parieto-frontal connectivity at the third step.

Finally, using the results of the resting-state analysis combined with previous knowledge derived from structural connectivity studies in macaques, we built and estimated a dynamic causal model of effective connectivity between the seven regions under the three tasks, which constitutes the main result of the present study.

2.3.1 Volume- and surface-based group maps of dorsal fronto-parietal cortex during saccades and hand and foot pointing

Whole brain activations resulting from the group level analysis are provided in our previous study (Pitzalis et al. 2019, Figure 6B-C), although the main aim of that analysis was showing the degree of responsiveness in the saccade and pointing tasks of three

medial parietal regions identified through an independent task. In line with the aims of the current work, in the present section, we will describe in more detail the activations evoked by saccades, hand pointing, and foot pointing only in the territories of our interest, i.e., the superior parietal and premotor cortex.

At the group level, we performed both a volume-based analysis (VBA) and a surface-based analysis (SBA): we show that VBA produced more robust activations in terms of peak height and cluster extent, while SBA better segregated between nearby foci, which was the main aim of our analysis.

Figure 2.1 (panel A) depicts a close-up on the posterior intraparietal sulcus territory, providing the activations resulting from our group level analyses. Indeed, results showed that in each of the three conditions, the VBA consistently showed a single activation peak in the pIPS (hand pointing: MNI coordinates -18 -64 55; T = 9.6; foot pointing: -24 -58 64, T = 6.5; saccades: -21 -64 52, T = 12.3), while the SBA consistently showed two peaks: a more medial one (hand pointing: -17 -65 53, T = 7.4; foot pointing: -19 -64 53, T = 6.5; saccades: -20 -64 52, T = 9.8), and a more lateral one (hand pointing: -25 -58 51, T = 7.8; foot pointing: -25 -58 50, T = 6.1; saccades: -25 -58 51, T = 13.5). Similarly, in the (hand pointing > baseline) AND (foot pointing > baseline) conjunction analysis, we detected a single peak in the pIPS territory in the VBA (-15 -64 55, T = 9.5) and two separate peaks in the SBA (medial: -19 -64 53, T = 6.5; lateral: -25 -58 50, T = 6.0). The same was true in the conjunction analysis of all the three conditions compared to baseline (VBA: -18 -64 55, T = 9.2; SBA: medial -19 -64 53, T = 6.5, lateral -25 -58 50, T = 6.0).

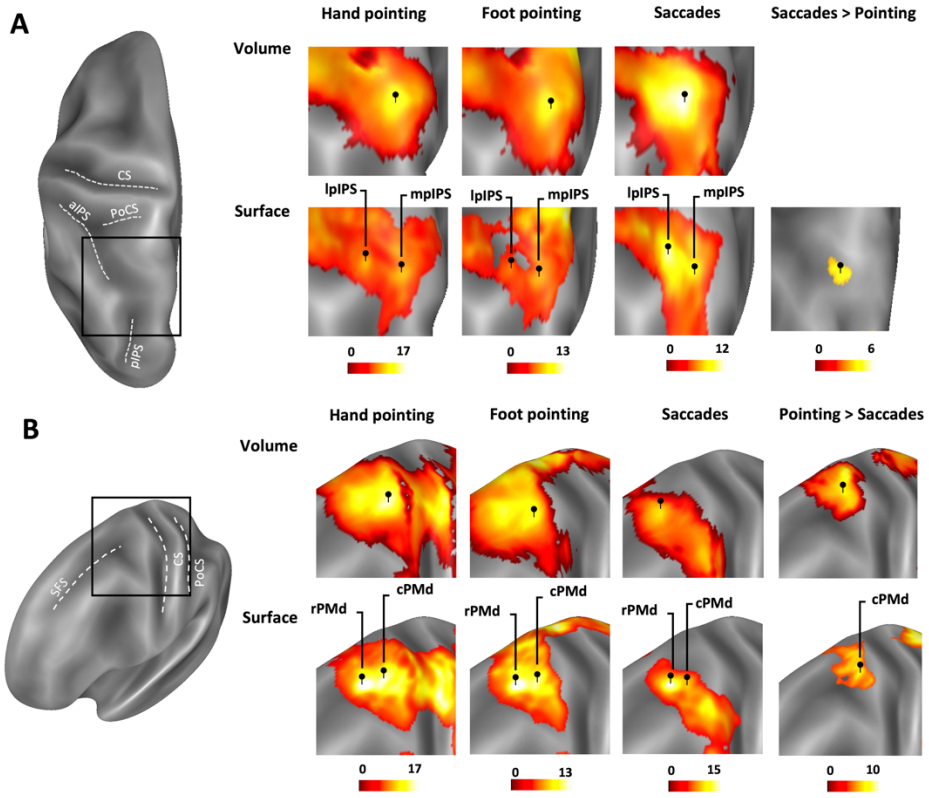

Figure 2.1. Group activations in the premotor dorsal and the posterior intraparietal sulcus territories. A) Comparison of the activation maps in the posterior intraparietal sulcus (pIPS) territory resulting from the volume-based (on the top) and the surface-based (on the bottom) analyses. For both analyses, the activations of each condition (hand pointing, foot pointing, and saccades) relative to the fixation are shown. The results of the (saccades > hand pointing) AND (saccades > foot pointing) conjunction analysis, i.e., saccades > pointing, are shown only in the SBA given that the VBA did not show significant activation. Both the activations corresponding to the lateral portion of pIPS and the medial portion of pIPS are labeled on the surface-based brain map and activation peaks are pinpointed in black in both VBA (one peak) and SBA (two peaks; see results section for more details). B) Comparison of the activation maps in the dorsal premotor cortex territory (PMd) resulting from the volume-based (VBA, on the top) and the surface-based (SBA, on the bottom) analyses. For both analyses, the activations of each condition (hand pointing, foot pointing, and saccades) relative to the fixation are shown, as well as the results of the (hand pointing > saccades) AND (foot pointing > saccades) conjunction analysis, i.e., pointing > saccades. Activation peaks are pinpointed in black in both VBA (one peak) and SBA (two peaks; see results section for more details). Both the activations corresponding to the caudal dorsal premotor cortex (cPMd) and the rostral dorsal premotor cortex (rPMd) are labeled on the surface-based brain map. In both A and B, the maps are

overlaid into the inflated Conte69 atlas (Van Essen et al. 2012) of the left hemisphere. Anatomical landmarks are also reported (SFS: superior frontal sulcus; CS: central sulcus; PoCS: postcentral sulcus; aIPS: anterior intraparietal sulcus; hIPS: horizontal intraparietal sulcus; pIPS: posterior intraparietal sulcus).

In both VBA and SBA we detected no significant differences in the activation maps within the pIPS territory when directly comparing the hand pointing and the foot pointing conditions. Intriguingly, in SBA an activation focus in the lateral portion of the pIPS, consistent with the lateral peak defined above (MNI coordinates: -24, -60, 51; T = 4.38; cluster size (kE) = 108), emerged when comparing saccades to the two pointing tasks [(saccades > hand pointing) AND (saccades > foot pointing) conjunction analysis]. This result is consistent with the preference of the lateral portion of the pIPS for saccadic movements in both monkeys (Snyder et al. 1997; Cui and Andersen 2007) and humans (Sereno et al. 2001). In the reverse contrast, i.e., (hand pointing > saccades) AND (foot pointing > saccades), we found no differences in the pIPS territory in both VBA and SBA. Conversely, coherently with the results by Heed and colleagues (Heed et al. 2011), we found pointing-related preference in the most anterior part of the superior parietal lobe (Supplementary Figure 1).

Within the PMd territory, as shown in Figure 2.1 (panel B), both VBA and SBA analyses detected no effector-specific significant differences in the activation maps when directly comparing the hand pointing and the foot pointing conditions, similar to what we observed in the pIPS. That said, both analyses revealed a possible, even if not clear, functional segregation of distinct subregions. Similarly to what we observed in the pIPS territory, the VBA consistently showed a single activation peak in the PMd in each condition compared to the baseline (hand pointing: MNI coordinates -27 -10 58; T = 13.8; foot pointing: -24 -7 61, T = 12.6; saccades: -24 -7 58, T = 9.5), while the SBA consistently showed two peaks: a more rostral one (hand pointing: -21 -7 52, T = 16.6; foot pointing: -21 -6 52, T = 15.6; saccades: -21 -6 52, T = 14.7), and a more caudal one (hand pointing: -25

-13 55, T = 13.3; foot pointing: -25 -13 55, T = 11.5; saccades: -26 -12 51, T = 8.5). Similarly, in the (hand pointing > baseline) AND (foot pointing > baseline) conjunction analysis, we detected a single peak in the PMd territory in the VBA (-15 -64 55, T = 9.5) and two separate peaks in the SBA (rostral: -21 -6 52, T = 15.6; caudal: -25 -13 55, T = 11.5). The same was true in the conjunction analysis of all the three conditions compared to baseline (VBA: -24 -7 58, T = 9.5; SBA: rostral -21 -6 52, T = 14.7, caudal -26 -12 51, T = 8.5). Noteworthy, results showed that only the caudal portion of PMd resulted to prefer pointing over saccades, as emerged from the (hand pointing > saccades) AND (foot pointing > saccades) conjunction analysis in both VBA (-24 -10 61, T = 6.7) and SBA (-26 -13 59, T = 6.21). The following steps of our work aimed at disambiguating the possibility of such functional segregation within the PMd.

To sum up, SBA suggested a possible functional distinction between two subregions within the pIPS, namely lpIPS and mpIPS, involved in all the three conditions; however, lpIPS was found to be more activated during saccades than during the pointing tasks. Similarly, both SBA and VBA analyses revealed a possible functional segregation between two portions within the PMd territory: a more rostral region involved to the same extent in all the three conditions, and a caudal region preferentially activated during pointing tasks.

2.3.2 Individual results and regions of interest selection

The next step aimed at verifying the possibility of mapping the regions resulting from group level activations at the single-subject level, with a special focus on the pIPS and PMd territories where adjacent, but functionally distinct, regions emerged. On the individual cortical surface, we were able to define seven regions: the medial posterior (mpIPS), the lateral posterior intraparietal sulcus (lpIPS), hPEc and hPE, the frontal eye fields (FEF), the caudal (cPMd) and the rostral dorsal premotor cortex (rPMd) (Figure 2.2).

We identified the regions from theoretically motivated contrasts, given the results of the SBA at the group-level, and with reference to anatomical landmarks. Each individual ROI

was identified by applying a watershed transform (as described in the Methods section) to the individual activation map to split it into a separate "neighborhood" for each activation peak in an objective manner, based on the spatial gradient of the activation map, resulting in regions of varying shape and size, bordered along the local minima of the map. As the whole activation map was segmented in this way, we then manually selected the regions of interest which best corresponded to the group peaks described in the previous section, using region-specific anatomical landmarks extensively described below. Importantly, since our aim was defining spatially distinct regions in an unbiased way, i.e., independently from their significant preference for one action over the other; therefore, no between-conditions contrasts were used to define individual ROIs.

mpIPS and lpIPS. The mpIPS was mapped from the (hand pointing AND foot pointing) > fixation conjunction analysis since this portion of the pIPS was active for pointing movements regardless of the effector (hand or foot), according to previous studies on humans (Heed et al. 2011, 2016) and our SBA results at the group-level. Furthermore, the anatomical location of the group peak we labeled as mpIPS is comparable with the putative medial intraparietal area (MIP), known to be preferentially involved in pointing and reaching movements, as suggested by previous human studies. Differently, we defined lpIPS from the eye > fixation t-contrast since this region was found to be more activated during saccades than during pointing. Consistently with Galati and colleagues (Galati et al. 2011), we marked the lpIPS territory as the junction between the horizontal segment of the intraparietal sulcus (hIPS) and its posterior segment (pIPS); the mpIPS was expected to be located in the medial bank of IPS (Grefkes et al. 2004), in the most anterior part of the pIPS, eventually leaning on the transverse parietal sulcus (TPS) (Galati et al., 2011), anteriorly to the parieto-occipital sulcus (POS) (similarly to the putative MIP defined by Connolly et al. 2003), but posteriorly to the subPS, which marks the posterior end of the hPEc territory (Pitzalis et al. 2019).

hPEc and hPE. hPEc was activated in both the pointing tasks regardless of the effector (Pitzalis et al. 2019), as opposed to hPE which resulted only from the foot pointing >

fixation t-contrast. We then mapped both regions from the same, commonly activated contrast (i.e., foot pointing > fixation t-contrast), to control for the eventual overlap between these areas. Consistently with Pitzalis and colleagues (Pitzalis et al. 2019), hPEc was expected to be located in the anterior part of the dorsal precuneate cortex, anteriorly to the subparietal sulcus (subPS) and posteriorly to the ascending ramus of the cingulate sulcus (Cgs), whereas the hPE anteriorly to hPEc, over the dorsal tip of the Cgs, and medially to the end of the postcentral sulcus (PCs).

FEF and PMd. In the frontal cortex, we defined FEF from the eye > fixation t-contrast. We expected the FEF to be located at the intersection between the precentral gyrus and the caudal end of the middle frontal sulcus (Vernet et al. 2014). As the SBA consistently showed two separate regions within the PMd territory across conditions, we attempted to map both of them from (hand pointing > fixation) AND (foot pointing > fixation) AND (saccades > fixation) conjunction analysis. However, in 5 out of 17 subjects it was not possible to segment the activation into more than one region, as the caudal portion of PMd was not reliably activated in all three conditions, being only subtly involved in saccades. Hence, we succeeded in defining a caudal (cPMd) and a rostral (rPMd) region, which were adjacent but still distinguishable, from the conjunction analysis of both pointing conditions, i.e., (hand pointing > fixation) AND (foot pointing > fixation) conjunction analysis. Importantly, we did not consider defining these two ROIs from different contrasts (i.e., the caudal one from the conjunction analysis of the two pointing conditions, and the rostral one from the conjunction analysis of all the three conditions) as this would have led to a risk of overlap between the two PMd subregions. Anatomically, the dorsal premotor region is a wide area limited rostrally to the postcentral sulcus, caudally to the anterior margin of the central sulcus, dorsally to the boundary between the lateral and mesial surfaces of the frontal cortex, and ventrally to the posterior prolongation of the inferior frontal sulcus (for a review see Ahdab et al. 2014). Here, we focused on specific premotor subregions located in the superior portion of the precentral gyrus. Based on previous evidence (Picard and Strick 2001; Chouinard and Paus 2006), we expected to find two subregions located medially with respect to the

omega shaped portion of the precentral gyrus known as the hand knob. A caudal PMd region was expected to extend from the rostral limit of the primary motor cortex, leaning just above the frontal eye fields (Rizzolatti and Luppino 2001; Mayka et al. 2006; Ahdab et al. 2014). The rPMd was expected to be placed anteriorly to its caudal counterpart (Picard and Strick 2001; Chouinard and Paus 2006) and extending in the posterior part of the superior frontal gyrus (Hirose et al. 2010), although there is still no clear accordance about the anatomical boundaries regarding the limits of the rostral portion of the PMd (Ahdab et al. 2014).

Overall, we succeeded in mapping the selected ROIs in the subjects, clearly distinguishing adjacent areas within the pIPS and the PMd territories (i.e., lpIPS and mpIPS, cPMd and rPMd). Mean coordinates and standard deviations of individual ROIs are provided in Supplementary Table 1. To check for the homogeneity between individual ROIs, we also created probabilistic ROIs (see Figure 2.3) by averaging the individual ones; then, we controlled for the degree of overlap across subjects (see Supplementary Figure 2.2). All the probabilistic ROIs showed an overlap reaching at least 75% of the subjects.

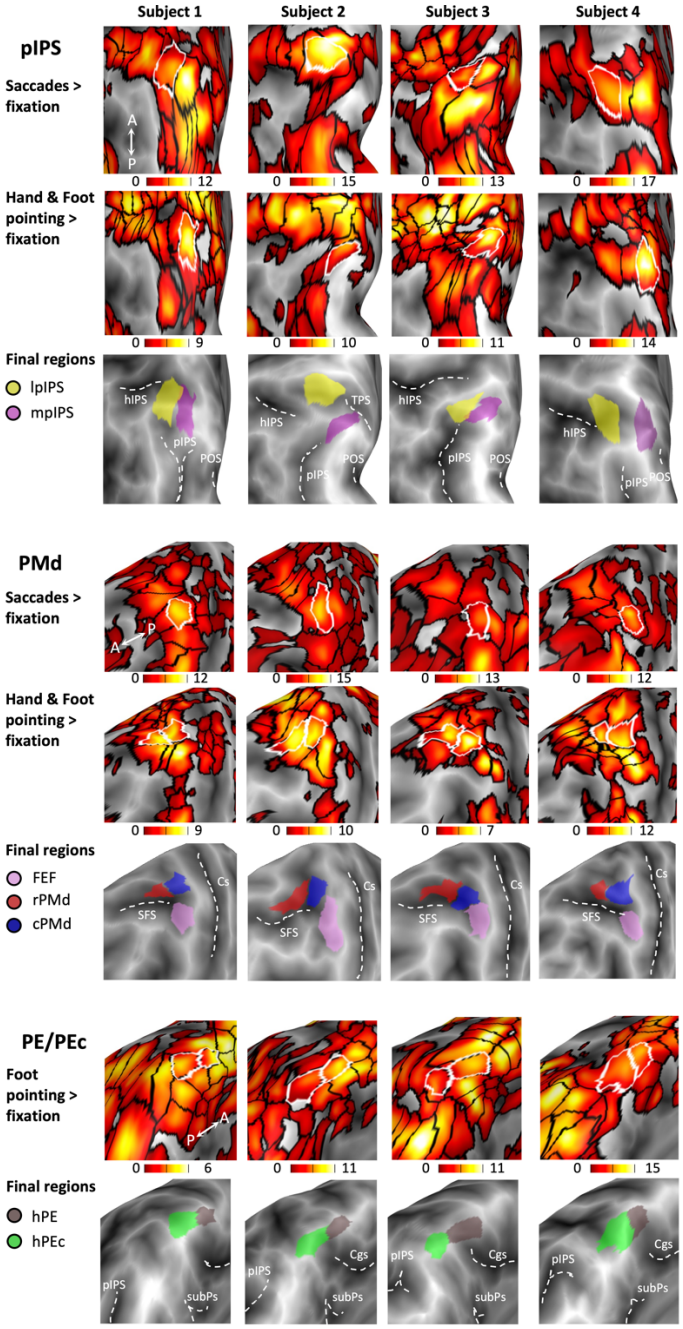

Figure 2.2. Individual ROI selection. The figure shows the mapping of each of the 7 ROIs for 4 representative subjects (columns). For each territory (upper panel: pIPS; middle panel: PMd; bottom panel: PE/Pec) individual activation maps (thresholded at t > 0) are shown as segmented by the watershed algorithm (black borders), with the selected ROI, after reduction to a maximum of 300 nodes, is denoted by white borders. Color scales are shown under each activation map. The final selected regions are depicted in the last row of each territory with different colors (lpIPS: yellow; mpIPS: purple; FEF: pink; rPMd: red; cPMd: blue; hPE: brown; hPEc: green) and are overlaid onto the individual surface along with anatomical landmarks (SFS: superior frontal sulcus; CS: central sulcus; hIPS: horizontal intraparietal sulcus; pIPS:

posterior intraparietal sulcus; TPS: transverse parietal sulcus; POS: parieto-occipital sulcus; subPS: subparietal sulcus; Cgs: cingulate sulcus). The antero-posterior axis is also represented for each territory.

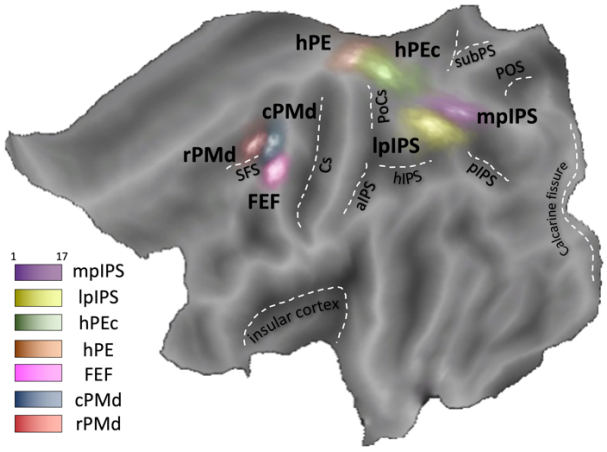

Figure 2.3. Probabilistic regions of interest. Probabilistic ROIs obtained by averaging individual ROIs, overlaid onto a flattened Conte69 brain atlas (left hemisphere). Each ROI is displayed in a color scale (lpIPS: yellow; mpIPS: purple; FEF: pink; rPMd: red; cPMd: blue; hPE: brown; hPEc: green) representing the degree of overlap across individual ROIs: the lighter the color (i.e., close to white), the higher the overlap of each node across the 16 individual ROIs. Anatomical landmarks are also reported (SFS: superior frontal sulcus; CS: central sulcus; PoCS: postcentral sulcus; aIPS: anterior intraparietal sulcus; hIPS: horizontal intraparietal sulcus; pIPS: posterior intraparietal sulcus; POS: parieto-occipital sulcus; subPS: subparietal sulcus).

2.3.3 Resting-state functional connectivity

We next set out a resting-state functional connectivity analysis to assess whether the correlation patterns in spontaneous fluctuations of the BOLD signal would suggest that some of our ROIs share similar functional properties. This analysis could shed some light on the functional differences between adjacent regions we found from the previous analyses. Results of the rs-fc analysis ($p < 0.0024$, corresponding to $p < 0.05$ Bonferroni corrected: see Figure 2.4 and Supplementary Table 2) showed that mpIPS is functionally

connected with hPEc (t16 = 4.08, p = 5.68 x 10-4) and both premotor areas (cPMd: t16 = 6.87, p = 3.83 x 10-6; rPMd: t16 = 8.92, p = 1.9 x 10-7). Similarly, a significant functional connectivity emerged between the hPEc and both the caudal (t16 = 7.32, p = 1.9 x 10-6) and the rostral (t16 = 7.5, p = 1.43 x 10-6) portions of the PMd, as well as between hPEc and hPE (t16 = 4.89, p = 9.71 x 10-5). lpIPS resulted to be connected with FEF (t16 = 5.57, p = 3.48 x 10-5) and with the adjacent area mpIPS (t16 = 4.77, p = 1.49 x 10-4). Also, the two subregions within the PMd territory appeared to be functionally connected with each other (t16 = 8.33, p = 4.3 x 10-7) and with FEF (rPMD: t16 = 5.15, p = 7.41 x 10-5; cPMd: t16 = 6.63, p = 5.67 x 10-6).

Overall, these results suggest that the connectivity of mpIPS is similar to that of the macaque area MIP, whereas the resting-state functional connectivity profile of lpIPS resembles that of the macaque area LIP. Also, the two PMds were found to have a different connectivity profile, being the connection with mpIPS stronger for the rPMd than for the cPMd (t14 = -4.06, p = 0.001), whereas the connection of the hPEc was stronger with the cPMd than the rPMd (t14 = 2.32, p = 0.036). Our findings were consistent with the anatomical studies on macaque areas that served as a model for our DCM analysis.

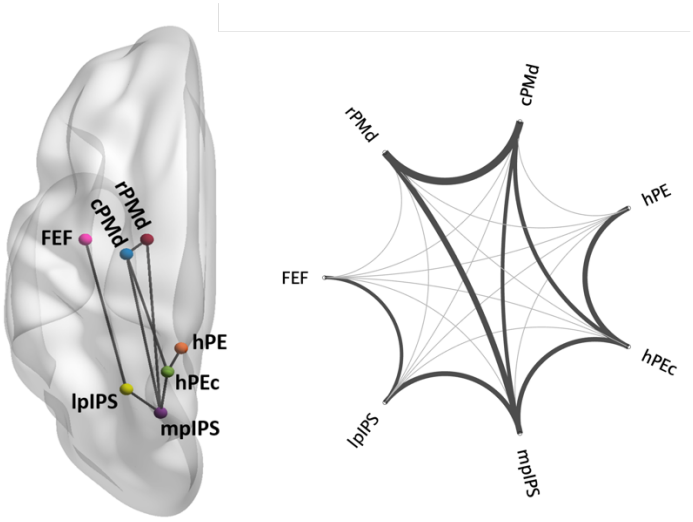

Figure 2.4. Resting-state functional connectivity results. The left panel shows significant correlations (p < 0.0024) across ROIs overlapped on the BrainNet Viewer template (Xia et al. 2013). Regions are labelled as follows: medial posterior intraparietal area: mpIPS; lateral

posterior intraparietal area: lpIPS; caudal hPE: hPEc; human PE: hPE; frontal eye fields: FEF; caudal dorsal premotor cortex: cPMd; rostral dorsal premotor cortex: rPMd. The right panel shows a graphical representation of the rs-fc results: significant correlations ($p < 0.0024$) are shown in dark gray; the width of the arrows is proportional to the strength of each connection, as represented by the average, normalized correlation coefficients ranging from 0.35 to 0.75. Non-significant correlations ($p > 0.0024$) are shown in light gray.

2.3.4 DCM analysis

To characterize the dynamic couplings within different parieto-frontal circuits involved in saccades, hand and foot pointing, we used the Dynamic Causal Modelling approach. We built the connectivity matrices according to the results of our resting-state functional connectivity analysis which suggested preferential fronto-parietal routes connecting specific brain regions (e.g., lpIPS and FEF), consistently with macaque studies.

Intrinsic coupling between nodes (A matrix). In order to build the architecture of the DCM model, the estimation of the intrinsic coupling between nodes was provided in the A matrix. Here, we modelled the connections between nodes according to our rs-fc results, which confirmed previous evidence emerged from tracer studies performed in macaque (Blatt et al. 1990; Stanton et al. 1995; Bullier et al. 1996; Matelli et al. 1998; Caminiti et al. 1999; Lewis and Van Essen 2000; Marconi 2001; Raos et al. 2004; Gamberini et al. 2009; Bakola et al. 2010, 2013, 2017) and a functional connectivity study on humans and macaques (Hutchison et al. 2012, 2013) (Supplementary Table 3). We assumed the following equivalence between macaque and human brain regions: F2/PMds, FEF/FEF, LIP/lpIPS, MIP/mpIPS, PE/hPE, PEc/hPEc. Briefly, we modelled the reciprocal connections between mpIPS and all the other modelled areas; those between lpIPS and both FEF and mpIPS; hPEc was supposed to be reciprocally connected with hPE, mpIPS and both PMds; we modelled the connections between FEF and both PMd and pIPS subregions, whereas the two premotor cortices were supposed to project, but not to receive, inputs from the hPE.

Results showed that in the leading diagonal, all the self-connections were negative except for the self-connection of lpIPS. For easiness of readability, the connectivity results will be described separately for each territory. The two regions in the posterior IPS (i.e., lpIPS and mpIPS) appeared to be positively and reciprocally connected; furthermore, mpIPS exerted a positive influence on all the modelled nodes (i.e., hPEc, hPE, lpIPS and both PMd), whereas lpIPS and FEF exerted a reciprocal inhibition.

The two PMd had two different patterns of connectivity: rPMd positively influenced FEF, but negatively influenced hPE and hPEc, whereas the opposite connections were subthreshold (FEF to rPMd: connection strength = 0, posterior probability = 0; hPEc to rPMd: connection strength = -0.06, posterior probability = 0.86). Instead, cPMd inhibited FEF, mpIPS and rPMd, receiving in return a positive influence from FEF and mpIPS, but no suprathreshold influence from rPMd (connection strength = 0, posterior probability = 0). hPE did not influence any modelled region but itself, whereas hPEc exerted a positive influence on hPE and a negative influence on mpIPS and cPMd (Figure 2.5).

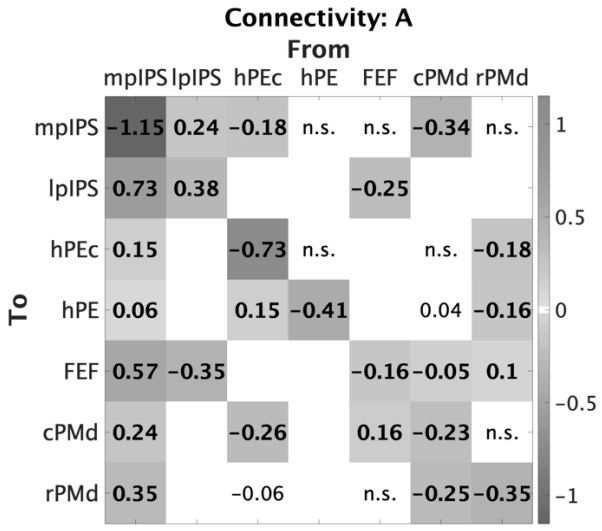

Figure 2.5. PEB Results- A Matrix. The figure shows the matrix of the effective connectivity of the unmodelled baseline. Connection strengths of excitatory (positive values) and inhibitory (negative values) couplings are displayed from light grey to dark grey. Values of connection strengths are also provided. Suprathreshold parameters (posterior probability > 0.90) are shown on shades of grey background, whereas subthreshold parameters are marked with "n.s." (i.e., non-suprathreshold), and non-modelled connections, i.e., whose priors are set to 0, are

displayed in white. Subthreshold parameters (0.70 < posterior probability < 0.90) are also provided and are shown on white background.

Effects of driving input (C matrix). The C matrix aims at disclosing the sensitivity of a region to the driving input stimulus, and we modelled it differently according to each condition. As input stimulus in the C-matrix, we separately modelled the direct influence of each condition "hand", "foot" and "saccade" on regions we hypothesized to be directly influenced by them. In the C matrix we modelled only the areas in the PPC since these nodes are supposed to encode the visuomotor properties of the target toward which eye or limb movements point. Given that mpIPS and hPEc were active in both hand and foot pointing conditions, we modelled the experimental inputs on both regions with the aim of examining the sensitivity of each of them to the driving inputs. We additionally modelled lpIPS as the only region directly influenced by the saccade driving input.

Parametrical Empirical Bayes (PEB) analysis results showed that foot pointing directly influenced both mpIPS and hPEc, while hand pointing exerted a direct effect on mpIPS only. A direct comparison between the driving inputs on mpIPS by means of a Bayesian contrast proved that foot pointing exerted a higher influence on mpIPS than hand pointing (Pp = 1, see Figure 2.6). Regarding the input stimulus in the "saccade" condition, we modelled lpIPS as the early perceptual station among the other candidate regions activated by this task; results showed this parameter being suprathreshold and positive.

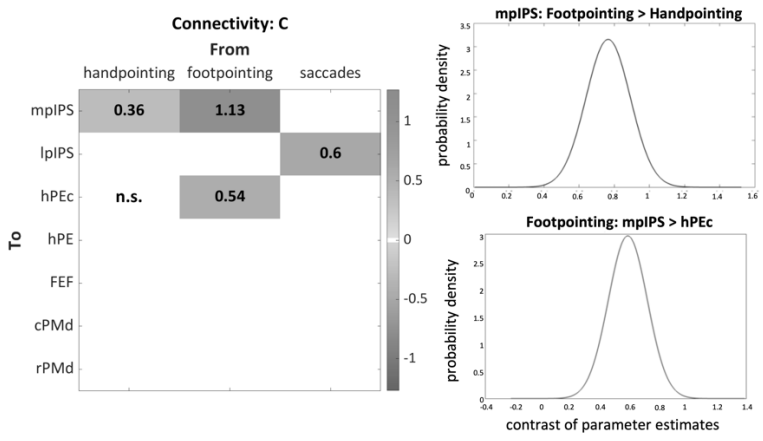

Figure 2.6. PEB Results-C Matrix. The left panel shows the matrix of the direct effect exerted by the inputs (i.e., stimuli of the hand pointing, foot pointing and saccades conditions) on the modelled ROIs (i.e., both mpIPS and hPEc in the two pointing conditions, only lpIPS in saccades). Only suprathreshold parameters (posterior probability > 0.90) are shown, whereas subthreshold parameters are marked with "n.s." (i.e., non-suprathreshold), and non-modelled connections, i.e., whose priors are set to 0, are displayed in white. Connection strengths of excitatory (positive values) input stimuli are displayed from light grey to dark grey. Values of connection strengths are also provided. The right panel of the figure also shows the Bayesian contrast over the comparison of the direct effects exerted by the two pointing conditions on mpIPS. Results showed that foot pointing exerted a higher influence on mpIPS than hand pointing (Pp = 1).

Task-specific modulation of connectivity (B matrices). To compute the influence of our tasks on connectivity among regions, we modelled three B matrices, one for each condition, aiming at assessing the dynamic couplings between the regions separately involved in each task, respecting two constraints: a) for each task, we included only the regions whose activation was reliable at both the group and the individual level in our surface-based analyses; b) we referred to the previous knowledge on the circuits separately involved in each task to model connections between the selected ROIs according to the above-defined constraint in the corresponding B matrix.

Hereafter we provide a detailed explanation of the parameters switched on in each B matrix (for a graphical representation, see also Supplementary Figure 3) along with the effective connectivity results of each condition (Figure 2.7).

We evaluated the mutual couplings between FEF and lpIPS, the latter being defined as the region of our GLM analysis with a preference for saccades compared to hand pointing and connected with FEF as resulted from the rs-fc analysis. PEB results showed that lpIPS exerted a positive influence on FEF, receiving inhibitory feedback.

As our GLM results showed that the rPMd is reliably engaged during saccades across subjects, as opposed to the cPMd, we also aimed at verifying the existence of a modulation exerted by this condition on the reciprocal connections between rPMd and FEF which we found to be functionally linked during resting-state. Differently, since no functional (see rs-fc results) nor anatomical (cfr. Supplementary Table 3) connections have been found between PMd and lpIPS, we did not model these parameters. The PEB analysis showed that rPMd inhibited FEF, whereas the coupling from FEF to rPMd did not exceed the threshold (connection strength = 0.16, posterior probability = 0.75).

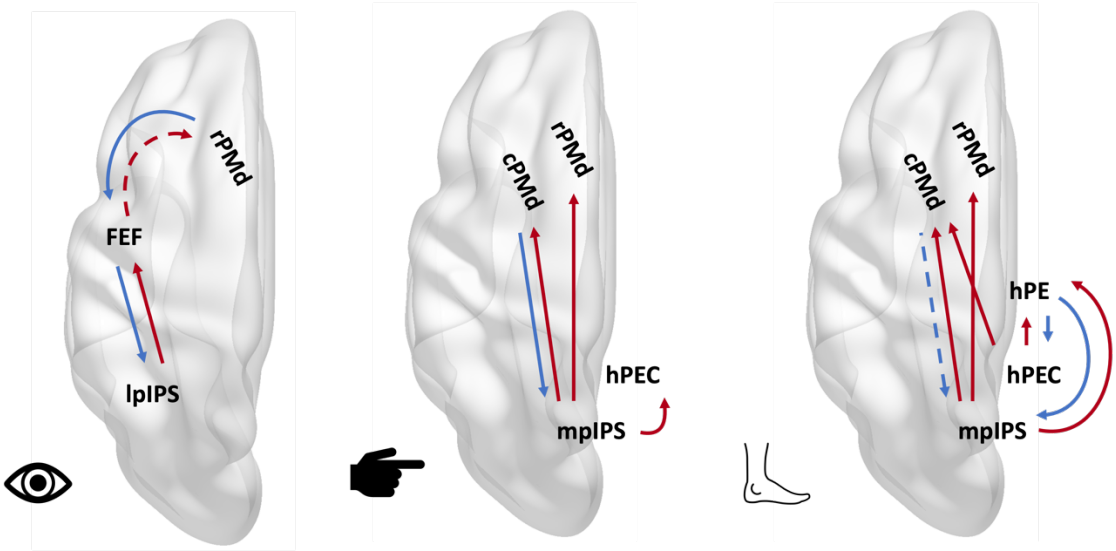

Figure 2.7. PEB Results- B Matrices. Schematic representation of each B matrix, separately for each condition. Connections with posterior probability > 0.75 are displayed: red lines denote excitatory connections, blue lines stand for inhibitory connections. Connections with probability between 0.75 and 0.90 are displayed as dashed lines.

Results of our both surface-based and rs-fc analyses led to the proposal of mpIPS as the homologue of macaque area MIP, since this area is activated during pointing, regardless of the effector, and is connected during resting-state with both subregions in the PMd. Accordingly, in the first B matrix we included both forward and feedback connections between mpIPS and the two PMds to characterize the eventual mutual interactions between these areas during hand pointing. We also verified the possibility of a

modulation exerted by this condition on the reciprocal connections between the two PMds. Results showed that mpIPS exerted a positive influence on both premotor areas, but only cPMd inhibited mpIPS even if this parameter was not suprathreshold (connection strength = -0.21, posterior probability = 0.76). Results of the Bayesian contrast on the connections from mpIPS to the premotor cortex showed that the modulation exerted by hand pointing was higher in the connection from mpIPS to cPMd than in that from mpIPS to rPMd (Pp = 0.98).

Several studies have suggested a role of PEc in pointing, in both macaques (Battaglia-Mayer et al. 2001; Ferraina et al. 2001; Hadjidimitrakis et al. 2015; Piserchia et al. 2016) and humans (Pitzalis et al. 2019); also, our fc-rs analysis showed that this area is connected with the dorsal premotor cortex, consistently with macaque data. Therefore, we aimed also at unveiling the eventual role of hPEc in hand pointing by modelling its reciprocal connections with mpIPS and both PMds. We found that mpIPS positively influenced hPEc, without receiving any feedback, whereas we found no modulation of hand pointing on the connections between hPEc and the two PMds.

Finally, even if there are few studies on foot pointing, they support evidence of involvement of both PE and PEc. Both regions exhibit motor and sensorimotor properties (Pitzalis et al. 2019; Sulpizio et al. 2020) and visual motion properties (Pitzalis et al. 2020; Di Marco et al. 2021), besides showing a preference for the lower visual field during pointing (Maltempo et al. 2021). Given the lack of evidence on the specific circuit involved in foot pointing, we modelled several connections to disentangle the roles of mpIPS, hPEc and hPE, and their eventual influence on both premotor regions. It is noteworthy that we did not model the hPE to directly influence the premotor cortex, since a reliable anatomical, afferent connection from PE to F2 has not been demonstrated in macaques (cfr. Supplementary Table 3), nor these regions appeared to be connected in our rs-fc analysis. Results showed that both mpIPS and hPEc exerted a positive influence on hPE and cPMd; however, they both received a feedback inhibition from hPE, whereas only mpIPS was inhibited by cPMd. Additionally, mpIPS also exerted a positive influence on

rPMd without receiving feedback. In contrast to the hand pointing condition, here the Bayesian contrast on the connections from mpIPS to the premotor cortices showed that the modulation exerted by foot pointing was lower from mpIPS to cPMd than from mpIPS to rPMd (Pp = 0.99).

A direct comparison between the foot pointing and the hand pointing conditions (Figure 2.8) showed that the connection from mpIPS to cPMd was higher in the hand pointing condition (Pp = 0.99), whereas the connection from mpIPS to rPMd was slightly higher in the foot pointing condition (Pp = 0.91).

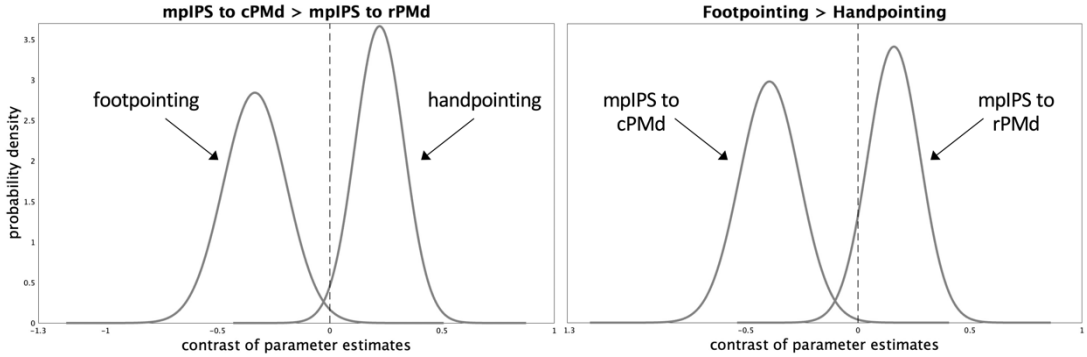

Figure 2.8. Bayesian contrasts over parameters of B-matrices. A) Comparison of the forward connections from the mpIPS to the two premotor cortices, separately for foot pointing (left curve) and hand pointing (right curve). Bayesian contrasts revealed that during hand pointing the forward connection from mpIPS was modulated more strongly when directed toward cPMd (connection strength: 0.66) than toward rPMd (connection strength: 0.44). The opposite pattern was found during foot pointing (connection strength of mpIPS to cPMd: 0.27; mpIPS to rPMd: 0.6). B) Comparison of parameters across conditions (namely, foot and hand pointing). The strength of the connection from mpIPS to cPMd (left curve) was higher during hand pointing (connection strength: 0.66) than foot pointing (connection strength: 0.27); conversely, the strength of the connection from mpIPS to rPMd (right curve) was higher during foot (connection strength: 0.6) than during hand pointing (connection strength: 0.44).

2.4. Discussion

The visuomotor transformations that enable individual actions in the environment are a crucial feature of the associative cortex and rely essentially on the involvement of areas

within the intraparietal sulcus, which are supposed to be differently specialized for one type of action or effector over the others. Despite extensive research on this topic, the functional organization of the human PPC is still a debated issue, due to anatomical, methodological, and conceptual tangles. Here, we attempted to contribute to this dispute by disambiguating the functional profiles of different areas in the pIPS, as well as their roles in the parieto-frontal circuits during resting state and visuomotor tasks. For the easiness of exposition, discussion has been divided into subheadings according to the three-step hierarchical analysis we performed.

2.4.1 Surface-based and Volume-based analyses

By employing both a surface-based analysis (SBA) and a volume-based analysis (VBA), we sought to explore the possibility of defining a functional segregation within the pIPS territory, which is supposed to be a mosaic of areas, each one specialized for different aspects of sensorimotor analysis.

With the individual surface-based approach, we successfully defined activation boundaries between adjacent areas in the pIPS, namely lpIPS and mpIPS. At the group level, on the one hand both areas resulted to be engaged during both pointing and saccades; on the other hand, the direct comparison between these tasks suggested a preference of the lpIPS for saccades over pointing regardless of the effector. Note that this result emerged only in the surface analysis; the reduction of multiple comparisons in SBA compared to VBA may account for the absence of this result in the VBA (Jo et al. 2007; Brodoehl et al. 2020), which also includes voxels outside the grey matter. Intriguingly, no region in the pIPS showed the reversed activation pattern, i.e., was more active during pointing than saccades. While the functional profile of lpIPS is similar to that of the monkey LIP, our results suggest caution when looking for homologies between mpIPS and MIP, since one would have expected the medial portion of the pIPS to exhibit a preference for pointing over saccades. This result is not completely surprising, though: previous studies (Hagler et al. 2007; Filimon et al. 2009) have provided similar results, leading to the hypothesis that pointing movements are not strong enough to activate

reach-related areas more than saccades (Filimon 2010). Overall, the results of our group analyses resemble the relative, rather than the absolute, preference of analogous segregated regions in the monkey pIPS for saccades or pointing (Snyder et al. 1997; Calton et al. 2002; Andersen and Cui 2009; see also the more recent paper by Liu et al. 2020). Notably, similarly to the findings of Heed and colleagues (Heed et al. 2011) and of Leonè and colleagues (Leoné et al. 2014), we detected a shared neural substrate for hand and foot pointing, possibly confirming a functional- rather than an effector-specificity within the pIPS. Conversely, anterior and medial regions of the PPC exhibit a subtle effector-selective preference as discussed in previous findings (Heed et al. 2011, 2016; Pitzalis et al. 2019).

Beyond the pIPS territory, in the dorsal premotor region we identified two areas, a more rostral one (rPMd), involved in all the conditions, and a more caudal one (cPMd), preferentially engaged in pointing tasks. At first glance, it might seem that this finding challenges the canonical view of PMd as being mainly a reach-related area. However, monkey studies have suggested that the PMd itself is not a homogeneous area, being instead composed of different subregions which share only partially overlapping functional properties (see for example Rizzolatti et al. 1998) that go beyond reaching-related features. For instance, some studies revealed a gaze-related discharge in PMd (Boussaoud et al. 1998; Jouffrais and Boussaoud 1999; Fujii et al. 2000; Lebedev and Wise 2001; Cisek and Kalaska 2002; Ohbayashi et al. 2003). In humans, an antero-posterior gradient within the PMd territory, compatible with a saccades-to-pointing preference continuum, has been previously detected (Filimon et al. 2009), a finding comparable with the functional dissociation between the two PMd regions we found in the present study. A collection of monkey studies by Pesaran and colleagues have suggested that in PMd both reaching-responsive (Pesaran et al. 2006) and saccade-responsive (Pesaran et al. 2010) neurons follow a relative reference frame, which depends upon the position of both gaze and hand, to encode the location of the target. Analogously, Gallivan and colleagues (Gallivan et al. 2011a) confirmed these previous results in humans as well, by using MVPA and employing cross-decoding between the left PMd and FEF related either to the

spatial position of a target or the effector used. Indeed, they found that both reaching, and saccade movement plans are spatially tuned to target locations and also showed that such spatial tuning is similar enough to allow cross-classifications across effectors, suggesting a shared relative position code.

Taken together, these findings suggest a shared spatial representation in this area regardless of whether the task to be performed is reaching an object or executing a saccadic movement. Even though the lack of evidence of possible segregation in the PMd territory in human fMRI studies prevents suggesting a strict homology with dissociated macaque premotor areas, we speculate that the hybrid functionality of the rPMd detected here resembles that of the PMd as described by Pesaran and colleagues in monkeys (Pesaran et al. 2006, 2010). Differently, the cPMd shows pure reach-related properties. Further studies may investigate to what extent it is possible to segregate regions in the human PMd territory based on their functional and/or anatomical features.

Overall, our study detected subtle differences in the activity pattern of adjacent areas. However, this finding is not enough to delineate the functional specificity of these areas. To deal with the complexity of the frontoparietal areas involved in visuomotor tasks, we implemented connectivity analyses which will be discussed in the following paragraphs.

2.4.2 Resting state functional connectivity

Resting state correlations may be interpreted as a neural signature of task-response properties of brain regions (De Luca et al. 2005; Vincent et al. 2006) and the rs-fc analysis has been used to constrain task-activation models (Fox et al. 2006; Dosenbach et al. 2007). In this vein, we attempted at detecting possible differences between adjacent regions in the pIPS and the PMd territory in their functional connectivity with other parietal and frontal areas. Results of rs-fc analysis highlighted the existence of parieto-frontal pathways similar to the ones observed in macaques during visuomotor tasks, consistent with the structural connectivity studies on macaque parietal areas. Indeed, the functional connectivity between mpIPS and the dorsal premotor cortices resembled that of the MIP-F2 circuit; similarly, the correlation between the spontaneous fluctuations of lpIPS and

FEF pointed toward a homology with the LIP-FEF circuit. Notably, as opposed to hPE, hPEc was found to be functionally connected with both PMds, presumably reflecting the anatomical connection between PEc and F2 (Caminiti et al. 1999; Marconi 2001; Bakola et al. 2010). Also, the significant seed-to-seed correlations between adjacent areas (i.e., the two PMds, hPE and hPEc, and the two subregions within the pIPS) reflected monkey data (Lewis and Van Essen 2000; Gamberini et al. 2009; Bakola et al. 2013, 2017).

Ultimately, the anatomical arrangement of mpIPS and lpIPS, their functional profile, and their connections with parietal and frontal areas, mark a neural signature of their homologies with monkey MIP and LIP and provide support for the neural architecture we modelled in the DCM analysis, discussed in the following section.

2.4.3 Effective connectivity within the effector-specific parieto-frontal circuits

Crucially for the present study, we aimed at achieving a broad comprehension of the effective connectivity between areas of the effector-specific parieto-frontal circuits underlying saccades, hand, and foot pointing, as suggested by previous and present findings.

As we expected, during saccades the input directly, and positively, affected lpIPS; furthermore, this region exerted a positive influence on FEF, receiving inhibitory feedback. This result suggests a feedforward-feedback loop between lpIPS and FEF, consistently with the serial activation of these areas during saccade planning and execution revealed by monkey studies (Snyder et al. 1997; Lawrence and Snyder 2006; Cui and Andersen 2007). Additionally, saccades negatively modulated the connection from rPMd to FEF, whereas we found only a subthreshold modulatory effect on the opposite connection. We cannot exclude that other brain regions not included here, e.g., supplementary eye fields (SEF), interact with rPMd during saccades execution. Indeed, as already speculated by Pesaran and colleagues (Pesaran et al. 2010), the recruitment of PMd during saccades might rely on inputs conveyed by the oculomotor control centers in the frontal cortex (namely, SEF or FEF). The functional meaning of the involvement of PMd during saccades is still unclear. The role of PMd is unlikely related to saccades'

motor commands, since PMd neurons have not been reported to consistently project to the superior colliculus or oculomotor structures (Fries 1985), nor to exhibit retinotopic saccadic responses. Conversely, it has been proposed that its connections with FEF (Thura et al. 2008), similarly to the one that emerged from our PEB results, subserve the bridge between hand and eye control, a result consistent also with Pesaran and colleagues' findings (Pesaran et al. 2006, 2010).

During pointing, the inputs exerted a direct influence on mpIPS, regardless of the effector, but this parameter was higher in foot than in hand pointing. The mpIPS region, similarly to macaque area MIP, might be involved in integrating the internal representation of both target and effector positions to compute a reach vector, i.e., the difference between the current and the desired effector position (Buneo and Andersen 2006; Blohm and Crawford 2007; Blohm et al. 2009; Vesia and Crawford 2012). As we predicted, in the modulatory matrices we found evidence of a feedforward-feedback loop between mpIPS and cPMd during pointing with both effectors, which points toward the view of a serial activation of parieto-frontal circuits during visuomotor tasks (Bencivenga et al. 2021). This neural architecture resembles the macaque MIP-F2 circuit responsible for the sensory-motor transformations that underlie pointing movements in an effector-independent fashion (Buneo and Andersen 2006). Also worthy of note is the comparison between the influences exerted by mpIPS on the two portions of the premotor cortex at rest and during the pointing tasks. In the rs-fc and the baseline connectivity (A matrix of the DCM), the mpIPS appeared to be more connected with the rostral rather than the caudal portion of the PMd. However, these links dynamically changed during the task: the "modulatory" B matrices showed that during hand pointing the connectivity profile of these regions is reversed compared to the intrinsic connectivity, as the mpIPS showed stronger connectivity with the cPMd, compared to the rPMd (mpIPS to cPMd= 0.66; mpIPS to rPMd= 0.44). This finding is consistent with the preferential activation of cPMd to hand movements, especially reaching and pointing ones (Filimon 2010). All in all, our results demonstrate that both premotor regions are involved in pointing movements with both effectors, likely being engaged in the coordinate transformations carried out during

motor execution. Furthermore, the differential pattern of connectivity stemming from mpIPS and reaching the premotor cortices depending on the effector to be used is in line with the view that action planning and implementation may be hierarchically organized. Accordingly, different levels of action representations ranging from effector independent, effector-dependent, to concrete representations, i.e., motor planning, converge in the parietal regions. Furthermore, these regions are reciprocally connected to the premotor regions, which instead hold effector-dependent representations, specific to the action to be implemented (Gallivan et al. 2013; Turella et al. 2020). Thus, the present results may indicate how parieto-frontal feedforward and feedback loops exchange the same effector-independent information common to either hand or foot actions, as recently proposed by comparing activations in analogous areas of individuals with dysplasia while reaching or grasping with their foot, and controls executing the same task with their hand (Liu et al. 2020). Further studies may investigate the differential contribution of the two PMd areas during visuomotor tasks, also taking into account their eventual links with M1 and subcortical structures.

In a previous study (Pitzalis et al. 2019) we reported a similar activity pattern of the hPEc in both hand and foot pointing, a result that is consistent with the absence of a somatotopic organization in this area, as opposed to what was observed in hPE (Breveglieri 2006; Gamberini et al. 2017). Interestingly, from a connectivity perspective, the hPEc showed effector-dependent dynamic couplings. First, the onset of the inputs directly affected hPEc only during foot pointing; consequently, the positive influence exerted by mpIPS seems to be the neural underpinning of the involvement of hPEc in hand pointing. Accordingly, one can argue that during foot pointing, besides the above-described mpIPS-cPMd loop, a parallel stream arises from hPEc, and then both circuits converge on somato-motor and premotor areas, namely hPE and cPMd. Here, different information, likely visuomotor and somato-motor, may be integrated through feedforward-feedback processes between frontal and parietal areas.

The distinct role of hPEc during hand and foot pointing deserves further consideration. As mentioned above, we found no effector-dependent activation patterns during pointing in either mpIPS or hPEc and, accordingly, dynamic couplings of mpIPS were similar during the two pointing conditions. In contrast, hPEc seemed to be involved in hand pointing due to the positive influence exerted by mpIPS but appeared to play an autonomous role in foot pointing. Distinct, intrinsic properties described in monkey MIP and PEc may account for this difference. It has been previously emphasized that both MIP and PEc are engaged during pointing and reaching (Filimon et al. 2007; Tosoni et al. 2008; Cavina-Pratesi et al. 2010; Vesia et al. 2010; Galati et al. 2011; Tosoni et al. 2015; Magri et al. 2019), are involved in broader visuomotor integration processing (Impieri et al. 2018; Gamberini et al. 2019), and their neurons discharge in response to visual and somatic stimuli. However, these two regions differ for their structural connectivity, since PEc receives vestibular and proprioceptive input (Bakola et al. 2010), unlike MIP. These two areas seem to represent space in different reference frames: whereas MIP/PRR refers to both eye-, hand- and head-centered frames (Batista et al. 1999; Mullette-Gillman et al. 2005; Pesaran et al. 2006; Bhattacharyya et al. 2009; Chang et al. 2009; Mullette-Gillman et al. 2009), PEc also encodes object locations in mixed body- and hand-centered references (Piserchia et al. 2016). Not lastly, only PEc responds to flow field stimulation (Squatrito et al. 2001; Raffi et al. 2002; Raffi et al. 2010; Raffi et al. 2011; Raffi et al. 2014; Pitzalis et al. 2019) and exhibits visual motion properties (Pitzalis et al. 2020; Di Marco et al. 2021), besides showing a preference for the lower visual field during visuomotor tasks (Maltempo et al. 2021). Given these peculiar features, it has been suggested that PEc encodes one's body posture in space (Breveglieri 2006), leading to the hypothesis that PEc is involved in locomotion (Breveglieri et al. 2008; Bakola et al. 2010; Raffi et al. 2014; Hadjidimitrakis et al. 2015; Gamberini et al. 2019), presumably integrating visually derived self-motion signals with motor leg movements (Pitzalis et al. 2019). Accordingly, we speculate that during foot pointing vestibular and proprioceptive inputs to PEc are strengthened, and that even if subjects lay in the scanner and are asked only to point towards a remembered target with their big toe, PEc encodes the body posture as one

would start locomotion, also by referring to a mixed hand/body-centered frame of reference. Instead, during hand pointing the transformation is necessarily executed with an eye-centered frame of reference starting from mpIPS, which receives weaker vestibular and proprioceptive inputs. Worthy of mention is also the evidence regarding the differential involvement of the PPC in the processing of motion-related features, such as depth and direction. Indeed, MIP has been shown to specifically encode the direction of the movement to be performed (Andersen and Buneo 2002), whereas PEc seems to be also engaged in estimating its depth especially in the phase of motor execution and relative to peripersonal space (Hadjidimitrakis et al. 2015). Even if to our knowledge there are no studies about the effector-dependent differences in encoding direction and depth during pointing, we may speculate that the estimated depth of the movement is of increasing relevance during foot pointing.

Further investigations are necessary to unfold the lack of hPEc dorsal premotor interactions during hand pointing. What is the next step of the information flow from hPEc? We cannot exclude that this area interacts with the arm-section of hPE, an area that still has to be thoroughly described.

2.4.4 Merging activation- and connectivity-based approaches

Our results suggest that the activation analyses only partially revealed differences between adjacent but distinct subregions in the pIPS and the PMd territory. For instance, mpIPS seemed to be recruited to the same extent during hand and foot pointing, but when looking at connectivity it clearly emerged a different connectivity profile between these two conditions. This finding does not point toward an incongruence between the two types of analyses, but rather emphasize their different ability in unveiling on the one hand, if some areas are recruited across conditions, on the other hand, how they are recruited across conditions. Also, the DCM analysis highlighted the possible forward (excitatory) and feedback (inhibitory) interactions between parietal and frontal areas. Future studies may aim at characterizing the functional meaning of the feedback-forward

influences occurring in each step of action planning and implementation (e.g., encoding of the visual properties of the stimulus, motor execution, online monitoring, etc).

2.5 Conclusions

Given the contradictory results on the segregation of the human PPC, we sought to perform a comprehensive analysis of brain networks differently involved in saccades and pointing. Rather than focusing on whether parietal subregions consistently and significantly prefer one action over the other, we wanted to show that spatially separate parietal subregions are differently interconnected with the premotor cortex, constituting distinct parieto-frontal circuits which are differently recruited by visuo-motor actions.

Our scope was threefold: as a starting point, we took advantage of individual surface-based analysis to increase the spatial accuracy in detecting differences in the pIPS and the PMd territories; then, we used rs-fc to define the brain architecture between the parieto-frontal areas we were interested in. At the endpoint, DCM allowed us to explain dynamic couplings between the same areas during visuomotor tasks, extending the findings of canonical activation analyses.

Despite that, some caveats are needed. We used a pointing rather than a reaching task, which also involves the transport of the forearm (Culham et al. 2006) and has been suggested to be more sensitive to the PRR properties. Furthermore, during our task subjects could not see their hand or foot while executing the movement. Despite being a common approach in fMRI studies on this topic, we cannot exclude that including the visual feedback through a visually guided pointing could change the couplings we reported in the present study. Also, we restricted the set of ROIs included in the connectivity analyses to fronto-parietal areas. We are aware that a wide range of areas, beyond the ones we considered here, may play a crucial role in visuomotor tasks such as pointing and saccades (for instance, areas in the ventral visual stream; for a review see Hutchison and Gallivan 2018). Nevertheless, we were forced to choose only some of them to account for the elevated computational effort that the DCM analysis requires when modeling a large number of regions. Thus, we included the main visuomotor areas

separately for each motor function. More research considering the role of a broader network of areas is needed to extend these findings.

The overall picture emerging from present and past studies is that an intrinsic specialization of fronto-parietal networks does exist, since they appear to be distinguishable depending on the function they subserve despite the involvement of common nodes during the implementation of similar tasks. Beyond a massive discrimination between actions, which reflects the distinct evolutionary, social, and functional meanings of saccades and pointing/reaching movements, in our study a more subtle distinction between effectors even in the same kind of visuomotor function emerges. Thus, our results confirm that a functional segregation of parietal and frontal areas solely based on their effector selectivity is difficult to obtain, as the last decades of research showed. On the other hand, the effective connectivity analysis allows a thorough characterization of specialized effector selective parieto-frontal networks recruiting common areas. Taken together, the present results are in line with the conception of the "dorsal visual stream" as made up of a multiplicity of functional streams that are composed of common areas (Galletti and Fattori 2018), which are not specific for one function or effector, but instead are dynamically activated or inhibited according to task to be performed. Our findings suggest caution when considering visuomotor functions and their underlying networks as independent of each other, with crucial implications in clinical practice.

CHAPTER 3

This chapter has been published in January 2021 as:

Bencivenga, F., Sulpizio, V., Tullo, M. G., & Galati, G. (2021). Assessing the effective connectivity of premotor areas during real vs imagined grasping: a DCM-PEB approach. NeuroImage, 230, 117806. https://doi.org/10.1016/j.neuroimage.2021.117806

Assessing the effective connectivity of premotor areas during real vs imagined grasping: a DCM-PEB approach

Federica Bencivenga,[1,2,3] Valentina Sulpizio,[1,3] Maria Giulia Tullo,[1,2,3] and Gaspare Galati[1,3]

[1] Brain Imaging Laboratory, Department of Psychology, Sapienza University, Rome, Italy

[2] PhD program in Behavioral Neuroscience, Sapienza University of Rome, Rome, Italy

[3] Cognitive and Motor Rehabilitation and Neuroimaging Unit, Santa Lucia Foundation (IRCCS Fondazione Santa Lucia), Rome, Italy

Abstract

The parieto-frontal circuit underlying grasping, which requires the serial involvement of the anterior intraparietal area (aIPs) and the ventral premotor cortex (PMv), has been recently extended enlightening the role of the dorsal premotor cortex (PMd). The supplementary motor area (SMA) has been also suggested to encode grip force for grasping actions; furthermore, both PMd and SMA are known to play a crucial role in motor imagery. Here, we aimed at assessing the dynamic couplings between left aIPs, PMv, PMd, SMA and primary motor cortex (M1) by comparing executed and imagined right-hand grasping, using Dynamic Causal Modelling (DCM) and Parametrical Empirical Bayes (PEB) analyses. 24 subjects underwent an fMRI exam (3T) during which

they were asked to perform or imagine a grasping movement visually cued by photographs of commonly used objects. We tested whether the two conditions a) exert a modulatory effect on both forward and feedback couplings among our areas of interest, and b) differ in terms of strength and sign of these parameters. Results of the real condition confirmed the serial involvement of aIPs, PMv and M1. PMv also exerted a positive influence on PMd and SMA, but received an inhibitory feedback only from PMd. Our results suggest that a general motor program for grasping is planned by the aIPs-PMv circuit; then, PMd and SMA encode high-level features of the movement. During imagery, the connection strength from aIPs to PMv was weaker and the information flow stopped in PMv; thus, a less complex motor program was planned. Moreover, results suggest that SMA and PMd cooperate to prevent motor execution. In conclusion, the comparison between execution and imagery reveals that during grasping premotor areas dynamically interplay in different ways, depending on task demands.

3.1 Introduction

The neural mechanisms underlying planning and executing a grasping movement, according to the visual features of an object, are still debated. Pioneer studies (Jeannerod et al., 1995; Fagg and Arbib, 1998; Rizzolatti and Luppino, 2001; Arbib and Mundhenk, 2005) enlightened the role of the "visuo-motor grasping circuit", which in macaques includes the anterior intraparietal area (AIP) and the ventral premotor cortex that corresponds to the cytoarchitectonically and functionally non-homogenous area F5 (Belmalih et al., 2009; Gerbella et al., 2011; Sharma et al., 2019; for a review, see Gerbella et al., 2017). According to these models, both areas seem to encode the goal of the action (Fogassi et al., 2001; Castiello and Begliomini, 2008) as well as the grip component of grasping, leading to the correct shape of the hand. Indeed, AIP encodes a 3D representation of the object to grasp and its affordances, while F5 stores a "vocabulary" where the action goals and the postures for grasping are represented, in order to select the most appropriate one according to the features of the object (for a review, see Castiello and Begliomini, 2008; Gerbella et al., 2017). A collection of positron emission tomography (PET), functional magnetic resonance imaging (fMRI) and transcranial magnetic

stimulation (TMS) studies has identified human homologues of these areas based on their similar functional and anatomical arrangement (Grafton et al., 1996; Faillenot et al., 1997; Binkofski et al., 1998; Culham et al., 2003; Culham 2004; Frey et al., 2005; Begliomini et al., 2007b; Dafotakis et al., 2008; Davare et al. 2009, 2010; for reviews, see also Davare et al., 2011; Gerbella et al., 2017). It has been proposed that some functional properties of these areas are shared across species. For instance, most neurons in AIP encode the object shape and, to a lesser extent, its size (Schaffelhofer and Scherberger, 2016); also in humans it has been proved that aIPs encodes intrinsic properties of the objects, such as their size, and not their extrinsic properties such as location (Monaco et al., 2015). Similarly, inactivation of both F5 (Fogassi et al., 2001) and PMv (Davare et al., 2006) results in an alteration of the grip but not of the transport component of grasping.

Following studies have suggested an extension of the macaque AIP-F5 circuit, focusing on the role of the dorsal premotor cortex (F2), traditionally known to be involved in reaching. Raos et al. (2004) demonstrated that this area is not only involved in the transport component of grasping, but also has a key role in keeping the motor representation of the object in memory and in updating hand movements (especially the configuration of fingers) as the hand approaches the object. Accordingly, it has been shown that some neurons in F2 are only tuned to reaching, others only to grasping, and others to both (Cao et al., 2013). More recently, a similar role of PMd during grasping has been found in humans by a wide range of studies using different techniques (Davare et al., 2006; Begliomini et al., 2007a; Nowak et al., 2009; Cavina-Pratesi et al., 2010; Gallivan et al., 2011b; Fabbri et al., 2016; Turella et al., 2019).

Castiello and Begliomini (2008) suggested that the areas of the grasping circuit are serially activated, since the information appears to flow from aIPs to PMv, then to PMd, and finally to M1 (F1 in macaques). The primary motor cortex is activated even prior to movement execution and is likely responsible for the motor output through the corticospinal tracts (CST) (Muakkassa & Strick 1979; Godschalk et al., 1984; Matelli et al., 1986; Dancause et al., 2006), besides contributing to the internal prediction of the

consequences of the movement (Seki and Fetz, 2012; Sun et al., 2015). A serial involvement of areas of the grasping circuit is also suggested by a series of human neurostimulation studies on precision grasping: whereas aIPs encodes for the visual representation of the object 270-220 ms before the fingers touch the object (Davare et al., 2007), PMv activates about 50 ms later (Davare et al., 2006). Finally, PMd activates around ~100 ms after the PMv (Davare et al., 2006).

Even if the supplementary motor area (SMA, F3 in macaques) was traditionally considered to be involved in the generation of internally driven complex movements (Orgogozo and Larsen, 1979; Roland et al., 1980; Goldberg, 1985), more recent studies have demonstrated an involvement of SMA in sequence planning (for a review, see Cona and Semenza, 2017) and visually guided movements such as reaching (Picard & Strick, 2003). Although SMA is not included in the grasping circuit, there is evidence that it might be involved in encoding some aspects of grasping movements, such as grip force scaling (Smith et al., 1981; Kuhtz-Buschbeck et al., 2001; Haller et al., 2009; White et al., 2013). Grip force is a crucial feature in grasping, since it must be modulated to grasp the object firmly, but without damaging it or let it slip (Johansson and Westling, 1984, 1988).

Dynamic Causal Modelling (DCM; Friston et al., 2003) is a framework for effective connectivity which allows testing hypotheses on the couplings among areas both in resting state (Friston et al., 2014) and during the execution of a task. Previous studies have applied DCM to fMRI data acquired during the execution of grasping; for instance, it has been proved that the dorsolateral (aIPs and PMv) and the dorsomedial (V6A and PMd) parieto-frontal circuits are differently modulated by grasping small or large objects (Grol et al., 2007). A DCM study by Begliomini et al. (2015) has shown that during a reach-to-grasp movement there is an increase in effective connectivity from aIPs to PMv, and from PMv to PMd. However, these studies did not explore the contribution of SMA in grasping; furthermore, they did not use commonly used objects, but manipulanda or boxes instead.

An attractive chance to disclose the underpinnings of motor processes is offered by the comparison between motor execution (ME) and imagery (MI). These two modalities recruit partially overlapping circuits: on the one hand, both seem to rely on a similar processing of motor temporal and spatial information, implemented by associative and premotor brain areas; on the other hand, it is still debated whether they share activity in M1 (for meta-analytic reviews, see Hètu et al., 2013; Hardwick et al. 2018; Papitto et al., 2020). However, striking evidences suggest that univariate fMRI analysis may not exhaustively account for eventual similarities or differences between these two modalities. By taking advantage of multivoxel pattern analysis (MVPA; Edelman et al., 1998; Haxby et al., 2001), it has been revealed that during motor tasks the main motor-related areas, included M1, encode the content of MI (Pilgramm et al., 2016) and that the overall neural representation of MI is similar but still distinct relative to ME (Zabicki et al., 2017; Monaco et al., 2020). By employing the multivariate Bayes (MVB) method (Friston et al., 2008), Park et al. (2015) found that movements were best predicted by M1 during ME, and by SMA during MI. An additional contribution potentially able to disentangle the neural substrates of ME and MI comes from effective connectivity approaches. In this vein, previous studies have clarified that during motor tasks the coupling between SMA and M1 is differently modulated by ME and MI (Solodkin et al., 2004; Kasess et al., 2008; Gao et al., 2011, 2014), e.g., during ME SMA exerted a positive influence on M1, whereas during MI the modulation on M1 became suppressive. These findings, combined with the above-mentioned MVPA studies, point toward the view that a similar, though not equal, implementation of the motor program is required during ME and MI and that, crucially, additional processes may take place during imagery to prevent the actual execution of the movement. However, the above-mentioned effective connectivity studies used imagery in low-demanding tasks (i.e. finger tapping).

Here, we provide the first attempt to apply DCM to imagery of a grasping movement by re-analysing previously collected fMRI data relative to execution and imagery of a pantomimed grasping of commonly used objects (Sulpizio et al., 2020). Several studies have pointed toward a neural similarity between pantomimed and actual movements

(Choi et al., 2001; Binkofski and Buxbaum, 2013). During grasping, slight differences in the activity of aIPs are found across pantomime and actual motor execution (Goodale et al., 2004; Hermsdörfer et al. 2007; Króliczak et al., 2007), presumably due to differences in the perceived goal of the action rather than in the motor planning per se. Notice that here we used pantomimed grasping to focus on the motor dynamics that finely regulate the planning and the execution of grasping, avoiding spurious contamination of the signal deriving from hand-object interactions. In the original study, we found a wide network of frontoparietal regions, such as aIPs, PMv, PMd and SMA, which are commonly activated by both imagery and execution of grasping coherently with the view of a similar recruitment of motor-related areas across modalities. In this vein, in the present study we sought to disentangle the direct and the modulatory effects of two exogenous variables (i.e., executed and imagined grasping) on a large motor network, including SMA. Accordingly, we used the computationally efficient Parametrical Empirical Bayes (PEB) approach recently introduced by Friston et al. (2015, 2016) to test both the feedback and the forward connections within our network of interest; by doing so, we hypothesized that we could get new insights on the involvement and the functional role of the key areas involved in grasping. Furthermore, we hypothesized that grasping execution and imagery would require a different involvement of premotor areas; thus, we expected the two conditions to differently modulate the effective connectivity among the key areas involved in grasping, in terms of the sign of the parameters (e.g., a connection would be positively modulated by grasping execution, and negatively modulated by imagined grasping) and of the connection strengths (e.g., reduced values of parameters in imagery relative to motor execution).

3.2 Methods

3.2.1 Participants

The present study is based on a reanalysis of BOLD data from a sample of twenty-five healthy subjects (22 females, mean age 26.5, s.d. 3.4) who participated to a previous study from our lab (Sulpizio et al., 2020). All participants were right-handed, as assessed by the

Edinburgh Handedness Inventory (Oldfield, 1971), had normal or corrected-to-normal vision, and gave their written informed consent to participate. The study was approved by the local research ethics committee of the IRCCS Fondazione Santa Lucia in Rome, according to the Declaration of Helsinki.

3.2.2 Procedure and experimental design

The experimental design is fully described in Sulpizio et al. (2020). Participants underwent an fMRI exam during which they were asked to execute a pantomimed grasping ("real" condition) or imagine the same movement ("imagined" condition). In both conditions, subjects saw the picture of an object, randomly chosen from a set of 36 black-and-white photographs of commonly used objects; in the "real" condition, participants were instructed to move the fingers and the wrist of their right hand simulating the grasping of the object, as if it was located in the proximity of their hand. In the "imagined" condition, participants had to imagine and plan the same pattern of movements without actually performing them.

Before entering the scanner, subjects were instructed on the task to perform, accounting for the trial timing and sequence; once in the scanner, they performed a short warm-up phase to familiarize with the setting. During the fMRI exam, an experimenter checked whether during the "real" condition participants moved their hand with the correct timing and according to the instructions, whereas during the "imagined" condition participants remained still.

The experiment used a block design. Each block lasted 16 seconds and was introduced by a written instruction (1 sec) which specified the condition (real or imagined); then, 8 consecutive trials, each lasting 1875 ms, were performed. Each trial started with the presentation in central vision of the graspable object photograph, followed by an inter-trial-interval of 1575 ms during which the subject had to perform or imagine (according to the specified condition) a "whole hand" or a "finger" grasping, depending on the visual stimulus (for more details, see Sulpizio et al., 2020). Graspable object photographs were presented for a very short time (300 ms) to reduce the impact of visual information

on BOLD activation. Grasping movements were indeed performed with respect to a "remembered" object not present anymore on the screen. Two runs were performed, each of them composed by 16 experimental blocks (8 for the real pantomimed grasping and 8 for the imagined grasping) plus 4 fixation blocks. Overall, the task consisted of 40 blocks and 256 experimental trials (128 for each condition).

3.2.3 Apparatus

Functional images were acquired at the Neuroimaging Laboratory (Santa Lucia Foundation) using a 3T Siemens Allegra MR system (Siemens Medical systems, Erlangen, Germany) equipped for echo-planar imaging with a standard head coil. Visual stimuli were presented by a control computer located outside the MR room, running in-house software (Galati et al., 2008) implemented in MATLAB (The MathWorks Inc., Natick, MA, USA). An LCD video projector with a customized lens was used to project visual stimuli to a screen placed at the back of the MR tube; participants watched visual stimuli through a mirror positioned inside the head coil. The timing of presentation of each stimulus was controlled and triggered by the acquisition of fMRI images.

We used blood-oxygenation level-dependent imaging (Kwong et al., 1992) to acquire echo-planar functional MR images (TR=2s, TE=30ms, flip angle=70◦, 64×64image matrix, 3 × 3 mm in-plane resolution, 30 slices, 2.5 mm slice thickness with no gap, ascending excitation order) in the AC–PC plane. Images were acquired starting from the superior convexity and extended ventrally; thus, images included the whole cerebral cortex, but the ventral portion of inferior temporal and occipital gyri. Also, a three-dimensional, high-resolution anatomical image was acquired for each participant (Siemens MPRAGE sequence, TR=2s, TE=4.38ms, flip angle=8◦, 512×512 image matrix, 0.5 × 0.5 mm in-plane resolution, 176 contiguous 1 mm thick sagittal slices). For each scan, we discarded the first four volumes to achieve steady-state, and the experiment started at the beginning of the fifth volume.

Each subject underwent a single acquisition session constituted by two functional scans, each lasting 5'28" (160 functional MR volumes), and one anatomical scan. In order to

minimize movements during the scans, subjects' head was stabilized with foam padding and with a chin rest mounted inside the head coil.

3.2.4 Preprocessing and surface reconstruction

A detailed description of the preprocessing and surface reconstruction steps is provided in our previous paper on the same dataset (Sulpizio et al., 2020). Briefly, we preprocessed and analysed images using SPM12 (Wellcome Department of Cognitive Neurology, London, UK) and FreeSurfer 5.1 (http://surfer.nmr.mgh.harvard.edu/).

We first analysed structural images following the "recon-all" fully automated processing pipeline implemented in FreeSurfer 5.1 (Dale et al., 1999; Fischl et al., 1999a,1999b; Desikan et al., 2006) in order to obtain a surface representation of each individual cortical hemisphere in a standard space. The surface reconstructions were transformed to the symmetrical FS-LR space (Van Essen et al., 2012) using tools in the Connectome Workbench software (https://www.humanconnectome.org/software/get-connectome-workbench), resulting in surface meshes with approximately 74K nodes per hemisphere.

Functional images were realigned within and across scans to correct for head movement and coregistered with structural MPRAGE scans using SPM12 (Wellcome Department of Cognitive Neurology, London, UK). Functional data were then resampled to the individual cortical surface using ribbon-constrained resampling as implemented in Connectome Workbench (Glasser et al., 2013), and finally smoothed along the surface with an iterative procedure emulating a Gaussian kernel with a 6 mm full width at half-maximum (FWHM).

Then, we analysed functional images for each participant separately on a vertex-by-vertex basis, according to the general linear model (GLM). Neural responses during "active" blocks (the two experimental conditions, "real" and "imagined") were modeled as box-car functions, convolved with a canonical hemodynamic response function and used as separate predictors in the GLM (one for each condition). Passive blocks (fixation) were not explicitly modelled as GLM regressors and were treated as part of the residual

variance. As nuisance regressors, we included the framewise displacement (FD), a subject-specific time-series index of the overall estimate of movement over time (Power et al., 2012). We computed FD as the sum of the absolute temporal derivatives of the six head-movement-related parameters (three for translations and three for rotations).

As a final step, we obtained group-level statistical parametric maps by implementing one-sample t tests, comparing signal in each condition relative to the baseline (i.e., real > fixation; imagined > fixation t-contrasts). Statistical maps were obtained with a cluster-forming threshold of $p < 0.001$; we also corrected for multiple comparisons at the cluster level ($p < 0.05$) through a topological false discovery rate procedure (Benjamini and Hochberg, 1995).

3.2.5 Regions of interest selection and time series extraction

Here, we sought to extend our knowledge on the grasping network, adding new light to previous human and monkey studies by providing an estimate of how brain areas interact during grasping movements and their imagination. Although in the GLM analysis reported in Sulpizio et al. (2020) (see also Figure 3.1) we observed an extended network of fronto-parietal brain regions involved in both grasping execution and imagery, we focused on a subset of areas basing on theoretical and methodological issues. Firstly, we included areas well known to play a crucial role during grasping (i.e., aIPS, PMv, PMd and M1) and/or during motor imagery (i.e., SMA) according to previous findings and similarly to previous DCM studies on this topic (Kasess et al., 2008; Gao et al., 2011; Begliomini et al., 2015, 2018), also following the model suggested by Castiello and Begliomini (2008). At difference, other brain areas (e.g., the cerebellum, prefrontal areas, V6A) are known to play a role during motor execution (e.g., broad visuomotor processes) or motor imagery but do not peculiarly encode grasping movement properties (Castiello and Begliomini, 2008; Gerbella et al., 2017). Moreover, given that at difference with previous DCM studies we included in the DCM analysis a large number of parameters by modelling reciprocal connections between ROIs (see 2.3.4), focusing on a larger set of ROIs would have further increased the computational load. Thus, we sought

to make the DCM analysis computationally more efficient by keeping the model as simple as possible (Stephan et al., 2010). One last issue worth mentioning was that the acquisition sequence prevented the inclusion of occipital and temporal areas, and of the cerebellum as well.

The five ROIs were defined on the cortical surface reconstruction of each individual hemisphere as the regions responding stronger to the real condition than the fixation one (real > fixation t-contrast). Each individual ROI was selected from the resulting statistical map using a threshold-free mapping, by selecting single activation peaks and their neighbourhood (for a maximum of 300 cortical nodes) through a watershed segmentation algorithm as applied to surface meshes (Mangan and Whitaker 1999). We also used anatomical landmarks as references for the selection of individual ROIs: thus, for instance, M1 was expected to be located near the "hand knob" in the precentral gyrus (Yousry et al., 1997), SMA in the dorsal medial wall, within the interhemispheric fissure, and aIPs at the junction between intraparietal sulcus and postcentral sulcus.

Although the choice of defining ROIs from the real > fixation map may seem biased toward motor execution at the expense of the imagined condition, our choice was motivated by theoretical and technical reasons. First, our group GLM analysis clearly identified a common network across conditions, where almost all the activated areas were recruited more strongly during the real than during the imagined condition (see also Sulpizio et al., 2020). Thus, with the scope of selecting the voxels more representative of the involvement of each region in a grasping task, we considered the real > fixation t-contrast as the most appropriate one, also given that the same criterion was previously adopted in DCM studies when comparing ME and MI (e.g., Kasess et al., 2008). While group-level results suggest that the statistical maps of the imagined condition are to a lesser extent representative of the recruitment of the areas of the grasping network, technical reasons led us to reject the possibility to use the conjunction map between execution and imagery. Indeed, a conjunction map is computed as the voxel-by-voxel minimum between the statistical maps of different conditions, in our case the two

conditions relative to the fixation. Given that the activations in the imagery task were overall locally lower than the activations in the "real" task, the conjunction map would have been nearly identical to the motor imagery contrast map, thus yielding to an inappropriate selection of the ROIs. A last worth mentioning technical consideration was that the watershed algorithm we applied to segment the individual activation maps uses the intrinsic spatial gradient of the contrast map, which is partially disrupted by taking at each point the minimum of two maps as happens when using conjunction maps. Not lastly, only during the real condition we found a reliable activation of M1, thus making other possible mapping criteria (i.e., imagined > fixation t-contrast; real > fixation & imagined > fixation conjunction analysis) unsuitable for the primary motor cortex. Consequently, only selecting ROIs from the real > fixation t-contrast would have allowed us to map all the ROIs from the same statistical map.

For each subject and region, we extracted "adjusted" time series from individual surface ROIs, i.e., after regressing out effects of no interest. To carry out the DCM analysis, a single representative timeseries was computed for each ROI retaining the first principal component (eigenvariate) of adjusted data.

3.2.6 Dynamic Causal Modeling

To evaluate the modulation exerted by real and imagined grasping on the effective connectivity between the selected ROIs, we used Dynamic Causal Modelling (DCM) (Friston et al., 2003), implemented in SPM12 (r7771). We hypothesized that both conditions exert a modulation on all the connections of our model, but that the two conditions would differ in terms of strength and sign of the parameters representing each modulated connection. For instance, we supposed that the parameter representing a specific connection in the "real" condition might have a higher value or a different sign respect to the parameter of the "imagined" condition for the same connection. Coherently with previous effective connectivity studies on MI and ME (Solodkin et al., 2004; Kasess et al., 2008; Gao et al., 2011, 2014), we also expected to find imagery-specific negative modulations that may account for actual movement inhibition.

Briefly, DCM uses an extended balloon model (Buxton et al., 1998; Friston et al., 2000) that explains neuronal dynamics through bilinear approximations. The following equation expresses the neuronal model that allows evaluating the changes in neuronal states over time:

$$\dot{z} = \left(A + \sum_{j=1}^{M} u_j B^j \right) z + Cu$$

where $z^{\cdot}$ is the derivative of the hidden neural state for each region, and u represents the experimental inputs (Dijkstra et al., 2017). The A matrix stands for the intrinsic coupling between nodes; the B matrix represents the modulatory effect exerted by specific inputs on the connectivity between nodes; the C matrix encodes the direct effect of a driving input on the hidden neural states.

3.2.7 Specification of the model: driving inputs and modulation of connectivity

DCM requires an a priori specification of a biologically and anatomically plausible model which explains how regions of interest interact; basing on this model, connectivity parameters are estimated. In the A matrix, our model included endogenous connections which have been reliably identified in anatomical studies in macaques (for a review, see Davare et al., 2011; for a detailed list of the considered monkey studies, see Supplementary Table 1). Note that, since anatomical studies have not proved the existence of reciprocal connections between aIPs and M1, PMd and SMA, these parameters were switched off (setting their prior expectation to zero and their variance close to 0). Furthermore, we did not centre the input; therefore, in our model the A matrix represents the unmodelled baseline connectivity, in absence of external stimulation (Zeidman et al., 2019a).

In our model, the B matrix consisted of all the possible modulatory effects of each condition on the exogenous connections modelled in the A matrix, except for the feedback exerted by M1 to the other areas. Indeed, differently from previous DCM studies (Begliomini et al., 2015, 2018), we decided to include in the B matrix not only

forward connections, but also the feedback ones in order to have a more complete view of how these areas interact during grasping.

In our task, the execution and the imagination of grasping are driven by a visual stimulus; however, since we were not interested in modeling the visual processing of the stimulus, we modelled both inputs (grasping execution and imagination) to exert a direct effect only on aIPs. Indeed, according to the model described by Castiello and Begliomini (2008) and to the DCM analysis performed by Begliomini et al. (2015, 2018), the visuomotor analysis of the to-be-grasped object is supposed to start from aIPs. Furthermore, TMS studies have supported this hypothesis showing that aIPs is involved in grasping ~50-100 ms before the premotor areas (Davare et al., 2006, 2007). The driven inputs of imagined and real conditions on aIPs stand for the C matrix.

3.2.8 Estimation of DCM and Parametrical Empirical Bayes (PEB)

To compare the changes in connectivity caused by the task, separately in the real and in the imagined condition, we used a DCM-PEB approach. Parametrical Empirical Bayes (PEB) (Friston et al., 2015, 2016) is a hierarchical Bayesian model that uses both non-linear (at first level) and linear (at second level) analyses. The main advantage of using PEB is to assess commonalities and differences among subjects in the effective connectivity domain at the group level and, thus, taking into account the variability in individual connections strength, i.e., the uncertainty over parameters represented by their covariance matrix. By doing so, this approach reduces the weight of subjects with noisy data (Zeidman et al., 2019b). In our study, we used the most recent PEB approach since we had specific hypotheses regarding the anatomical constraints of our model but not the direction and the strength of our parameters, especially in the imagined condition.

Time series extracted from individual ROIs were carried into DCM analysis for the first level, in which a fully connected model (with previously hypothesized constraints) was estimated for each subject. The inversion (estimation) of the model uses the Variatonal Laplace estimation scheme (Friston et al., 2007), which allows finding the predicted time series that matches the observed time series as much as possible, minimizing movement

of the parameters from their prior values. By doing so, the score of the quality of the model, i.e., the (negative) variational free energy, may be maximized finding the neural parameters which offer the best trade-off between model accuracy and complexity.

Before computing the analyses at the group level, we checked that for each subject the variance explained by the model was at least of 10%, as an index of the success of model inversion (Zeidman et al., 2019a); one subject did not respect this constraint and was excluded from further analyses. Then, we collapsed DCMs from the remaining 24 subjects in order to perform PEB second level (between subjects) analysis over the first-level DCM parameter estimates. We chose to carry out separate PEB analyses, one for the A matrix and another one for B and C matrices. Indeed, since our analysis involved a large number of parameters, we wanted to avoid dilution of evidence effect, reducing the search space (Zeidman et al., 2019b). Furthermore, since we were interested only in the group means, we did not model other between-subjects effects. As a consequence, we used a between-subject design matrix X = [1…1]T.

Having estimated the full model (with all connections of interest switched on) for each subject, the PEB approach requires to perform Bayesian model reduction (BMR) and Bayesian model Average (BMA).

Briefly, BMR is a particularly efficient form of Bayesian model selection (BMS) that, using a greedy search, automatically compares the full model with 256 models where one or more connections, which have the least evidence, are pruned out and thus switched off, whereas the parameters with the most evidence are kept stable (Friston et al., 2016; Friston and Penny, 2011; Pinotsis et al., 2016). Indeed, each reduced model has a probability density over the possible values of parameters (connection strengths) that maximizes the score for the quality of the model (Zeidman, 2019a).

Finally, we performed BMA analysis to average the parameters across models, weighted by the evidence of each model (Hoeting et al., 1999; Penny et al., 2006; Rosa et al., 2012).

Finally, we used a threshold based on free energy, taking into account the covariance of parameters, to evaluate whether a parameter contributed to the model evidence. We selected parameters keeping only those with strong evidence, i.e., posterior probability > 0.95; this value represents the probability of the parameters of being present vs absent.

In order to compare the strength in effective coupling between the two conditions, we computed Bayesian contrasts (Dijkstra et al., 2017) over the parameters of the B matrix that exceeded the threshold. After having computed the posterior mean (m), variance (v) and probability of the contrast, we evaluated the posterior distribution over it. This procedure allowed us to take into account the uncertainty of the estimated parameters.

3.3 Results

3.3.1 Whole-brain analysis and ROIs selection

A detailed description of the whole-brain GLM analysis is provided in our previous study on the same dataset (Sulpizio et al., 2020). Figure 3.1 shows an overlap of the group activation maps, as resulting from the two conditions, overlaid onto the flattened atlas Conte69. Since the present study focuses on the contralateral hemisphere to the moving hand, only results in the left hemisphere are shown.

In both the real > fixation and the imagined > fixation t-contrast a wide frontoparietal network emerged. Frontal activations encompassed premotor areas (e.g., PMd, PMv) and, in the dorsal medial wall, an activation of SMA emerged. The parietal activations included the posterior intraparietal sulcus (pIPs), with the adjoining superior (SPL) and inferior (IPL) parietal lobules, and the supramarginal gyri (sMg). In this territory, we found a strong focus of activation in aIPs.

Notably, at difference with the imagined condition, during pantomimed grasping the frontal activation encompassed the hand territory of the left primary motor and somatosensory areas (M1 and S1).

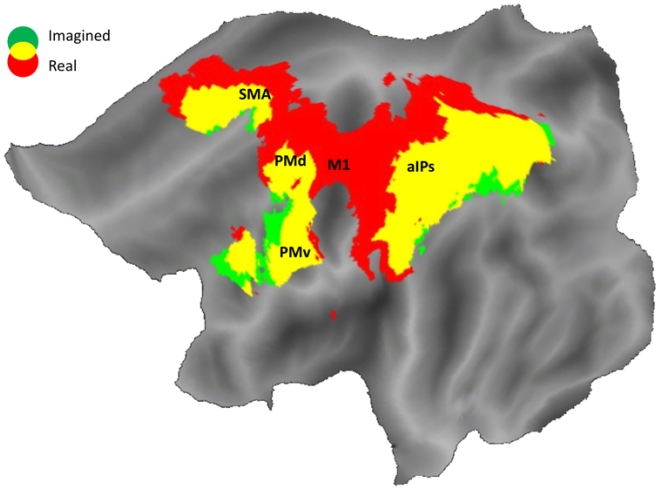

Figure 3.1. Whole-brain results. Superimposition of the group-activation map associated to the real > fixation t-contrast (in red) and to imagined > fixation t-contrast (in green); commonly activated brain areas are displayed in yellow. The maps are overlaid into the flattened Conte69 atlas (Van Essen et al., 2012) of the left hemisphere. Main activations are labelled as follows: M1, primary motor cortex; aIPs, anterior intraparietal area; PMd, dorsal premotor cortex; PMv, ventral premotor cortex; SMA, supplementary motor area.

To perform the following DCM analysis, we selected for each subject the regions of interest from the individual cortical surface, inspecting the real > fixation statistical map. The activation plots of the ROIs across the two conditions are provided in the Supplementary Figure 1.

To provide a visual representation of the anatomical location of the ROIs, we combined them across subjects to create probabilistic maps. Figure 3.2 shows the probabilistic ROIs overlaid onto the inflated Conte69 atlas surface (Van Essen et al. 2012). Table 1 also shows mean coordinates of individual ROIs, along with their standard deviations. The location of the probabilistic ROIs resembled the location of the activated foci across both conditions (except for M1).

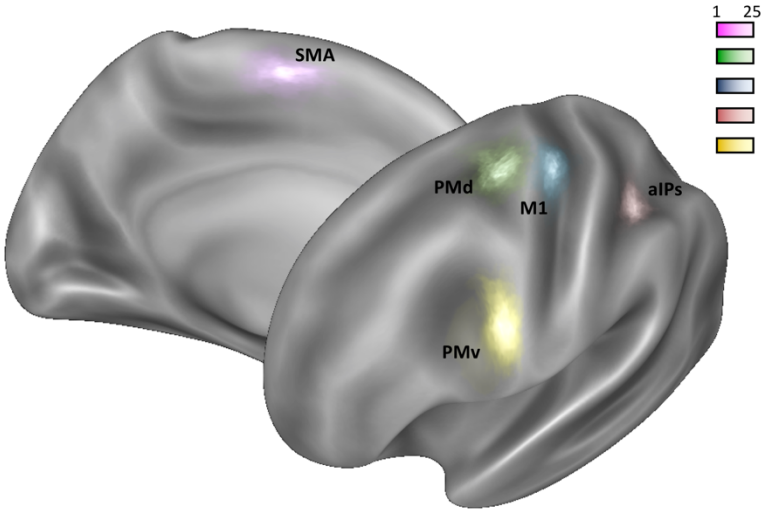

Figure 3.2. Anatomical location of regions of interest (ROIs). The ventral premotor area (PMv) is shown in pale yellow, the dorsal premotor area (PMd) in pale green, the primary motor cortex (M1) in blue, the anterior intraparietal area (aIPs) in pink, and the supplementary motor area (SMA) in purple. Probabilistic ROIs are overlapped onto an inflated Conte69 brain atlas (left hemisphere) in different views (dorsolateral and medial). The color scale represents the proportion of subjects whose ROI included that node: the lighter the color (i.e., close to white), the higher the probability that the node is common across the 25 individual ROIs.

Region	**MNI Coordinates**		
	x	***y***	***z***
aIPs	-37 ± *2,3*	-40 ± *2,9*	42 ± *3,2*
M1	-35 ± *3,3*	-22 ± *4,2*	57 ± *5,9*
SMA	-5 ± *1,2*	-5 ± *5,2*	58 ± *3,2*
PMd	-26 ± *3,8*	-11 ± *2,2*	54 ± *5,7*
PMv	-50 ± *4,1*	5 ± *2,4*	31 ± *5,5*

Table 3.1. Mean peak coordinates and standard deviations of individual ROIs.

3.3.2 DCM analysis

The A matrix represents the baseline connectivity, i.e., the intrinsic coupling between nodes. The leading diagonal of the A matrix (Figure 3.3) shows the values of self-connections, which are unitless log scaling parameters scaled up or down the default value of -0.5 Hz (Zeidman et al., 2019a). This means that a positive value stands for an increase in the inhibition of the region, representing its reduced responsivity to the inputs from the network. Our results showed that all the self-connections had negative values, except for M1 and aIPs, even if this parameter did not reach the threshold (connection strength = 0.109, posterior probability = 0.92).

For the other connections, the values resulting from the analysis represent the rate of change, in units of Hz, in the activity of one area ("destination"), caused by the change of the activity in the "source" area. Thus, positive values mean excitatory influences, whereas negative values stand for inhibitory influences. Our results showed that M1 and SMA had a reciprocal negative influence, whereas the connection from SMA to PMv was excitatory. Connections from PMd were excitatory on M1 and SMA, inhibitory on PMv. Finally, PMv had a positive influence on M1, a negative influence on aIPs and PMd.

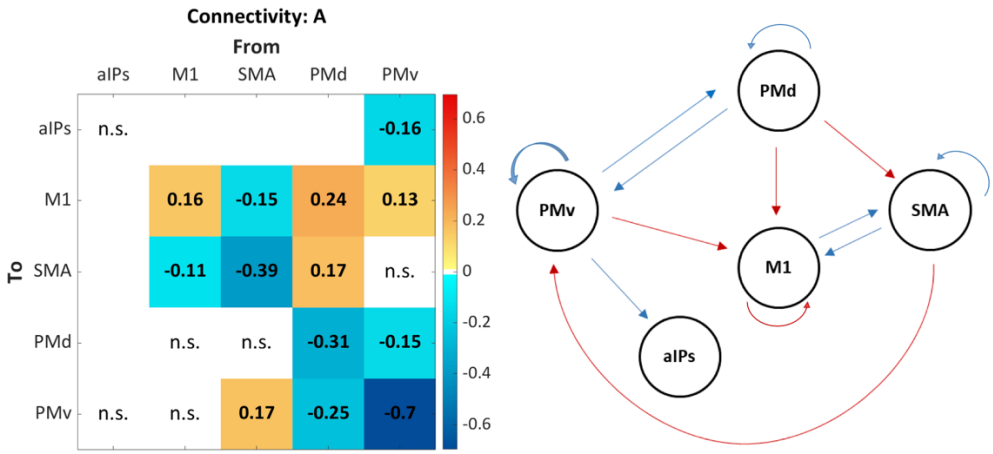

Figure 3.3. PEB results – A matrix. The left side of the figure shows the matrix of the effective connectivity of the unmodelled baseline; only suprathreshold parameters (posterior probability > 0.95) are shown, whereas subthreshold parameters are marked with "n.s." (i.e., non-

suprathreshold), and non modelled connections, i.e, whose priors are set to 0, are displayed in white. Connection strengths are represented in a scale from yellow to dark red, if excitatory, and from turquoise to dark blue, if inhibitory. Values of connection strengths are also provided. The right side of the figure also shows a schematic representation of the corresponding matrix, displaying only suprathreshold connections: line thickness reflects the strength of the respective connection; red lines denote excitatory connections, blue lines stand for inhibitory connections.

In the B ("modulatory") matrix, the values resulting from the analysis represent the rate of change, in Hz, in the coupling from an area ("source") to another one ("destination") caused by the experimental input. In the real condition, the major positive modulatory effect of executed grasping propagated from aIPs to PMv, followed by the strong inhibitory feedback exerted by PMv to aIPs. PMv exerted a positive influence on M1, PMd and, to a lesser extent, on SMA. In turn, only PMd had a negative influence on PMv. In the imagined condition, a positive influence from aIPs to PMv and from SMA to PMd emerged; moreover, there was an inhibition of PMv exerted by PMd (Figure 3.4).

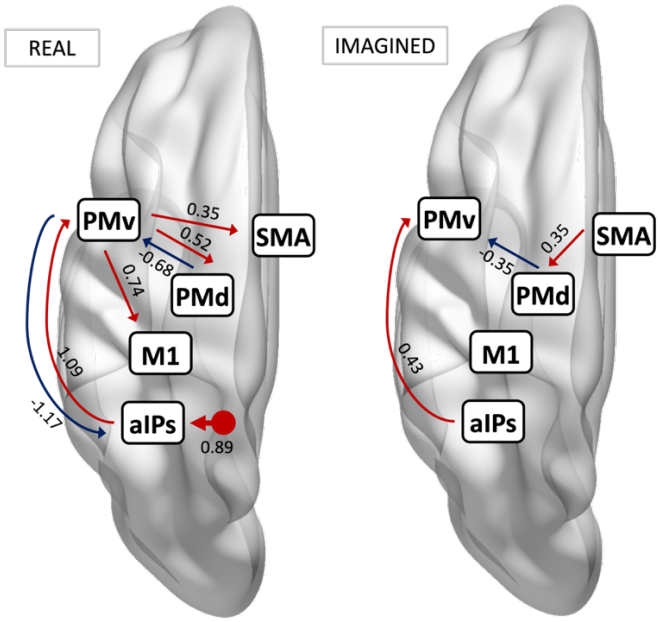

Figure 3.4. PEB results – B and C matrices. Schematic representation of the matrices, separately for the real (left) and the imagined (right) conditions. Only suprathreshold connections (posterior probability > 0.95) are displayed: red lines denote excitatory connections, blue lines stand for inhibitory connections. Connection strengths are also provided along with each connection.

Results of Bayesian contrasts (real > imagined) performed over connections that exceeded the threshold in both conditions are shown in Figure 3.5. There was a 100% posterior probability that in the real condition the coupling between aIPs and PMv was higher than in the imagined condition; similarly, inhibition exerted from PMd to PMv was higher in the real than in the imagined condition (posterior probability = 0.96).

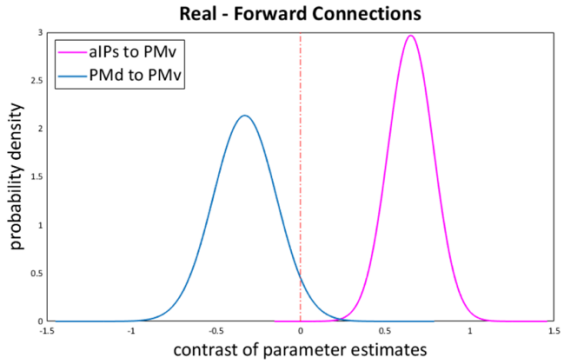

Figure 3.5. Bayesian contrast over parameter estimates (real > imagined). Plot of the probability density function of the contrast over parameter estimates that exceeded the threshold (posterior probability > 0.95) in both conditions: connection from aIPs to PMv (in purple) and connection from PMd to PMv (in blue). Both contrasts have a posterior probability higher than 0.95 (aIPs to PMv: 1; PMd to PMv: 0.96); thus, both connections are higher in the real than in the imagined condition. However, the direction of the contrast is different among the two connections: the posterior mean of the contrast of the forward connection from aIPs to PMv is positive, i.e., this connection is more excitatory in the real than in the imagined condition; instead, the posterior mean of the contrast of the feedback connection from PMd to PMv is negative, meaning that this connection is more inhibitory in the real than in the imagined condition.

3.4. Discussion

The main aim of our study was to evaluate whether effective connectivity adds some useful insight into the functioning of the visuo-motor grasping circuit, by comparing dynamic couplings during grasping execution and imagery. Our results confirm and extend the knowledge on the functional role of the areas serially involved in grasping.

3.4.1 Pantomimed grasping

As the classic view of the grasping circuit suggests (Jeannerod et al., 1995), our model confirms that during real grasping the first node involved in the analysis of the stimulus is aIPs (driven input), which has been shown to be activated even during object fixation (Taira et al., 1990; Sakata et al., 1995; Murata et al., 2000).

As emerged from the results of the modulatory matrices, during real grasping all the forward connections among traditional grasping-related areas (aIPs, PMv, PMd, M1) are excitatory (i.e., represented by positive values of posterior estimates); on the contrary, all the feedback couplings are inhibitory. The functional meaning of this evidence might be that the representation stored in the previously activated area is updated based on the new features of the object, processed by the following activated nodes of the circuit. This hypothesis suggests that the role of premotor areas does not run out when the information flows to the following activated areas. Otherwise, the inhibitory feedback couplings might be necessary to downscale the excitation of the previously activated areas. Anyway, both hypotheses support the serial involvement of the areas in the grasping circuit, as suggested not only by the classic models of this circuit but also by human TMS studies (Davare et al., 2006, 2007).

Accordingly, once the network is activated through aIPs, our results show that the visuo-spatial representation of the object is conveyed to PMv to select the motor program (e.g., hand posture) appropriate to the object and to encode the timing of the intrinsic hand muscle recruitment (Olivier et al., 2007). As the next step of the information flow, our results underline the role of PMd and SMA, both receiving an excitatory influence by PMv. Both areas may have a key role in integrating different aspects of the grasping movement, processing low-level features of the movement at high-level processing stages.

Regarding PMd, Fabbri et al. (2016) showed that PMd encodes the number of digits as well as object visual properties. Accordingly, an fMRI adaptation study (Monaco et al.,

2015) has shown that while aIPs adapts only to object size, PMd adapts to both object size and location; thus, this area integrates both extrinsic and intrinsic features of the object to plan how to make contact with the object, correctly positioning the fingers. Therefore, it is plausible that PMd updates information previously processed by PMv.

Differently from previous DCM studies, we chose to include SMA in our model, since it seems to be involved in grip force scaling, even if there is no evidence that SMA processes the force per se (White et al., 2013). It has been suggested that grip force relies on an internal representation of the object mechanical properties (Flanagan and Wing, 1997) and that, once the most appropriate internal model of the object dynamics has been selected, its implementation might rely on the activity of cerebellum and SMA (Bursztyn et al., 2006; White et al., 2013). Accordingly, our results suggest that the motor program selected by PMv is conveyed to SMA, as this area may be responsible for the integration of the force variation with other features of grasping movement (e.g., timing), at a high-level processing stage (Haller et al., 2009).

The last step of the grasping movement requires the execution of the motor program, which is supposed to be conveyed to the primary motor cortex, responsible for the motor output through the cortico-spinal tracts. Raos et al. (2004) suggested that the connection from F2 to M1 might be responsible for the control of forelimb actions. Thus, contrary to the traditional view which supposes that PMv activates directly M1, Castiello and Begliomini (2008) hypothesized that the connection from PMd to M1 might be the last step of the grasping circuit. However, when these authors tested this network hypothesis with a DCM study (Begliomini et al., 2015), they did not find a significant modulation of grasping on the connection from PMd to M1, while the other connections were significantly modulated by the task (from aIPs to PMv and from PMv to PMd). On the same line, our results showed that M1 receives an excitatory influence only from PMv, and not from PMd; thus, our model supports the classic theories of the visuo-motor grasping circuit (Jeannerod et al., 1995; Fagg and Arbib, 1998; Rizzolatti and Luppino, 2001; Arbib and Mundhenk, 2005).

To sum up, our results support the view of a hierarchical organization of the cortex postulated by Rizzolati et al. (1998), where action representation spans from the abstract encoding of the goals to the concrete representation of motor features (Turella et al., 2019). Indeed, a collection of studies performed with MVPA (Gallivan et al., 2011a, 2011b; Gallivan et al., 2013; Turella et al., 2019) has revealed that goal-related features of actions are encoded by aIPs and PMv, coherently with macaque findings (Fogassi et al., 2001; Castiello and Begliomini, 2008), whereas other areas, as PMd, are responsible for lower-level motor features. Similarly, our findings suggest that planning a grasping movement requires the encoding, in PMv, of a "general" motor program, which is then updated processing low-level motor features of the object (e.g., grip force, wrist orientation, configuration of fingers) that allow grasping it appropriately. These additional features, encoded by SMA and PMd, are not necessary to grasp the object, but allow carrying out a more careful and precise movement.

Since we did not find a direct connection of SMA and PMd to M1, similarly to the finding of Begliomini et al. (2015), it is still unclear how these areas update the motor execution encoding for high-level features. Moreover, our results show that, differently from PMd, SMA does not exert a negative feedback on PMv. It has been reported that all premotor areas project to the spinal cord, but in different ways (Dum and Strick, 2005). Indeed, PMv has limited access to motoneurons (Martino and Strick, 1987; He et al., 1993; Shimazu et al., 2004) compared with SMA and PMd. Furthermore, even if PMd projects to the spinal cord, this area does not seem to play a direct role in movement execution, being more involved in action selection (Halsband et al., 1993; Rushworth et al., 1998). Accordingly, our results suggest that PMd sends back an updated motor program to PMv, which in turn conveys it to M1, refining motor execution. Differently, since SMA directly projects to the hand motoneurons (Dum and Strick, 1996; Maier et al., 2002), it may influence the motor execution without conveying the updated motor program to the primary motor cortex through PMv.

3.4.2 Imagined vs Pantomimed grasping

The PEB results of the C matrix did not confirm that imagery exerts a direct effect on aIPs. This result is consistent with studies that have suggested that the activation of aIPs depends on the perceived goal of the action (Fogassi et al., 2001; Hamilton and Grafton, 2006; Króliczak et al., 2007; Tunik et al., 2007). Accordingly, it might be supposed that imagery activates aIPs less than ME in the univariate analysis and does not exert a direct effect on aIPs in the effective connectivity one, because imagined actions are perceived as less purposeful than executed pantomimed actions. Furthermore, as stated above, we chose to model the input to have a direct effect only on aIPs, even if both conditions arise from a visual cue; indeed, we were not interested in analysing the visual processing of the stimulus, and the acquisition sequence itself excluded the possibility of modelling occipital areas. However, it has been shown that during imagery there is a major contribution of visual cortices (Guillot et al., 2009; Jiang et al., 2015); therefore, it is unsurprising that during imagery aIPs is not the first involved node in our model.

In the present study, we also aimed at testing the hypothesis that real and imagined grasping would require a different involvement of premotor areas, exploring the difference in couplings between our regions of interest across the two conditions. As expected, our results suggest that during the imagined condition a different connectivity pattern emerges. aIPs exerts a positive influence on PMv, but to a lesser extent than during real grasping; PMv does not exert feedback inhibition on aIPs. A potential explanation of the latter finding may be that during MI the absence of the concrete implementation of the movement prevents the online update of the information stored in aIPs. Indeed, aIPs jointly represents abstract and concrete action properties (Turella et al., 2019) and is known to be involved in online monitoring (Davare et al. 2007; Tunik et al., 2007; Dafotakis et al., 2008), a process that likely takes place thanks to cortico-cortical and cortico-cerebellar loops. This collection of evidence confirms the flexible organization of aIPs that subserves the ability to react to unexpected environmental demands (Turella et al., 2019).

Alongside the aIPs-PMv circuit, the PEB results of the imagined condition show that the motor program appropriate to the object, encoded by PMv, is not conveyed to M1, which is not activated even in our group analysis (Sulpizio et al., 2020), nor to SMA and PMd. Thus, the motor program seems not to be updated by higher-level processing stages encoded by PMd and SMA, suggesting that during imagery a less complex motor program is planned. Despite that, both SMA and PMd seem to play a role during imagery, since SMA activates PMd, which in turn inhibits PMv. It has been proved that both areas are involved during imagery, and PMd receives inputs from visual areas (Marconi et al., 2001; Simon et al., 2002), even if we did not model these connections. Also, PMd is involved in the selection of the kind of action to be performed (Hoshi and Tanji, 2007). Accordingly, our results suggest that SMA and PMd may cooperate to prevent that the action would be performed, since a crucial input to PMd seems to derive from SMA at difference with executed grasping; this evidence possibly confirms the existence of imagery-specific processes that prevent the execution of the motor plan.

Differently from previous DCM studies on motor imagery during low-demanding tasks such as finger tapping (Kasess et al., 2008; Gao et al., 2014), our model did not show a suppressive influence of SMA on M1. The lower complexity of the movements to be performed, as well as the exclusion of PMd in the above-mentioned DCM studies, may account for the dissimilarity between previous and present DCM results. The study from Park et al. (2015) also points toward this interpretation, since it showed that the predictive role of SMA during imagery differed across tasks (namely, hand grasping and rotation). Moreover, since our results show that M1 is not activated by PMv and PMv is inhibited by PMd, one may speculate that during imagined grasping there is no need for SMA to inhibit the primary motor cortex.

The comparison between imagined and real grasping further supports the abstract-to-concrete action representation in the cortex previously discussed. Indeed, the abstract representation of motor plan during grasping was found to be shared across ME and MI in higher-level areas as aIPs (Monaco et al., 2020), and this might explain the cross-

condition involvement of the aIPs-PMv circuit in our PEB results. Moreover, PMd was found to represent actions in both ME and MI, irrespective of the complexity of the motor tasks; more intriguingly, this area lacks of generalization across ME and MI during grasping (Monaco et al., 2020), whereas it shows a more similar representation across modalities during low-demanding motor tasks (Zabicki et al., 2007). The above-described and the present findings yield to the suggestion that different, and presumably task-dependent, neural mechanisms take place in PMd. Accordingly, the crucial role of PMd in deciding the kind of action to be performed (Hoshi and Tanji, 2007) may account for differences between MI and ME, and this property be emphasized when dealing with complex motor movements and their inhibition.

Also the distinct roles of M1 during MI and ME deserve further considerations. The contribution of the primary motor cortex during imagery is controversial, since different techniques and approaches have resulted in contradictory findings. Indeed, some studies have suggested that M1 encodes high-level motor properties such as the goal of the action both in ME and MI (Alexander and Crutcher 1990; Ashe et al., 1993; Georgopoulos and Grillner, 1989; Kalaska and Crammond, 1992; Gallivan et al., 2011a; Pilgramm et al., 2016; Turella et al., 2019), whereas several fMRI activation studies have failed in revealing a consistent contribution of M1 during MI. However, methodological limits (such as the lack of spatial specificity of canonical, volumetric fMRI analyses) may account for eventual null findings; different fMRI techniques, such as MVPA, have indeed suggested that M1 decodes the content of MI (Pilgramm et al., 2016). Of utmost relevance is the usage of high-resolution fMRI (7T) to disentangle the contribution of different layers of the primary motor cortex during MI, compared to ME (Trampel et al., 2011; Persichetti et al., 2020). Monkey (Weiler et al., 2008; Mao et al., 2011) and human (Huber et al., 2017) studies have indeed revealed layer-specific connections of M1, where the superficial layers orchestrate the cortico-cortical connections, whereas the deeper ones are responsible for the generation of cortico-spinal outputs. Accordingly, the usage of the vascular space occupancy (VASO) method that increases the spatial specificity removing the vasculature bias (Turner, 2016; Huber et al., 2018), combined with high-resolution

fMRI (7T), revealed that the superficial layers are recruited during both MI and ME; conversely, the motor outputs are generated in the deeper layers of M1 only during ME (Persichetti et al., 2020). Thus, M1 presumably holds, albeit for short periods, high-level motor properties processed by premotor regions. Despite our attempt to increase spatial accuracy by using a surface-based ROIs selection, our analysis may have not reached such degree of specificity.

3.4.3 Limitations

One limitation of the present study is that we used pantomimed instead of actual grasping. This choice is quite common among fMRI studies due to the difficulty of performing real grasping in the MR environment (Shikata et al., 2003; Simon et al., 2002; Johnson-Frey et al., 2005; Bozzacchi et al., 2012; Makuuchi et al., 2012), especially if the objects to grasp are commonly used objects and not boxes or manipulanda. Moreover, in order to test our hypothesis on motor dynamics during grasping, pantomime allowed us to avoid that hand-object interactions (i.e., touching the object) would result in the activation of sensorial areas, which might superimpose the activation of the motor ones. However, it might be useful to test whether our model is reliable also during actual grasping, despite the tactile stimulation caused by the interaction with the object.

We are aware that grasping execution involves a broader range of areas, for instance prefrontal areas (e.g., dorsolateral and ventrolateral prefrontal cortex) or pre-SMA (F6 in macaques), which interact with motor areas and may play a crucial role in motor dynamics (Gerbella et al., 2017). Similarly, imagery involves also visual (Jiang et al., 2015) and frontal areas such as the dorsolateral prefrontal cortex (Hardwick et al., 2018). Beyond the exclusion of some areas (e.g., cerebellum, occipital and temporal areas) due to the acquisition sequence, we chose not to include other areas in our model to focus on brain regions known to peculiarly encode grasping movement properties; furthermore, this allowed us to keep the DCM model as simple as possible, reducing the number of possible parameters of interest.

3.5 Conclusions

The present study provides the first attempt to study execution and imagery of a grasping movement with a DCM-PEB approach, focusing on premotor dynamics.

On balance, we succeeded in enlightening the role of areas recently found to be involved in grasping; moreover, our model provides new evidence of the functioning of the whole grasping circuit, clarifying the ambiguous last steps of the circuit that involves PMd, PMv, and M1. This is the first attempt to analyse connectivity in the grasping network by using the DCM-PEB approach and a surface-based analysis. Furthermore, differently from previous DCM studies, the evaluation of feedback connections allowed us to make inferences also on the serial activation of these areas, an information otherwise impossible to detect by using canonical fMRI analysis. Finally, the comparison between real and imagined grasping reveals that premotor areas dynamically interplay in different ways, depending on task demands.

Overall, our study suggests that disengaging from an activation perspective, where a similar recruitment of motor-related areas has been found in ME and MI, effective connectivity may provide an explanation on substantial similarities and differences between imagined and executed grasping. Indeed, the task-dependent interactions revealed by DCM can be only partially explained by the slighter recruitment of the areas within the grasping network we detected in the whole-brain activation maps (Sulpizio et al., 2020). If so, we would have found that the same connections were modulated by both conditions, but to a lesser extent during imagery. Our results suggested that this is true only for a few connections. Such findings could be useful when using MI in rehabilitation protocols of post-stroke patients (Page et al., 2007) and applied to brain computer interface (BCI) (Green and Kalaska, 2011), as well as when evaluating the effectiveness of such procedure (Doyon et al., 2003; Nyberg et al., 2006; Bajaj et al., 2015).

Further studies might extend the circuit of interest as previous functional connectivity studies (Hutchison and Gallivan, 2018) to understand whether other brain areas,

excluded from our model, may account for differences in connectivity during imagined and executed grasping. It would be also useful focusing on the visual processing of the stimulus, especially for the imagined condition, or evaluating how intra-hemispheric couplings are modulated by the interhemispheric connections.

CHAPTER 4

This chapter has been published in March 2023 as:

Bencivenga, F., Tullo, M. G., Sulpizio, V., & Galati, G. (2023). Interhemispheric interplay between the left and right premotor cortex during grasping as assessed by dynamic causal modelling. Scientific Reports, 13(1), 4958.

https://doi.org/10.1038/s41598-023-31602-y

Interhemispheric interplay between the left and right premotor cortex during grasping as assessed by Dynamic Causal Modelling

Federica Bencivenga,[1,2,3] Maria Giulia Tullo,[4] Valentina Sulpizio,[2,3] and Gaspare Galati[2,3]

[1] PhD Program in Behavioral Neuroscience, Department of Psychology, "Sapienza" University of Rome, Rome, Italy

[2] Brain Imaging Laboratory, Department of Psychology, "Sapienza" University of Rome, Rome, Italy

[3] Cognitive and Motor Rehabilitation and Neuroimaging Unit, Santa Lucia Foundation (IRCCS Fondazione Santa Lucia), Rome, Italy

[4] Department of Translational and Precision Medicine, "Sapienza" University of Rome, Rome, Italy

Abstract

Research on the contribution of the ipsilateral hemisphere to unilateral movements, and how it is mediated by transcallosal connections, has so far provided contradictory findings. By using Dynamic Causal Modelling (DCM) and Parametric Empirical Bayes (PEB) analyses applied to fMRI data, we sought to describe effective connectivity during

pantomimed and imagined right-hand grasping within the grasping network, namely the anterior intraparietal sulcus (aIPs), ventral (PMv) and dorsal (PMd) premotor cortex, supplementary motor area (SMA) and primary motor cortex (M1). The two-fold aim of the present work was to explore a) whether right and left parieto-frontal areas show similar connectivity couplings, and b) the interhemispheric dynamics between these regions across the two hemispheres.

We detected a network architecture comparable across hemispheres during executed but not imagined grasping movements. Furthermore, during pantomimed grasping the interhemispheric crosstalk was mainly driven by premotor areas: we found an inhibitory influence from the right PMd toward the left premotor and motor areas and excitatory couplings between homologous ventral premotor and supplementary motor regions.

Overall, our results support the view that dissociable components of unilateral grasping execution are encoded by a non-lateralized set of brain areas complexly intertwined by interhemispheric dynamics, whereas motor imagery obeys different principles.

4.1 Introduction

Despite the major recruitment of the contralateral hemisphere, the ipsilateral motor and premotor cortex participate in refining the execution of unilateral movements. Interhemispheric dynamics driving such contributions are mediated by transcallosal fibers in the corpus callosum (Zarei et al., 2006) and are supposed to act bidirectionally. The underlying neurophysiological mechanisms are known as interhemispheric inhibition (IHI) and facilitation (IHF) and in humans they can be directly tested using transcranial magnetic stimulation (TMS). Pioneer studies on these mechanisms have described IHI as the inhibition of the motor cortex ipsilateral to the moving hand exerted by the contralateral motor (Ferbert et al., 1992) and premotor (Mochizuki et al., 2004) cortex. During unilateral movements, such a mechanism is functional to prevent mirror motor command of the contralateral body part which must be kept still (Mayston et al., 1999). These findings have challenged the contralateral control tenet, namely the

assumption that each hemisphere controls the contralateral portion of the body exclusively based on inputs from motor and sensory crossing fibres.

While this evidence is roughly straightforward for simple movements, more complex movements have been proved to rely on a more bilateral involvement of both motor and premotor areas, which may likely require a different interhemispheric balance with respect to the above-described one. Multiple evidence points toward this view in the case of grasping movement, whose planning and execution depend on the bilateral activity of the anterior intraparietal sulcus (aIPs), ventral (PMv) and dorsal (PMd) premotor cortex, and supplementary motor area (SMA). TMS studies have shown that a bilateral virtual lesion of aIPs is necessary to impair hand shaping during grasping (Davare et al., 2007). Similarly, lesions to both the left and right PMv lead to an impairment in motor planning during right-hand grasping, since this area bilaterally encodes hand posture, whereas only the left PMv is responsible for the hand muscle recruitment hence being more directly involved in movement execution (Davare, 2006). A body of literature using multivoxel pattern analysis (MVPA) applied to functional magnetic resonance imaging (fMRI) data has suggested that bilateral parietal and premotor regions encode limb-independent, high-level neural representations of the movement plan (Gallivan et al., 2013) entailing the processing of temporal and spatial information both during motor execution and imagery (Monaco et al., 2020; Papitto et al., 2020). An intriguing debate has been raised on the role of the ipsilateral motor cortex (iM1), whose activity is only marginally reported by fMRI activation studies. Davare and colleagues (Davare et al., 2007) reported that interfering with the activity of iM1 during grasping alters the timing of muscle recruitment. fMRI studies have proved that activity in the ipsilateral motor cortex increases with movement complexity (Verstynen et al., 2005); similarly, Verstynen and Ivry (Verstynen & Ivry, 2011) have shown that fluctuations in the activity of iM1 correlate with the activity in the contralateral motor cortex (cM1) and that this correlation is higher for complex movements. A possible explanation is that iM1 provides additional resources to correctly perform complex movements, coordinating the sequencing of muscle recruitment (Davare et al., 2007)·(Yarosh et al., 2004).

Studying interhemispheric inhibitory and facilitatory mechanisms through fMRI is challenging since the blood oxygenation level dependent (BOLD) signal is much more influenced by excitatory rather than inhibitory spikes. A study conducted by Bestmann and colleagues (Bestmann et al., 2008) sought to draw a broader picture of these phenomena by combining TMS and fMRI during a left-hand grip task. These authors found an inhibitory pattern at rest linking the left PMd with the right M1 and PMd, which turned to be facilitatory during the task. Together, this body of evidence strengthens the controversies surrounding different facets of interhemispheric motor dynamics, such as their directions and involved nodes, suggesting that they may not be univocal but rather task-dependent.

A more recent line of research is getting advantage of connectivity approaches to investigate the task-dependent interplay between brain areas. In this scenario, the analysis of effective connectivity performed through Dynamic Causal Modeling (DCM, (K. J. Friston et al., 2003)) may overcome fMRI limits by describing inhibitory and excitatory modulations between brain areas driven by experimental inputs. This approach has already been exploited to investigate interhemispheric couplings during hand movements. During a fist-closing movement, Grefkes and colleagues (Grefkes et al., 2008) have shown that motor areas contralateral to the moving hand exert a suppressive influence on the ipsilateral motor areas. Gao and colleagues (Gao et al., 2014) provided evidence of a modulation of the connectivity from the contralateral toward the ipsilateral SMA during execution and to less extent during imagery of a right-hand finger tapping movement. A study by Begliomini and colleagues (Begliomini et al., 2015) focused on the interhemispheric couplings between homologous areas during grasping and reported modulation of the connectivity from the left aIPs to the right aIPs, and between the left and right PMd.

Additional insights on the contribution of the ipsilateral hemisphere to unilateral movements can be provided by comparing motor execution to motor imagery. These two processes recruit partially overlapping brain circuits dealing with action planning (Hashimoto & Rothwell, 1999; Lorey et al., 2011; Munzert et al., 2009; Sulpizio et al., 2020).

Although univariate fMRI analyses may have failed in detecting right-hemisphere activations for right-hand imagined movements, MVPA studies revealed cross-modal decoding in bilateral parietal areas (Monaco et al., 2020; Zabicki et al., 2016), supporting the view that such areas encode both abstract and concrete action properties (Turella et al., 2020). This paves the way to the investigation of right-hemisphere dynamics during both executed and imagined actions, a matter being neglected by previous DCM studies (Gao et al., 2014; Kasess et al., 2008) that focused only on the contralateral hemisphere to the executed/imagined unilateral movements.

To tackle this issue, we used DCM and parametrical empirical Bayes (PEB; (K. Friston et al., 2015)). We adopted a similar procedure to that of our previous study (Bencivenga et al., 2021) in which we analysed left intrahemispheric couplings during a right-hand pantomimed grasping, and showed a serial involvement of aIPs, PMv, PMd, and M1, plus an additional role of SMA. Our previous findings (Bencivenga et al., 2021) supported the well-known contribution to grasping movement of each of these areas, being aIPs encoding the 3D representation of the object to be grasped, the PMv storing a "vocabulary" of grasp postures and goals, the PMd controlling finger configuration, and SMA controlling grip force scaling and sequence planning (Castiello & Begliomini, 2008; Gerbella et al., 2017; White et al., 2013), by providing additional evidence on the way these areas interplay during grasping movements. We also found that a similar, but less complex, motor program is planned during the imagination of the same movement. In the present study, using the same dataset we aimed at assessing the role of the homologous areas in the right hemisphere, as well as their interhemispheric dynamics. If the same processes are shared across hemispheres, the network should not only be bilaterally activated but also susceptible to interhemispheric crosstalk and similar intrahemispheric modulations despite movement lateralization. Conversely, if hemispheric-specific mechanisms occur, the bilateral activation of the network would be explained by different connectivity patterns. Furthermore, since movement execution and imagery tap into similar neural mechanisms, these statements should hold in both conditions, at least for higher-level processing areas such as the parietal regions.

To answer this challenging question, we conducted two separate DCMs: one exclusive for the right hemisphere, and the other leveraging intra-hemispheric results to estimate inter-hemispheric connections in a computational efficient fashion (Razi et al., 2017). We hypothesized that we could observe in the right hemisphere a network architecture similar to the one we found in the left hemisphere (Bencivenga et al., 2021), confirming the existence of a bilateral network whose functions are shared across hemispheres; we also hypothesized that this bilateral circuit would be modulated by interhemispheric homologous and non-homologous bilateral couplings.

Our study stands out from the above-mentioned ones as we focused on a complex movement pantomimed execution and imagination, exploring the connectivity architecture within a wide bilateral network including parietal, premotor, and motor areas, finally investigating interhemispheric links between homologous and non-homologous brain regions. Furthermore, we exploited the hierarchical modeling implemented through PEB to run separate estimations of left and right couplings, whose empirical priors were subsequently used to estimate an interhemispheric model in a more robust and less computationally expensive way.

We provide evidence that unilateral pantomimed grasping, but not its imagination, elicits similar mechanisms in both hemispheres whose crosstalk is mediated by both excitatory and inhibitory influences.

4.2 Methods

4.2.1 Participants and tasks

In the present study, we reanalyzed BOLD data from a sample of twenty-five right-handed healthy subjects (22 females, mean age 26.5, s.d. 3.4) who participated in a previous study from our lab (Sulpizio et al., 2020) after giving their written informed consent. The study was approved by the local research ethics committee of the IRCCS Fondazione Santa Lucia in Rome, in accordance with the Declaration of Helsinki.

The fMRI exam consisted of the execution of a right-hand pantomimed grasping movement ("pantomimed grasping" condition) or its imagination ("imagined grasping" condition). The experiment was structured as a block design in which pantomimed and imagined grasping blocks were alternated with fixation blocks. Each block lasted 16 seconds and was introduced by a written instruction (1 sec), followed by 8 trials. In each trial an object was shown in central vision for 300 ms, randomly chosen from a set of 36 black-and-white photographs of commonly used objects that elicited "whole hand" or "finger" grasping movements, followed by an interval of 1575 ms during which the subject had to perform or imagine the movement. Participants were instructed to imagine the object located in the proximity of their right hand, therefore excluding the transport component of the grasping movement. For further details on the protocol, see (Sulpizio et al., 2020).

4.2.2 Image acquisition and analysis

MR images were acquired at the Neuroimaging Laboratory at Santa Lucia Foundation through a 3T Siemens Allegra system. One structural image per subject was acquired through a Siemens MPRAGE sequence (TR=2 s, TE=4.38 ms, flip angle=8°, 512 × 512 image matrix, 0.5 × 0.5 mm in-plane resolution, 176 contiguous 1 mm thick sagittal slices) and processed using FreeSurfer 5.1 (http://surfer.nmr.mgh.harvard.edu/) to obtain a surface representation of the individual cortex in a standard space, which was then transformed in the FS-LR space (Van Essen et al., 2012) with 74k nodes per hemisphere through the Connectome Workbench software (https://www.humanconnectome.org/software/get-connectome- workbench).

Two functional image time series per subject, each including 8 pantomimed grasping, 8 imagined grasping, and 4 fixation blocks, were acquired using a gradient-echo EPI sequence (TR=2 s, TE=30 ms, flip angle=70°, 64 × 64 image matrix, 3 × 3 mm in-plane resolution, 30 slices, 2.5 mm slice thickness with no gap, ascending excitation order), corrected for head movements and coregistered to the structural images using SPM12 (Wellcome Department of Cognitive Neurology, London, UK), resampled to the individual surfaces using ribbon-constrained resampling as implemented in Connectome

Workbench (Glasser et al., 2013), and smoothed along the surface with an iterative procedure emulating a Gaussian kernel with a 6 mm full width at half-maximum (FWHM).

Functional images were analyzed for each participant separately on a vertex-by-vertex basis, according to the general linear model (GLM), with execution and imagination blocks modeled as box-car functions convolved with a canonical hemodynamic response function, and framewise displacement (FD), a subject-specific time-series index of the overall estimate of movement over time (Power et al., 2012), used as a nuisance regressor. Group-level statistical parametric maps of the activation in each condition relative to the baseline (i.e., pantomimed grasping > fixation; imagined grasping > fixation t- contrasts) were obtained with a cluster-forming threshold of $p < 0.001$ and corrected for multiple comparisons at the cluster level ($p < 0.05$) through a topological false discovery rate procedure (Chumbley et al., 2010).

4.2.3 Region definition

We selected five regions of interest (ROIs) per hemisphere, namely the anterior intraparietal sulcus (aIPs), the ventral (PMv) and the dorsal (PMd) premotor cortex, the supplementary motor area (SMA), and the primary motor cortex (M1). ROIs were defined on the cortical surface reconstruction of each individual hemisphere as the regions responding stronger to the pantomimed grasping condition than the fixation (pantomimed grasping > fixation t-contrast). We applied a watershed segmentation algorithm (Mangan & Whitaker, 1999) on the statistical parametrical maps ($p < 0.5$) and selected single activation peaks and their neighborhood for a maximum of 300 cortical nodes. Finally, for each defined region and subject, we retained the first principal component (*eigenvariate*) of the adjusted timeseries to be entered in the DCM analysis. A regional analysis on the right-hemisphere ROIs was also performed to address the recruitment of each of these regions during motor imagery and pantomime.

4.2.4 Dynamic Causal Modeling

We assessed right-hemisphere and interhemispheric dynamics during the execution and imagination of a pantomimed grasping through Dynamic Causal Modeling (DCM) (K. J. Friston et al., 2003), implemented in SPM12. DCM estimates effective connectivity in terms of changes in neuronal states over time, by computing the intrinsic coupling among nodes (A matrix), the activation of the circuit exerted by a driven input (C matrix), and the modulatory effect of input on the connectivity between nodes (B matrix).

The interhemispheric model we aimed to test is composed of ten regions (5 per hemisphere), therefore requiring the estimation of a large number of parameters. In the DCM estimation, any model with more than 8 brain regions is estimated by setting some constraints on the model priors to avoid the potentially redundant parameterization of large DCMs. The built-in solution for that is to estimate the task-based functional connectivity, and then use its results to inform the priors of the effective connectivity analysis. Another valid procedure is suggested by Razi and colleagues (2017). Whenever a network can be meaningfully split into subnetworks, the authors propose to estimate effective connectivity in each subnetwork, and then use such results to estimate the whole network connectivity (Razi et al., 2017).

Following this approach, we proceeded by conducting separate DCM-PEB analyses for each hemisphere and then used their results to inform the priors of a third, interhemispheric DCM. Note that the results for the left hemisphere have been discussed in a previous study (Bencivenga et al., 2021).

We built the connectivity model based on macaque tracer studies which offer the possibility to disambiguate the directionality of the fibers linking brain areas. The network architecture we tested here was the same we adopted for the left hemisphere in our previous work: in the A matrix ("baseline connectivity"), we included all the possible feedback and forward coupling among ROIs, except for the reciprocal connections between aIPs and the premotor and motor cortex (i.e., SMA, PMd, and M1) for which no anatomical evidence was provided by macaque tracer studies (Boussaoud et al., 2005;

Dancause et al., 2007; Dum, 2005; Geyer et al., 2000; Jenny, 1979; Lanz et al., 2017; Leichnetz, 1986; Luppino et al., 1993, 1999; Marconi et al., 2003; Matelli et al., 1986; McGuire et al., 1991; Rouiller et al., 1994; Ruddy et al., 2017; Stepniewska et al., 1993) (see Supplementary Table 1 for the full list).

When testing the modulatory effect of the imagined and the pantomimed grasping on the effective connectivity between brain areas (B matrices), we investigated all the possible connections (forward and feedback) within the grasping network, but the ones from M1 to premotor areas. We modeled both pantomimed and imagined grasping conditions to exert a direct input only on aIPs (C matrix), as the entry hub of the grasping network devoted to the first processing stage for grasping movement, namely 3D encoding of visual stimuli. Figure 4.1 shows a graphical representation of the model architecture we tested.

Testing the same network architecture across hemispheres and conditions fulfilled the central scope of the present work, i.e., to address effective connectivity modulations in the grasping network based on the task (imagery or execution) and the hemispheric laterality (ipsilateral or contralateral to the moving hand). Note that, as we will discuss in the Results section, the "imagined grasping" condition yielded scarce whole-brain activations in the right hemisphere, but regional activations in the grasping network areas were significantly detected. We feel that this is an additional incentive to test whether a connectivity analysis could provide more insights than a massive univariate analysis in detecting the right-hemisphere contribution during right-hand grasping imagery.

Bayesian contrasts (Dijkstra et al., 2017) over the parameters that exceeded the threshold a) in both right and left DCMs for each condition, or b) within the right DCM in both conditions were implemented to evaluate differences between hemispheres and conditions.

Having estimated the two single-hemisphere DCMs, we built an interhemispheric model by using the group posterior estimates of the single-hemisphere DCMs to inform the

priors for a new estimation (Razi et al., 2017), building the model to keep only the parameters that exceeded the threshold in the single-hemisphere DCMs. In addition, we modeled interhemispheric bilateral couplings in line with anatomical evidence from macaque tracer studies, that supported the existence of bilateral interhemispheric connections between all the selected ROIs, except for the connections between aIPs and all the contralateral non-homologous regions (see Supplementary Table 1). Baseline (A matrix) connectivity was tested in all these connections. In the B matrices, we tested the modulation exerted by the two conditions on the bilateral connections between parietal and premotor areas, and the unilateral connections from premotor to motor areas, hence excluding connections from the right or left M1 toward the contralateral SMA, PMv, and PMd.

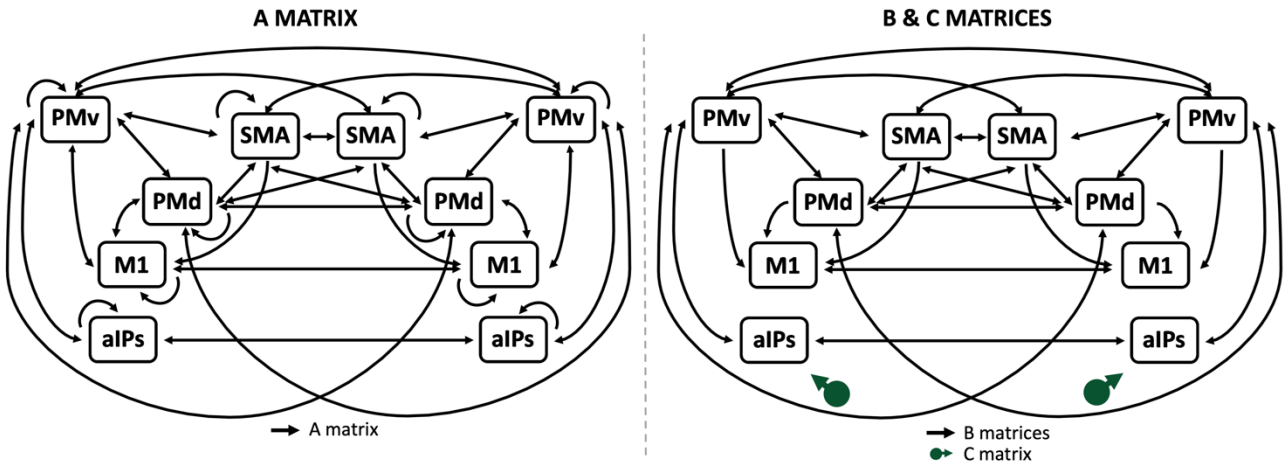

Figure 4.1. Model for the effective connectivity analysis. Black arrows represent connectivity between brain regions as modelled in the A (baseline; left panel) and B (modulatory; right panel) matrices. Modelled driven input (C matrix) are shown as green arrows in the right panel.

4.2.5 Estimation of DCM and parametrical empirical Bayes (PEB)

We specified and inverted the full DCMs for each individual using the Variational Laplace estimation scheme (K. Friston et al., 2007). We next checked that all subjects had a good model estimation by controlling for the variance explained by the model. Subjects

with a lower value than 10% were excluded from the group analysis, in agreement with standard practice for DCM (Tak et al., 2021).

A parametric empirical Bayes (PEB; (K. Friston et al., 2015; K. J. Friston et al., 2016)) approach was then used to determine group results through separate analyses for the A matrix, and the B and C ones. This analysis acts as a hierarchical model in which empirical priors at the group level could shrink the estimates at the individual level toward those that reach the maximum of the model evidence. Bayesian Model Reduction (BMR; (K. J. Friston et al., 2016; K. Friston & Penny, 2011; Pinotsis et al., 2016)) and Average (BMA; (Hoeting et al., 1999; Rosa et al., 2012)) were used to prune the connections with the least evidence and average the parameters. Finally, we evaluated whether a parameter contributed to the model evidence by retaining only those with strong evidence of being present vs absent, namely those with posterior probability > 0.95 accordingly to a threshold based on free energy.

4.3 Results

Results are organized into four sections. We will first describe right-hemisphere whole-brain and regional activations evoked by pantomimed and imagined grasping movements. Then, we will focus on how the parietofrontal network entailing grasping actions is selectively modulated by grasping execution and imagery. In line with the separate analyses we performed, we will describe right-hemisphere couplings, compare them with the left-hemisphere ones, and then highlight the interhemispheric dynamics.

4.3.1 Whole-brain and regional activations

During the pantomime of a grasping movement, activations were bilaterally detected in parietofrontal areas, including the intraparietal sulcus, premotor and motor areas, and prefrontal ones. Differently, motor imagery drove activation in the same parietofrontal network predominantly in the left hemisphere, as in the right one a subtle involvement of supplementary motor cortex, premotor cortex, and postero-occipital regions was detected (Figure 4.2).

Five regions of interest (ROIs) were defined in each individual hemisphere based on the activation during the pantomimed grasping condition: anterior intraparietal sulcus area (aIPs), the ventral (PMv) and dorsal (PMd) premotor cortex, the supplementary motor area (SMA) and the primary motor cortex (M1).

A regional analysis was conducted to detect the recruitment of each ROI during the pantomimed and the imagined grasping condition, extending the results of the mass univariate group analysis. Results showed that all right-hemisphere ROIs were also significantly activated ($p < 0.05$ FDR corrected for the number of regions) during grasping imagery (Figure 4.3; see Supplementary Figure 1 in (Bencivenga et al., 2021) for similar results in the left hemisphere) with the following statistical values: aIPs rh ($t_{24} = 3.66$, $p = 0.001$), M1 rh ($t_{24} = 3.18$, $p = 0.001$), SMA rh ($t_{24} = 3.57$, $p = 0.002$), PMv rh ($t_{24} = 2.28$, $p = 0.017$) and PMd rh ($t_{24} = 1.77$, $p = 0.042$).

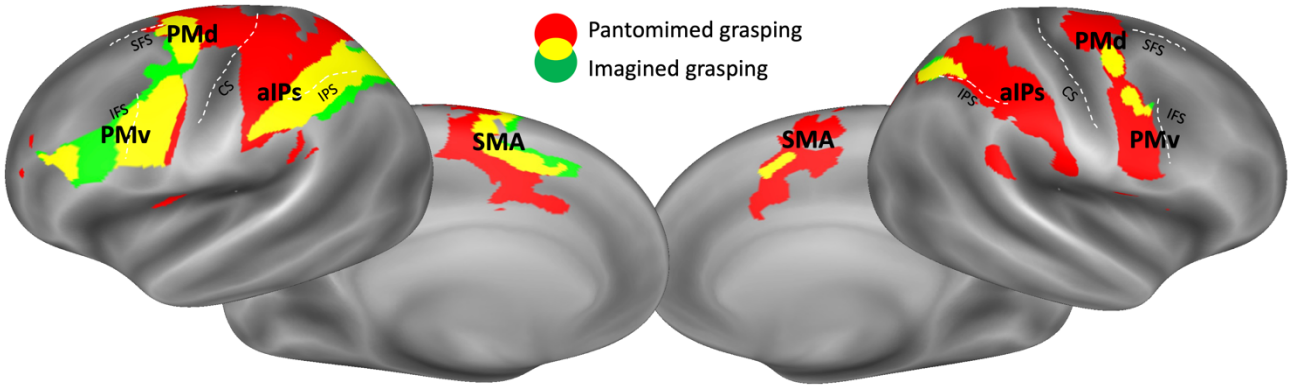

Figure 4.2. Group whole-brain results. Superimposition of the group activation maps resulting from the pantomimed grasping > fixation (in red) and the imagined grasping > fixation t-contrasts (in green) and average location of right hemisphere regions of interest (ROIs). Overlapping activated right brain regions across the two conditions are displayed in yellow. Maps are overlaid into an inflated Conte69 atlas (Van Essen et al., 2012) of the right hemisphere. Average location of aIPs (anterior intraparietal sulcus area), PMv (ventral premotor area), PMd (dorsal premotor area), SMA (supplementary motor area), and M1 (primary motor cortex) is represented through black edges and labelled arrows. Anatomical landmarks are also reported (SFS: superior frontal sulcus; IFS: inferior frontal sulcus; CS: central sulcus; IPS: intraparietal sulcus).

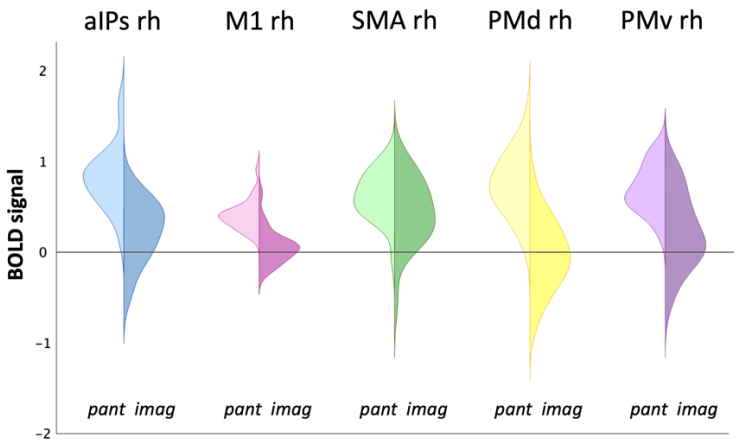

Figure 4.3. Plots of the activations of the right regions of interest (ROIs) in the pantomimed grasping and imagined grasping conditions. Violin plots showing the distribution of the activation of the selected ROIs across subjects are displayed for each right-hemisphere region, i.e., aIPs (blue), M1 (pink), SMA (green), PMd (yellow), and PMv (purple). The left side of the violins represents the pantomimed grasping condition ("pant"), and the right side the imagined grasping condition ("imag").

4.3.2 Right-hemisphere DCM-PEB results

22 subjects out of 25 reached an explained model variance higher than 10% and were included in the PEB analysis. Results of the A matrix representing the baseline connectivity pattern are shown in Supplementary Figure 1.

The core of our work was to describe how pantomimed or imagined movements perturb parietofrontal connectivity, as described by the B and C matrices of the DCM analysis.

The "pantomimed grasping" condition exerted a direct effect on the right aIPs (C matrix). Results of the B "modulatory" matrix showed a strong positive modulatory effect propagating from aIPs to PMv, followed by inhibitory feedback exerted by PMv toward aIPs. This is evidence of a feed-forward parietofrontal loop subserving grasping movements. PMv exerted a positive influence on M1, PMd and SMA. In turn, only PMd had a negative influence on PMv. PMd inhibited SMA (Figure 4.4, left panel).

In the "imagined grasping" condition, the driven effect on aIPs (C matrix) did not exceed the threshold. In the B "modulatory" matrix, we found a positive influence from aIPs to

PMv, and a feedback inhibition from PMv to aIPs. PMv and SMA were linked by excitatory/inhibitory connections (Figure 4.4, right panel).

Across conditions, no differences were found in the aIPs to PMv ("Pantomimed grasping" = 0.61, "Imagined grasping" = 0.56, Posterior probability pp of the Bayesian contrast = 0.61) and in the PMv to SMA ("Pantomimed grasping" = 0.35, "Imagined grasping" = 0.32, Pp = 0.58) connections.

Comparison between left- and right-hemisphere DCM-PEB results

In the present section, we will compare the results of the right hemisphere DCM (B and C matrices) with the left hemisphere ones presented in our previous work (Bencivenga et al., 2021). We will also describe the suprathreshold (Posterior Probability > 0.95) Bayesian contrasts aimed to compare connection strengths of common modulated connections across the two hemispheres (Figure 4.5).

As first striking evidence, connectivity patterns were extremely similar across hemispheres during pantomimed movements, but not their imagination.

In the "pantomimed grasping" condition, the positive forward connections from aIPs to PMv and PMv to M1 were stronger in the left than the right hemisphere (aIPs to PMv: LH = 1.09, RH = 0.61, Pp = 0.99; PMv to M1: LH = 0.74, RH = 0.33, Pp = 0.99). This is compatible with the predominance of left-hemisphere couplings for right-hand movements. The other forward connections (PMv to PMd and SMA) were not significantly different across hemispheres. The only feedback inhibitory connection differing across hemispheres was PMd to PMv (LH = -0.68, RH = -0.4, Pp = 0.96). Note that the connection from PMd to SMA was modulated in the right, but not the left hemisphere.

In the "imagined grasping" condition, only the positive influence from aIPs to PMv was common across hemispheres, without significant differences between left/right connection strengths (LH = 0.43, RH = 0.56, Pp = 0.83). This bets against the predominance of left-hemisphere couplings for right-hand imagined movements. Positive modulation

from SMA to PMd and negative modulation from PMd to PMv were exclusively found in the left hemisphere.

4.3.3 Interhemispheric DCM-PEB results

In the interhemispheric DCM model, 23 out of 25 subjects reached an explained model variance higher than 10%, being therefore included in the PEB analysis.

In the "pantomimed grasping" condition, the majority of interhemispheric connections were inhibitory: negative inputs were exerted from the right PMd toward the left primary motor (M1) and premotor (PMv, PMd, SMA) cortex. Noteworthy, the left SMA and PMv exerted a positive modulation of their right homologue areas, whereas the right SMA contributed to increasing activation in the left PMv (Figure 4.4, left panel).

Only an inhibitory modulation exerted from the right PMd toward the left M1 was detected in the "imagined grasping" condition (Figure 4.4, right panel). Such inhibition was stronger than in the "pantomimed grasping" condition, likely accounting for the suppression of the motor output (Posterior estimate "Pantomimed grasping" = -0.26; Posterior estimate "Imagined grasping" = -0.5; Pantomimed grasping > Imagined grasping Pp = 0.97).

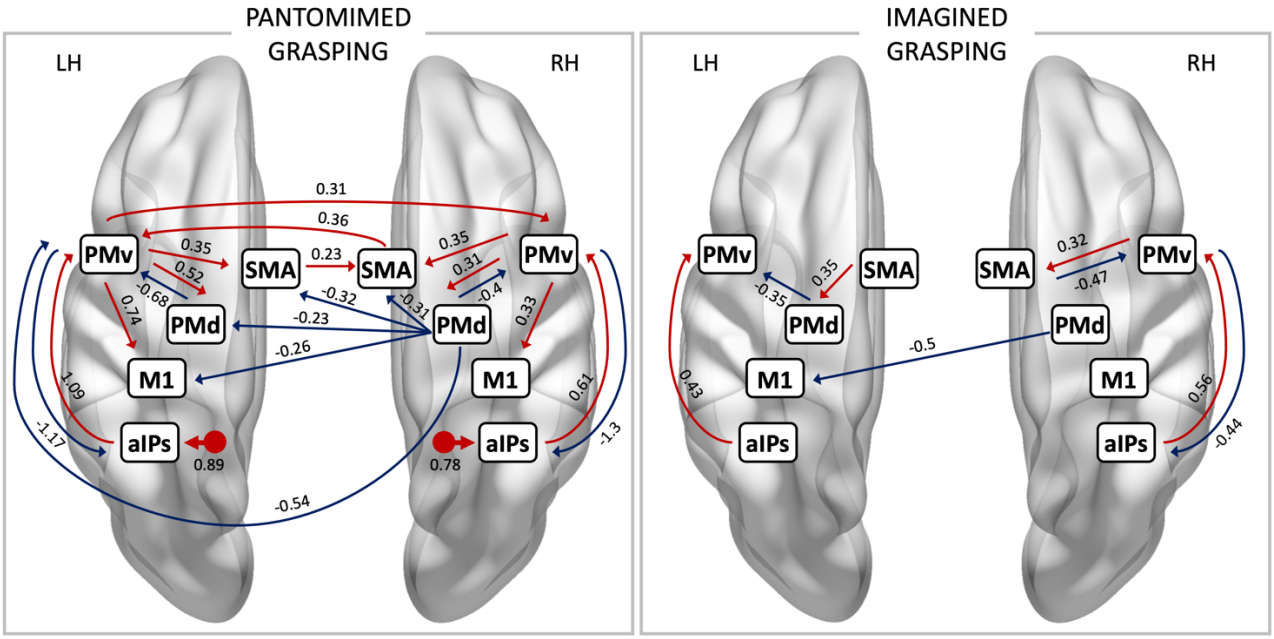

Figure 4.4. *PEB results – B and C matrices.* Schematic representation of the direct (C matrix) and modulatory (B matrix) effect on the effective connectivity within the network, separately for the

pantomimed grasping (left panel) and the imagined grasping (right panel) condition. Only suprathreshold parameters (posterior probability > 0.95) are shown: red lines denote excitatory connections; blue lines stand for inhibitory connections. The direct effect (C matrix) on aIPs, where exceeding the threshold, is displayed as a dot with a left/right arrow. Connection strengths are also reported. Regions are denoted as aIPs (anterior intraparietal sulcus area), PMv (ventral premotor area), PMd (dorsal premotor area), SMA (supplementary motor area), and M1 (primary motor cortex).

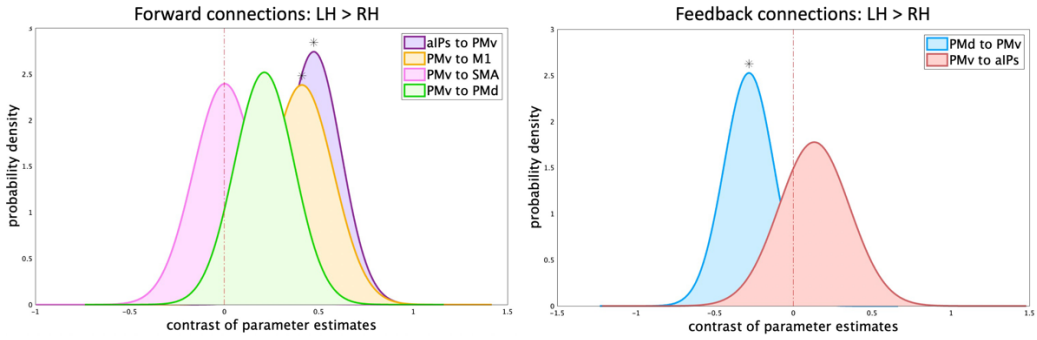

Figure 4.5. *Bayesian contrast over parameter estimates (LH > RH) in the "pantomimed grasping" condition.* Plot of the probability density function of the contrast over parameter estimates that exceeded the threshold (posterior probability > 0.95) representing the same connection in both single-hemisphere DCM. Connections are subdivided into Forward (left panel: PMv to SMA in pink, PMv to PMd in green, PMv to M1 in yellow, aIPs to PMv in purple) and Feedback (right panel: PMd to PMv in blue, PMv to aIPs in red). A red dotted line denotes the 0 point. Contrasts whose posterior is higher than 0.95 are marked with an asterisk above the probability density curve. If the curve is on the right (i.e., mean higher than 0) the connection is higher in the left vs the right hemisphere; conversely, if the curve is on the left (i.e., mean lower than 0) the connection has lower connection strength in the left vs the right hemisphere.

4.4 Discussion

"Contralateral control" is the core tenet of motor functioning, supported by the anatomical arrangement of motor and sensory fibers. Notwithstanding, multiple pieces of evidence agree that this is only half the story, as the contribution of the ipsilateral hemisphere holds a fundamental role in successful motor planning and execution. The advent of more sophisticated methods to assess connectivity within and between

hemispheres, such as new TMS protocols and fMRI data analysis techniques, has boosted knowledge on the topic.

While TMS is an ideal candidate to infer the causal impact of one brain region on an interconnected area and ensures high temporal resolution, it can hardly deal with the complexity of a network consisting of multiple hubs that exert a reciprocal influence. Indeed, the majority of studies using TMS to assess interhemispheric dynamics have focused on the M1 activity, as the increase or decrease in amplitude of the motor-evoked potential (MEP) recorded through electromyography has been used as a hallmark of neural inhibition or facilitation.

DCM applied to fMRI data can be a valid method to detect complex interactions within a wider network and to assess directional influences between brain areas besides M1. Since caution is necessary when relating BOLD signal increases or decreases to actual neural states, we will discuss our results in light of those deriving from both techniques, being aware that it is not possible to find strict homologies.

As we evaluated the effective connectivity within the grasping network during the pantomime of right-hand grasping movements and their imagination, we will discuss our results separately for each experimental condition.

4.4.1 Pantomimed grasping

The first evidence drawn from the "pantomimed grasping" condition pointed toward striking similar network connectivity across hemispheres: the dynamic interactions occurring between right parieto-frontal areas were similar to those of the left hemisphere, even though connection strengths were overall lower, a result highly consistent with that found by Begliomini and colleagues (Begliomini et al., 2015). The signal spanned from aIPs to PMv, was susceptible to modulations by PMd and SMA, and finally reached M1. Notably, only the forward excitatory connections from aIPs to PMv and from PMv to M1 were stronger in the left vs the right hemisphere.

Beyond confirming the wide involvement of a bilateral parieto-frontal network during grasping, our results suggest that very similar mechanisms occur across hemispheres in

terms of network functionality. As we already discussed in our previous work relative to the left-hemisphere results (Bencivenga et al., 2021), we suggest that a general motor program for grasping is planned by the aIPs-PMv circuit, whereas PMd and SMA encode high-level features of the movement. Notably, the excitaxwtory input from the right PMv to the right M1 supports the view that the ipsilateral M1 provides additional resources when performing unilateral complex movements even if the amount of activation detected by fMRI is extremely low. Together, these findings support the key role of the ipsilateral hemisphere in the planning and execution of a complex unimanual action, whereby hand actions are supported by limb-invariant representations in parietal and frontal areas (Gallivan et al., 2013).

The crucial issue we revamp here is that interhemispheric connections may bridge the two hemispheres to allow sharing of resources and information for a successful motor plan. For this reason, the second step of our work sought to describe interhemispheric dynamics occurring during the task. When comparing our results with previous findings, we are aware that the heterogeneity in the protocols, techniques, and tasks used to investigate interhemispheric dynamics may lead to apparently contradictory results. For instance, we observed a massive interhemispheric inhibition spanning from the right to the left hemisphere, whereas interhemispheric facilitation occurred in the opposite direction. Noteworthy, this latter pattern reverses the inhibition occurring at baseline (A matrix), therefore being a hallmark of the connectivity modifications depending on the current motor state, i.e., active or passive. While a short and a long latency interhemispheric inhibition emerges from contralateral PMd to M1 at rest (Ni et al., 2009), some studies have pointed out that interhemispheric dynamics change during the transition from a motor state to another, reflecting the switch from motor planning to implementation. For instance, Liuzzi and colleagues (Liuzzi et al., 2011), using a simple right-hand reaction time task, recorded a biphasic pattern of modulation exerted from the right PMd toward the left M1, namely early and late latency facilitation respectively evoked by movement selection and execution, while M1-M1 interactions were modulated only right before movement onset. With the current experimental design, we could not

decompose grasping movements into planning and implementation phases, therefore future studies will be aimed at disentangling dynamic changes in interhemispheric connectivity according to each stage of the movement.

The role of the right PMd in driving the inhibition toward the left premotor and motor cortex deserves a spotlight. PMd covers a key role in decision making and is a central structure for the selection and initiation of voluntary actions (Cisek & Kalaska, 2005; Hoshi & Tanji, 2007). In agreement with that, it has been suggested that PMd is responsible for the top-down processing of movement control both within and across hemispheres (Hinder et al., 2012). Beyond PMd, our data show that in the case of grasping movements, the left PMv is the central hub of the network as it groups inputs from the ipsilateral and the contralateral hemispheres.

Worthy of mention is the role of the left SMA which, together with the left PMv, exerts a positive influence on its right homologue. Notably, a similar modulation was found by Gao and colleagues (Gao et al., 2014) during a finger tapping task, supporting the idea that the information transfer between bilateral SMAs plays a crucial role in both unimanual and bimanual movements (Grefkes et al., 2008; Seitz et al., 2004; Stancak, 2003). Still, a different role of left and right SMA, independently of the effector (left or right hand), was suggested by White and colleagues (White et al., 2013) in a TMS study on grip force. According to these authors, the left SMA is crucial for predicting the required grip force, overall encoding object dynamics, whereas the right SMA is more likely involved in the translation of object representation into motor commands. In line with this view, our results suggest that object dynamics encoded in the left SMA may converge in the right SMA, integrated with the generated motor command, and transferred back to the left PMv to drive the last stages of motor planning and execution.

TMS studies have consistently detected an interhemispheric inhibition between the two motor cortices, a result that we failed to replicate. Methodological and theoretical issues can account for this discrepancy. First, we did observe M1-M1 inhibition at rest, therefore our results must be interpreted by accounting for the evidence that this baseline inhibitory pattern is not strengthened or reduced during motor execution or imagery, in

other words no task-dependent modulation emerged in the B matrix. Moreover, it has been suggested that iM1 shapes the muscular command in different ways depending on the stage of the motor execution, according to which this area can drive inhibitory or facilitatory inputs (Duque et al., 2005; Murase et al., 2004) and shows unspecific activity for right- or left-hand movements during planning, which turns to be specific during execution (Gallivan et al., 2013). Although here we could not account for this distinction, on a deeper analysis the comparison between present and previous findings suggests that, during simple movements, a strengthening of the cM1-iM1 crosstalk is necessary (see the DCM study by (Grefkes et al., 2008)), whereas complex movements might rely upon a premotor rather than a direct motor interhemispheric modulation (see also (Begliomini et al., 2015)).

4.4.2 Grasping imagery

When imagining the grasping movement, a different scenario emerged. A first striking difference uncovered by the whole-brain activation maps is the only subtle involvement of the right hemisphere during grasping imagery, a result that suggests a contralateral hemisphere dominance in motor imagery vs the bilateral involvement of the network during motor execution.

In line with that, only partial similarities in the effective connectivity across the two hemispheres were revealed by the DCM. Differently from what we described for the pantomimed grasping, the connection from aIPs to PMv was equally modulated in both hemispheres. Furthermore, SMA and PMd cooperated to inhibit PMv only in the left hemisphere. Conversely, in the right one a loop directly linking SMA and PMv emerged, as well as an inhibition from the right PMd to the left M1. Presumably, these dynamic interactions both drive motor imagery and concur to prevent excitation from the left PMv toward M1, resulting in the suppression of the motor output. This latter interpretation is in line with the concept of an "impulse-control" mechanism aimed at preventing overt activity in the right hand (Gueugneau et al., 2013).

Overall, these results point toward a different role of the right and left hemispheres during motor imagery. A previous study on motor imagery in stroke patients found that only right hemisphere damage impaired the timing estimation of imagined movements, sparing that of real movements (Malouin et al., 2012). These authors suggested that the right hemisphere is crucial for maintaining spatial information over time when internally simulating the motor pattern. As SMA is a key node in temporal processing (Coull et al., 2015), our results may be interpreted from the perspective that temporal encoding of the imagined movement may be processed by the right SMA and then this information is transferred to the right PMv to coordinate the imagined movement.

Together, we can conclude that motor execution and imagery share neural effector- and task-independent representations in high-order areas such as aIPs, whereas lower-order areas as SMA and PMd deem with effector- and task-dependent representation (Gallivan et al., 2013; Monaco et al., 2020; Zabicki et al., 2016), a result confirmed by the different connectivity patterns we found across hemispheres and condition. This is in line with previous studies showing that motor planning triggers the recruitment of common areas to both motor execution and imagery (Hashimoto & Rothwell, 1999; Lorey et al., 2011; Munzert et al., 2009; Sulpizio et al., 2020).

Future studies may be designed with the specific aim to address the different functional contributions of the two hemispheres to motor imagery vs execution with compelling implications for rehabilitation practice, for instance guiding the choice of target areas for brain computer interfaces (BCI) protocols using MI on post-stroke patients.

4.5 Conclusion

With the present study, we adopted a novel methodological approach to investigate interhemispheric dynamics during unilateral complex movements. Our results endorse the idea of a complex interplay both within and between hemispheres during grasping movements, whereby dissociable components of unilateral grasping are encoded by a non-lateralized set of brain areas entailing the abstract action representations (Turella et

al., 2020), whereas the more concrete action representations may be task- and limb-dependent. As grasping execution directly targets bilateral aIPs (C matrix) and grasping imagery is subtended by different hemispheric contributions, we argue that the ipsilateral hemisphere signal does not merely reflect an efference copy of the contralateral motor command, but rather an active contribution to the refinement and implementation of the motor plan.

Our study is not exempt from limits. First, we used a pantomime movement, that only partially share neural representations with actual grasping including contact with the graspable object. Also, we focused on a set of ROIs to keep a reasonable number of nodes within the network, including areas within the dorsoventral visual stream well-known to be key areas in the grasping network.

Further studies on the interhemispheric dynamics are advisable to inform clinical research on the spread of information along the corpus callosum supporting complex motor functions in pathological conditions. Unwanted bilateral muscle activity for unilateral actions may be induced by lesional events directly damaging the corpus callosum, but also by aging, which incurs the degradation of callosal fibers (Baliz et al., 2005; Bodwell et al., 2003; Hoy et al., 2004). Recovery of impaired motor functions post-stroke is known to be supported by interhemispheric connectivity. A recent study showed that the contralesional aIPs supports grasping movements performed with the stroke-affected hand, overall suggesting that the contralesional hemisphere can reallocate resources to the ipsilesional one (Hensel et al., 2022). The understanding of interhemispheric mechanisms may boost rehabilitation programs in the case in which age, strokes, traumatic brain injury, or temporary limb immobilization foster a re-balance of the bridges between hemispheres.

CHAPTER 5

Behavioral, kinematic, and physiological evidence of target updating during reach-to-grasp actions in a virtual environment

Federica Bencivenga[1,2,3], Michelangelo Tani[1], Sarah Boukarras[4,5], Cristina Ottaviani[4], Gaspare Galati[1,2], and Matteo Candidi[4,5]

[1] Brain Imaging Laboratory, Department of Psychology, "Sapienza" University of Rome, Rome, Italy

[2] Cognitive and Motor Rehabilitation and Neuroimaging Unit, Santa Lucia Foundation (IRCCS Fondazione Santa Lucia), Rome, Italy

[3] PhD Program in Behavioral Neuroscience, Department of Psychology, "Sapienza" University of Rome, Rome, Italy

[4] Department of Psychology, "Sapienza" University of Rome, Rome, Italy

[5] Social Neuroscience Lab, Santa Lucia Foundation (IRCCS Fondazione Santa Lucia), Rome, Italy

Abstract

We live in a non-stationary environment which constantly provides us with multiple action possibilities and often requires us a sudden modification of our motor actions while we are implementing them. Research on visuomotor functions has attempted to investigate action monitoring, conflict, and resolution by using in most cases non-ecological paradigms. Here, we implemented a grasping task combining virtual reality (VR) and motion tracking. Participants (N = 26) performed individual or joint grasping (i.e., together with a virtual avatar) actions toward a virtual bottle-shaped object that could be grasped with a power or precision grip depending on trial-by-trial instructions. Crucially, in 30% of trials a target update occured, hence forcing participants to rapidly adapt their motor behavior shifting from a precision to a power grip or vice versa. Although actions were taking place in a virtual world and no real interaction with the objects was present, we observed real-life motor kinematics with precision and power grip differing for grip aperture and wrist height. Kinematics were also susceptible of

modulation during joint action thanks to sensorimotor simulative mechanisms driven by the observation of the other's actions. In addition, following a trial in which a target perturbation occurred, accuracy was higher and the time to attain maximum wrist height increased. This indicate that our behavior and kinematics rapidly adapt to embrace the possibility of living in an unpredictable world: after an unexpected event and the necessity to modify on flight one's own movement, behavior is rapidly optimized toward reiterative but still infrequent events.

5.1 Introduction

The environment constantly provides us with multiple action possibilities. When interacting with the external world, following contextual cues we must select among all the possibilities the most appropriate behavior to match our action goals. However, the environment is never stationary, often requiring us a sudden modification of our motor actions while we are already instantiating them. Thus, our actions undergo a continuous online monitoring and update.

Research on visuomotor functions has tried to investigate action monitoring, conflict, and resolution using paradigms as the target jump. In this paradigm, while participants are performing reaching movements the target suddenly changes its location. As a response to such an unexpected event, hand movements are not abruptly interrupted and then rearranged, but smoothly updated without undue delay. At the neural level, while the hand is still moving according to the preplanned trajectory, an updated plan including the trajectory correction is encoded in parallel to the initial plan (Archambault et al., 2011). This points towards a coexistence of neural signals about the execution of a specific hand trajectory together with those concerning a different trajectory, overall being consistent with the affordance competition hypothesis (Cisek and Kalaska, 2010). Less is known about these mechanisms during more complex actions such as grasping. Previous studies have adopted paradigms including a change after movement onset of object size

(size-perturbation paradigm; Paulignan et al., 1991), or orientation (Tunik et al., 2005). However, the extent to which these paradigms extend to real life scenarios is still unclear.

In many cases, our actions are also embedded in social exchanges where we must take into account the others' behavior and eventual unpredictable changes in the other's intentions. A valid model of ethologically-relevant category of behavior are joint actions, namely motor interactions in which two or more agents share a common goal (Sebanz et al., 2006). Social motor interactions are scaffolded on neural networks partially overlapping the ones supporting individual actions, including the mirror neurons system (Rizzolatti et al., 2004), and the overlap between these mechanisms can be the key through which interactive actions can moderate impairments during the execution of purposeful actions in apraxic patients (Candidi et al., 2017). During social motor interaction, we must integrate action observation, prediction, and control of our personal motor behavior. In other words, our muscular synergies are shaped by the representation of interpersonal synergies and affected by the simulation of the other's movements (Candidi et al., 2015). It is foregone that also error monitoring mechanisms can be shared across individual and joint actions (see Moreau et al., 2020). Hence, by providing the opportunity to investigate how monitoring of individual and social movements and goals interplay with each other (Vesper et al., 2016), joint actions can offer insights into the ability to rapidly adapt one own's motor behavior.

In this work, we implemented a grasping task combining virtual reality (VR) and motion tracking. We adapted a paradigm introduced by Sacheli and colleagues (Sacheli et al., 2012, 2015; Moreau et al., 2020) with the ultimate goal of making it suitable for functional magnetic resonance imaging (fMRI) implementation (see Chapter 6). Participants' hand movements were reproduced on a first-person virtual avatar in a realistic environment where they could perform individual or joint grasping movements toward a rectangular-shaped bottle. In the former case, a light could appear on the top or bottom part of the bottle, indicating subjects to perform a power or precision grip ("Move" condition). During joint actions, participants were also asked to synchronize their grasping

movements with those executed by a virtual partner. We distinguished between two separate conditions: in the "Guided" condition, participants performed the same task as the "Move" condition but were asked to grasp either the upper or the lower part of the bottle, depending on a light appearing on the bottle, while at the same time matching the partner's grasping in time. Conversely, in the "Interactive" condition, they were asked to grasp the bottle depending on the action of the virtual partner (see Methods section for details), while matching both in time and space the partner's grasping movements and ignoring the lights appearing on the bottle. We also disambiguated between imitative and complementary actions by asking participants to perform the same or the opposite movement cued by the bottle's lights or the partner's movements, expecting to find evidence of visuo-motor interference in the social condition (Sacheli et al., 2012, 2015). Crucially, in 30% of trials, participants were required to rapidly adapt their motor behavior based on a switch in the spatial location of the non-social cue ("Move" and "Guided" condition), or a sudden change in the trajectory of the virtual avatar's movements ("Interactive" condition). We measured behavioral (e.g., accuracy, reaction times), kinematic (e.g., wrist height, grip aperture), and physiological (i.e., heart rate) indices, comparing socially and non-socially cued conditions, complementary and imitative actions, and perturbed vs non perturbed trials.

We expected social interactions during joint actions to modulate performances by requiring the integration and prediction of visual and sensorimotor information about both one's own and the other's actions. Indeed, joint action contexts can modulate motor activity by coupling together perception and action in a top-down fashion (Prinz, 1990; Bolt and Loehr, 2020). We also tested the hypothesis that social interactions could modulate kinematic indices of participants' grasping movements by eliciting simulative motor mechanisms and the activity of the autonomic nervous system, as assessed by heart rate variability. Moreover, we analyzed if being forced to perform a motor correction in response to a target update driven by social or non-social cues could influence behavior and kinematic movement properties in the current and the following trial, expecting to find in this latter case the typical post-error mechanisms detected in

motor and non-motor tasks, such as post-error slowing (PES; Rabbitt, 1966; Debener et al., 2005; Eichele et al., 2010).

On a side note, our study provides the first implementation of this paradigm in a virtual environment setting, whereby participants do not interact with real objects to grasp. Hence, we tested whether our paradigm could distinguish kinematic properties of the movement (e.g., grip aperture, wrist height) associated with different grip configurations (i.e., precision vs power grip) despite the absence of an interaction with a real object. This would validate the virtual reality paradigm for the following fMRI implementation (see Chapter 6).

5.2 Methods

The experiment was built in Unity (v. 2019.4) using Unity Experiment Framework (UXF; v2.4.3) and custom scripts. The used Virtual Reality headset was HTC Vive Pro Eye (HTC Corporation, New Taipei, Taiwan), through which we could also record eye movements. For hand movement tracking we used the Leap motion controller (Ultraleap, San Francisco, California, United States). We located the device on a desk, while the participant's hand was lying over it, supported by the chair arms. A custom GUI was created to calibrate the position of the actor avatar based on the arm length of each subject.

5.2.1 Subjects

Twenty-six subjects participated in the study (7M; 27.9 ± 5.86 y). Participants were right-handed, as assessed by the Edinburgh Handedness Inventory (Oldfield 1971), and had normal or corrected-to-normal vision. Participants gave their written informed consent to participate in the study. The study was approved by the local research ethics committee of the IRCCS Fondazione Santa Lucia in Rome, according to the Declaration of Helsinki.

5.2.2 Experimental paradigm

In a virtual environment, two avatars faced each other, sitting at opposite sides of a table. One avatar (actor avatar) reproduced real-time tracked participant's movements; the other one (partner avatar) was programmatically animated. As a starting position, the right hand of both avatars was placed over the table. A white rectangular platform was placed under the actor avatar's hand. The virtual camera was located at the height of the actor's eyes; therefore, the participant could see his/her right forearm and hand, the table, and the partner. The partner's face was hidden by a panel.

At the center of the table, two bottle-shaped objects were located. Bottles were composed of two superimposed rectangles with diameters of different sizes (the lower one larger, the higher one smaller) and provided by a button. From the subject's perspective, the buttons on the left bottle were white, whereas those on the right bottle were green. The partner avatar executed right-hand movements toward the bottle with white buttons. In a mirror way, participants were asked to perform right-hand movements toward the bottle with green buttons (Figure 5.1).

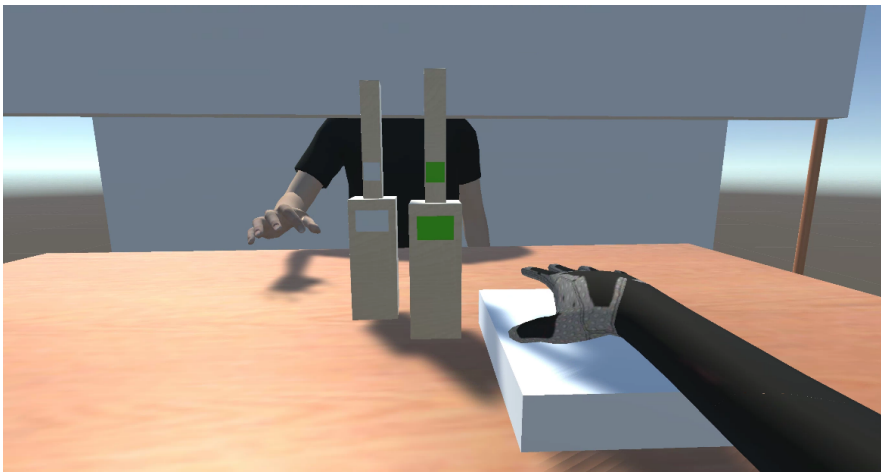

Figure 5.1. Virtual reality scene from a first-person perspective.

The experiment was conceived as a 2x2x2x2 factorial design. We implemented a mixed design, whereby one factor ("Instruction") varied between blocks, whereas the others ("Movement", "Correction", "PreviousCorrection") were event-related.

- "Interactive" blocks: the partner could perform a precision/power grip, with (1/3 trials) or without (2/3 trials) change of intention (= Correction). The upper or lower button of the subject's bottle was enlightened, eventually spatially updating during the trial (1/3 trials). The participant was asked to perform the same/opposite movement with respect to the partner, trying to synchronize his/her movement with the partner.
- "Guided" blocks: the partner could perform a precision/power grip, with (1/3 trials) or without (2/3 trials) change of intention (= Correction). The upper or lower button of the subject's bottle was enlightened, eventually spatially updating during the trial (1/3 trials). The participant was asked to perform the same/opposite movement with respect to the bottle, trying to synchronize his/her movement with the partner.
- "Move" blocks: the partner was still. The upper or lower button of the subject's bottle was enlightened, eventually spatially updating during the trial (1/3 trials). The participant was asked to always perform the same movement with respect to the bottle. In this case, the movement time was not beaten by the partner's movement. This was considered a control condition targeting individual actions and the ability to rapidly update motor behaviors.

The "PreviousCorrection" factor disambiguated trials that were ("YES") or not ("NO") following a perturbed trial.

Block- and trial- instructions were auditory stimuli created through speech synthesis using Amazon Polly, and then cut to achieve a preset duration using GarageBand 10.4.7. At the beginning of each block, subjects heard a 0.6s cue according to the "Instruction" factor. 5 stimuli were created in English and Italian (female voice): "Avatar", "Bottle", "Move". Each of these words corresponded to an experimental or control condition: respectively, subjects could follow the Avatar's movement ("Interactive") or the bottle's lighting while the partner was moving ("Guided") or still ("Move"). The comparison between the Interactive and the Guided conditions was used to disambiguate social and

non-social cued movements. In both conditions, subjects were required to synchronize with their partner's movements.

At the beginning of each trial in the "Interactive" and the "Guided" blocks, a trial-specific instruction (0.2s; male voice) addressed whether subjects should perform the same ("Same" condition) or the opposite ("Opposite" condition) movement. The distinction between the two was introduced to discriminate between imitative ("Same") or complementary ("Opposite") reach-to-grasp action. "Move" trials were tested only under "imitative" conditions ("Same"). An additional 0.1s delay was provided after the trial-specific instruction to get the participant ready for the incoming trial.

In 33% of the trials, the partner or the bottle cue could change while paßrticipants were performing the movement. Unperturbed trials occurred with twice the probability, implying that perturbed trials violated participants' expectations. According to the "Instruction" factor, participants had to adjust their trajectory to react to unexpected events, eventually correcting their own reaching trajectory and grip type.

Three additional confounding variables were balanced and pooled together:

a. Participant's grip type: in the "Interactive", "Guided" and "Move" blocks, participants were required to execute a power or precision grip with the same probability. In this experimental setup the two movements suffered from a spatial bias, being distinguishable more for the reaching than for the grasping phase. In all the analyses but kinematics we decided to model the grip type as a confounding variable.

b. Congruency between visual cues: social (partner's) and non-social (bottle's) cues could suggest the same movement ("congruent") or not ("incongruent"). In the "Interactive" and "Guided" blocks, we modeled an equal number of "congruent" and "incongruent" trials to discriminate whether the subject was attending to the social or the non-social cue.

c. "Correction of no-interest": in each trial, the partner's and the bottle's corrections never occurred together, whereas *one* or *any* of the two occurred with the same probability. In other words, whenever a correction-of-interest was present (i.e., bottle's correction in the "Guided" blocks; partner's correction in the "Interactive" blocks) a correction-of-no-interest (i.e., bottle's correction in the "Interactive" blocks; partner's correction in the "Guided" blocks) was never present. Whenever a correction-of-interest was absent, a correction-of-no-interest could equally be present or not. This check was necessary to discriminate whether the subject was indeed correcting his movement following the correction performed by the partner or the bottle, according to each block instruction. Note that the partner's corrected movements were smoothed in time and space, whereas the buttons could just turn on or off, with no transition between the two states. To match the two corrected movements, we considered creating a probability cloud between the two states, and proportionally increase or decrease the amount of light on each button. However, we reasoned that if buttons gradually and slowly transited from one state to another, in the "Guided" blocks the subjects could be tempted to synchronize with the amount of light emission during time, rather than with the partner's movement.

In each run, each combination between the 6 factors (3 of interest, 3 of no interest) occurred once in the case of correction trials, and twice in the case of no-correction trials.

Overall, 20 trials for each combination of "Corrected" trials with the other levels were created (e.g., 20 Interactive Same Corrected trials), whereas 40 trials were implemented for each combination of "Uncorrected" trials, balanced between the presence or the absence of a correction of no-interest (e.g., 40 Interactive Same Uncorrected trials).

Trials were distributed across 5 runs, each including 15 blocks (6 Interactive, 6 Guided, 3 Move) composed of 4 trials.

To keep consistent with the fMRI implementation of the task (see Chapter 6), subject-specific trial lists were created to optimize the HRF response by counter-balancing the

sequence of trials and blocks. We assigned a random partner animation video to each trial, balanced across conditions (e.g., each condition included an equal repetition of each of the 20 possible animations). A variable ISI following a truncated exponential distribution (min = 0.5s, max = 5s, mean = 2s) was added to the duration of the partner's movement, and the resulting sum was used to define trial duration (ITI). For consistency, the same procedure was used to define trial duration during "Move" blocks, although no movement was actually executed by the partner.

We recorded the timing at which the movement started (i.e., the actor raised the hand from the starting platform), and the touch of the button occurred. Kinematics of the right index, thumb, wrist and elbow as reconstructed by the actor avatar movement were also recorded at the Unity frame rate (~60FPS).

5.2.3 Partner's movements and bottle's lighting

Partner avatar's movements were created based on kinematic recordings of naturalistic grasping movements performed by a human toward a bottle-shaped object similar to the above-described virtual one. The upper (*thinner*) part of the bottle could be grasped with a precision grip (Pr), whereas the bottom (*thicker*) part with a power grip (Po). 5 recordings for each grip type were obtained. Motion capture data were applied on a Caucasian male virtual avatar using MotionBuilder 2011 (Autodesk, Inc., San Rafael, CA). 3ds Max 2011 was used to render the data. Recordings were manipulated to obtain "corrected movements" by mixing up the first key frames of one grip type with the last key frames of the other grip type. Therefore, we created 5 power-corrected (PoC) and 5 precision-corrected (PrC) clips, representing grasping movements in which the partner's reaching trajectory shifted from the upper to the lower button (i.e., switching from a precision to a power grip; PoC) or vice versa (PrC). The mean duration of the clips was 3.08s (± 0.26).

From each clip, we extracted kinematics by tracking the 3D frame-by-frame position of the wrist, the index, and the thumb of the partner avatar's right hand using the built-in tracker provided in UXF. Note that the grasping movements suffered a spatial bias:

precision grasping movements reached a higher height, being directed toward the upper button. This implies that the most striking difference between precision and power grasping movements was the height of the hand, rather than the grip aperture, namely that the upcoming grip type could be predicted from the reaching phase. Hence, we averaged the vertical position (MeanY) of the wrist, index finger, and thumb for each frame. For simplicity, we will refer to this measure as the hand height.

We then proceeded by identifying the timing at which the initial grip configuration became evident, i.e., a clear distinction between the intention of performing a power or precision grip emerged. Furthermore, we wanted to identify the moment when a correction occurred, i.e., when a change in trajectory signaled the shift from a precision to a power grip or viceversa. To this aim, we calculated the frame-by-frame hand height difference, which we compared across animation types.

In Power Corrected (PoC) movements, the hand height continuously increases until the correction occurs; in Precision (Pr) movements, it keeps increasing until touch. Instead, during Power (Po) and the beginning of Precision corrected (PrC) movements, in the first part of the movement the height of the hand gradually increases, but soon the curve flattens. We retained the points demarking such difference for each animation starting with a precision movement (5 PoC, mean = 0.27s; 5 Pr, mean = 0.28s; see "initial grip configuration" window in grey in Figure 5.2). Ideally, this marks a clear point signaling the (initial) intention to perform a precision vs a power grip. We used these timings to set the moment when one of the two lights on the bottle should be turned on. This visually cued the initial movement to be performed in the Guided and Move conditions.

The second challenge was to set the timing for the target update. During the first part of Power Corrected (PoC) animations, the hand height is continuously increasing. However, whenever the change in intention occurs, it suddenly decreases. In mathematical terms, this corresponds to the first negative successive difference of hand height (see the blue "correction window" in Figure 5.2). We retained the frame of its occurrence for each of the PoC animations (5 values, mean = 0.7s). We then reasoned that

in the last part of PrC movements the hand height suddenly increases, stepping above the maximum height reached by any Power movement. Hence, we first retained the highest hand height across Power movements, and then we found the moment when the hand height exceeded that threshold for each PrC animation (5 values, mean = 0.73; see the orange "correction window" in Figure 5.2).

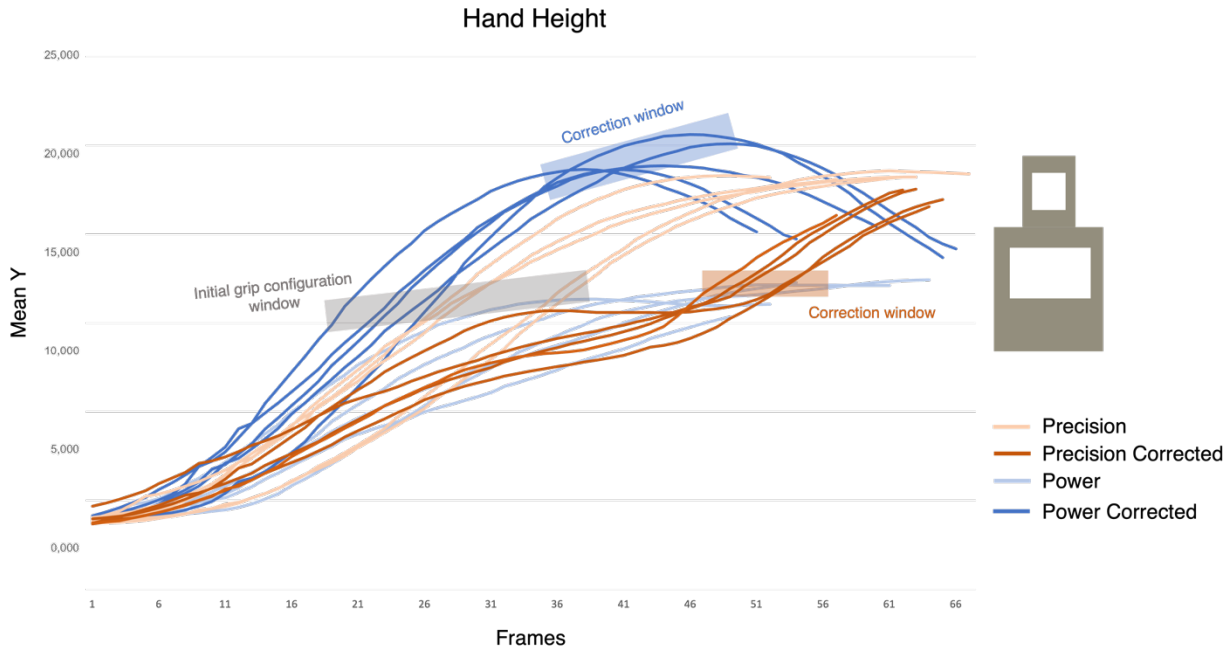

Figure 5.2. Kinematics of the virtual avatar animation. The plot shows the hand height for each of the animations where the avatar performed a Precision (salmon), Power (pale blue), Precision Corrected (orange), or Power Corrected (blue) movement. Kinematic curves are cut at the bottle contact time. Grey, blue and orange shaded rectangles represent the window where we detected the initial grip configuration (grey, signaling the distinction between power or precision movements), and the correction windows for power corrected (blue) and precision corrected (orange) movements.

5.2.4 Physiological recordings

We used the Bodyguard 2 device (Firstbeat Technologies Ltd., Jyväskylä, Finland) to record heart rate as beat-to-beat intervals in ms. Heart rate variability (HRV) was assessed by computing the root mean square of successive beat-to-beat interval differences

(RMSSD), which reflects vagal regulation of HR (Task Force, 1996). Outlier and artifact detection as well as HRV analyses were performed using Kubios HRV software (Tarvainen, Niskanen, Lipponen, Ranta-Aho, & Karjalainen, 2014). Here, we will use the term HRV to refer to RMSSD.

5.2.5 Data Analysis

Data analysis was performed using R and JASP.

We analyzed the following variables:

- Fixation on objects of interest: a collider object was attached to the actor or the partner's hand and to the green buttons on the actor's bottle to count the number of times participants were fixating them. This analysis served as a check to control whether participants fixated more the partner during Interactive vs Guided movements. We expected that the three conditions did not differ for the number of fixations on the actor's hand nor the buttons. Also, we predicted that participants would have fixated more the down button during power and more the up button during precision movements.
- Behavioral variables: accuracy; reaction time; grasp asynchrony (only in Joint Action blocks); time-to-contact (i.e., the time between the start of the movement and the first contact with the virtual bottle).
- Kinematic variables: grip aperture, computed as the Euclidean distance between thumb and index fingertips; maximum grip aperture latency in percentage relative to the whole movement; maximum wrist height; maximum wrist height latency in percentage. To compute the latencies of grip aperture and wrist height, we retained participants' movements starting from the 20% of movement onset to the object contact. This excluded the very first part of the movement, as the starting position of the hand was open and relaxed on the chair arm.
- Physiological variables: heart rate variability. Note that HRV analyses were performed only on blocks and not on trials because of evident temporal constraints relative to the experimental design (block duration ~20 seconds, trial duration ~5

seconds). Indeed, ultra-short periods of recording have been proven to be reliable if performed on a temporal window of a minimum of 10 seconds, under certain conditions (Salahuddin et al.,2007), which was further confirmed by an investigation on a very large sample (N = 3387; Munoz et al., 2015).

For dependent variables other than number of fixations, accuracy, and HRV, we eliminated trials in which participants failed to grasp the correct target; we also retained only RT>0 and RT<2s. We detected and removed the outliers (mean ± 2sd) for each analysis relative to each dependent variable.

We analyzed separately Individual ("Move") and Joint ("Interactive" and "Guided" conditions) and disambiguated the effects relative to Correction, Previous Correction, and, where applicable, Movement and Instruction. For kinematic variables, we also considered the different grip types.

To check if our variables were normally distributed, we used the Shapiro-Wilk test from the R package "rstatix". In the case of HRV analysis, we normalized the distribution of the data with log10 function. Number of fixations were analyzed using a repeated measures factorial ANOVA. Accuracy scores were evaluated using non-parametric factorial Analysis of Variance (ANOVAs). All the other variables were analyzed using mixed linear models ("lmer" function), modeling subjects as random variables. Post hoc tests were carried using the "emmeans" function.

Results were considered significant if the p-value was smaller than a threshold of 0.01.

5.3 Results

Results will be subdivided into fixation analysis, physiological, behavioral, and kinematic variables. Behavior and kinematics will be described separately for joint and individual actions.

5.3.1 Fixation analysis

Fixations on the actor's hand were higher in the Move than Guided ($p = 0.003$) and Interactive ($p = 7.2 \times 10^{-13}$) condition, and higher in the Guided than Interactive condition ($p = 0.002$). Conversely, fixations on the partner's hand were higher in the Interactive than Move ($p = 4.4 \times 10^{-15}$) and Guided ($p = 9.3 \times 10^{-14}$) conditions, as expected. Both buttons were fixated more in the Guided and Move condition vs Interactive (button down Move – button down Interactive, $p = 7.5 \times 10^{-6}$; button down Guided – button down Interactive, $p = 0.03$; button up Move – button up Interactive, $p = 1.01 \times 10^{-7}$; button up Guided – button up Interactive, $p = 5.3 \times 10^{-8}$; see Figure 5.3).

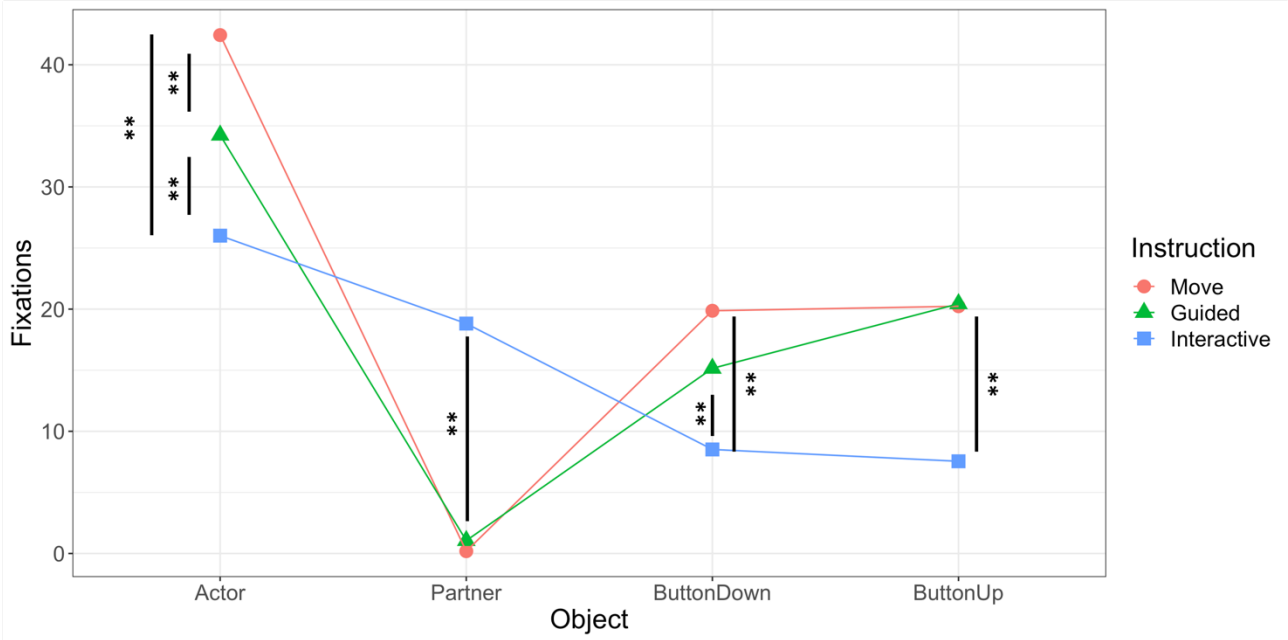

Figure 5.3. Mean number of fixations for each object of interest, separately for each Instruction block. Asterisks represent significant comparisons (** $p<0.01$; * $p < 0.05$).

When comparing grip types, objects and correction, we observed that when the movement wasn't perturbed, participants fixated more the down vs up button during power grips ($p = 0.049$); and more the up vs down button during precision grips ($p = 8.04 \times 10^{-8}$); instead, without any correction, they fixated both buttons at the same extent. No difference was found in the number of fixations on the actor's and partner's hand across grip types. However, we found that participants tended to perform more fixations on

their hand when they had to correct their movement on flight vs when this wasn't required ($p = 7.9 \times 10^{-7}$; Figure 5.4).

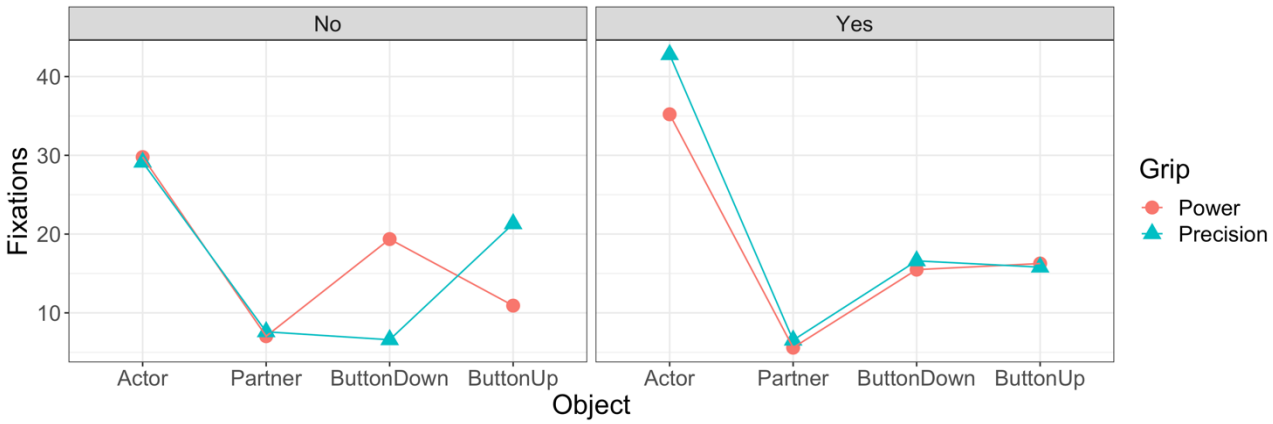

Figure 5.4. Mean number of fixations for each object of interest, separately for each Grip type (orange or turquoise lines) and Correction (left panel = no; right panel = yes).

5.3.2 Physiological results: HRV

A linear mixed model showed a significant effect of Instruction ($F = 4.82$, $p = 0.008$), and post hoc tests showed that HRV was significantly higher in Interactive vs Move and Guided blocks, whereas no difference occurred between Move and Guide blocks (Figure 5.5).

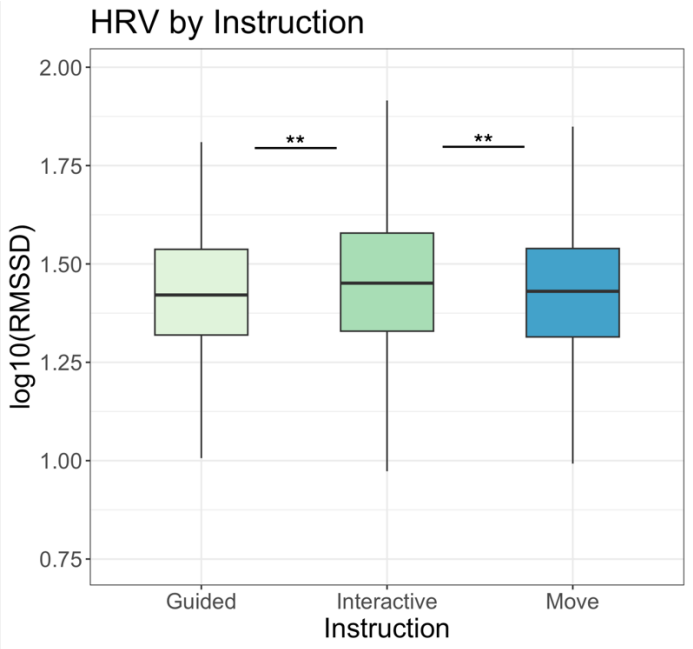

Figure 5.5. Box plots showing mean HRV across "Instruction" conditions. Asterisks represent significant comparisons (** $p<0.01$; * $p < 0.05$).

5.3.3 Behavioral results

Table 1 summarizes the mean percentage of correct answer across each combination of "Instruction", "Movement", and "Correction".

INSTRUCTION	MOVEMENT	CORRECTION	ACCURACY
Guided	Opposite	No	97%
Guided	Opposite	Yes	92%
Guided	Same	No	98%
Guided	Same	Yes	92%
Interactive	Opposite	No	93%
Interactive	Opposite	Yes	92%
Interactive	Same	No	94%
Interactive	Same	Yes	92%
Move	Same	No	99%
Move	Same	Yes	89%

Table 5.1. Mean Accuracy percentage scores for each level of Correction (No = left panel; Yes = right panel), Instruction ("Guided", "Interactive", "Move"), and Movement ("Opposite", "Same").

As a first step, we compared grasp asynchrony between the Guided and Interactive conditions, Correction vs NoCorrection and PreviousCorrection vs NoPreviousCorrection (Figure 5.6). This served as a control analysis to test if the necessity to adapt movements in space based on the lights on the bottle could distract participants from the request to adapt movements in time based on the partner's movements. A linear

mixed model showed that the difference between the two conditions held only for trials where neither the current nor the previous trial were perturbed, leading to higher asynchrony in the Guided vs the Interactive condition (p = 0.004).

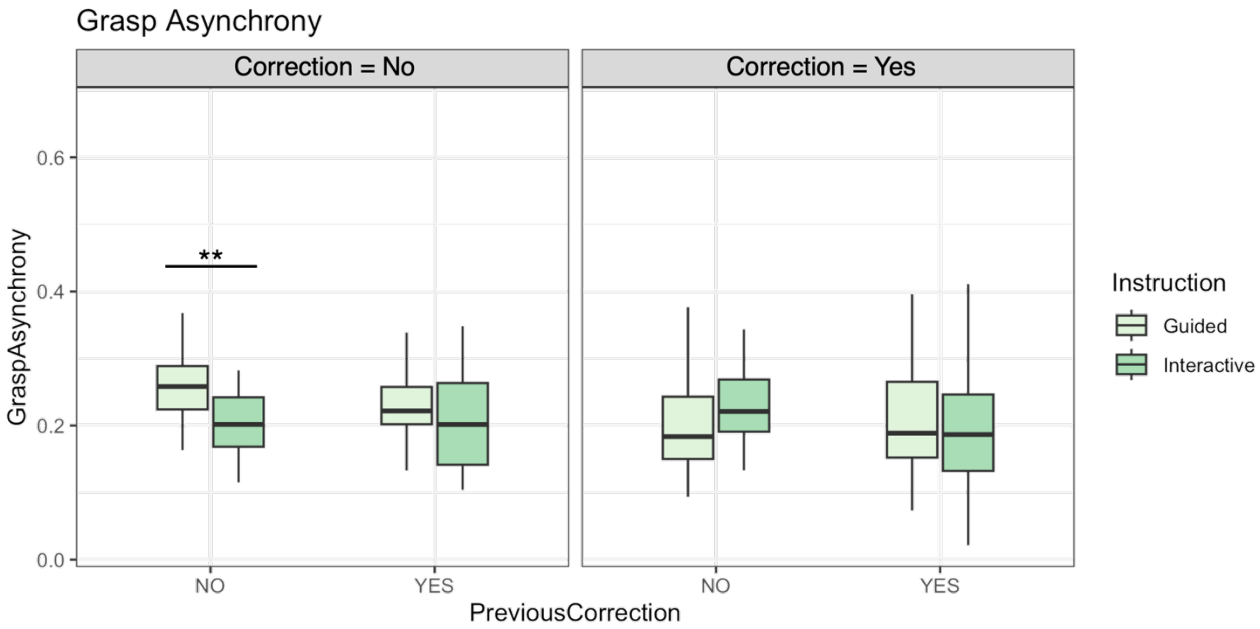

Figure 5.6. Box plots showing mean Grasp Asynchrony for each level of Previous Correction (NO, YES) and Correction (No = left panel; Yes = right panel) in Joint action blocks. Asterisks represent significant interaction effects (** p<0.01; * p < 0.05).

We then proceeded by testing different hypotheses for individual and joint actions. Specifically, we expected Correction and Previous Correction to modulate accuracy, time to contact and reaction times in both individual and joint actions. However, we tested the hypothesis that interacting with a partner, especially when reading the other's intentions was crucial to attain the task goal, could have modulated these effects.

Individual actions

A non-parametric ANOVA on accuracy scores using Correction, PreviousCorrection, and their interaction as factors showed only a significant effect of Correction (F = 20.1, p = 10^{-4} x 2.7): accuracy was lower in trials with vs without a motor correction (Figure 5.7).

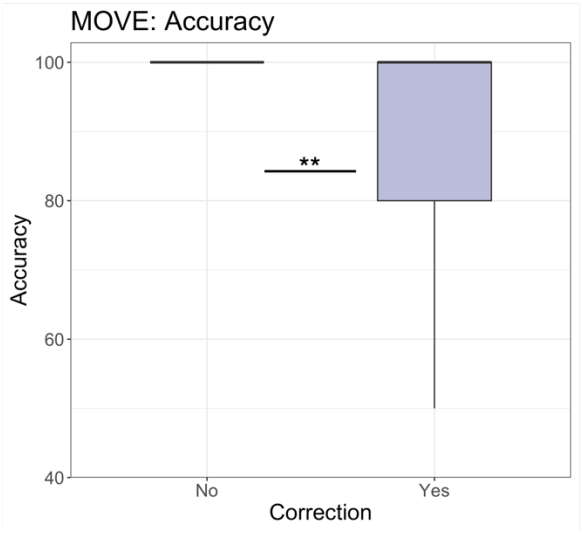

Figure 5.7. Box plot showing the distribution of Accuracy by each level of Correction (No, Yes) in "Move" blocks. Asterisks represent significant comparisons (** p<0.01; * p < 0.05).

A linear mixed model revealed that the Time-To-Contact was higher when a correction was required in the current trial ($p < 0.001$) or the previous ($p = 0.01$) compared to when no correction was needed, but there was no significant interaction between the two factors was found ($p = 0.98$) (Figure 5.8).

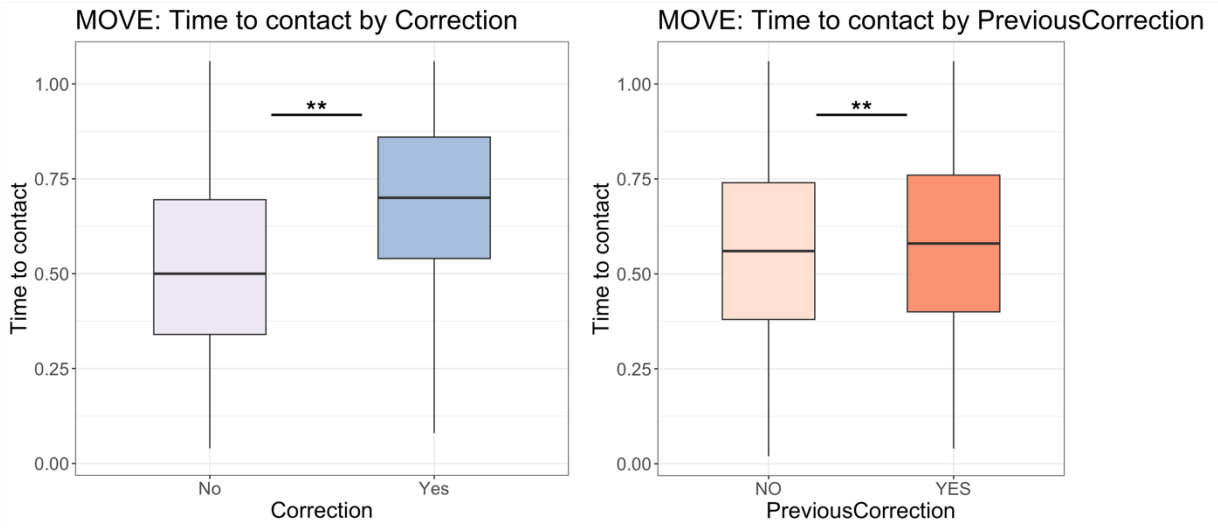

Figure 5.8. Box plots showing mean Time To Contact in Correction (left) and PreviousCorrection (right) trials in "Move" blocks. Asterisks represent significant comparisons (** p<0.01; * p < 0.05).

No effects were found on RTs.

To sum up, trials whereby a motor correction occurred led to worse performance and slower movements. Motor correction also influenced the following trial, increasing movement but not reaction times, or affecting accuracy.

Joint actions

A non-parametric ANOVA on accuracy scores using Correction, Previous Correction, Movement, Instruction, and their interaction as factors showed a significant effect of Previous Correction ($F = 15.94$, $p = 10^{-4} \times 7.9$) and its interaction with Correction ($F = 4.1$, $p = 10^{-4} \times 0.04$). Accuracy were higher in trials requiring a motor correction, but if a motor correction was requested in the previous trial, this pattern reversed (Figure 5.9).

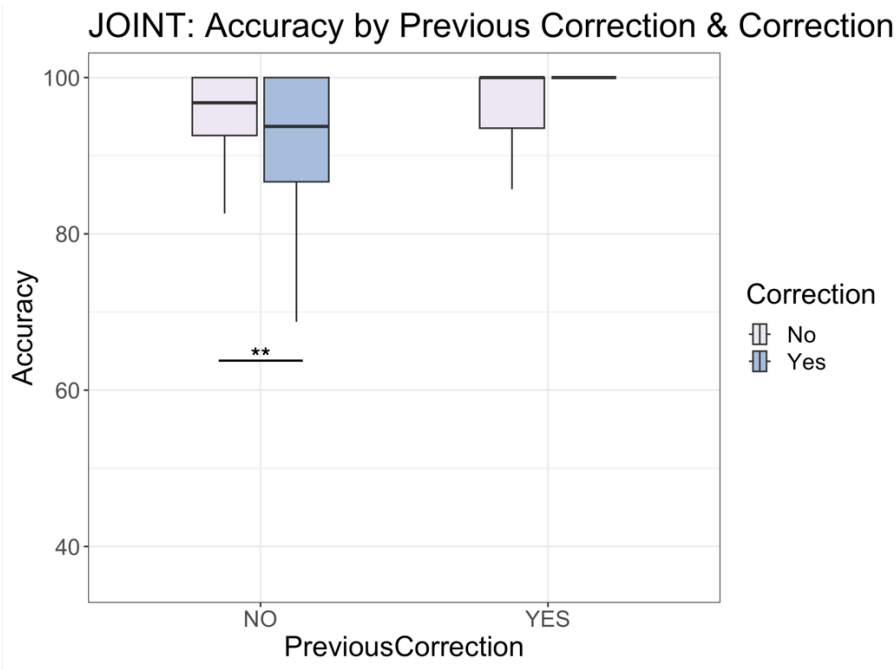

Figure 5.9. Box plots showing mean Accuracy scores in Correction and PreviousCorrection trials averaged across "Joint" blocks. Asterisks represent significant interaction effects (** $p<0.01$; * $p < 0.05$).

A linear mixed model on Time-To-Contact using Correction, Previous Correction, Movement, Instruction and their interaction as factors showed a significant main effect

of Instruction ($p = 10^{-2} \times 6.3$), Correction ($p < 0.01$) and of their interaction ($p = 10^{-2} \times 6.3$). Time-To-contact was slower if a correction is required, and in Interactive compared to Guided but only when a motor correction doesn't take place (Figure 5.10).

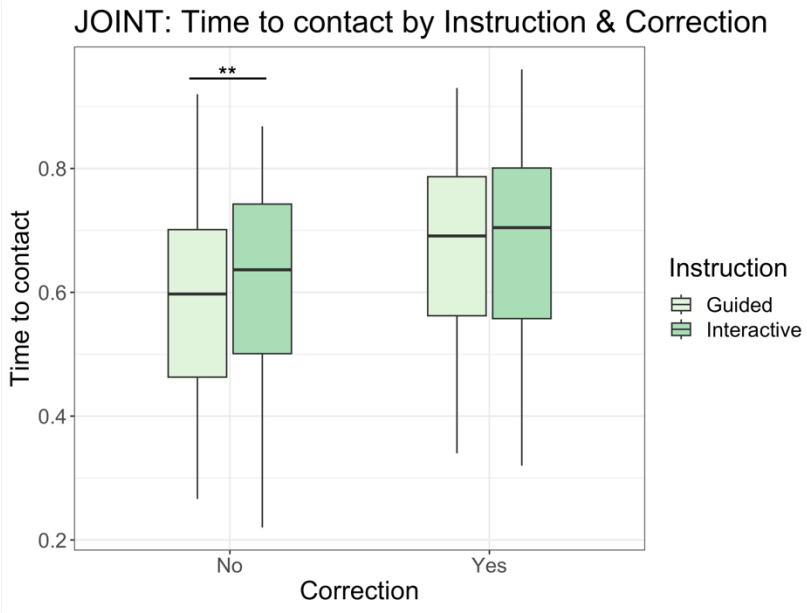

Figure 5.10. Box plots showing mean Time To Contact in Correction trials, separately for "Guided" and "Interactive" blocks during joint actions. Asterisks represent significant interaction effects (** $p<0.01$; * $p < 0.05$).

We also found a tendency toward significance of a three-way interaction of Instruction, Movement and Previous Correction ($F = 6.13$, $p = 0.013$): a significant difference between Guided and Interactive (i.e., Guided faster than Interactive) was found only in Same trials that were not preceded by correction trials (Figure 5.11).

Figure 5.11. Box plots showing mean Movement Time according to "Instruction" (Guided or Interactive), "PreviousCorrection" (YES or NO) and "Movement" (Opposite or Same) in joint actions. Asterisks represent significant interaction effects (** p<0.01; * p < 0.05).

A linear mixed model on RTs using Previous Correction, Movement, Instruction and their interaction as factors showed a significant main effect of Instruction (p = 0.0022), and a tendency toward significance of Movement (F = 5.3, p = 0.011). RTs were higher in Interactive and Opposite movements (Figure 5.12).

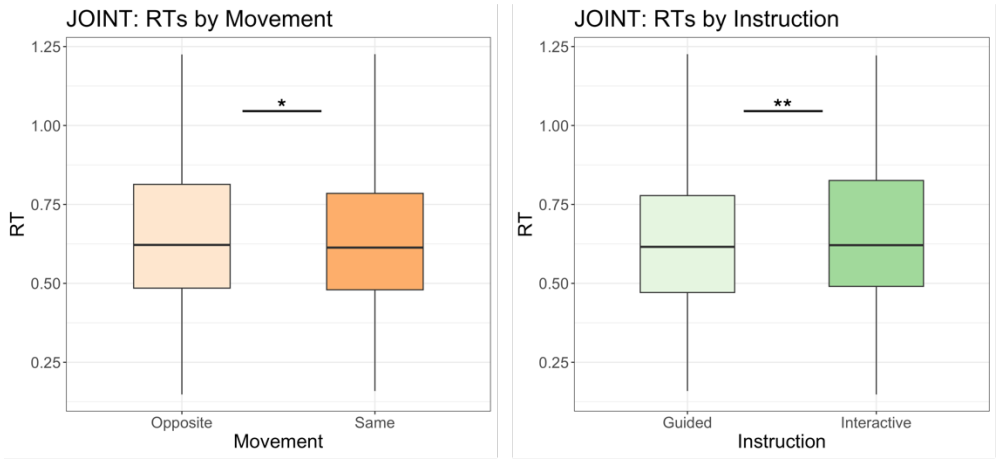

Figure 5.12. Box plots showing mean Reaction Time (RT) according to "Movement" (left) and "Instruction" (right) factors in joint actions. Asterisks represent significant comparisons (** p<0.01; * p < 0.05).

5.3.4 Kinematic results

Differently from behavioral analyses, kinematic analyses included the distinction between precision and power grips. They were performed to attain a three-fold aim. First, we wanted to validate the VR protocol assessing its validity in distinguishing precision and power movements. This analysis mainly targeted the wrist height and grip aperture. In a second place, we aimed to verify if experiencing a perturbation in the current or the previous trial could affect the temporal evolution of the movement kinematic properties. Finally, we hypothesized that simulative motor processes during social interactions could impact kinematics.

Individual actions

A linear mixed model on maximum wrist height using Correction, Grip, and their interaction as factors showed a main effect of Correction ($p = 10^{-8} \times 3.7$), Grip ($p = 10^{-15} \times 2.2$), and a significant interaction Correction*Grip ($p = 10^{-15} \times 2.2$) that fully explained the main effects. Indeed, only in trials without a motor correction the maximum wrist height was higher in precision than power grip. A similar effect was found for maximum grip aperture, whereby we obtained a significant main effect of Grip ($p = 10^{-7} \times 4.4$), which was explained by its interaction with Correction ($p = 10^{-3} \times 8.1$): only in trials without a motor correction the maximum grip aperture was higher in power than precision grip (Figure 5.13).

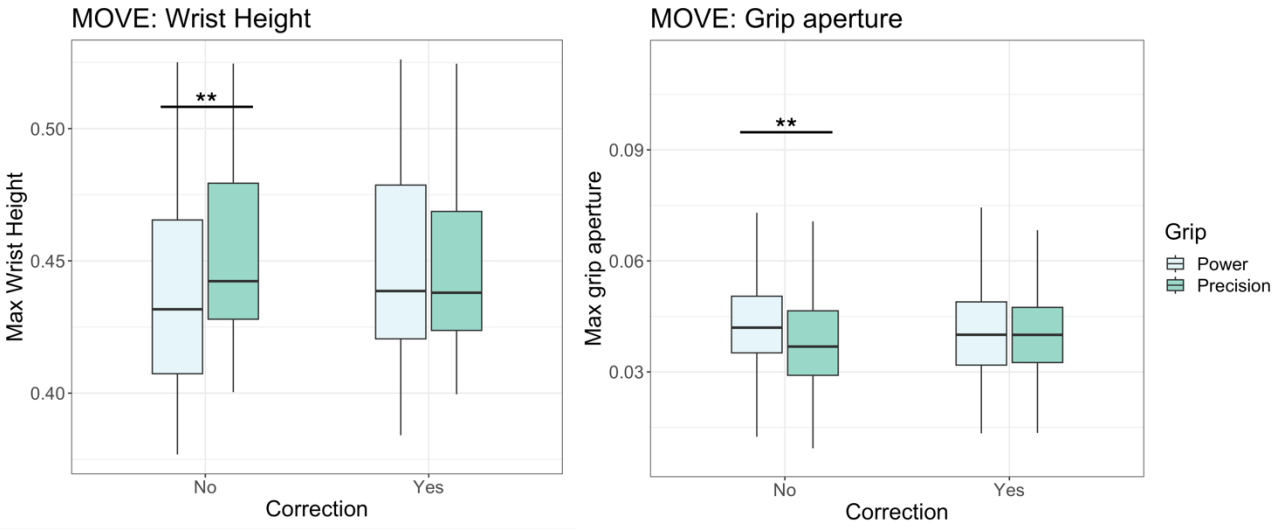

Figure 5.13. Box plots showing mean maximum wrist height (left panel) and grip aperture (right panel) averaged separately for each "Correction" and "Instruction" level in individual ("Move") actions. Asterisks represent significant interaction effects (** p<0.01; * p < 0.05).

A linear mixed model on maximum wrist height latency % using Correction, Grip, and their interaction as factors showed a main effect of Correction ($p = 10^{-3} \times 5.8$), Grip ($p = 10^{-15} \times 2.2$), and a significant interaction Correction*Grip ($p = 10^{-6} \times 8.1$). Participants reached the maximum wrist height later during the movement in precision compared to power grips; in power grips, trials with a correction speeded the latency of the wrist height. Finally, a tendency toward significance was found in the interaction between Correction and Previous correction ($p = 0.018$), whereby in trials requiring a motor correction, the latency was higher if a correction occurred also in the previous trial (Figure 5.14).

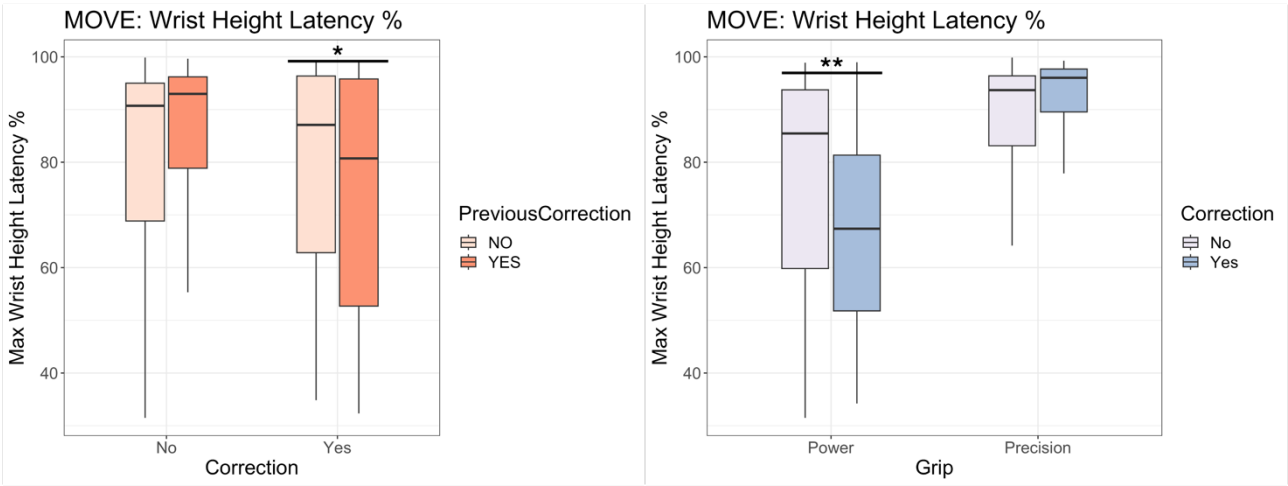

Figure 5.14. Box plots showing mean maximum wrist height latency in percentage relative to the full movement (left panel) and grip aperture (right panel) averaged separately for each "Correction" and "Instruction" level in individual ("Move") actions. Asterisks represent significant interaction effects (** p<0.01; * p < 0.05).

Results of the linear mixed model on the latency of maximum grip aperture showed only a significant main effect of Grip ($p = 10^{-7} \times 3.9$), being higher in power vs precision grips (Figure 5.15).

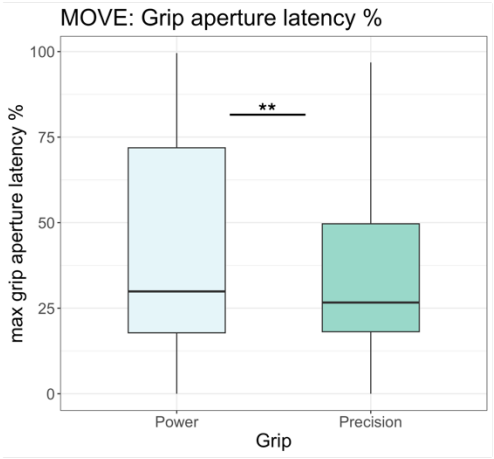

Figure 5.15. Box plots showing mean maximum grip aperture latency in percentage relative to the full movement averaged separately for each Grip type in individual ("Move") actions. Asterisks represent significant comparisons (** p<0.01; * p < 0.05).

Joint actions

A linear mixed model on maximum wrist height using Instruction, Correction, Movement, Grip, and their interaction as factors showed a main effect of Correction ($p = 10^{-15} \times 2.2$), Grip ($p = 10^{-15} \times 2.2$), and Movement ($p = 10^{-4} \times 4.3$) and a significant interaction Correction*Grip ($p = 10^{-15} \times 2.2$). Wrist height was higher for precision grips, but it was also differently modulated by motor corrections, being higher in correction trials for power grips, and no-correction trials for precision grips. Wrist height was also higher for complementary vs imitative movements (Figure 5.16).

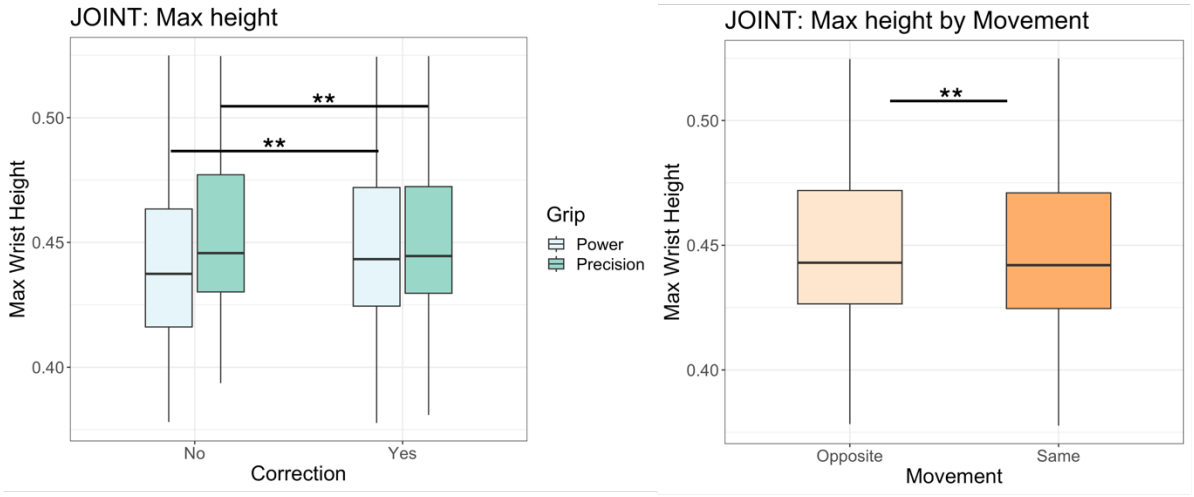

Figure 5.16. Box plots showing mean maximum wrist height averaged separately for each Grip type and Correction level (left panel) and Movement (right panel) in Joint actions. Asterisks represent significant comparisons (** $p<0.01$; * $p < 0.05$).

When analyzing the maximum grip aperture, we found a main effect of Instruction ($p = 10^{-4} \times 8.6$) and Grip ($p = 10^{-15} \times 2.2$), and a significant interaction Correction*Grip ($p = 10^{-6} \times 3.7$). Grip aperture was higher in power vs precision grip. Moreover, it was higher in precision grip when a correction took place, while it was higher in power grip when no correction occurred (Figure 5.17).

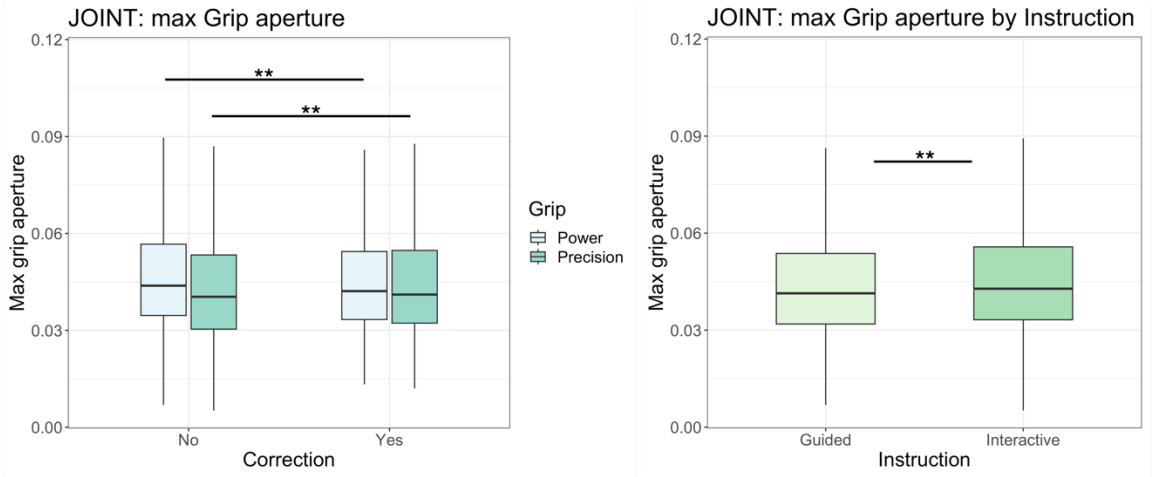

Figure 5.17. Box plots showing mean maximum grip aperture averaged separately for each Grip type and Correction level (left panel) and Instruction (right panel) in Joint actions. Asterisks represent significant comparisons (** p<0.01; * p < 0.05).

A linear mixed model on maximum wrist height latency % using Instruction, Correction, Movement, Grip, and their interaction as factors showed a main effect of Correction ($p = 10^{-7} \times 1.8$), Grip ($p = 10^{-15} \times 2.2$), and a significant interaction Instruction*Correction ($p = 10^{-2} \times 8.9$). In guided trials with a correction, participants reached faster the maximum wrist height. Latency was higher for precision vs power grips (Figure 5.18).

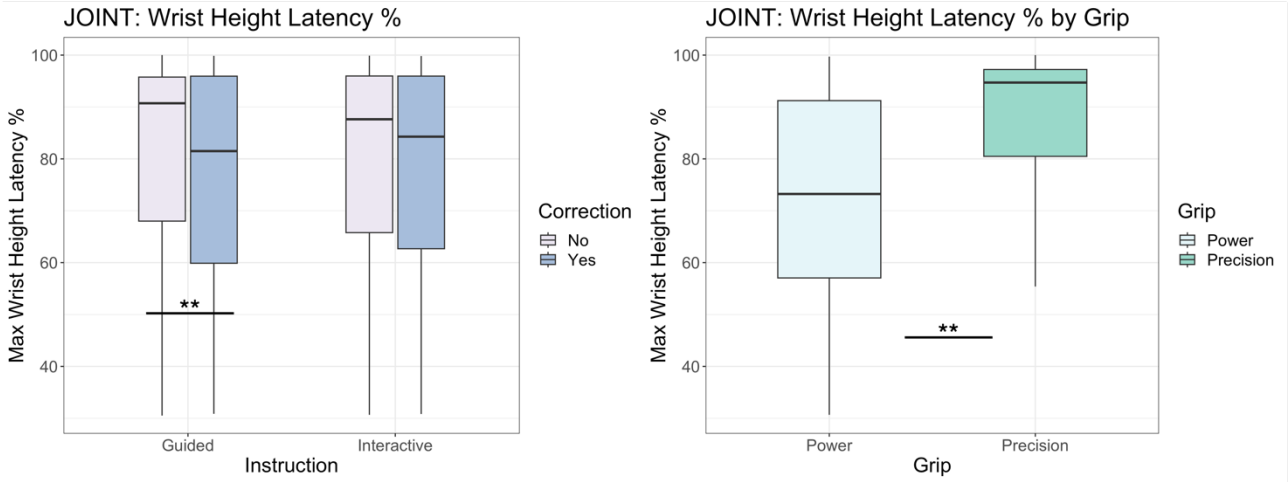

Figure 5.18. Box plots showing mean maximum wrist height latency in percentage relative to the full movement averaged separately for each Instruction and Correction level (left panel) and Grip (right panel) in Joint actions. Asterisks represent significant comparisons (** p<0.01; * p < 0.05).

The same analysis on maximum grip aperture latency % only revealed a main effect of Correction ($p = 10^{-5} \times 5.9$) and Grip ($p = 10^{-15} \times 2.2$), with values being higher in trials where a correction occurred and in power grips (Figure 5.19).

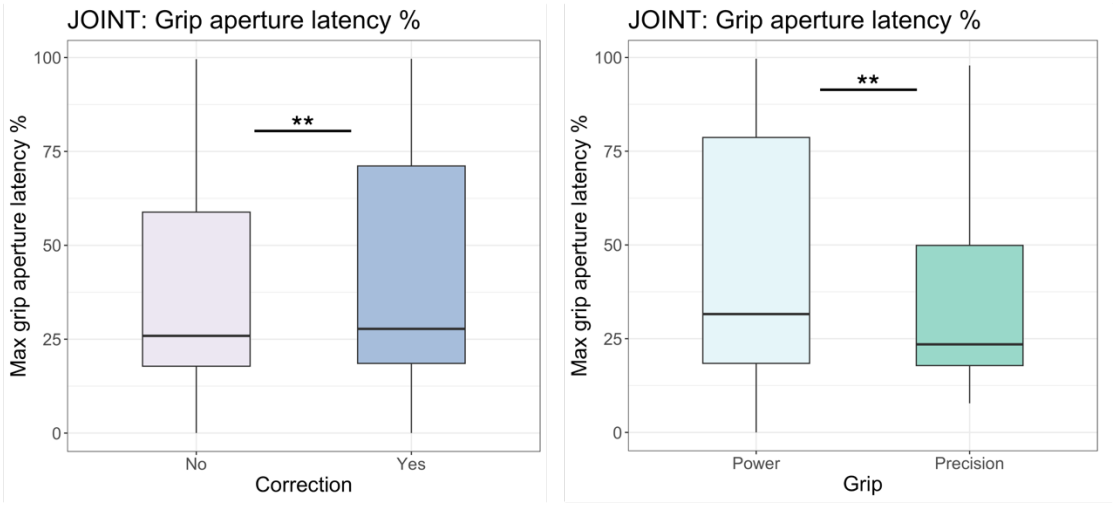

Figure 5.19. Box plots showing mean maximum grip aperture latency in percentage relative to the full movement averaged separately for each Correction level (left panel) and Grip (right panel) in Joint actions. Asterisks represent significant comparisons (** $p<0.01$; * $p < 0.05$).

5.4 Discussion

In this study, we aimed to investigate fast motor corrections in response to unexpected external events in a virtual reality grasping task. As our exchanges with the environment are often embedded in social scenarios, we tested the eventual influences of social interactions on action update by measuring behavioral, physiological, and kinematic indices during individual and joint actions.

5.4.1 Methodological considerations

In building the paradigm, we attempted to carefully balance all these experimental factors to make the task suitable for following fMRI investigation. Hence, while sharing most features with similar grasping paradigms adopted in our previous behavioral and neuroimaging studies (Sacheli et al., 2015; Moreau et al., 2020), this task has been designed to achieve a higher degree of similarity of contextual cues across conditions. Thus, we rearranged the non-socially cued condition ("Guided"). In the previous studies, trials in the "Guided" blocks were introduced by a high or low pitch sound, indicating to execute a precision or a power grip. Hence, participants knew from the very beginning of the trial the final grip configuration to achieve. On the other hand, during the "Interactive" condition the trajectory of their movement toward the target evolved

together with that of the partner, and it wasn't possible to predict in advance the final grip configuration. Furthermore, to counterbalance social and non-social contributions in "imitative" and "complementary" actions, "same" and "opposite" conditions were introduced also in the "Guided" condition.

To overcome these uncontrolled differences between the two conditions, we cued the grip type by lighting up one of the two target buttons on the bottle to indicate a power (bottom button) or precision (upper button) grip. We tried to match in time social and non-social cues and spatial update. To this end, we extracted the timing at which the partner's movements signaled a change of intention and used them to cue the lighting on the bottle. In a control condition ("Move"), participants moved at their own pace, spatially tuned to the light on the bottle, without any kind of social interaction. In joint actions, fulfilling the goal could require adapting to the virtual partner's action in time and space ("Interactive" condition) or only in time, while adapting in space to the light cue appearing on the bottle ("Guided" condition). Finally, an online target update was made possible by switching the bottle's light after movement onset. One could argue that being the Guided condition more challenging in terms of divided attentional processes, participants could make more mistakes and fail to adapt in time with the virtual partner. Fixation analyses suggested that participants were performing a very small amount of fixations on the partner during Guided condition, therefore they were likely using peripheral vision to check the other's movement timing. However, the two joint conditions showed comparable accuracy scores and grasp asynchrony, as the only significant difference in synchrony we found was modulated by a co-occurrence of other factors (i.e., no-correction, no-previous correction trials). We conclude that during the Guided condition participants could attain both task demands without worsening their performance.

Notably, HRV was higher in the Interactive condition than in the Move and Guided ones, with no difference occurring between the last two. These differences are unlikely explained by different task difficulty, as accuracy was comparable across conditions. We

believe that this result is entirely linked to socially-driven effects via vagally-mediated inhibition of the sympathetic system. Adapting one's own movement in time and space to a partner, trying to delineate the other's motor intentions, can stress cognitive flexibility, attentional mechanisms, and self-regulation, all variables linked to heightened heart-rate variability (Thayer and Lane, 2000; Forte et al., 2019; Deits-Lebehn et al., 2023).

In the next subparagraphs, we will discuss the kinematic analyses we conducted to reveal whether the virtual reality implementation of the task succeeded in distinguishing different grip type configurations. We will then discuss the effect that fast motor correction stressing the error monitoring system exerts on behavioral and kinematic indices both across consecutive trials and within each perturbed trial. Eventual modulation of these processes driven by social interactions will be signaled.

5.4.2 Kinematic indices and their modulation by social interactions

Despite the absence of real hand-object interaction, we expected hand movement kinematics to distinguish power and precision grip configurations in terms of different grip apertures. Given the peculiar spatial features of our task, we also expected to find a difference in the height of the wrist. Indeed, in our setup the power and precision grips are always executed with the same spatial pattern (namely, towards the lower and the higher part of the bottle, respectively). Our results confirmed these predictions. During individual actions, the height of the wrist was higher for precision vs power movements, and the grip aperture was bigger for power vs precision movements whenever a motor correction did not take place. We also found that the latency of the maximum wrist height was slower in precision than power grips, being the target farther from the hand starting position for precision vs power movements. Intuitively, the latency of the maximum grip aperture was slower in power than precision grips.

While confirming these results, joint actions enhanced the differences between the two grip types whenever a correction occurred: power corrected movements reached higher wrist height and smaller grip aperture than non-corrected movements, while precision movements showed the opposite trend. Overall, these results are in line with the non-

virtual version of the paradigm implemented by Sacheli and colleagues (2015), hence indicating that participants effectively preshaped for a different configuration grip before being forced to a change of trajectory and hand shaping.

We also found evidence of a sensorimotor simulation induced by Joint actions. The maximum grip aperture was overall wider during the "Interactive" than the "Guided" condition. The target update in the Guided condition, which was abrupt (vs. the smoothed change in the trajectory of the partner's movement in the "Interactive" condition), led to a faster change in the participant's trajectory. Indeed, we found a lower latency of maximum wrist height during the Guided vs the Interactive condition.

Overall, these results confirm that we could distinguish between different grip configurations despite no real hand-object interaction taking place and that interactive behaviors could modulate kinematic properties of participant's movements.

5.4.3 Intra- and inter-trial effects of fast motor corrections

Performing a fast motor correction led to different effects based on whether actions were carried out in an individual or social context. In the former case, the rapid target update induced more errors and increased the movement time compared to unperturbed trials. Only the movement time was affected by target update during joint actions, where it was likely associated with increased latency to attain the maximum grip aperture. During the more demanding joint actions, accuracy was somewhat preserved during perturbed trials, but the update of the movement trajectory was susceptible to interference from inter-trial effects. Such effects can be partially explained in light of the conflict monitoring theory (Botvinick et al., 2001). According to this theory, after committing errors motor responses are partially inhibited, namely the threshold in M1 to elicit an overt action increases. Simultaneously, more efficient attentional processes and post-error focusing (Verguts et al., 2011) take place in task-related brain areas. At behavioral level, these mechanisms emerge through a number of effects such as post-error slowing (PES), improvements in accuracy (PIA), and reduction of interference (PERI) that are partially independent of each other. Their (eventually co-) appearance also depends on the task

difficulty (Danielmeier et al., 2011). Post-error adjustments are supposed to be triggered by top-down signals rising from the performance monitoring system and probably share underlying mechanisms with those intervening after infrequent events (Notebaert et al., 2009).

We believe we tapped into such mechanisms when analyzing the effects on accuracy, RTs, and Time-To-Contact in the trials following a motor correction. Contrary to the typical occurrence of the PES effect, we did not detect effects on RTs in individual or joint actions. This is entirely foreseen as our participants were not asked to perform the movement as quick as possible, but at their own (individual) or the partner's (joint) pace. However, the perturbation occurred in the previous trials affected other high-level motor properties of the reach-to-grasp trajectory. During individual actions, we observed that following a perturbed trial the Time-To-Contact increased, i.e., participants executed the movement more slowly, compared to the trials that were not preceded by a perturbed trial. During joint actions, the necessity to synchronize the movement with the partner likely compensated for this effect. Here, differently from individual, less demanding actions, accuracy increased after correction trials. Furthermore, having executed a motor correction in the previous trial improved performance during perturbed trials. This suggests that after an unpredictable target update, participants could adaptively change their response threshold to embrace the possibility that another unpredictable event could occur as they were acting in a non-stationary environment, ultimately becoming more cautious (Dutilh et al., 2012). This hypothesis is also suggested by the increased time to attain the maximum wrist height we detected. In sum, after the unexpected event and the necessity to modify on flight one's own movement, behavior is rapidly optimized toward reiterative environmental demands, potentially because the most recent, "novel", and rarer evidence is prioritized.

5.5 Conclusion

Overall, we succeeded in creating a grasping paradigm to identify mechanisms of online update of movements based on social or non-social cues. While reaching ceiling effect in

the accuracy score, the task was still very demanding and engaging, therefore making the paradigm suitable for the fMRI implementation of the study which will be described in Chapter 6. However, the present study is not exempt from limitation.

First, we could not match the two joint action conditions in every aspect. Indeed, in the "Guided" condition the cue was provided as a light, which only had two states: on or off. Instead, in the "Interactive" condition the grip type was cued by a natural movement executed by the partner, who gradually shifted towards a power or precision grip, or eventually changed the trajectory to simulate the occurrence of a change in intentions. One possibility was to create a "probability cloud" where the light was gradually turned on or off. However, this would have interfered with the request of synchronize in time with the partner's movement, which was common across the two conditions as a form of joint action.

On a technical note, while the hand was laying on the virtual cushion and the chair arm in the real world, the starting position of the fingers was free, and participants were not instructed to join index and thumb at the beginning of the trials. Thus, some behavioral analyses on grip aperture reported in the literature (Candidi et al., 2017) could not be replicated. Furthermore, with the current experiment we could only perform analyses of the HRV on blocks, hence modeling only the "Instruction" condition.

Together, the consistence of our results with the previous studies on a similar paradigm supports the validity of the usage of virtual reality settings to investigate fast motor adaptation and social interactions.

CHAPTER 6

Scripts to run MOTUM in Unity and the custom skeleton we created for the QTM software are available as Package at the following link:

https://github.com/fbencive/Unity-MOTUM

MOTUM: a Motion Online Tracking Under MRI system

Federica Bencivenga[1,2,3], Federico Giove[4], Steve Gazzitano[2], and Gaspare Galati[1,2]

[1] Department of Psychology, "Sapienza" University of Rome, Rome, Italy

[2] Cognitive and Motor Rehabilitation and Neuroimaging Unit, Santa Lucia Foundation (IRCCS Fondazione Santa Lucia), Rome, Italy

[3] PhD Program in Behavioral Neuroscience, Department of Psychology, "Sapienza" University of Rome, Rome, Italy

[4] Marbilab, Enrico Fermi Centre, Rome, Italy

Abstract

Attempts to implement realistic body-environment interactions during fMRI experiments have resulted in the development of expensive, hardly reproducible, and task-specific setups. Here, we introduce MOTUM, a motion online tracking under MRI system. MOTUM uses an amagnetic motion tracking setup to track body parts' movements and reproduces them in real-time in virtual reality environments, wherein both the requisites of realism and experimental control are met. We tested MOTUM during a grasping task (N = 2) including joint actions performed with a virtual avatar, individual actions, and action observation. As a safe check, we estimated to what extent participants' movements affected the quality of the recorded brain signal. Then, we proceeded to show the potentialities of this system to dissociate socially and non-socially

prompted motor goals and detect the neural underpinnings of fast hand movement corrections in response to unpredictably changing task demands. We end by discussing other potential applications of this system, ultimately claiming that it can potentially revolutionize real life neuroscience research.

6.1 Introduction

Body-environment motor interactions can be acknowledged between the most theoretically and methodologically challenging topics in neuroimaging research. The richness of the motor behaviors driving our exchanges with the environment is hard to replay in experimental setups, whereby the necessity of controlling confounding variables leads to studying motor control under simplified, almost impoverished, conditions, where movement is paradoxically constrained. This limit massively affects research in the domain of visuomotor functions, namely the mechanisms through which objects' properties are extracted by visual inputs and turned into motor actions (e.g., pointing, reaching, or grasping). Most of our knowledge of such behaviors comes from experiments where participants reach simplified targets, e.g., dots in the space, or grasp ad hoc created objects with simple geometrical configurations (e.g., manipulanda).

This issue hits even heavier neuroimaging experiments. During electroencephalography (EEG), magnetoencephalography (MEG), and functional magnetic resonance imaging (fMRI) recordings, participants' movements must be limited due to structural, mechanical, and technical constraints. For instance, body movements can affect the quality of the recordings, resulting in enhanced noise in the recorded signal. Such practical issues have led neuroscientific research to an extreme simplification of the body-environment interactions we daily experience, overall setting boundaries to our knowledge of the neural correlates of motor control. It is therefore unclear how well current theories on motor control are valid under more naturalistic and dynamic real-life situations.

To overcome such issues, fMRI studies aimed at unraveling the neural substrates of hand-object interactions such as reaching or grasping movements have adopted workarounds.

They include the projection of 2D visual stimuli on a mirror placed in the scanner in place of the presentation of real, 3D objects. In these studies, participants were required to execute pantomime movements pretending that the images showed real objects located near their hand (Przybylski et al., 2017; Sulpizio et al., 2020). Nevertheless, action representations, especially in high-order cognitive (e.g., parietal) areas, are affected by the realness of the objects to interact with (Króliczak et al., 2007). Another option is to use real objects under MRI, which is not exempt from issues, though. Jody Culham's group has introduced the "Grasparatus" (Culham et al., 2003), implemented by applying a 5° tilt to the shallow ramp and a 20-30° tilt to the participant's head using foam. With this apparatus, subjects could see their own hand movements and interact with real objects located on a bracket above the MRI table. However, to widen the range of objects to be presented additional devices must be set up. For instance, Brandi and colleagues (2014) have introduced the "Tool-Carousel", a box with six compartments that can hold different objects and be turned around its central axis; Nowik and colleagues (2019) developed a new version of the "Grasparatus", consisting of two rotating drums connected with side panels and a conveyor belt, on top of which the objects were mounted; Knights and colleagues (2022) have used a turntable. In most cases, objects have been created using a 3D printer.

While with these setups true hand-object interactions can be achieved, the number of available action possibilities is limited. These setups successfully tap into static motor control, i.e., conditions where action planning straightforwardly turns into motor commands, but they can't deal with dynamic motor control, i.e., the way motor plans are updated and adapted *while movement unfolds*. This is a central issue for real-life neuroscience that should take into account daily challenges to our motor behaviors, e.g., whenever we must correct our movements while they are being implemented. Some attempts to create ad-hoc settings to target dynamic motor control have been made. For instance, to investigate the neural encoding of obstacles during grasping movements toward a target, Chapman and colleagues (2011) used a platform positioned over participants' hips on top of which they positioned both the objects to be grasped and a

set of handles to be manipulated to move cylinders, acting as obstacles impeding to grasp the target object. The drawback is that the handles were meant to be manipulated by an experimenter located inside the scanner room. In another study aimed to infer the neural mechanisms dealing with adaptive behavior in response to unpredictable changes in the object's orientation, an experimenter was present in the scanner room to manipulate the object's orientation (Baltaretu et al., 2020). In both cases, the role of the experimenter was crucial, and a cautious implementation of the experiment was necessary to respect the timeline of the experimental paradigm.

In this paper, we significantly boost neuroimaging research toward easily and replicable dynamic motor behaviors by introducing the MOTUM (Motion Online Tracking Under MRI) system, a methodology able to overcome current limits in the neuroscience of motor control by using virtual reality combined with an MRI compatible motion tracking system. Virtual reality makes it possible to create naturalistic environments with a high degree of control, therefore fitting the idea of realistic, but still manipulable, scenarios. Using MOTUM, participants can act in these environments by means of a virtual 1st person avatar, whose movements are created and updated according to the real-life position and rotation of the participants' body parts. This is achieved using a set of MRI-compatible cameras performing an online tracking of body position and an amagnetic glove to track finger movements, both broadcasting information to a VR software (Unity 3D). To test MOTUM, we adapted a joint grasping paradigm developed by Sacheli and colleagues, whose behavioral and kinematic features and neural correlates have already been extensively described in a collection of studies (Sacheli et al., 2012, 2015; Moreau et al., 2020). In this task, participants interacted with a virtual partner and were asked to on-flight adjust their grip type in response to unpredictable changes in the task demands. While describing the results of this experiment as an example of how MOTUM can overcome the limited landscape of body-environment interactions feasible in the MRI setting, we will also discuss the potentiality of this system to boost real-life neuroscience in the wider frame of body representation and body-environment interactions.

6.2 Methods

We will start the methods section by describing how we implemented the motion tracking system, the challenges we faced in doing so, and the way we tried to optimize the system given the constraints of the scanner room we operated in.

MOTUM is composed of three main parts (Figure 6.1): three cameras to track hand and forearm movements, an amagnetic glove to track finger movements, and VR glasses.

The first component of the system is a set of cameras to track markers we positioned on participants' right arm, overall reconstructing its rotation and position in the space. Related to that, we faced three main issues: a) the optimal positioning of the cameras allowing us to track markers that were partially inside the MRI coil; b) the optimal positioning of the markers on the arm to build up a skeleton-like configuration; c) the training of a model that could leverage acquired knowledge on the mechanical properties of the movement to be executed to eventually compensate for a sub-optimal tracking of the markers during the whole fMRI acquisition.

The second component of MOTUM is an amagnetic glove to track the flexion and extension of the fingers. Theoretically, by positioning markers on each finger we could have tracked their movements using the same camera system we adopted to track arm movements. However, we had a limited number of cameras (only 3) and it would have been necessary to use at least three markers for each finger (one for each joint). With this setup, it would have been nearly impossible to avoid markers' collinearity. Hence, the usage of a glove was the best workaround possible. Viceversa, getting rid of the cameras and using the glove only wouldn't have allowed us to track arm position and rotation in the space: the glove is made to track only the fingers, and not the wrist nor the forearm.

The third component of our system is the glasses to display a stereoscopic view. Indeed, all the inputs on subjects' movements converge into a virtual reality environment. In doing so, we dealt with the issue of tailoring the virtual environment to individual

features such as the pupillary distance, the real length of participants' arms, and their general comfort when carrying out the movement.

In the next paragraphs, we will describe the features of the camera system, the glove, and the VR glasses. Then, we will start describing the acquisition protocol we used. Finally, we will discuss how we tailored the environment view to each participant for our specific task and virtual scenario. The endpoint of the method section will be the description of the task we used to validate the system and the fMRI data analyses.

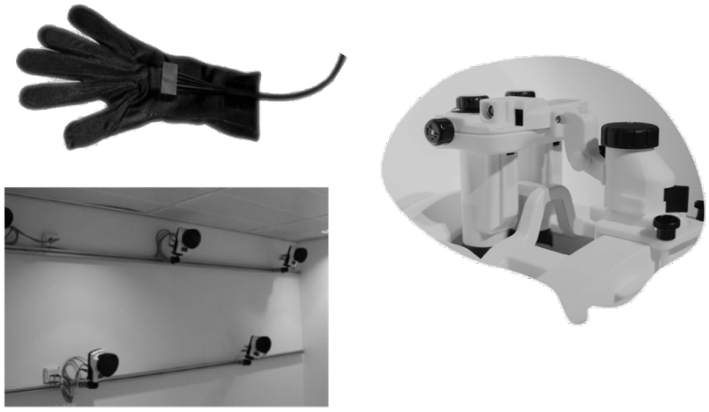

Figure 6.1. Components of MOTUM system: the amagnetic glove, the MRI-compatible cameras, and the VR glasses.

6.2.1 Camera system

A Qualisys MRI-compatible motion capture system was used to track arm and wrist position and rotation movements via the Qualysis Track Manager (QTM) software.

Three electromagnetically shielded cameras (Oqus 310; diameter 12cm) were mounted in the scanner room, facing the entrance of the scanner (see Fig. 6.2). Three is the minimum number of cameras to perform a 3D reconstruction of markers' position in space. As participants were to execute the movement with the right hand, after several attempts we achieved the best configuration possible for our scan room: we distributed the cameras along the frontal wall of the scanner, positioning the first camera (n° 1) slightly farther the left side and last camera (n° 3) slightly farther on the right side of the wall facing the scanner. Cameras were also distributed in slightly different positions along the vertical

and z-axis, the last one being achieved by manipulating each camera support. This allowed us to achieve the deepest view possible, partially covering the inside of the scanner where the participants' hand was supposed to be located. Figure 6.2 reports a schematic representation of camera positioning including the distance between the cameras and with the isocenter of the scanner.

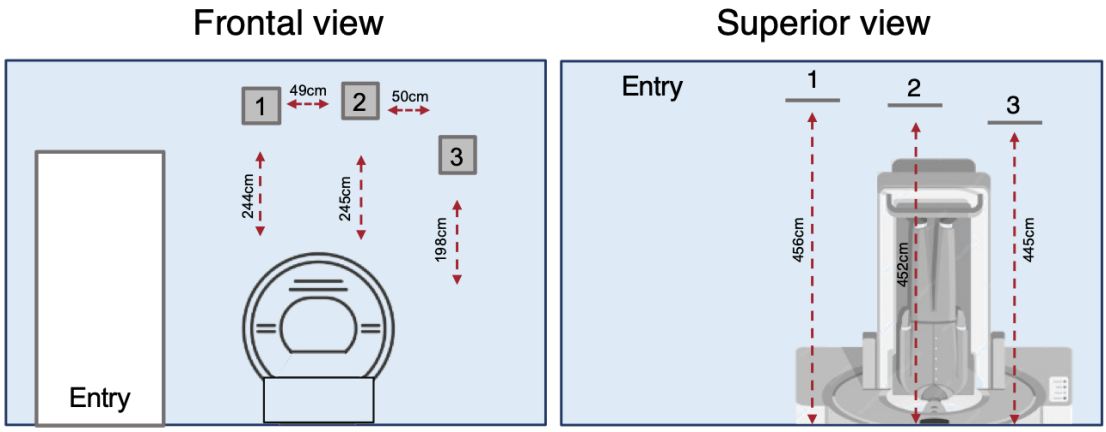

Figure 6.2. Schematic representation of the camera positioning from a frontal and a superior view of the scan room. Distances are computed respect to the isocenter of the scanner.

A crucial point to perfectly calibrate the system was to block unwanted static reflections. To do so, we turned off the scan screen (making sure it resulted black) and then used the built-in "Auto-mask" function that creates masks over eventual phantom markers.

System Calibration

The first step of the acquisition was the system calibration. This step serves to define the position of the world relative to the cameras, and that of each camera relative to the others. Calibration must be performed before each acquisition session.

As a first step, we moved the MRI table forward to reach the entrance of the scanner, at 1063mm from the magnet isocenter.

The system calibration is performed by using two calibration objects. One of the two objects, i.e., the reference object, is a stationary L-shaped structure with four markers on it. The reference object serves to define the origin and orientation of the coordinate system to be used. We positioned it at the top-left corner of the MRI table (Figure 6.3). The other object, i.e., the calibration wand, is a T-shaped object (length = 301.4 mm) with two markers at the two opposite extremes. The calibration is performed by doing a 60s recording during which the calibration wand is moved by an experimenter in the environment in the 3 axes. Throughout the acquisition, it is fundamental to avoid that the experiment's body or the wand itself could cover the view of the markers on the L-shaped object. This registration is used to generate data defining the location and the orientation of the cameras relative to the reference object.

To keep consistent with standard neuroimaging practice, we set the coordinate system orientation as follows: the vertical axis was identified as the Y-axis (positive = up), whereas the horizontal axis corresponded to the X-axis (positive = right). Due to the shifted location of the reference object with respect to the magnet isocenter, the origin of the system was translated as follows: X = 315 (i.e., the horizontal displacement of the L-shaped object's corner and the isocenter of the scanner); Y = 0; Z = 1063.

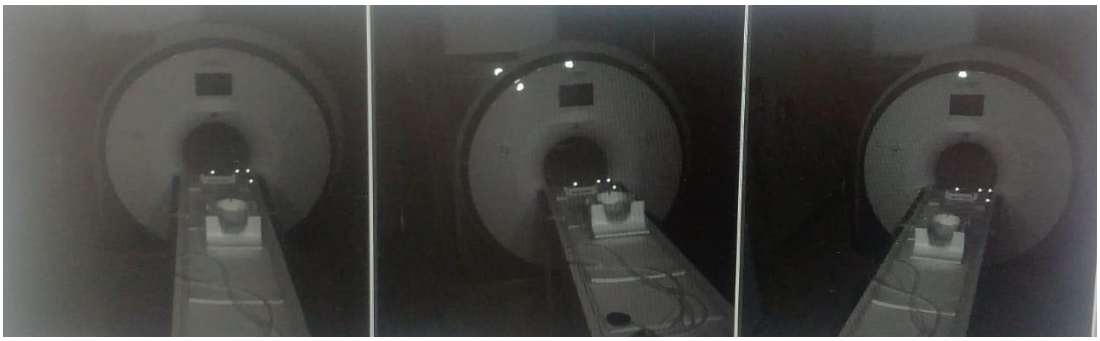

Figure 6.3. Calibration setup from the three camera views. The L-shaped object with 4 markers is in the upper right corner of the scanner table.

Markers' positioning

One key point for the cameras to correctly track the markers was to avoid their collinearity. To overcome this issue, we used cushions to slightly tilt participants' arm so that the height of the elbow, the forearm, and the wrist was higher than the height of the hand.

We used five markers (12.5mm diameter) that were positioned on the subject's right arm and hand as follows: 1) on the outer elbow (bony prominence), 2) on the forearm, 3) on the outer (pinky side) and 4) the inner (thumb side) bones of the wrist, and 5) below the ring finger's knuckle of the right hand, in agreement with the marker description provided by QTM (Animation-Marker-Set) (Figure 6.4). Note that all the markers but the one on the elbow (1) and the forearm (2) were positioned on top of the amagnetic glove. The markers were positioned in a way not to form a straight line relative to each other: they were slightly displaced along the horizontal axis to avoid marker collinearity.

Figure 6.4. Location of the 5 markers on the participant's arms, following the Qualysis Animation Marker Set manual.

6.2.2 Amagnetic glove

To track the fingers' movements, we used an amagnetic right-hand glove (Fifth Dimension Technologies; 5DT Glove Ultra 14 sensors MRI compatible). In our experience, the glove is larger than the medium hand size. Therefore, to increase its stickiness to the skin we placed a rubber glove on top of it. We used different glove sizes (XS, S, M) depending on participant's hand size.

The amagnetic glove must be calibrated for each participant in order to set the maximum and the minimum flexion values for each finger. These values were set by asking each participant to perform 4 types of movements:

1. Fist with the thumb flexed in the most internal part of the hand;
2. Thumb flexion with the other fingers extended;
3. Open hand;
4. Flat hand.

The maximum and minimum flexion values could be stored for successive loading.

6.2.3 Virtual reality glasses

To reproduce the VR environment, we used the NordicNeuroLab VisualSystem HD which can display a stereoscopic view with high visual fidelity and without compromising the picture refresh rate. Each display (left or right) is driven separately via a standard HDMI port. The images were projected from Unity to the two displays by adapting a NordicNeuroLab Unity package available on Github (https://github.com/nordicneurolab/vshd-unity-example).

To achieve the highest comfort, the pupillary distance and the distance of the glasses from participants' eyes could be set via small wheels located on the device.

6.2.4 Acquisition procedure

Subject preparation

Each acquisition started with the camera calibration as described above.

After entering the scanner room, subjects were asked to sit on the MRI table and wore the NordicNeuroLab VisualSystem HD. The glasses were turned on to allow participants to see the environmental scene and regulate the pupillary distance and the position of the glasses. Afterward, subjects wore the amagnetic glove and a rubber glove on top of it and performed the four movements previously described useful to calibrate the amagnetic

glove. Each movement to be performed was cued by an example image that was delivered on the screen.

Next, the glasses were turned off and participants were asked to lie on the MRI table, wearing headphones. The coil was placed on their heads, and the glasses were placed on top of the coil. Participants were asked to regulate the distance of the glasses to ensure comfort. The subject's right hand was sustained by cushions to ensure comfort and the five markers were positioned on the arm.

AIM recording

A key feature of the Qualisys Track Manager (QTM) software is the possibility to create an automatic identification of markers (AIM). With this function, QTM automatically identifies and labels movement trajectories, a crucial aid to maintaining a stable reproduction of the movement even when markers are not completely visible during the entire movement. AIM must be generated by a trial in which the specific motion one is going to track is recorded, in our case consisting of a set of repetitions of the grasping movement. It is crucial that the markers are correctly tracked throughout the whole AIM trial. We experienced that this was hardly achievable when participants were completely inside the scanner as during the acquisition of MRI images. Hence, we decided to acquire the AIM trial when participants were lying on the MRI table but not within the scanner. After the montage of the glove and the markers, the MR table was moved until ~35cm from the magnet's isocenter. From this distance, we ensured that all the markers were clearly visible, and asked participants to perform a grasping movement. Starting with their right hand laying along their right hip and leg, participants were instructed to raise their right arm toward their belly (elevating it, moving it backward, in the direction of their head, and the left part of their body), finally getting their thumb and index closer in space as to grasp a virtual object. Then, they carefully came back to the starting position. An experimenter inside the scanning room checked the amplitude of the movement and that the markers were visible during the entire movement. A 60s capture of the movement was performed in QTM, and this recording was then used to boost the

automatic identification of trajectories by creating an AIM model. Using the built-in function "skeleton solver", we applied to the AIM model a custom skeleton we created, whereby the five markers were connected by "bones" (figure 6.5), and bones formed "segments". The QTM real-time protocol was used to stream in real time skeleton data to the Unity software.

Note that as AIM models are learning models, they benefit from new trials added to the model providing more examples of distances and angles between markers, i.e., depending on participants' arm length. Therefore, each participant's recording was added to the previously stored AIM information to help the software apply the model more easily for future participants.

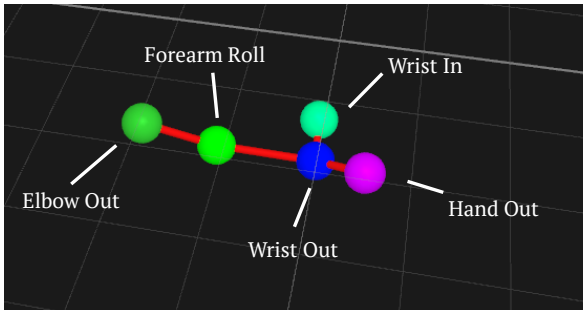

Figure 6.5. Real-time reconstruction of the model created by the AIM, whereby markers were connected by "bones".

Environment calibration

Once the AIM was accomplished, the table entered the scanner until reaching the magnet isocenter, and the 3D glasses were turned on, therefore allowing the participant to see again the virtual scene.

Participants were asked to reproduce the grasping movement they performed during the AIM recording. Kinematic skeleton data from QTM and the glove were fed into Unity and used to animate a 1st person humanoid avatar through custom scripts. In this way, participants could see their hand movements reproduced on the avatar. Using a

customized user interface (see Figure 6.6), the experimenter modified the virtual environment position to match the amplitude of the movement participants performed during the creation of the AIM. In this phase, it was crucial to make sure that the position of the virtual bottle was inside a space range within which the markers' position could be detected by the camera. As a further check, in this phase the starting platform and the buttons on the bottle turned red every time they were touched by the participant's hand. This provided an additional visual cue to be sure that the virtual touch truly occurred.

The GUI was also used to cue the participants on the movements to be executed to calibrate the glove; select the language of the experiment; enter details on the participant ID code and the number of the run to be launched; regulate environment settings such as the position relative to the participant's view and the size of the bottle; regulate camera settings, such as 3D distortions, field of view (FOV) and pupillary distance.

While the subjects' right hand was positioned over cushions, a virtual platform was inserted in the virtual scene, acting as a starting point for the subject's movement.

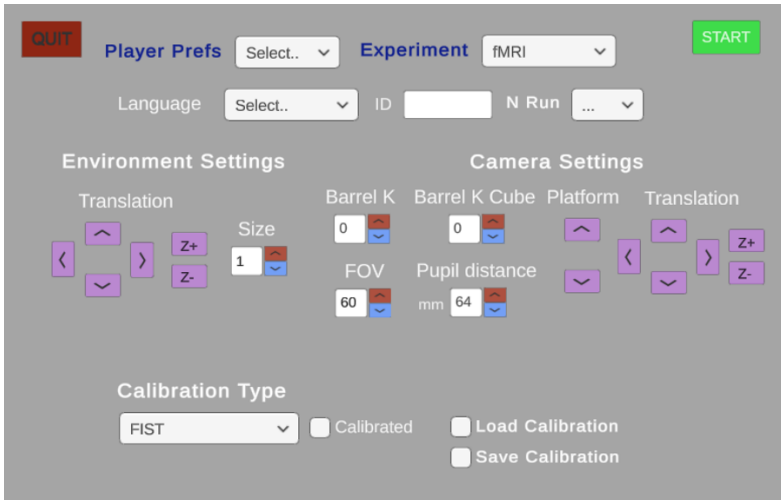

Figure 6.6. Environmental setup GUI. The user interface was created to choose the kind of experiment to be performed (behavioral or fMRI), the audio language, set the participant ID and the run to be performed. Further sections were aimed to translate the environment in the three dimensions (e.g., moving the table away from the hand), the 1st person avatar, raising the starting platform over the table. Furthermore, some properties of the 3D view could be adjusted, i.e., the Barrel K and Barrel K Cube (implemented within the Nordic NeuroLab Unity

package available at https://github.com/nordicneurolab/vshd-unity-example), the field of view (FOV) and the pupillary distance.

6.2.5 Subjects and experimental paradigm

Two subjects participated in the pilot fMRI study, one female (aged 24) and one male (aged 29). To be sure that the arm was at the edge of the entrance of the scanner, we recruited participants taller than 170cm. This ensured that the markers on the arm would have been visible from the cameras during the whole acquisition. Participants were right-handed, as assessed by the Edinburgh Handedness Inventory (Oldfield 1971), and had normal or corrected-to-normal vision. Participants gave their written informed consent to participate in the study. The study was approved by the local research ethics committee of the IRCCS Fondazione Santa Lucia in Rome, according to the Declaration of Helsinki.

Experimental stimuli and paradigm

The experiment was built in Unity (v. 2019.4) using Unity Experiment Framework (UXF; v2.4.3).

A detailed description of the experiment is provided in Chapter 5, where data relative to the behavioral implementation of the paradigm are discussed. Figure 6.7 shows the VR environment from a first-person perspective. Note that respect to the behavioral version of the experiment described in Chapter 5, the bottles are closer to the participant. Hence, the movement must be performed backward. We reasoned that moving forward would have required a bent forearm as starting position, which was hardly achievable due to the constraints of the scanner tube. We tried several options. For instance, we asked the pilot subject to start the movement with their forearm horizontally laying on their belly, however in this case the movement was too wide, and the camera couldn't appropriately track the markers. We could have designed a device to constrain more the arm's position, but again, this would have interfered with the markers' tracking. Overall, we believe that

we found the best workaround possible to obtain a reach-to-grasp movement limiting the risk of losing the arm tracking.

Figure 6.7. Virtual reality scene from a first-person perspective. Note that respect to the behavioral experiment, here the bottles were closer to the participant's view. Therefore, the participants were required to move their hand backward, i.e., as if the bottles were located on their belly.

The experiment was a 2x2x2 factorial and mixed design, whereby one factor ("Instruction") varied between blocks, whereas the others ("Movement" and "Correction") were event-related. Relative to the behavioral implementation of the paradigm, two block conditions were added to isolate neural correlates of action execution ("Move") and observation ("Observe"). We also modeled three rest blocks for each run. "Observe" and "Rest" trials were introduced by the auditory repetition of the block instruction (i.e., "Observe" or "Rest"), pronounced by a male voice and cut at 0.2s.

A summary of each block is provided below:

- "Interactive" blocks: the partner could perform a precision/power grip, with (1/3) or without (2/3) correction. The upper or lower button of the subject's bottle was enlightened, eventually correcting during the trial (1/3). The participant was asked

to perform the same/opposite movement with respect to the partner, trying to synchronize his/her movement with the partner.

- "Guided" blocks: the partner could perform a precision/power grip, with (1/3) or without (2/3) correction. The upper or lower button of the subject's bottle was enlightened, eventually correcting during the trial (1/3). The participant was asked to perform the same/opposite movement with respect to the bottle, trying to synchronize his/her movement with the partner.
- "Move" blocks: the partner was still. The upper or lower button of the subject's bottle was enlightened, eventually changing during the trial (1/3). The participant was asked to always perform the same movement with respect to the bottle. In this case, the movement time was not beaten by the partner's movement. This was considered a control condition to isolate brain areas involved in the planning and execution of a visually-cued grasping movement.
- "Observe" blocks: the partner could perform a precision/power grip, with (1/3) or without (2/3) correction. The lights on the bottle's buttons were never turned on. The participant was only asked to observe the performed movement. This condition isolated the action observation network.
- "Rest" blocks: the partner was still. No light on the bottle's buttons was turned on. The participant was asked to stay still and observe the visual scene.

In each run, each combination between the 6 factors (3 of interest, 3 of no interest) occurred once in the case of correction trials, and twice in the case of no-correction trials.

Overall, 20 trials for each combination of "Corrected" trials with the other levels were created, whereas 40 trials were implemented for each combination of "Uncorrected" trials, balanced between the presence or the absence of a correction of no-interest.

Trials were distributed across 5 runs, each including 21 blocks (6 Interactive, 6 Guided, 3 Move, 3 Observe, 3 Rest) composed of 4 trials. A rest block never occurred as the first block, but it occurred always as the last block of each run.

Subject-specific trial lists were created to optimize the HRF response by counter-balancing the sequence of trials and blocks. We assigned a random partner animation video to each trial, balanced across conditions (e.g., each condition included an equal repetition of each of the 20 possible animations). A variable ISI following a truncated exponential distribution (min = 0.5s, max = 5s, mean = 2s) was added to the duration of the partner's movement, and the resulting sum was used to define trial duration (ITI). For consistency, the same procedure was used to define trial duration during the "Rest" and "Move" blocks, although no movement was executed by the partner.

We recorded the timing at which the movement started (i.e., the actor raised the hand from the cushion), and the touch of the button occurred. Kinematics of the right index, wrist, and elbow as reconstructed by the actor avatar movement were also recorded at the Unity frame rate (~60FPS).

The mean block duration was 23.56s for Subject 1 and 23.42s for Subject 2. Each run lasted 8 minutes and 20 seconds.

6.2.6 fMRI acquisition

MR images were collected using a 3T scanner (Siemens MAGNETOM Prisma) equipped with a 64-channel head coil.

Acquired structural images included a T1-weighted structural image with a MPRAGE (magnetization-prepared rapid gradient-echo) sequence with perspective motion correction and selective reacquisition of data corrupted by motion based on interleaved 3-D EPI navigators (Tisdall et al., 2012; Hess, Tisdall, Andronesi, Meintjes, & van der Kouwe, 2011). Volumetric imaging included 176 slices, isotropic resolution = 1 mm3, TR = 2500 msec, TE = 2 msec, inversion time = 1070 msec, flip angle = 8°.

Functional, whole-brain MR images were acquired with a T2*-weighted gradient-echo EPI sequence, a multiband factor of 6, and an isotropic voxel size of 2.4 mm3 (60 slices, field of view = 208 × 208 mm2, TR = 800 msec, TE = 30 msec, flip angle = 52°, no in-plane acceleration; Xu et al., 2013; Feinberg et al., 2010; Moeller et al., 2010). The number of

volumes in each run was subject-specific, depending on the individual trial list. For both participants 1 and 2, we acquired 627 volumes in each run. Data acquisition in each functional run began with 3.2 s of rest to approach steady-state magnetization.

Two spin-echo EPI volumes with phase encoding in opposite directions, no multiband acceleration, and the same geometrical and sampling properties of functional runs were acquired for field mapping (TE = 80 msec, TR = 7000 msec).

6.2.7 fMRI data analysis

Data were processed using fMRIprep (Glasser et al., 2013). An iterative procedure emulating a Gaussian kernel with a 4 mm full width at half-maximum (FWHM) was used to smooth the data. We analyzed functional images for each participant on a vertex-by-vertex basis, implementing a General Linear Model (GLM) in SPM12. Each trial was modeled as a canonical hemodynamic response function time-locked to the trial onset. Rest blocks and error trials were not explicitly modeled as GLM regressors and were thus treated as part of the residual variance.

To estimate the amount of head movement, we computed the framewise displacement (FD) as an estimate of the amount of instantaneous head movement at each time point (Power et al. 2012). We included the FD and the DVARS (i.e., the spatial standard deviation of successive difference images; Smyser et al., 2011) as movement regressors.

Trial-specific functions and head FD regressors entered in two separate GLMs aiming to further control the amount of arm movement. We first retained the movement of the index relative to the wrist and of the wrist relative to the elbow to obtain an estimate of the absolute hand (H) and forearm (FA) movements. For each of these measures we computed the framewise displacement (FD_H and FD_{FA}).

In the first GLM, we resampled the FD_H and FD_{FA} to the TR time (0.8) and used them as regressors. We then obtained a statistical map showing the brain voxels whose activity correlated with the amount of hand and forearm movement, cleaned by the effects of the

experimental variables. Results from this GLM were used to visualize how much arm movement affected the BOLD signal in each participant.

In a second GLM, we summed the FD_H and FD_{FA} within each trial and used them as parametric regressors, therefore cleaning the signal for hand and forearm motion artefacts. Results from this second GLM were used to perform t-tests to compare signal between conditions at the single-subject level.

For all the analyses, results were obtained defining clusters of adjacent vertices surviving at least an uncorrected voxel-level threshold of $P < 0.001$; then, statistical maps were corrected for multiple comparisons at the cluster level ($P < 0.05$) through a topological false discovery rate procedure based on random field theory (Chumbley et al. 2010).

6.2.8 Behavioral and kinematic measures

We evaluated the accuracy percentage scores. Also, we computed the maximum grip aperture (i.e., the maximum Euclidean distance between the thumb and the index), and the maximum wrist height excluding the error trials.

After the scan, participants were asked to fill out a six-item questionnaire to assess the degree of embodiment (Tieri et al., 2015; Botvinick & Cohen, 1998). Two measures are obtained: 1) feeling of ownership, i.e., the degree to which the participants felt that the virtual arm belonged to them (average of responses to Items 1-2; Item 3 acted as a control); 2) agency, i.e., the feeling to be in control of the virtual hand's action (average of responses to Items 4-5; Item 6 acted as a control).

6.3 Results

Results will be divided into two main sections. The first section will show the results of the check we performed to exclude that the arm movements performed by the subjects could result in a wide contamination of the brain activity as estimated by the BOLD signal. The second section will test task-based hypotheses about the brain areas

preferentially engaged in the execution or the observation of complex motor actions and the implementation of fast hand movement corrections.

6.3.1 Behavioral and kinematic measures

Accuracy was high in both Subject 1 and 2 (see Table 1). The difference between power and precision maximum grip aperture was not significant ($p = 0.17$, $T = 1.36$ in Subject 1; $p = 0.93$, $T = 0.09$ in Subject 2), whereas the difference in wrist height was significant ($p = 1.04 \times 10^{-15}$, $T = 8.55$ in Subject 1; $p = 2.95 \times 10^{-9}$, $T = 6.13$ in Subject 2).

INSTRUCTION	MOVEMENT	CORRECTION	ACCURACY	
			Subject 1	Subject 2
Guided	Opposite	No	97.5%	100%
Guided	Opposite	Yes	65%	75%
Guided	Same	No	100%	97.5%
Guided	Same	Yes	95%	95%
Interactive	Opposite	No	100%	90%
Interactive	Opposite	Yes	90%	100%
Interactive	Same	No	100%	97.5%
Interactive	Same	Yes	95%	100%
Move	Same	No	100%	100%
Move	Same	Yes	100%	95%

Table 1. Accuracy percentage scores during the task, separately for each combination of the three experimental factors and each participant.

As assessed by the Embodiment Questionnaire, both participants showed high levels of feeling of ownership (7.5/10 Subject 1; 7/10 Subject 2) and agency (8.5/10 Subject 1; 7.5/10 Subject 2).

6.3.2 Movement artefacts

First, as a control check, we controlled the head FD in each session and participant (Figure 6.8). Only one frame exceeded the threshold of 0.9mm (Subject 1). The estimated head motion was higher for Subject 1 than 2.

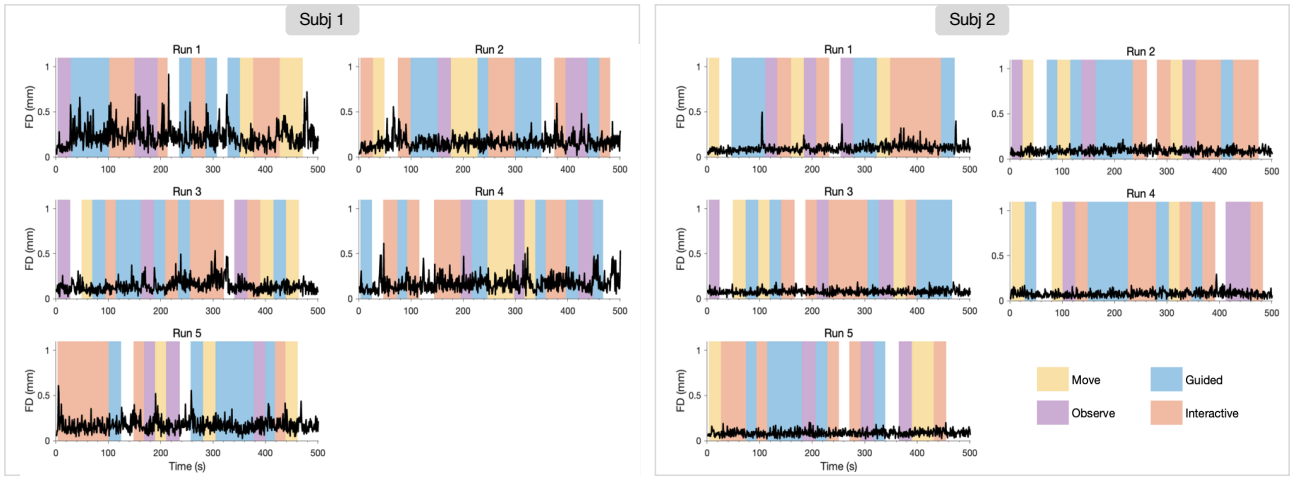

Figure 6.8. Visualization of framewise displacement (black lines in each subplot) as a function of time for each run in Subject 1 and 2. Experimental blocks are visually represented as colored stripes (yellow = "Move", blue = "Guided", purple = "Observe", orange = "Interactive). White stripes represent rest blocks.

Hand movement correlated with stronger activity of the left premotor cortex and superior temporal sulcus in both subjects. Subject 1 also showed motion-related activations in the supramarginal gyrus. Forearm movements correlated with activity mainly in the right hemisphere, including the intraparietal sulcus, secondary somatosensorial areas, and the superior temporal sulcus (Figure 6.9).

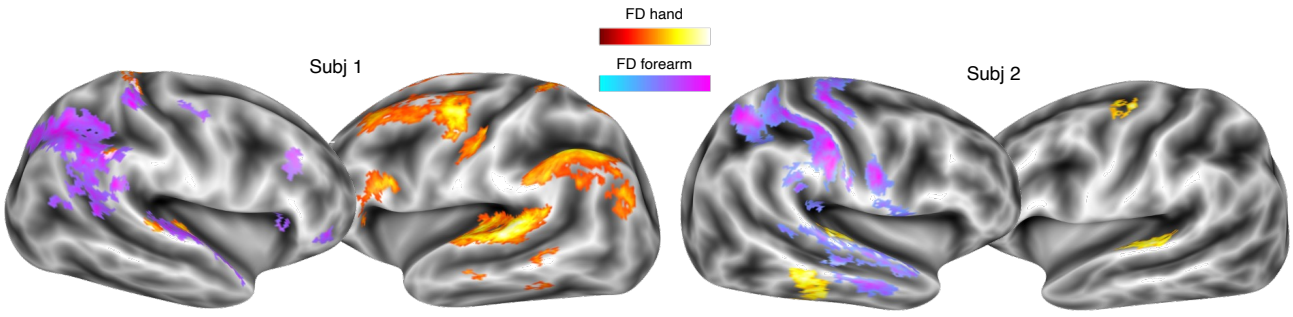

Figure 6.9. Brain activity correlating with hand and forearm absolute movements, as indexed by the framewise displacement (FD) estimates.

6.3.3 Task-evoked activations

Grasping execution vs observation. Both "Move" and "Observe" conditions led to the activation of the early and high visual cortex, second somatosensory areas, and IPS (including aIPs). Despite the correction for the hand and forearm movement estimates, during grasping execution a clear activation of the left M1 was observed. "Move" also activated supplementary motor areas in the bilateral medial wall (Figure 6.10).

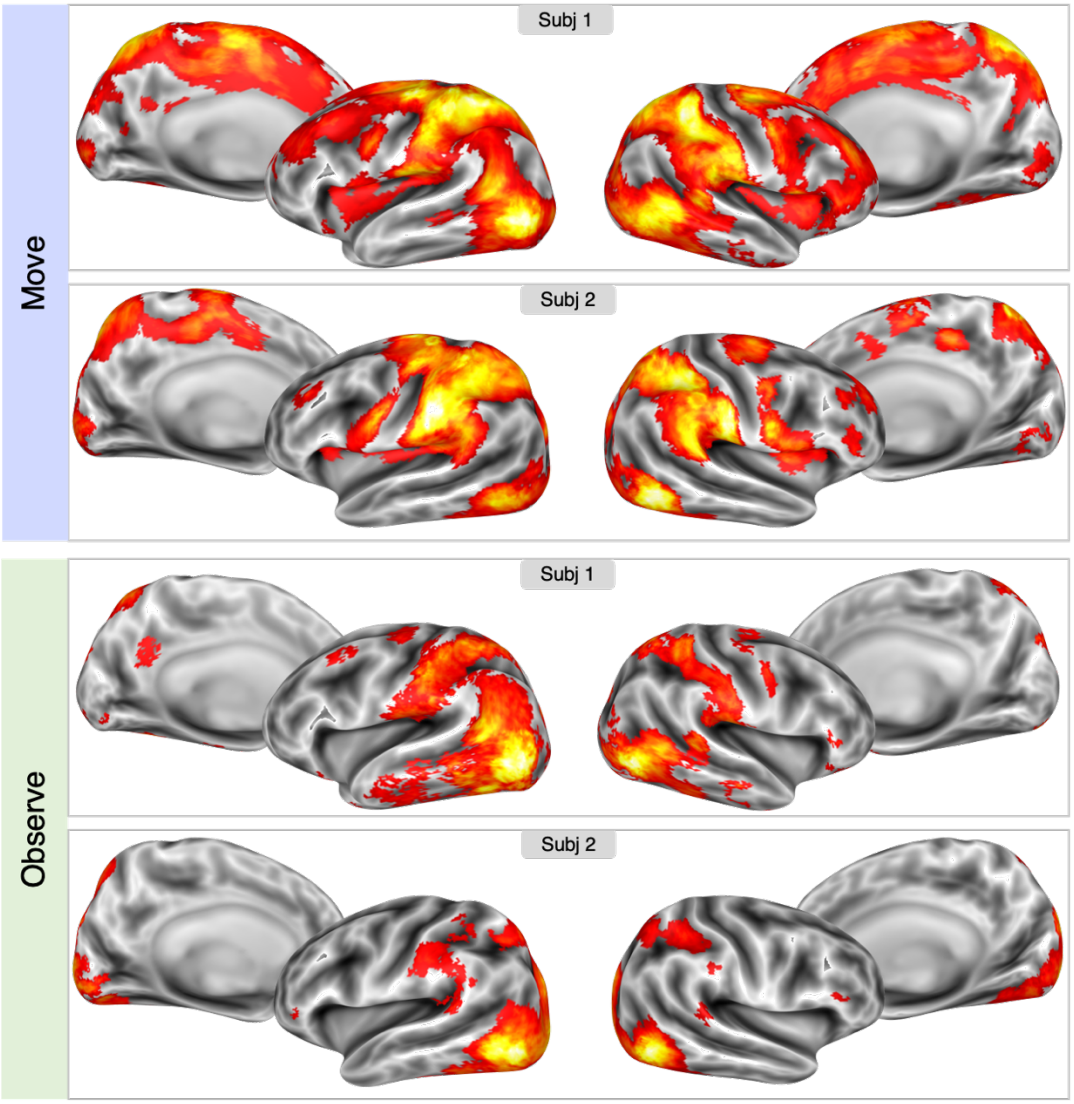

Figure 6.10. Single-subject whole brain activations: "Move" and "Observe". The top panel shows activations detected in the "Move" condition vs. baseline; the lower panel shows activations detected in the "Observe" condition vs. baseline, separately for Subject 1 and 2. Activation maps are overlaid into the inflated individual surface of both hemispheres.

Activations during action execution were stronger than during action observation in the left motor cortex and the bilateral premotor (PMd, PMv) and parietal (S2, aIPs) areas, and SMA in the medial wall. Compared to grasping execution, observation activated more strongly the action observation network (AON) (Rizzolatti & Craighero, 2004) including the high-visual cortex in the occipital and temporal lobes (e.g., extrastriate body area) (Figure 6.11).

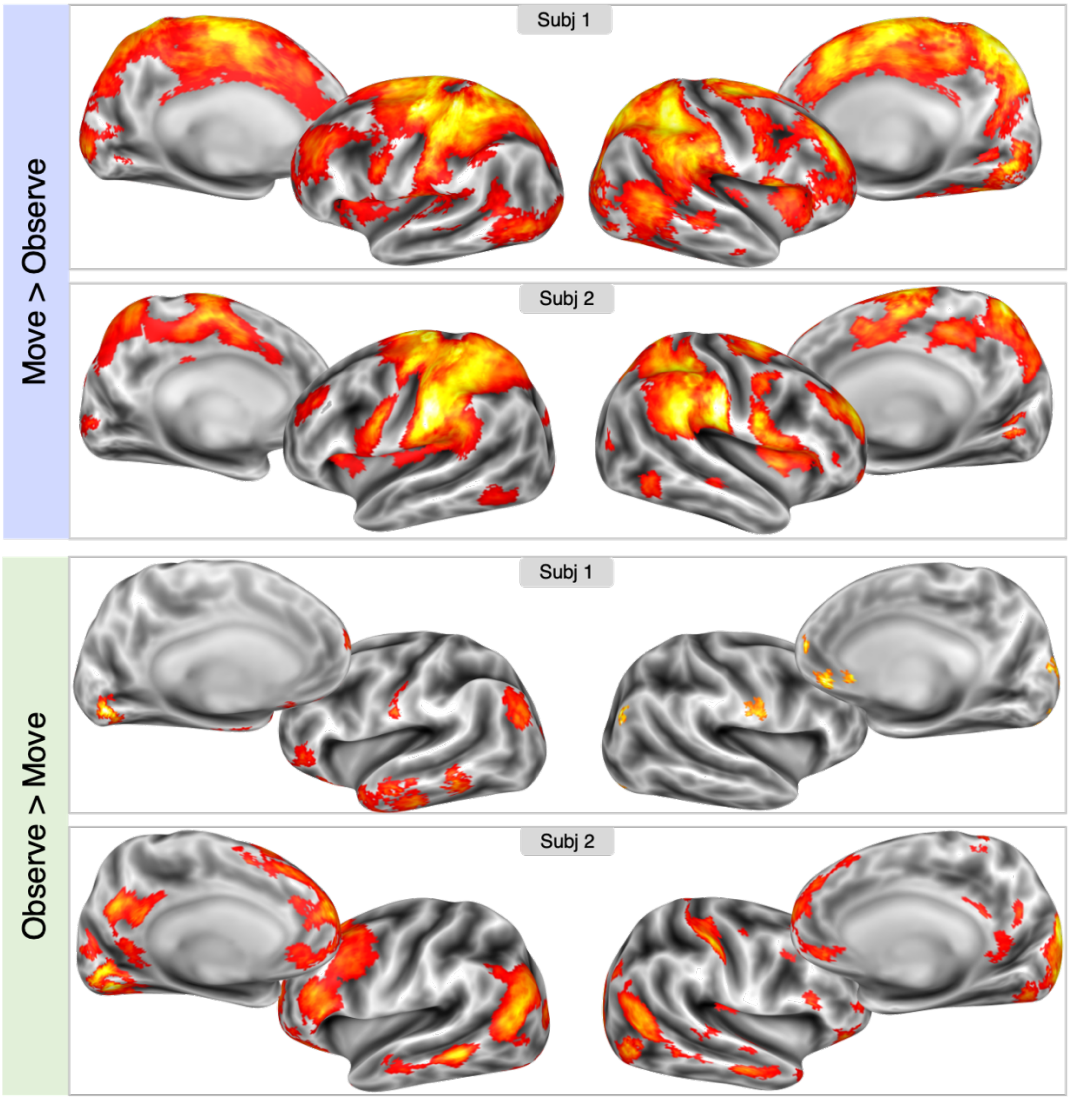

Figure 6.11. Single-subject whole brain activations: "Move" vs "Observe". The top panel shows activations detected in the "Move>Observe" t-contrast; the lower panel shows activations detected in the "Observe>Move" t-contrast, separately for Subject 1 and 2. Activation maps are overlaid into the inflated individual surface of both hemispheres.

Joint grasping: social vs non-social cues. When the participant's movement was cued by the avatar's movement (Interactive), we observed a stronger activation of EBA in both subjects and hemispheres, and of the intraparietal sulcus, including aIPs, in one subject (Subj 1). Instead, when the participant's movement was cued by the light on the bottle (Guided), activations were sparser, mainly located in the orbitofrontal cortex (right: Subj1; left: Subj2), and the supramarginal gyrus in Subject 2 (see Figure 6.12).

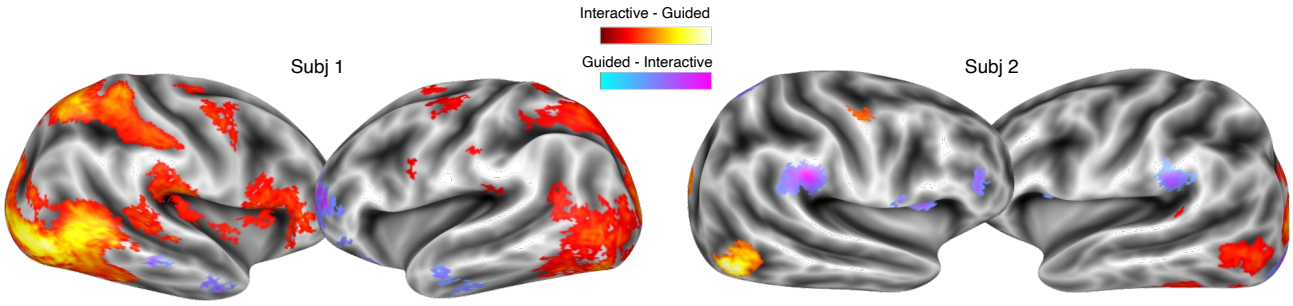

Figure 6.12. Single-subject whole brain activations: "Interactive" vs "Guided". Activations detected in the "Interactive>Guided" t-contrast are shown in red-to-yellow shades; activations detected in the "Guided>Interactive" t-contrast are shown in blue-to-purple shades. Results are displayed separately for Subject 1 and 2. Activation maps are overlaid into the inflated individual surface of both hemispheres.

A comparison between complementary ("Opposite") vs imitative ("Same") actions provided different results between the two participants, hence precluding to drive strong inferences. We will therefore report them only in a descriptive manner. When merging the two joint conditions, we found that in Subject 1 complementary actions recruited more the superior parietal lobe and the bilateral premotor cortex than imitative ones. The same comparison in the Guided conditions only revealed the activation of the left superior parietal lobe and a medial portion of it likely corresponding to PEc, whereas the

Interactive condition only engaged more occipital areas. In Subject 2, the comparison between complementary and imitative behaviors led to significant results only in the "Interactive" condition, whereby complementary actions activated more than imitative ones the bilateral dlPFC and SMG (Figure 6.13).

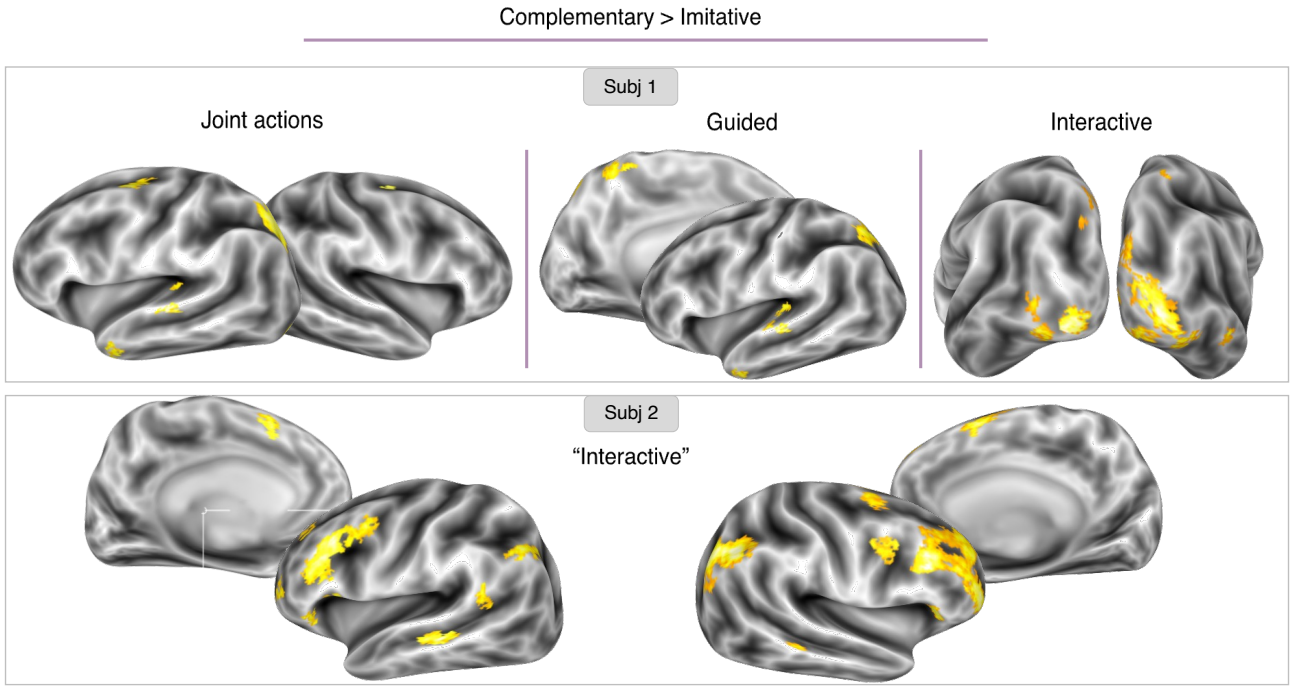

Figure 6.13. Single-subject whole brain activations: "Opposite" > "Same" across "Instruction" conditions. Activations detected in the "Opposite>Same" t-contrast are shown in red-to-yellow shades. Results are displayed separately for Subject 1 and 2 for each condition in which complementary and imitative actions led to different brain activations, i.e., "Joint" ("Interactive" and "Guided"), "Guided", and "Interactive" for Subject 1, and only "Interactive" for Subject 2. Activation maps are overlaid into the inflated individual surface of both hemispheres.

Motor correction. When an on-flight correction of the preplanned movement was required in the "Move" condition, we observed heightened activation of bilateral PMd, aIPs, and SMG in Subject 2. Instead, observing a correction performed by the actor avatar induced higher activation in the left aIPs in Subject 1 (Figure 6.14).

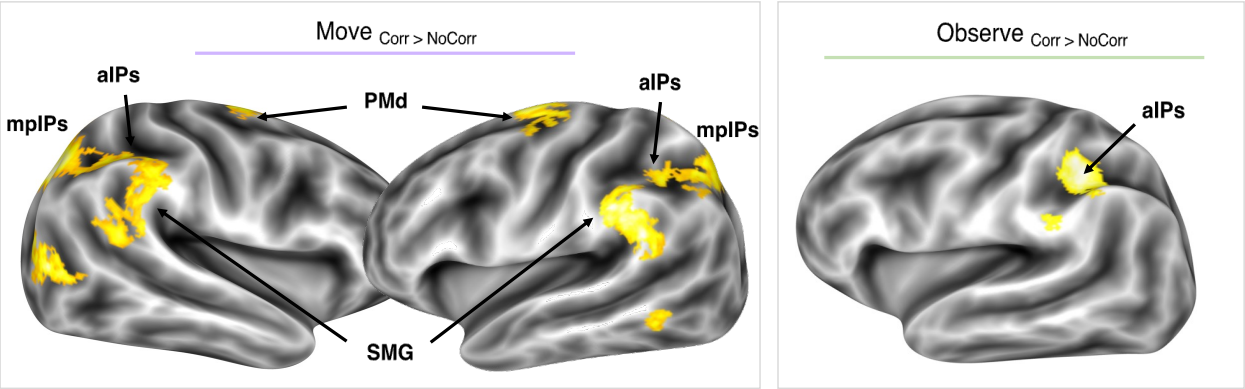

Figure 6.14. Single-subject whole brain activations: Corr>NoCorr in control conditions. Activations detected in the Corr>NoCorr contrast during the "Move" (left panel) and "Observe" (right panel) conditions. Results are displayed for Subject 2 ("Move") and 1 ("Observe"). Activation maps are overlaid into the inflated individual surface of both hemispheres.

During the Joint action conditions, the on-flight correction was supported by stronger activation in the supramarginal gyrus, the anterior cingulate, and the right dlPFC, the latter one only in Subject 2 (Figure 6.15). On a more fine-grained analysis, no significant activations were found in the "Guided" condition when comparing correction vs non-correction trials, whereas in the "Interactive" condition we found activity in SMG and dlPFC in both subjects (Figure 6.16).

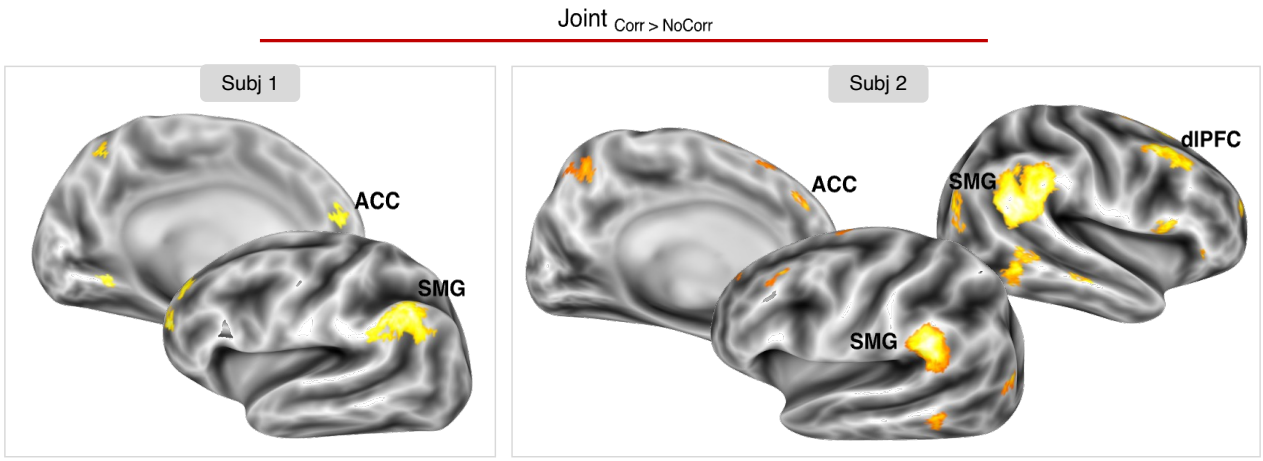

Figure 6.15. Single-subject whole brain activations: Corr>NoCorr during joint actions. Activations detected in the Corr>NoCorr contrast in the two "Joint action" conditions, i.e., averaging "Interactive" and "Guided" conditions. Activation maps are overlaid into the inflated individual surface of both hemispheres.

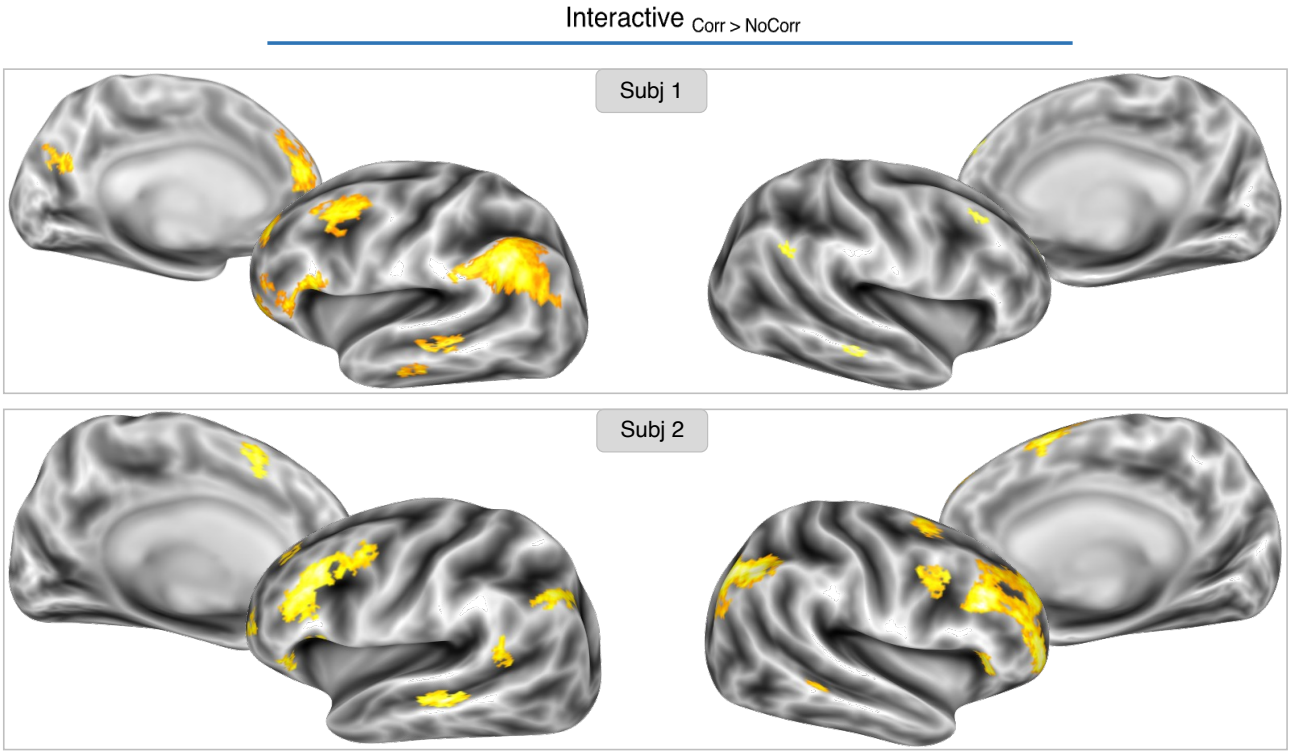

Figure 6.16. Single-subject whole brain activations: Corr>NoCorr in the "Interactive" condition. Activations detected in the Corr>NoCorr contrast in the "Interactive" and "Guided" conditions. Activation maps are overlaid into the inflated individual surface of both hemispheres.

6.4 Discussion

We developed a motion online tracking system under MRI (MOTUM), unique in the world to our knowledge, to combine motion tracking and virtual reality in real time. We tested MOTUM in a paradigm requiring dynamic motor control, here tested through fast hand motor corrections. We will start discussing the potential methodological issues related to movement artefacts. Afterward, we will discuss the fMRI activations of the two participants who performed the grasping task. The very small sample demands extreme

caution when interpreting the results, however we believe they might provide an overview of the possibility of using MOTUM to study dynamic motor control in a potentially more efficient, reproducible, and realistic manner with respect to previously developed systems.

6.4.1 Methodological considerations

When implementing the tracking system, we faced several challenges. The hardest achievement was to maintain the tracking of markers which were partially inside the scanner during the whole acquisition. To overcome this issue, we adopted some workarounds on the marker positioning to reduce the risk of collinearity (i.e., slightly dislocating them on the horizontal plane). More recently, we tested whether this goal can be achieved by using smaller markers (5mm diameter). However, we haven't acquired data with smaller markers yet, and more tests would be necessary to verify this possibility. Another critical point of our system is that we only have the minimum number of cameras possible (i.e., three) and all of them are located in the wall that faces the scanner. In a recent test, we used two additional cameras that we positioned on the wall standing on the left side of the scanner, hence tracking the position of the markers from a completely new side view. A preliminary test confirmed that using 5 rather than 3 cameras could achieve a more stable tracking of the markers. We will test the potentialities of this setting in the future.

A second key point was the type of movement to be performed inside the scanner. We had to adapt the movement both to the constraints of the MRI scan and the risk that other body parts could cover the markers while the movement was being executed. In the configuration we adopted, in the starting position participants are lying on the MRI table with their right hand along their hips; when performing the task, they move their hand toward their belly to grasp the virtual bottle. This body posture is clearly different from that participants experience in the virtual world, where the first-person avatar is sitting at a table with the right hand extended in front of him/her. Nevertheless, both participants experienced embodied of the virtual hand, as assessed by the scoring of the

Embodiment Questionnaire, overall reporting high levels of feeling of ownership and agency. We conclude that the immersivity of the environment we created was strong enough to counter the discrepancy between the real and virtual body posture.

One possible drawback of MOTUM is that the amount of body motion could affect the recorded signal. To run out this possibility, we first checked and then regressed out the amount of head movements during the scan. A visual inspection of the first derivative of head movements revealed only one critical timepoint in the whole scan of one participant. Nevertheless, hand and forearm movements still affected neural signal, as revealed by the first GLM we implemented using the first derivative of arm movement as additional regressors. To further control for that, following analyses were performed by adopting a parametric GLM, i.e., including a trial-by-trial estimate of arm movements. Results from these analyses suggest that the amount of movement in our specific task didn't affect the brain signal in a way that precludes making inferences on the ongoing neural processes.

6.4.2 Movement observation and execution

Consistently with the well-known network subserving grasping (for a review see Gerbella et al., 2017), when performing a grasping movement, but not when observing its execution, we detected the activation of several areas including aIPs, PMv, PMd, SMA and M1. The opposite contrast revealed the activation of the temporo-occipital nodes of the action observation network (AON), which constitutes the neural substrate for action understanding (Rizzolatti e Craighero, 2004) and of the bilateral aIPs. The activation of this area may be entirely task-related, as during grasping actions aIPs has been associated with both goal-based motor control and the coding of others' observed action goals, overall representing action goals and intentions independently by the actor (self, or another person; Fogassi et al., 2005; Hamilton & Grafton, 2006). To achieve this goal, aIPs is involved in creating a *prediction* of such motor intentions based on the simulation of sensory-motor cues (Kilner et al., 2007), and forward such predictions to PMv (Tunik et al., 2005).

The core of the present study was to evaluate whether MOTUM could achieve the goal of targeting dynamic motor control, implemented as fast hand movement corrections in response to abruptly changing environmental demands. This is indeed the true rationale behind the usage of such a complex system in this task.

Despite the motor correction occurring in a short time, which could be challenging to detect through BOLD signal, the results we obtained by comparing trials with vs without motor correction are in line with theories of motor control and previous findings. First, we showed that performing a motor correction while acting alone ("Move" condition), or observing another person performing a motor correction ("Observe" condition), enhanced activity in the aIPs, the parietal grasp-related region, in the left hemisphere. This is in agreement with the idea that aIPs encodes both self and others' goals, as we mentioned above. Moreover, Rice and colleagues (2006) showed that perturbation of aIPs using TMS distrupts grasping behaviors when applied during error correction, but not detection.

Implementing (but not merely observing) a motor correction also activated the superior parietal lobe, SMG, and PMd. The first result is not surprising, given that the motor correction didn't only imply a change in the grip type, but also in the reaching trajectory, therefore recruiting reach-related parietal areas such as mpIPS and hPEc (Bencivenga, Tullo et al., 2023). Beyond being part of the reaching circuit, PMd is a well-known critical region for action selection and, in the context of our experiment, might trigger the initiation of the correct response (Christensen et al., 2007; Schubotz, 2007). Finally, it has been suggested that SMG activity is modulated by the detection and correction of "low-level" sensorimotor errors, including the discrepancy between motor commands and their effects as the movement unfolds, for instance in cases of trajectory deviations (Krigolson and Holroyd, 2006, 2007). In this guise, SMG appears to be critical for switching motor plans by suppressing the present (but incorrect) motor plan (Rushworth et al., 2001; Hartwigsen et al., 2012), overall playing a key role in action conflict monitoring. More broadly, SMG is part of the temporo-parietal junction, playing a key

role in detecting matches and mismatches between expected and actual sensory, motor, or cognitive events (Doricchi et al., 2022) and constructing a predictive model of attention (Wilterson et al., 2021). We speculate that during our task the SMG and the aIPs interplay in comparing the predictions on the plant's future state (i.e., the efference copy, according to the Optimal Feedback control theory; Todorov, 2004) and the actual sensorimotor feedback. As during ongoing grasping movements aIPS has been suggested to perform such iterative comparisons to assure that the current grasp plan matches the current context and sensorimotor state (Tunik et al., 2006), SMG may participate in this process with its domain-unspecific role in supporting the detection of the mismatch and providing a sophisticated form of motor learning.

Surprisingly, trials with vs without a motor correction didn't elicit stronger activity of the frontal grasp-related area, i.e., PMv. We speculate that while power and precision grips may be differently encoded in parietal areas, using MOTUM we didn't elicit strong kinematically different motor properties between the two grip types. Indeed, we didn't detect a significant difference in grip aperture between precision and power grip (a difference that we instead found in the behavioral version of the task, see Chapter 5). The switch from one to the other might therefore not trigger corrective responses in PMv.

6.4.3 Joint actions

Next, we examined joint actions in which one own's goal must be achieved simultaneously with another person but based on the other's behavior in one case ("Interactive") and on a non-social cue in the other ("Guided"). The two conditions provided an identical visual input, and both required to pay attention to the other's behavior in order to synchronize one own's movement with the avatar. Therefore, the true difference between the two is in the action goal: to follow the partner (i.e., a social cue) or the light on the bottle (i.e., a non-social cue).

The comparison between the two conditions showed that acting in response to social cues increases activation in the temporo-occipital nodes of AON (e.g., EBA) in both participants, while also showing presumably attention-related effects in the parietal lobe

in one participant. Activations in the non-social cued condition vs the social-cued one were instead sparser between the two subjects, preventing driving general inferences.

During joint actions, regardless of the action goal (follow the avatar or the light), trials with motor correction led to stronger activity of the SMG and ACC when compared to no-correction trials. Our findings confirm and shed new light on those obtained by Moreau and colleagues (2020) using source analysis applied to EEG data recording during a "real-life" (and not virtual) implementation of the task we used here. In trials where a correction was necessary to achieve the task goal, the Authors recorded the error-related negativity potential (ERN; Falkenstein et al., 1991; Gehring et al., 1993) rising from frontal areas and the Positivity error potential (Pe; Falkenstein et al., 2000) from the parietal cortex during motor corrections. We speculate that ACC can be the source of ERN, as previously found (Carter et al., 1998; van Veen, et al., 2001), and linked to the detection of "high-level errors" (i.e., failure to meet a goal; Krigolson & Holroyd, 2006), conflict monitoring (Botvinick, et al., 2001; Yeung, et al., 2004) or action outcome predictions (Alexander & Brown, 2011; Quilodran, et al., 2008). SMG may instead be the source of the Pe recorded by Moreau and colleagues, and, as already occurring during the non-joint actions (i.e., "Move" condition), it deals with "low-level" sensorimotor errors. Several studies have also claimed a role of the TPJ in the "theory of mind", which could explain its higher contribution under the "Interactive" condition, whereby it is fundamental to read and update the other's intentions. Surprisingly, we didn't find activation of aIPs during motor correction in joint actions, as opposed to what we observed when participants performed a correction during individual actions ("Move") or observed a correction ("Observe"). However, the effects we find are driven by the "Interactive" condition, where the replanning of one's own actions is driven by the detection of a violation of the others' action predictions. In this case, heightened activity of SMG and the dorsolateral prefrontal cortex. The latter one may be the source of the greater ERN mean amplitude that Moreau et al. (2020) found in the interactive vs control condition in their study using a paradigm similar to ours.

6.5 Conclusions

We succeeded in implementing a unique motion tracking system under MRI and provided encouraging preliminary data about its possibility to target dynamic motor control. However, some methodological caveats are needed.

First, we used MOTUM in a paradigm requiring a continuous tracking of hand movements. To be sure that the markers located on the hand could enter the camera view range throughout the whole movement, we only recruited participants taller than 170cm.

Second, the grasping movement was executed towards a virtual object. This was necessary because introducing a real object in the scanner, e.g., a wooden bottle in our case, would have blocked the camera view, therefore making it impossible to track the movement. Nevertheless, we are very aware that while providing visual feedback about the movement, our study didn't tackle the sensorimotor feedback induced by contact with the objects. Combining MOTUM with amagnetic haptic devices that could provide haptic feedback when entering the space of a virtual object may overcome this limitation.

Although we only tested MOTUM during hand movements, we feel confident that its implementation to track and reproduce movements from other body parts (e.g., lower limbs) could be even easier, as they are completely out of the scanner. This paves the way for a wide range of real-life actions to be performed during fMRI scans, potentially impacting multiple neuropsychological research fields, including spatial navigation (e.g., participants could walk in virtual environments). Another attractive advantage of virtual reality is that both the environment and the movement itself can be manipulated to eventually reproduce unrealistic events. For instance, in the field of body representation and peripersonal space studies, a distortion of the body properties (e.g., limb length or size) could be online applied; in the study of visuomotor functions, limb trajectory can be suddenly altered (e.g., inducing prismatic-like effects). To conclude, we believe that MOTUM could completely revolutionize current fMRI paradigms.

CHAPTER 7

This work was developed during my 4-month internship (in 2023) at the DavareLab at the King's College of London. I was funded by a Mobility Grant (Sapienza University of Rome) and the Network of European Neuroscience Society (NENS) Exchange Grant. The goal of my internship was to develop knowledge and practical skills in the usage of transcranial magnetic stimulation (TMS) to study the neurophysiology of movement control. With a completely different approach with respect to my previous knowledge about motor control studied with fMRI, I dealt with the temporal evolution of motor planning and implementation, and the way our brain encodes forces and kinematics to accomplish hand object interactions.

Unravelling the contribution of cortico-cortical inputs to M1 in sensorimotor processing during skilled grasp: a directional TMS protocol

Federica Bencivenga[1,2,3], Alexander Pleger[4], Aneirin Potter[5], Marco Davare[5]

[1] Brain Imaging Laboratory, Department of Psychology, "Sapienza" University of Rome, Rome, Italy

[2] Cognitive and Motor Rehabilitation and Neuroimaging Unit, Santa Lucia Foundation (IRCCS Fondazione Santa Lucia), Rome, Italy

[3] PhD Program in Behavioral Neuroscience, Department of Psychology, "Sapienza" University of Rome, Rome, Italy

[4] Institute of Sports Science, Faculty of Humanities, Leibniz Universitat Hannover

[5] School of Life Course and Population Sciences, Faculty of Life Sciences and Medicine, King's College London, SE1 1UL, London

Abstract

Grasping and lifting objects necessitates anticipatory planning of fingertip forces. However, when objects have complex geometry, for example an asymmetric center of mass, fingertip forces are further scaled based on the fingertip positioning relative to the object's center of mass, a process only taking place after object contact. Thus, skilled grasp control arises from a sophisticated interplay between anticipatory and feedback control mechanisms. The relative weighting between anticipatory and feedback mechanisms depends on the degree to which one can predict fingertip positioning before object contact, for example through prior experience with the object. In the present experiment, we varied the predictability of fingertip positioning, hypothesising that this would modify the reliance on anticipatory vs. feedback mechanisms in high vs. low predictable fingertip positioning conditions, respectively.

We then probed the effect of a shift from anticipatory to feedback control mechanisms on corticospinal excitability (CSE) using a directional transcranial magnetic stimulation (TMS) protocol, by applying postero-anterior (PA) or antero-posterior (AP) induced currents.

We asked participants (n=21) to grasp and lift a symmetrically shaped object with an asymmetrical center of mass while minimizing tilting. Fingertip positioning could be either visually cued (i.e., constrained) or freely chosen (i.e., unconstrained), thus altering the reliance on anticipatory vs. feedback control mechanisms, respectively (as in Davare et al. 2019). Single pulse TMS was delivered just after object contact in a PA or AP configuration. While PA TMS led to short latency motor evoked potentials (MEPs), AP TMS delayed MEP onset by 1.2 ms on average, likely as AP currents preferentially activate late I-wave inputs to corticospinal neurons. We found that the increased weighting of sensorimotor feedback processing in the unconstrained vs. constrained condition had no differential effects on the MEP amplitude in either PA or AP TMS conditions. Interestingly, we found changes in MEP latencies depending on the grasp

context: the differential MEP latency between AP and PA TMS conditions was larger in the unconstrained (t_{20}=2.75; p=0.012) compared to the constrained grasp.

These findings suggest that increased reliance on feedback control mechanisms is driven by late I-wave pathways, likely mediating cortico-cortical inputs to the primary motor cortex. We ultimately suggest that MEP latency, as assessed by directional TMS protocols, can be a neurophysiological biomarker for probing the integrity of sensorimotor processing during skilled hand movements.

7.1 Introduction

Anticipatory control based on sensorimotor memory is fundamental for dexterous object manipulation. An efficient grasp control requires optimized force-to-position coordination, namely the ability to coordinate fingertip forces in a flexible manner that depends on the fingertips' location on the object relative to its center of mass (CoM) (Fu et al., 2010; Mojtahedi et al., 2015). Anticipatory mechanisms predicting fingertip contact points and forces well before object contact overperform reflex-driven corrective mechanisms by bypassing the delay and noise intrinsic to feedback signals (Gordon et al., 1993; Burstedt et al., 1999; Salimi et al., 2000). However, in most cases we can grasp an object in many ways, e.g., locating our fingertips at very variable positions. This sets a limit to the reliability of the sensorimotor memory. For instance, during repetitive grasping of the same object, the inevitable noise in motor planning and/or execution results in wide inter-trial variability in fingertip positioning. Such variability must be counteracted using sensory feedback of digit placement to modulate fingertip forces (Fu et al., 2010; Mojtahedi et al., 2015). This brings to a trial-by-trial update of the internal sensorimotor object representation and continuous refinement of the predictive lift planning for the next trials. Hence, a subtle balance between sensorimotor memory and sensory feedback is required.

During everyday object manipulation, we must deal with accurate planning for both object weight and weight distribution. When grasping objects with non-uniform weight

distribution (e.g., a hammer or a box with unequal distributed content), compensatory torques must be applied to prevent tilt (Salimi et al., 2000). During two-digit manipulation, at a high-level planning process (i.e., motor equivalence) this task can be accomplished by modulating either the position (a) or the force (b) of the finger located on the heavy object side: we can place it higher (a) or exert a larger vertical loading force (b) respect to the digit located on the light object side. The first solution is mechanically less expensive. Individuals tend to optimize forces to a safety margin, namely to exert grip forces just slightly above the minimum necessary to keep the object stable (Johansson and Westling, 1984). Increasing the vertical spacing between the centers of pressure of the two fingers implies a smaller energy cost than implementing a largely asymmetric digit load force (Fu et al., 2010).

To distinguish the relative contribution of sensorimotor memory vs sensory feedback, previous studies have adopted grasp paradigms of symmetrically shaped objects with asymmetric CoM where digit position could be free or constrained by visual cues providing information on the optimal fingertip positioning (Fu et al., 2010; Mojitahedi et al., 2015; Davare et al., 2019). Intuitively, when the digit position is constrained, its inter-trial variability is reduced. This results in higher reliability of the sensorimotor memory acquired from previous trials in predicting digit forces and smaller feedback gains (Johansson and Cole 1992; Johansson and Flanagan 2009; Westling and Johansson 1984). Conversely, when fingertip position is unconstrained (i.e., forces are unpredictable), planned digit forces will be rapidly updated based on the sensory feedback about digit placement just after object contact (Fu et al., 2010; Mojtahedi et al., 2015; Davare et al., 2019).

To date, it's still unclear how and where these processes are encoded in the brain. It has been proposed that the primary motor cortex (M1) stores the internal representation of digit forces experienced during previous lifts and updates such memory by processing the sensory inputs from S1 (Chouinard et al., 2005; Loh et al., 2010; Nowak et al., 2004). However, other cortical regions, e.g., anterior intraparietal sulcus (aIPs), ventral and

dorsal premotor cortex (PMv, PMd), participate in this process (Davare et al., 2006, 2007; Loh et al., 2010; Marnewerck et al., 2018, 2020). Here, we contend that it's not M1 *per se* to store sensorimotor memory, but that it receives this information from other cortico-cortical inputs and contributes to its rapid update based on the sensory feedback.

We tested this hypothesis by implementing a directional transcranial magnetic stimulation (TMS) protocol while participants lifted an object with asymmetrical CoM. We probed corticospinal excitability by delivering a posterior-anterior (PA) or an anterior-posterior (AP) current at the object contact onset. These two current directions are supposed to recruit different intracortical circuits in M1. While PA currents preferentially evoke highly synchronized descending volleys in the corticospinal tract, AP-induced volleys are often less synchronized and more variable within- and between-subjects. AP and PA currents primarily generate late I-wave and early I-waves activity respectively, likely due to differences in their preferential site of activation. Consequently, the latency of motor evoked potentials (MEP) is delayed in AP compared to PA stimulation (Di Lazzaro et al., 2012; Di Lazzaro and Rothwell, 2014). Furthermore, as axonal depolarization is sensitive to the current direction, distinct populations of neurons are preferentially targeted by different current directions. Therefore, we reasoned that AP stimulation protocols should be more sensitive at probing cortico-cortical inputs to M1, likely conveying sensorimotor information from surrounding areas, such as PMv, PMd, and S1. Standing this hypothesis, we expected corticospinal excitability evoked by AP stimulation to be modulated by sensorimotor uncertainty more than PA stimulation. We tested differences between both MEP amplitude and latency induced by AP and PA stimulation under constrained and unconstrained grasping. We hypothesize that both the shape and the peak amplitude of the MEP waveform could carry information about the contribution of cortico-cortical inputs to M1 reflecting heavier sensorimotor processing.

7.2 Methods

7.2.1 Participants

We recruited 26 participants (mean age = 26 ± 5; 15 females) with normal or corrected-to-normal vision, no history of neurological disease, musculoskeletal disorders, or upper limb injury. Participants were assessed for handedness (Oldfield 1971) and screened for potential risk of adverse reactions to transcranial magnetic stimulation according to the published guidelines (Rossi et al. 2009) using the TMS Adult Safety Screen (Keel et al. 2001). The experimental protocol was approved by the ethical committee of King's College London.

7.2.2 Grip Device

The device used in the present study has been described in depth in previous works (Lukos et al., 2007; Fu et al., 2010; Davare et al., 2019). Concisely, the device was a grip-lift manipulandum in an "inverted T-shape". The horizontal base contained three compartments in which 3D-printed cuboids that were identical in appearance were placed. The cuboid in the rightmost compartment contained a 400 g mass while the others were hollow so that the device's mass distribution was shifted to the right of its vertical midline. When lifting the object, this imbalance induced an external torque of 255 Nmm, which participants needed to compensate for to maintain the horizontal base level. The total weight of the manipulandum, including the cuboids, amounted to 790 g (see Figure 7.1).

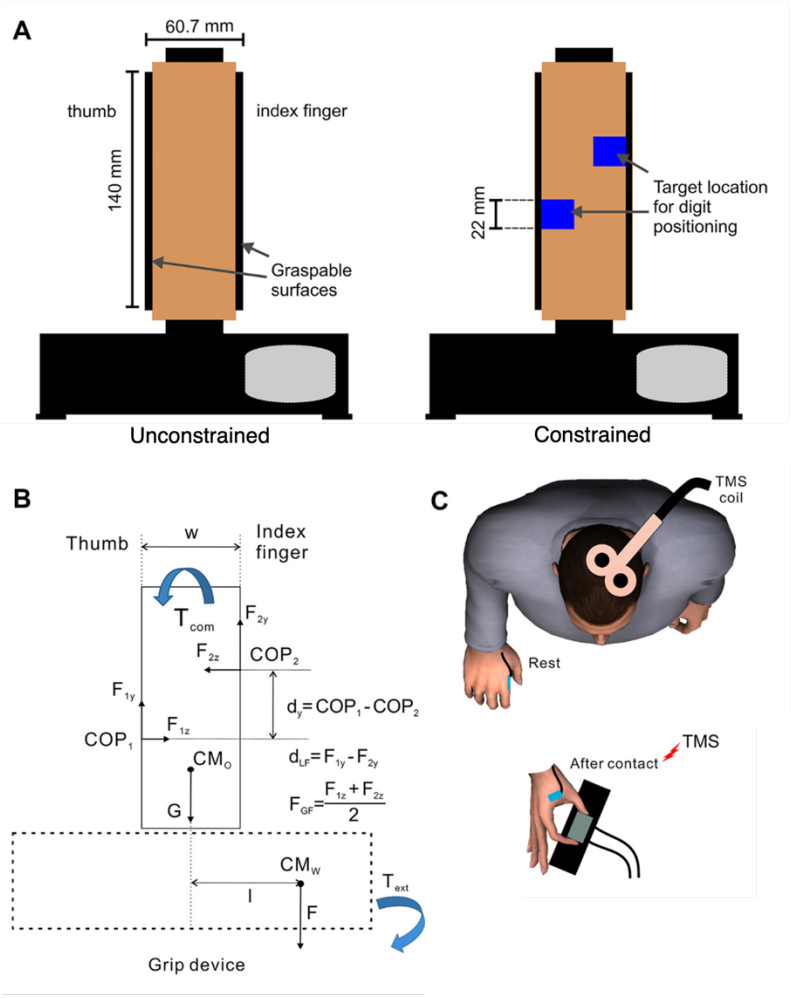

Figure 7.1. Experimental setup. A: grip device used for the two experimental conditions. In the Constrained condition, visual cues (blue markers) indicated participants where to place the thumb and index fingertips. B: object body diagram shows forces acting on the object, gravity (G, F) acting on the object center of mass (CMO) and added mass (CMw), and forces exerted by the thumb (F1) and index fingertip (F2) in the normal (z) and tangential (y) directions through their centers of pressure (COP1 and COP2, respectively). The vertical distance between COP1 and COP2 is defined as dy, the difference between F1y and F2y is defined as dLF, and the average of F1z and F2z is defined as grip force (FGF). Subjects were required to exert a compensatory moment (Tcom) to counter the external moment (Text) caused by the 400-g mass (CMw) inserted in the rightmost compartment acting at a distance (I) from the center of the object. C: single-pulse transcranial magnetic stimulation (TMS) was applied over the left M1 at object contact. Adapted with permission by Davare et al., 2019.

Two six-dimensional force/torque sensors (Nano-25; ATI Industrial Automation, Garner, NC) were affixed to the vertical segment of the manipulandum. These sensors were concealed by a cover plate, and grip surfaces consisting of two plates covered with sandpaper were mounted to the transducers. The sensors allowed us to measure grip and load forces and calculate the center of pressure of the thumb and index finger.

7.2.3 Experimental task

Subjects were seated at a table with the grip-lift device placed in front of them. The object's start position did not face forward (i.e., parallel to the edge of the table), but was rotated in a counterclockwise direction at a 30° offset. This position optimized the biomechanical wrist rotation useful to grasp the object itself. At the beginning of each trial, the subject held on to a rod securely fixed to the table to ensure the repeatability of the starting position as well as arm posture. They were instructed to reach for and grasp the device upon receiving an auditory "go" signal, using only thumb and index fingertips, at a self-selected pace. After grasping the object, the task entailed lifting it approximately 10 cm vertically off the table while trying to minimize any tilting. Subjects were required to hold the object in this elevated position for about 1 s before placing it back on the table following a second auditory cue.

Two conditions were established concerning the provision of predictive information and digit positioning: subjects could either choose freely where to position their fingertips on the grasping surfaces (unconstrained; low predictability), or they were presented with visual cues indicating where to grasp (constrained; high predictability). For the placement of the markers in the high-predictability condition, subjects performed 15 practice trials in the low-predictability condition, and the average digit position across these trials was marked with electrical tape. Tape color and size were the same across all sessions.

7.2.4 TMS procedure and EMG recording

Electromyographic (EMG) activity of the first dorsal interosseus (FDI) of the right hand was recorded using differential surface electrodes placed over the muscle's belly. The

reference electrode was placed on the dorsal surface of the head of the fifth metacarpal. The experimenter ensured that all electrodes remained in place throughout the experiment. The signals were sampled at X kHz and amplified (Neurolog NL844 EMG amplifier, Digitimer, Welwyn Garden City, UK). Data acquisition was performed using a Power 1401 CED data acquisition interface with Signal software (Cambridge Electronic Design, Cambridge, UK).

Transcranial magnetic stimuli (TMS) employing a monophasic current waveform were applied using a figure-of-eight coil (loop diameter 8) connected to a Magstim model 200 stimulator (Magstim, Whitland, UK). For 9 participants we used a DUOMAG MP 70BF figure of 8 butterfly coil with 2 x 70mm windings and an external wing diameter of 9cm. The TMS coil was positioned to target the left M1 region and optimized to elicit motor-evoked potentials (MEP) amplitude in the FDI muscle (Davare et al., 2009; Parikh et al., 2020). We targeted only this muscle following the results by Davare et al. (2019) who found that CSE changes are muscle-specific, targeting only the index finger because it shows greater contact point variability during unconstrained grasping, while the thumb is used as a "pivot". Active motor threshold (AMT) was determined for currents in both the anterior-posterior (AP) and posterior-anterior (PA) directions, respectively. It was defined as the minimum stimulus intensity required to elicit 50 μV peak-to-peak MEPs in five out of ten trials, while the subject held the object the object approximately 10 cm above the table without tilting.

The peak-to-peak amplitude of MEPs of the FDI muscle was measured to quantify corticospinal excitability at object contact.

Following the method by Federico and Perez (2017), the MEP onset was determined as the point in time when rectified EMG signals exceeded two standard deviations of the mean background EMG. The background EMG was measured from the beginning of the recording until 5ms before the stimulus artifact, for a total time of 45ms. MEP onset latencies were computed for each trial per subject and condition. Trials were identified as outliers and removed from further analysis if MEP onset, MEP amplitude, and/or time to peak deviated more than two standard deviations from the mean. We computed the

difference in onset latencies of MEPs elicited by AP directed current vs PA for each condition. We also quantified the variability of MEP latencies, i.e., the onset latency dispersion.

During the experimental procedure, single-pulse TMS stimuli were delivered at the moment of object contact. Subjects completed blocks of 25 trials, within which five did not involve TMS stimulation. These trials were presented in a randomized order. Subjects performed four blocks encompassing all possible combinations of predictability and TMS directions (PAcon; PAuncon; APcon; APuncon).

To ensure a balanced experimental design, one half of the subjects started the experiment with the PA condition, followed by the AP condition, while the other half completed the experiment in opposite order. The sequencing of the predictability condition was pseudorandomized.

7.2.5 Statistical Analyses

To check the distribution of finger positioning during the trials in the constrained vs unconstrained grasping, we run a mixed model on delta finger position (i.e., thumb – index height) using trial number (from 1 to 25) and condition (constrained, unconstrained) as fixed factors and subjects as random variables. We expected delta finger position to became stationary only during the course of the constrained blocks.

To evaluate condition-dependent effects on the difference between AP and PA stimulation, we first computed the difference in amplitude and latency values between AP and PA, i.e., delta amplitude and latency. Then, we run separate paired t-tests comparing these delta mean values between the constrained and unconstrained condition.

Analyses were performed using R and JASP.

7.3 Results

Although we recruited 26 participants, we had to discard 5 of them because of missing or noisy data. Hence, the analyses were only performed on 21 participants.

The mixed model implemented on the delta finger position (i.e., thumb – index height) revealed a significant effect of Trial Number (ChiSquared = 7.06, Pr = 0.007) and an interaction between Trial Number and Condition (ChiSquared = 8.36, Pr = 0.004). In particular, in the unconstrained condition the delta finger position increased during the trials (Figure 7.2).

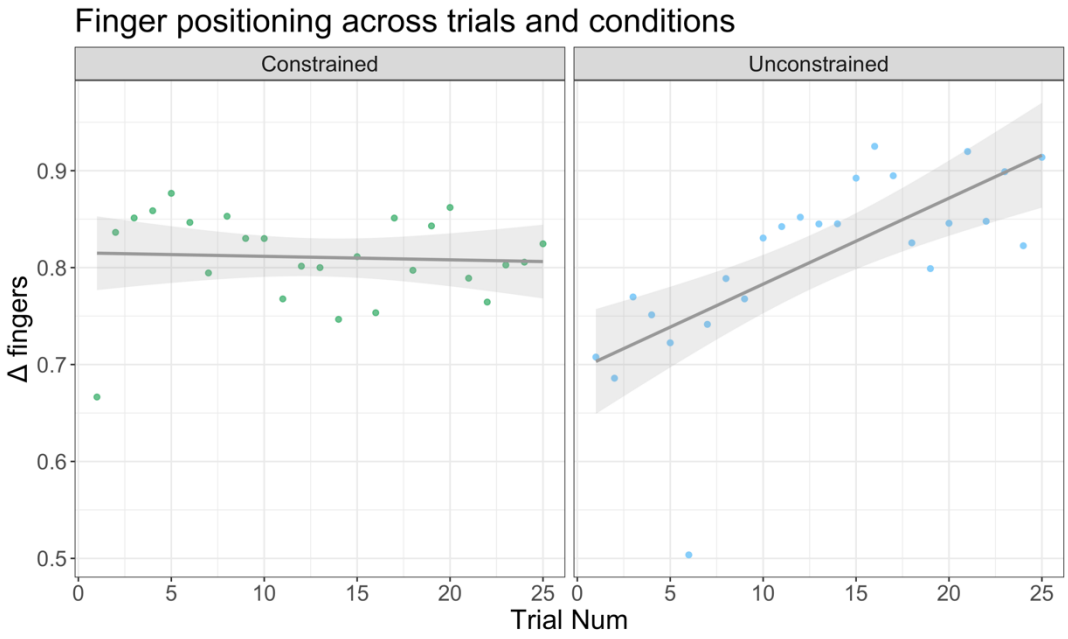

Figure 7.2. Evolution of distance between thumb and index finger on the T-shaped object at contact across the trials (from 1 to 25).

The paired t-tests (Figure 7.3) showed higher scores in the unconstrained vs constrained condition for the mean delta latency (t_{20}=2.75; p=0.012).

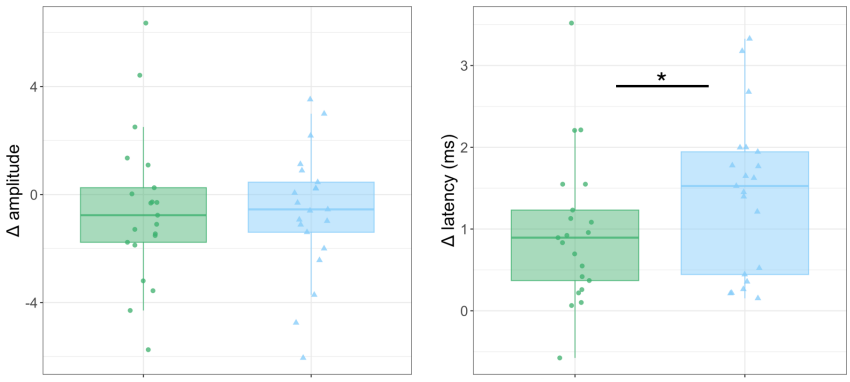

Figure 7.3. Difference between constrained and unconstrained conditions in delta amplitude and latency means.

7.4 Discussion

In the present study, we probed a directional TMS protocol to provide a neurophysiological hallmark of the complex balance between sensorimotor feedback and anticipatory control. We showed that when the reliance on previously stored sensorimotor memory is not sufficient to support a skilled grasping movement, the onset of the motor potentials evoked by AP stimulation is further delayed compared to a grasp context with lower sensorimotor uncertainty. We will discuss this finding in light of the cortico-cortical pathways tapped by different coil orientations during single pulse TMS stimulation.

7.4.1 Cortical pathways triggered by AP and PA stimulation

A single TMS pulse over the primary motor cortex (M1) activates the axons of excitatory synaptic inputs to corticospinal neurons (CSNs). The observed MEP is generated by descending activity in the corticospinal tracts in which a series of volleys of activity can be detected. The earliest wave (direct; D-wave) originates from the direct activation of axons of CSNs; later waves (indirect; I-waves) are thought to result from mono- (early I waves) and polysynaptic (late I waves) inputs to CSNs. Different coil orientations can target different sets of waves. While latero-medial (LM) stimulation targets D-waves, PA gradually targets the I waves (i.e., I1..I2..I3) via monosynaptic inputs to CSNs inducing highly synchronized corticospinal activity. Finally, AP stimulation tends to recruit more indirect inputs to CSNs (i.e., I3 waves) eliciting less synchronized corticospinal activity, which ultimately results in delayed MEP latencies (2-3 ms later than PA; Di Lazzaro et al., 2012). For this reason, late I-waves potentially targeted by PA and AP are supposed to be generated by different excitatory polysynaptic inputs (Ni et al., 2011). PA is supposed to target deep neuronal populations projecting to the pyramidal layer V (L5) neurons, while AP targets more superficial ones (layers 2-3; Aberra et al., 2020; Sommer

et al., 2013). Overall, based on the stimulation direction TMS can recruit different cortical elements.

This idea has been confirmed by several studies disambiguating how these different pathways contribute to motor tasks and can be modulated by stimulation of other brain areas.

A first study by Federico and Perez (2017) provided evidence that late synaptic inputs triggered by AP stimulation are preferentially involved in power vs precision grip. A more subtle analysis relative to the different grip types was conducted by Davis and colleagues (2022). As somatosensory inputs are more relevant during precision vs power grip (Gentilucci et al., 1994; Lei et al., 2018), Davis et al. (2022) provided evidence that during precision grip neuronal populations stimulated by AP coil orientation are more sensitive to S1-M1 interactions, raised via polysynaptic thalamo-cortical pathways triggered by the short afference inhibition (SAI) protocol. Other possible inputs to M1 arise from the premotor cortex and the cerebellum. Based on the evidence that PMv, similarly to S1, has dense connections with the superficial M1 layers (L2-L3, i.e., those targeted by AP stimulation; Ghosh & Porter, 1988, Mao et al., 2011, Sommer et al., 2013), Casarotto and colleagues (2023) applied a PMv-M1 cortico-cortical paired associative stimulation (ccPAS) protocol with different coil orientations during power and precision grasping. They found that AP direction preferentially modulated precision grip likely through the mediation of M1 I2-wave intracortical circuits that interact with monosynaptic projections coming from PMv (Cattaneo et al., 2005). The Authors claim that this result is a hallmark of stronger sensorimotor integration required by precision vs power grip. Finally, AP latency was found to be correlated with the functional connectivity of M1 with the premotor cortex (Volz et al., 2015). The contribution of the premotor cortex to AP inputs is also supported by a multi-scale model of TMS-induced neural activation in M1 proving that AP activates the rostral M1 by triggering premotor pyramidal cells (Aberra et al., 2020). Beyond the cerebral cortex, AP and PA coil orientation may reflect separate connections from the cerebellum with different

conduction times (Spampinato et al., 2020) and functional outcomes: cerebellar activity triggers AP inputs during model-based learning and PA inputs during model-free learning (Hamada et al., 2014).

Overall, these studies provide different accounts for the modulatory effect exerted by other cortical regions on AP inputs. These apparently contradictory findings are explained by the fact that TMS is biased to trigger the pathways that are recruited during each specific task (Di Lazzaro et al., 1998). Hence, the source of inputs to M1 captured by AP stimulation is task-dependent. In most cases, the goal of these studies was to compare precision and power grasping. We are instead the first to provide evidence of a modulation of AP latency exerted by predictive vs. feedback-related motor control. To understand which cortical circuits may potentially be responsible for the effect we observe, we will proceed by addressing cortical contributions to the online update of sensorimotor memory.

7.4.2 Possible sources of late synaptic inputs to M1 during online update of sensorimotor memory

Grasping an object while preventing tilting, spilling, or dropping is supported by sensorimotor learning, i.e., the possibility to optimize motor skills guided by sensory information (Seidler et al., 2013). The pioneering work by Johansson and Westling (1988) suggested for the first time that the information about grip forces influences the preparatory grip force in the following trials. It has been suggested that sensorimotor memory is stored in M1. A first study by Chouinard and colleagues (2005) showed that repetitive stimulation of M1 disrupted the scaling of forces based on information acquired during a previous lift. Loh and colleagues (2010) compared the MEPs recorded when preparing to lift an object of unknown weight preceded by either a heavy or a light object, showing that the MEP amplitude was larger when the lifted object was preceded by a heavy relative to a light object.

A key point in anticipatory control is that predictions of the consequences of our movement in terms of changes in the external world and our own body are conveyed in the form of "efference copy" from M1 to S1 (Miall & Wolpert, 1996). Before movement

initiation, S1 activity can be decoded from preceding activity in M1 (Umeda et al., 2019) and disruption of M1, but not S1 (Schabrun et al., 2008, Parikh et al., 2020), impairs the retrieval of learned digit forces stored in sensorimotor memory. At object contact, somatosensory signals (exafference and reafference) elicited by mechanoreceptors are conveyed within the order of dozens of milliseconds to S1 and trigger eventual corrective mechanisms. Indeed, throughout the movement, S1 activity can be decoded from both M1 and afferent activities (Umeda et al., 2019). Online sensory feedback is then used to assess the accuracy of the motor plan and update the sensorimotor memory. When grasping an object with an asymmetrical center of mass without any clue on fingertip positioning, digit forces are modulated as a function of digit position on a trial-to-trial basis (Fu et al. 2010; Mojtahedi et al. 2015). This information follows the opposite cortical pathway as the anticipatory force, i.e., being broadcasted from S1 to M1. The integrity of both regions is therefore critical to accomplish the task. A recent work by Parikh and colleagues (2020) showed that continuous theta burst stimulation (cTBS) on S1 and M1 impaired the ability to modulate digit forces to position during unconstrained grasping.

It is therefore possible to deduct that the effect we found of higher sensorimotor processing during unconstrained grasping on MEP latency evoked by AP stimulation is explained by cortico-cortical inputs linking S1 and M1. This would reflect greater processing of proprioceptive and tactile inputs reaching S1 to scale digit forces, supported by the finding that late I-waves, compared to early I-waves, are much more affected by cutaneous afferent inputs (Tokimura et al., 2000), and would be in line with the study by Davis and colleagues (2022). However, predictive grip force scaling and sensorimotor feedback processing are complex mechanisms that are unlikely supported exclusively by sensorial and motor areas, and some studies have challenged the claim that M1 alone can store and update sensorimotor memory.

For instance, an elegant study by Dafotakis and colleagues (2008) showed that TMS applied over PMv prior to object contact interfered with the predictive scaling of grip forces according to the most recent lift. In contrast, at object contact, TMS over aIPs

disrupted the reactive adjustment of grip force to the novel mass of the object. No effects were found when stimulating M1. These results are consistent with previous findings about the role of aIPs in grip force scaling (Davare et al., 2007) and online grasping configuration adjustments (Tunik et al., 2005). Moreover, while PMv seems to play a pivotal role in finger positioning, PMd seems to be involved in the recruitment of proximal muscles responsible for the lifting phase. A series of fMRI works by Marneweck and colleagues (2018, 2020) has partially confirmed these results by showing that a broad network including cerebellar lobules I-IV, BA44, PMv and aIPs (but not M1 or S1) are both involved in grasp configuration and matching predicted and actual digit positioning and forces.

Although our study design couldn't disambiguate between all these possible sources of the effect we observed, we speculate that S1-M1 circuit redefines the sensorimotor memory based on the sensory feedback, but then this information must be conveyed to other brain regions in the grasping circuit for efficient online adjustments of the motor plan. As S1 doesn't show direct anatomical connections with PMv (Dancause et al., 2005, 2006), nor aIPs (Borra et al. 2008), M1 is the only possible target of incoming proprioceptive and tactile information from S1. The signal from M1 could then propagate back to the premotor cortex or even reach aIPs for a more efficient motor correction involving both force modulation (aIPs, PMv) and digit positioning (PMv, PMd). This interpretation merges apparently contradictory findings about the role of M1 in storing sensorimotor memories and/or feedback processing by hypothesizing that multiple areas can play a different role in such a process whose nature still needs to be ascertained. Overall, we believe that anticipatory and feedback-control mechanisms are distributed, rather than localized, functions.

7.5 Conclusion

Using a directional TMS protocol during skilled grasping, we showed that increased reliance on feedback control mechanisms is driven by late I-wave pathways, likely mediating cortico-cortical inputs from S1 to M1. Future studies may address the

contribution of other brain regions driving inputs to M1 to update the motor plan, for instance using double coil paradigms to rule out the role of the PMd-M1 and PMv-M1 circuits in this process.

In the current study, we failed to replicate the results obtained by our previous single-pulse PA TMS paradigm on the same task. In Davare et al. (2019), we found higher MEP amplitude in unconstrained vs constrained grasping. A methodological difference can account for this unconfirmed result. In our previous paper, stimulations were performed using a different TMS threshold, i.e., 80% rMT, because stimulations occur at two time points: during midreach, and at contact. Instead, we chose to deliver TMS pulses at 1mV, computed during muscle contraction, i.e., while holding the graspable object.

An intriguing further step would be to assess whether the asymmetric biomechanical capabilities of the thumb and index (Salimi et al 2000) affect the task. This could be achieved by alternating blocks where the CoM is shifted to the right, to blocks where the CoM is shifted to the left.

Understanding how the brain integrates previous experience, stored as sensorimotor memory, and flexibly adapts it based on the feedback it receives from the external world, would be fundamental to plan rehabilitation and targeted motor trainings to restore or improve dexterous manipulation skills. For instance, anticipatory planning is impaired in unilateral spastic cerebral palsy (USCP) (Gutterman et al., 2021), and patients with Parkinson disease can't take advantage of sensorimotor memories gained from previous manipulations, therefore showing that dopamine depletion impairs implicit learning of digit placement and forces during grasp (Lukos et al., 2010).

We ultimately contend that MEP latency, as assessed by directional TMS protocols, can potentially be a neurophysiological biomarker for probing the integrity of sensorimotor processing during skilled hand movements.

CHAPTER 8

General discussion

Action is the only way we can modify our state in the world and exert an influence on it. In this thesis, I've mainly focused on the way we interact with the external world using our hands – to reach, grasp, and lift objects. In studying the neural mechanisms underlying this ability, I have faced methodological, technical, and conceptual challenges.

First: cognitive functions are an emergent property of the brain. This doesn't mean that we must neglect each component's unique properties, but we must frame them in a more complex system within which they acquire new functionalities based on the interaction with other components. In the first part of this thesis, I have stressed the importance of studying the brain circuitries responsible for the planning and implementation of visuomotor functions. The spotlight in this case is on the parietofrontal circuits subserving different actions (e.g., grasping, pointing, saccades) that can be performed with different effectors (e.g., hand, foot, eyes). In Chapter 2, I have pointed out that the boundaries between action- and effector-selective parietal and frontal subregions are blurred and no strict dichotomies between them can be defined. Pending this assumption, segregation still emerges as a relative preference for one action or effector over the others. I have shown that succeeding in the aim of distinguishing adjacent but functionally distinct brain regions requires an accurate structure-to-function mapping tailored to the individual sulcal configuration. Driving general (group-level) inferences on the distinct functionalities of segregated areas in the parietal cortex means finding homologies between individuals (and, on a more general extension, between species). However, to succeed in this aim, it is fundamental to start from the differences, i.e., what makes each individual (and species) unique. Once accomplished this, I went a step further providing evidence that according to which effector is used (e.g., hand or foot) the very same action-specific circuit (e.g., reaching circuit) can show a different behavior, being differently driven by the contribution of effector-specific brain areas. For instance, during hand pointing mpIPS excited hPEc and premotor areas, whereas during foot

pointing, in addition to these connections, the foot-specific parietal region hPE excited hPEc.

In Chapters 3 and 4, I have focused on the very well-known grasping circuit, this time comparing motor execution and imagery to reveal how different task demands modulate the grasping network within and between hemispheres. I have shown that brain activation analyses can only provide information on the different extent to which these areas are engaged across the tasks (imagery or execution). Instead, connectivity analyses have shown that beyond modulating connection strength, motor imagery and execution also rely on a different interplay between areas in the grasping circuit, leading to task-dependent interactions. Also, I have identified similar interregional couplings in both hemispheres despite the movement being unilateral. In all these studies, I provided evidence of a forward-feedback loop linking parietal and frontal areas, that support the view of a directional preference of the information flow and a continuous exchange of information within these networks.

While providing insights into the functioning of parietofrontal circuits during visuomotor tasks, these studies reflect a bias in the research of motor control. We tend to study a dynamic concept (action) with conceptually static paradigms. This is embedded in the way we think about actions in cognitive science. For instance, the most used example to refer to grasping actions is "grasping a cup of coffee". This tells us two things. First, researchers can't survive without coffee. Second, the way we think about action is an oversimplification of the dynamic scenarios we are embedded in. In Chapter 5, I have tried to provide an example paradigm of naturalistic environments in which we daily act, wherein our actions must be rapidly updated, and social interactions take place. From a technical point of view, with that study we observed real-life motor kinematics although actions were taking place in a virtual world and no real interaction with the objects was present. In addition, the study suggested that our behavior and kinematics rapidly adapt to embrace the possibility of living in an unpredictable world: after an unexpected event

and the necessity to modify on flight one's own movement, behavior is rapidly optimized toward reiterative but still infrequent events.

The paradigm I have introduced in Chapter 5 is just an example of realistic and dynamic motor actions. A crucial issue I faced was to make this kind of action suitable for investigation in a neuroimaging setting with the ultimate goal of investigating their neural underpinnings. It is intuitive to think that dynamic actions are just scaffolded on the very same neural mechanisms of actions in a static environment. However, the picture can be more complex, as motor control theories have tried to point out. Nevertheless, to my knowledge, these theories have rarely been tested in truly dynamic environments, often due to a scarcity of technologies to reproduce realistic scenarios. We tried to significantly depart from previous literature in the field by building a motion tracking system inside the MRI scanner room that can potentially challenge the way we approach scientific research questions.

As a drawback, none of the previous studies included the interaction with a real object. Haptics is instead a crucial source of information that shapes our motor commands. In a study with Marco Davare (in prep.), we showed that combining virtual reality and haptic feedback recruits corticospinal tracts to the same extent of real hand-object interactions: touching a virtual object with haptic feedback doesn't lead to smaller excitability of the CST when compared with the contact with a real object. Instead, a virtual touch that is only visual, but lacks haptic feedback, can't trick the motor system. This is because somatosensory feedback provides a continuous update on the body-environment state that is fed via S1 to M1 and motor planning-related areas. In Chapter 7, I tested the refinement of digit forces while grasping and lifting an object with an asymmetrical center of mass. I leveraged TMS for its good temporal resolution and the possibility to test corticospinal excitability. The adoption of a directional paradigm allowed us to infer that trial-to-trial variability in digit positioning and forces stresses corticocortical inputs to M1 as a hallmark of strong sensorimotor processing.

Together, I believe that the studies I presented here represent a personal journey toward a real-life neuroscience that can address the richness of naturalistic motor behavior.

Epilogue: thoughts from real conversations

I am fully aware that motor control doesn't cover only visuomotor functions and crosses many other cognitive domains. Although hand-object interactions constitute my main topic of interest, my curiosity has never been limited to it but spans different research themes that somehow intersect motor control. This has been made possible by the chances I had to discuss such research topics with researchers I met during these three years. These experiences opened my mind to new perspectives that are only tangentially related to my PhD focus.

The present section reports some considerations born from such conversations that I think will help me to contextualize my research in the future. The aim here is to raise questions whose answers are (at least for now) out of my league. I will therefore tackle concepts such as evolution, tool use, and extended cognition without any ambition of being exhaustive on these topics.

"Neuroscience needs evolution"

I borrowed this title from a paper in a theme issue edited by Paul Cisek and Benjamin Hayden in 2022 and that completely revolutionized the way I approached the motor control domain: from an evolutionary perspective.

Our brain has evolved for one scope only: to widen the range of our action possibilities. This is evident from the fact that the two regions in the brain that have mostly increased in size and complexity during evolutionary history are the parietal and the prefrontal cortex (PFC). The parietal cortex is intrinsically a bridge between perception and action and is involved in motor planning: in other words, it is responsible for complex, goal-directed, and future-oriented behaviors. On the other side, the prefrontal cortex itself can be seen as an extension of the premotor cortex, and prefrontal functions can be conceptualized as an abstraction of action selection mechanisms (Fine and Hayden, 2022).

According to this hypothesis, the core function of the PFC is the potentiation and depotentiation of action plans at different levels of abstraction.

The study of the human brain cannot get rid of an evolutionary perspective, which has been neglected by human neuroscientific research for a long time. It is impossible to understand the present shape of the human brain and behavior neglecting how the evolutionary pressure has boosted human abilities to increase the chance of survival (e.g., via upright posture, and the consequent differentiation between limb functions). Looking at the past helps to understand the present and the future: as the evolutionary pressure has shaped our ancestors' brains, it will continue to do so for the following ages. These changes intrinsically encompass both brain structure and function. At a smaller scale, structural and functional differences characterize individuals and mark the distinction between those who have some peculiar, acquired expertise in complex motor functions, and those who have lost the possibility to implement even basic motor functions.

This doesn't mean that we are what we inherited. We are the way we transformed what we inherited to guarantee better functioning and higher probabilities of survival. Also, interacting with the world often means *using* the world to widen our action possibilities. In a paradigmatic shift, neuroscience is moving from the way our actions in the world shape the world, to the way how they shape ourselves. Striking evidence of that comes from the study of tool use, which has profoundly and progressively shaped our brain anatomy, society, and cognition. In the next paragraph, I will try to underline the way the shift from "object" to "tool" use has contributed to the evolution of the brain – especially PPC – overall influencing and being influenced by the progression of visuomotor functions.

From the hand-as-tool to the tool-in-hand

Literally two weeks before the deadline for the submission of the present thesis, I attended a game-changer talk by Emiliano Bruner. His work explores the evolution of visuomotor integration functions from a completely different perspective: evolutionary anthropology, neuroarchaeology, and paleoneurology.

Bruner's work starts from the assumption that *technology* in terms of tool fabrication and usage is among the most prominent features of the Homo sapiens (or, according to Henri Bergson, "Homo faber"). Bipedalism freed the hands and upper limbs from locomotion, paving the way for tool use. *Tooling* has further shaped the brain, especially the parietal cortex, which is by far the region in the brain that has undergone the most substantial morphological evolution (Weidenreich, 1941). The expansion of the parietal bone and cortex and the outfolding of the parietal sulci are typical of modern humans, being absent in Neanderthals and apes, and ultimately constituting a demarcation between the modern human lineage and the others (Bruner et al., 2018). Object manipulation, tool use, and constructive skills are sophisticated products of visuomotor functions. Bruner collected evidence of the lack of visuospatial specialization in Neanderthal vs Homo Sapiens. For instance, Neanderthals didn't make throwing tools (e.g., arches): such a lack of projectile technology may be explained by weak visuospatial ability and eye-hand coordination. Neanderthals also relied on the usage of the mouth as a "third hand", likely to supply scarce hand abilities (Bruner and Lozano, 2014). Another example comes from the evidence that the most archaic tools had big dimensions, requiring to be held with a power grip configuration; during evolutionary history, tools assumed smaller sizes and elongated shapes, thus implying a form of somatic and perceptual specialization in hand-tool interactions including precision and "squeeze" grip. This change observed in the structural properties of the tools evolved simultaneously with the expansion of the SPL, ultimately suggesting that a neural specialization co-evolved with a sensorimotor specialization (Bruner et al., 2023).

As I had the chance to discuss with Alessandro Farnè in Lyon (as part of the Young Investigator Training Program), a key point is that the process of using an external tool is rooted in the experience of *using our own body* as a tool: for instance, the finger to indicate and obtain an object; the mouth and the voice to communicate; and, of course, our hands. Indeed, the ability to interact with the environment requires a definition of the boundaries of our physical self (Goldring & Krubitzer, 2020). The strict link between the usage of our body parts and external objects entails the concept of peripersonal space

(or response field; Bufacchi and Iannetti, 2018). The inner knowledge of our body is one of the most stable representations our brain holds. Nevertheless, starting from the seminal work by Iriki and colleagues (1996) on monkeys, studies on the effects of tool use on body perception showed that the hand representation is dynamic as it can be expanded and contracted depending upon tool (Farnè and Ladavas, 2000; see Maravita and Iriki, 2004 for the first review on the theme and, more recently, Maravita and Romano 2018). Tools can also function as sensory extensions of the user's body (Miller et al., 2018) and modulate sensorimotor representations underlying action, with effects on hand kinematics. Once again, all these processes occur in the PPC as an interface between body and environment in a dynamic, gradual, and flexible architecture.

Studies on tool use and its relationship with body representations can be contextualized in the broader frame of extended, embodied, and enactive cognition – all supporting the idea that cognition can be built by the dynamic interactions between brains, bodies, and material environments (Hutto and Myin 2013; Malafouris 2013). However, most of the studies in this direction are human-centered. That is, when the man "believes he is photographing the outside world he is often observing and depicting himself" (Ramon y Cajal, "Advice for a Young Investigator", 1897). Stepping outside the human species, novel insights can be obtained by studying how other living organisms use the environment to enrich themselves. In the next subparagraph, I will provide an example by discussing studies on motor control in climbing plants.

"I act, therefore I am": lessons from movement control in climbing plants

At the beginning of my third year as a PhD student, I met Bianca Bonato, currently postdoc researcher at the University of Padua under the supervision of Umberto Castiello. Her work on the climbing plants and their grasping-like behavior opened my mind to a new perspective on motor control.

The way organisms explore the environment, interact with it, and use it to ensure their own survival share common features across species, including plants, animals, and even unicellular organisms. This assumption fits well with the lines of research that have

challenged the notion of "cognition" as something that occurs exclusively within the brain. According to this view, cognition can be "distributed" among individuals of the same species (e.g., bees), "embodied", namely encapsulated in the body, or even "extended" when it involves external physical objects that become part of the individual's cognitive system, as the webs for spiders (Parise et al., 2020). In this paragraph, I will share some considerations on the research field that focus on reach-to-grasp behavior in climbing plants, whereby the bond between the plants and their support is considered an example of "extended cognition".

Climbing plants need to grow vertically to maximize their light acquisition. This survival necessity yields them to support searching and attachment mechanisms driven by visual, acoustic, and chemosensory perception. Back in the 19th century, Charles Darwin described the movement of plants during their approach to a support as circumnutation, a set of elliptical movements around the elongation axis aimed to search for climbable supports (Darwin, 1907). This behavior shows surprising similarities to primates' reach-to-grasp behavior.

Kinematic studies on reach-to-grasp plant movements have revealed that climbing plants extract the graspable features of the supports, using them to execute the most appropriate motor program. For example, plants show a speed-accuracy trade-off, whereby they decrease their movement speed for complex to-be-grasped objects (Ceccarini et al., 2020) and size their movements based on the support diameter, optimizing their energy expenditure (Guerra et al., 2019). Plants have also evolved a motor accuracy mechanism through which they monitor and eventually correct in flight their movement through submovements (Ceccarini et al., 2020) also when the root and the aerial signals are contradictory (Guerra et al., 2022). In this latter study, the Authors manipulated the support size to create incongruency between the above- and under-ground thickness (perturbed conditions; see Figure 8.1a-8.1b) and compared plants' kinematics to control conditions where the support size was constant in its whole length (Figure 8.1c-8.1d).

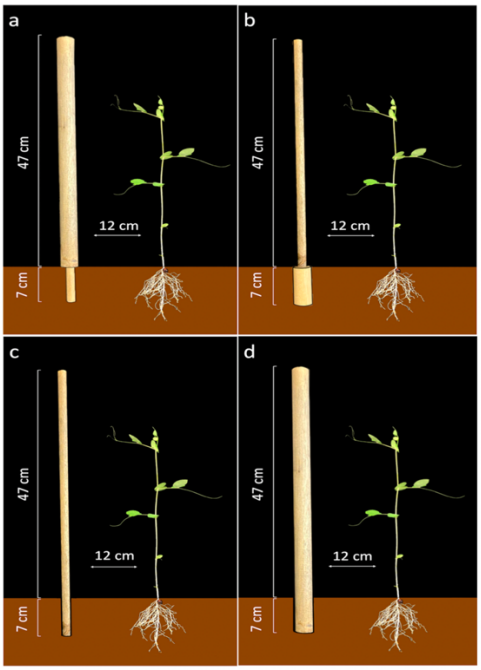

Figure 8.1. A & B) Perturbed conditions, where the support is thinner (A) or thicker (B) under the ground vs above the ground; C & D) Control conditions with thinner (C) or thicker (D) support.

Results showed that a crosstalk between roots and aerial information occurred in the perturbed conditions, as if the plants were aware of the mismatch between the under- and above-ground signals: they flexibly adjusted their motor behavior to such unexpected situation, scaling their movement to effectively wrap around the support. For instance, in the condition where the support was thicker above the ground, the tendrils' maximum velocity was higher, and their aperture was wider.

This evidence suggests that plants form an anticipatory behavior, namely their immediate actions are endowed with the endpoint of the movement itself, but that this behavior is susceptible to online modifications and updates. The Authors frame their results into the proprioceptive feedback mechanisms through which humans correct their motor trajectory based on limb position. In other words, plants, similarly to humans, would be physically self-aware and leverage this knowledge to interact with the environment making support-specific "decisions", a process that may fall under the umbrella term of "high-level processing".

One might be tempted to interpret plant's motor behavior using neuropsychological terms, referring to the notion of "intentionality" and challenging the idea that a neural system is necessary to exhibit such sort of behavior. This would reflect the tendency to extend human processes and their nomenclatures to other species/behaviors. But it is no secret that neural processes have, at their very essence, chemical, and biological basis, on top of which cognitive processes have been established. We should not neglect this assumption when studying human behavior as well.

So, my unsolved question is: should we redefine the relationship between mind, body, and environment, or rebuild our notions on "consciousness", "awareness", and "intentionality"? And how can research in the motor field unfold such issues? Movement is, among the cognitive functions, the one that fills the bridge between the self and the external world and can be objectively measured, e.g., through kinematic indices. These unique features make it ideal to perform a cross-species comparison.

I will conclude this section with a quote from Umberto Castiello (2023): "So far, we have explored a world depending on the central nervous system (CNS) and of course the CNS is a possibility... But it's not the only one".

Supplementary Material

Chapter 2

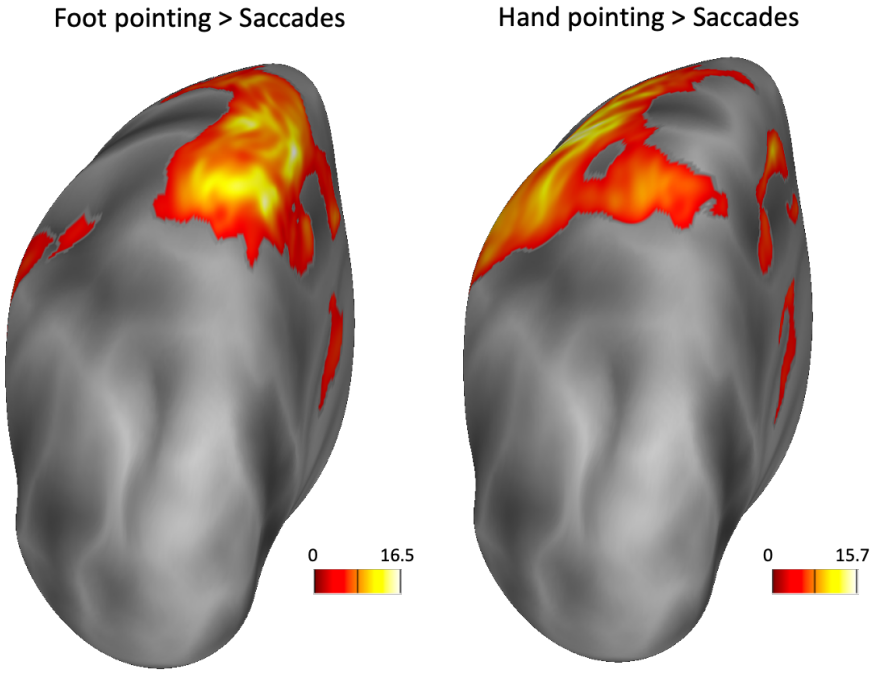

Supplementary Figure 1. *Surface-based group activations in the posterior parietal cortex for the hand pointing > saccades and the foot pointing > saccades (p<0.001 at the voxel level, p<0.05 FDR corrected at the cluster level).*

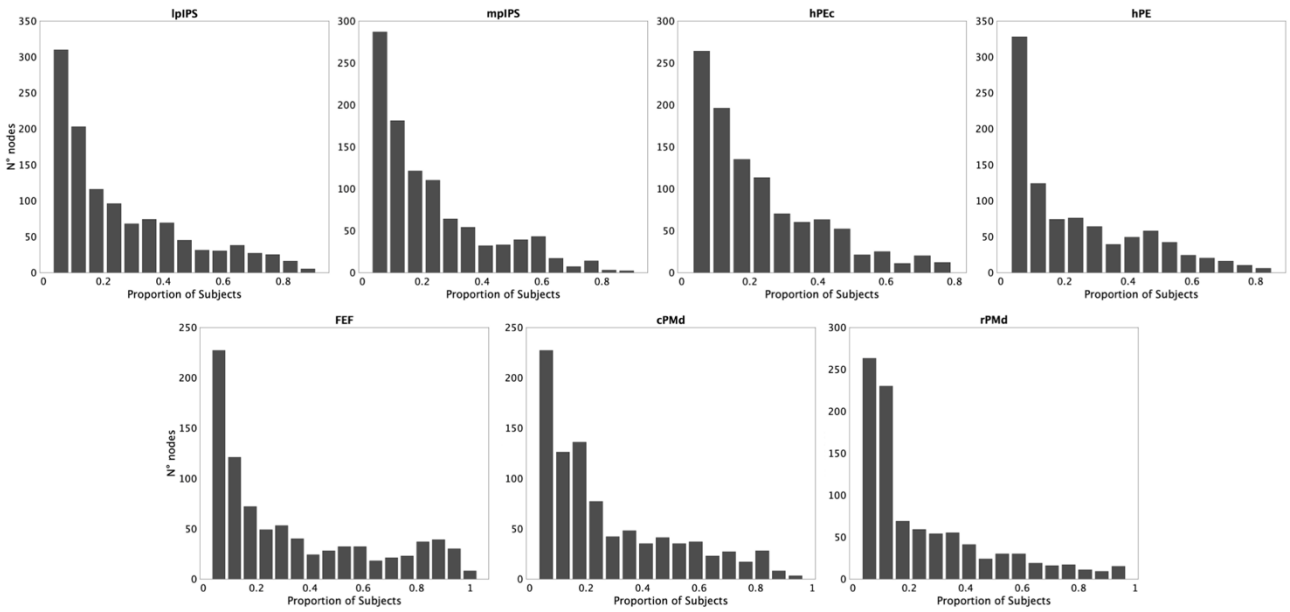

Supplementary Figure 2. *Overlap across subjects of the nodes belonging to each probabilistic ROI.* For each ROI (lateral posterior intraparietal area: lpIPS; medial posterior intraparietal area: mpIPS; caudal hPE: hPEc; human PE: hPE; frontal eye fields: FEF; caudal dorsal premotor cortex: cPMd; rostral dorsal premotor cortex: rPMd), the X-axis

represents the proportion of subjects (ranging from 0 to 1) whose ROIs shared a certain number of nodes (on the Y-axis). All the ROIs reached a maximum overlap of at least 0.75% of the subjects despite inter-individual differences.

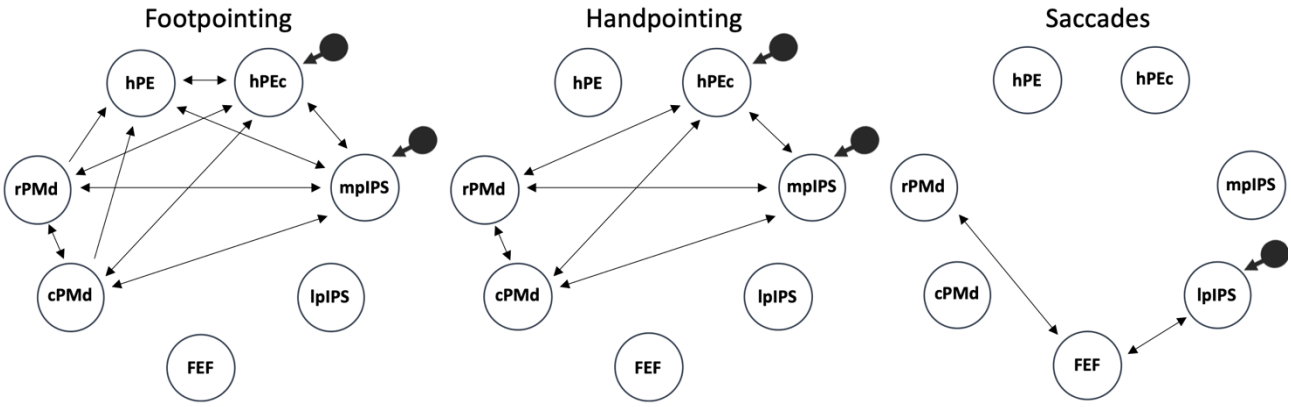

Supplementary Figure 3. *Schematic representation of the B and C Matrices.* Graphical representation of the implemented DCM model for the B matrices. For each condition (namely, hand pointing, foot pointing, and saccades), circled arrows stand for the modeled parameter of the C matrix. Instead, black arrows represent the connections we modeled in the corresponding B matrix; note that in this latter case the arrows also represent the direction of each connection.

Region	**MNI Coordinates**		
	x	***y***	***z***
mpIPS	-17 ± *2,1*	-66 ± *1,8*	54 ± *3,1*
lpIPS	-27 ± *2,8*	-58 ± *2,3*	53 ± *4,8*
hPEc	-15 ± *3,6*	-52 ± *3,7*	67 ± *4,7*
hPE	-11 ± *2,7*	-44 ± *3,2*	70 ± *3,2*
FEF	-39 ± *4,1*	-7 ± *1,3*	50 ± *2,1*
cPMd	-27 ± *2,2*	-12 ± *0,9*	54 ± *4,3*
rPMd	-21 ± *0,6*	-7 ± *2,9*	52 ± *2,3*

Supplementary Table 1. *Mean peak coordinates and standard deviations of individual ROIs.*

	lpIPS	mpIPS	hPEc	hPE	cPMd	rPMd
FEF	**Z = 0.23** T = 5.57 $p = 3.48 \times 10^{-5}$	Z = 0.14 T = 2.66 $p = 9.3 \times 10^{-3}$	Z = 0.08 T = 1.98 $p = 3.4 \times 10^{-2}$	Z = 0.09 T = 2.57 $p = 1.1 \times 10^{-2}$	**Z = 0.34** T = 6.63 $p = 5.67 \times 10^{-6}$	**Z = 0.32** T = 5.15 $p = 7.41 \times 10^{-5}$
lpIPS		**Z = 0.27** T = 4.77 $p = 1.49 \times 10^{-4}$	Z = 0.01 T = 0.08 $p = 4.7 \times 10^{-1}$	Z = -0.04 T = -0.93 $p = 8.2 \times 10^{-1}$	Z = 0.23 T = 2.83 $p = 6.63 \times 10^{-3}$	Z = 0.23 T = 3.14 $p = 3.61 \times 10^{-3}$
mpIPS			**Z = 0.29** T = 4.08 $p = 5.68 \times 10^{-4}$	Z = 0.05 T = 1.13 $p = 1.4 \times 10^{-1}$	**Z = 0.28** T = 6.87 $p = 3.83 \times 10^{-6}$	**Z = 0.51** T = 8.92 $p = 1.9 \times 10^{-7}$
hPEc				**Z = 0.42** T = 4.89 $p = 9.71 \times 10^{-5}$	**Z = 0.32** T = 7.32 $p = 1.9 \times 10^{-6}$	**Z = 0.24** T = 7.5 $p = 1.43 \times 10^{-6}$
hPE					Z = 0.11 T = 0.95 $p = 5.1 \times 10^{-2}$	Z = 0.05 T = 2.7 $p = 1.8 \times 10^{-1}$
cPMd						**Z = 0.61** T = 8.33 $p = 4.3 \times 10^{-7}$

Supplementary Table 2. *Results of the resting-state functional connectivity (rs-FC) analysis.* For each connection between each pair of regions, mean and standard deviations (SD) across individual, Z-transformed connectivity values are shown, along with t-values and uncorrected p-values of the one-sided one-sample t-test. Mean Z-values of significant connections ($p < 0.0024$) are bolded.

From / *To*	**F2**	**FEF**	**LIP**	**MIP**	**PE**	**PEc**
F2		Hutchison 2012, 2013		Raos 2004 Marconi 2001 Matelli 1998		Marconi 2001 Caminiti 1999
FEF	Hutchison 2012, 2013		Bullier 1996 Blatt 1990	Hutchison 2012, 2013		
LIP		Stanton 1995 Blatt 1990		Lewis 2000		
MIP	Bakola 2017	Bakola 2017 Hutchison 2012, 2013	Bakola 2017		Bakola 2017	Bakola 2017
PE	Bakola 2013			Bakola 2013		Bakola 2013
PEc	Bakola 2010			Gamberini 2009	Gamberini 2009	

Supplementary Table 3. *Anatomical macaque studies proving the existence of anatomical connections among regions of interest* (F2/PMd, FEF/FEF, LIP/lpIPS, MIP/mpIPS, PE/hPE, PEc/hPEc). Empty cells stand for anatomical connections not reliably identified in macaques (i.e., reciprocal connections between F2 and LIP, FEF and PE, FEF and PEc, LIP and PE, LIP and PEc, and the connection from PE to F2), or self-connections.

Chapter 3

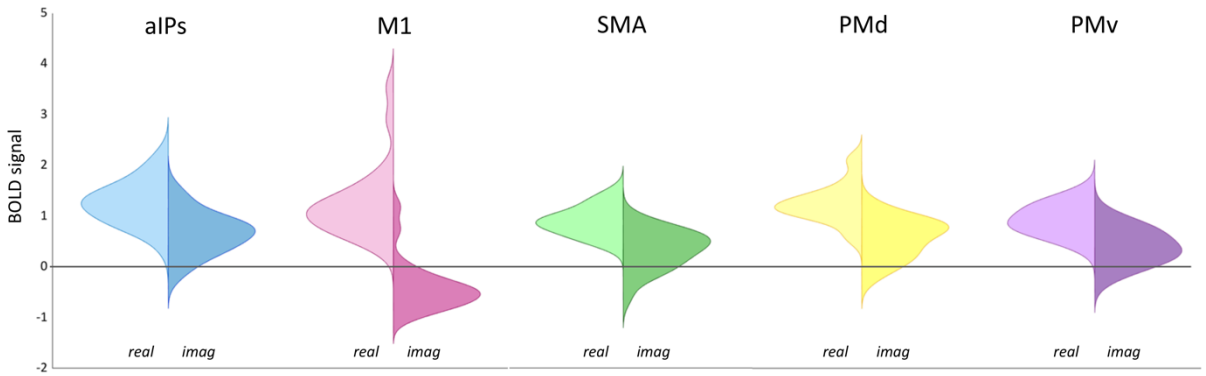

Supplementary Figure 1. *Plots of the activations of the regions of interest (ROIs) in the imagined and the real condition*. Violin plots showing the distribution of the activation of the selected ROIs across subjects are displayed for each region. The right side of the violins represents the imagined condition (*imag*), the left side the real condition (*real*).

From / To	**AIP**	**F1**	**F3**	**F2**	**F5**
AIP					Luppino et al., 1999; Borra et al., 2008
F1			Luppino et al., 1993; Dum et al., 2005	Dum et al., 2005	Dum et al., 2005
F3		Stepniewska et al., 1993; Rouiller et al., 1994		Stepniewska et al., 1993; Luppino et al., 1993	Stepniewska et al., 1993; Luppino et al., 1993
F2		Dum et al., 2005	Luppino et al., 1993; Dum et al., 2005		Marconi et al., 2001
F5	Luppino et al., 1999; Ghosh et al., 1995; Borra et al., 2008	Dum et al., 2005	Dum et al., 2005; Ghosh et al., 1995	Dum et al., 2005	

Supplementary Table 1. *Anatomical studies proving the existence of anatomical connections among regions of interest* (AIP/aIPs, F1/M1, F3/SMA, F2/PMd, F5/PMv). Empty cells stand for anatomical connections not reliably identified in macaques (i.e., reciprocal connections between AIP and F1, AIP and F3, AIP and F2), or self-connections.

To	**aIPs.LH**	**M1.LH**	**SMA.LH**	**PMd.LH**	**PMv.LH**	**aIPs.RH**	**M1.RH**	**SMA.RH**	**PMd.RH**	**PMv.RH**
aIPs.LH					Luppino 1999					
M1.LH			Luppino 1993 Dum & Strick 2005	Matelli 1986 Geyer 2000	Dum & Strick 2005		Jenny 1979 Leichnetz 1986 Rouiller 1994	Rouiller 1994	Rouiller 1994 Ruddy 2017	Dancause 2007
SMA.LH		Stepniewska 1993 Rouiller 1994		Stepniewska 1993 Luppino 1993	Stepniewska 1993 Luppino 1993		Rouiller 1994	McGuire 1991 Rouiller 1994	Rouiller Ruddy 2017	Dancause 2007
PMd.LH		Matelli 1986 Dum & Strick 2005	Luppino 1993 Dum & Strick 2005		Matelli 1986 Marconi 2001		Marconi 2003 Boussaoud 1995 Lanz 2017	Marconi 2003 Lanz 2017	Marconi 2003 Lanz 2017	Marconi 2003 Dancause 2007 Lanz 2017
PMv.LH	Luppino 1999	Dum & Strick 2005	Dum & Strick 2005	Matelli 1986 Dum & Strick 2005			Dancause 2007 Lanz 2017	Dancause 2007 Lanz 2017	Dancause 2007 Lanz 2017	Boussaoud 1995 Dancause 2007 Lanz 2017
aIPs.RH										Luppino 1999
M1.RH		Jenny 1979 Leichnetz 1986 Rouiller 1994	Rouiller 1994	Rouiller 1994 Ruddy 2017	Dancause 2007			Luppino 1993 Dum & Strick 2005	Matelli 1986 Geyer 2000	Dum & Strick 2005
SMA.RH		Rouiller 1994	McGuire 1991 Rouiller 1994	Rouiller 1994 Ruddy 2017	Dancause 2007		Stepniewska 1993 Rouiller 1994		Stepniewska 1993 Luppino 1993	Stepniewska 1993 Luppino 1993
PMd.RH		Marconi 2003 Boussaoud 1995 Lanz 2017	Marconi 2003 Lanz 2017	Marconi 2003 Lanz 2017	Marconi 2003 Dancause 2007 Lanz 2017		Matelli 1986 Dum & Strick 2005	Luppino 1993 Dum & Strick 2005		Matelli 1986 Marconi 2001
PMv.RH		Dancause 2007	Dancause 2007	Dancause 2007	Boussaoud 1995	Luppino 1999	Dum & Strick 2005	Dum & Strick 2005	Matelli 1986	

		Lanz 2017	Lanz 2017	Lanz 2017	Dancause 2007 Lanz 2017				Dum & Strick 2005	

Supplementary Table 1. Anatomical macaque studies proving the existence of anatomical connections among regions of interest of the left and right hemisphere (aIPs, PMv, PMd, SMA and M1). Homologous regions (e.g., aIPs in the two hemispheres) are supposed to be reciprocally connected. Green cells represent existent anatomical connections; white cells stand for anatomical connections not reliably identified in macaques, or self-connections.

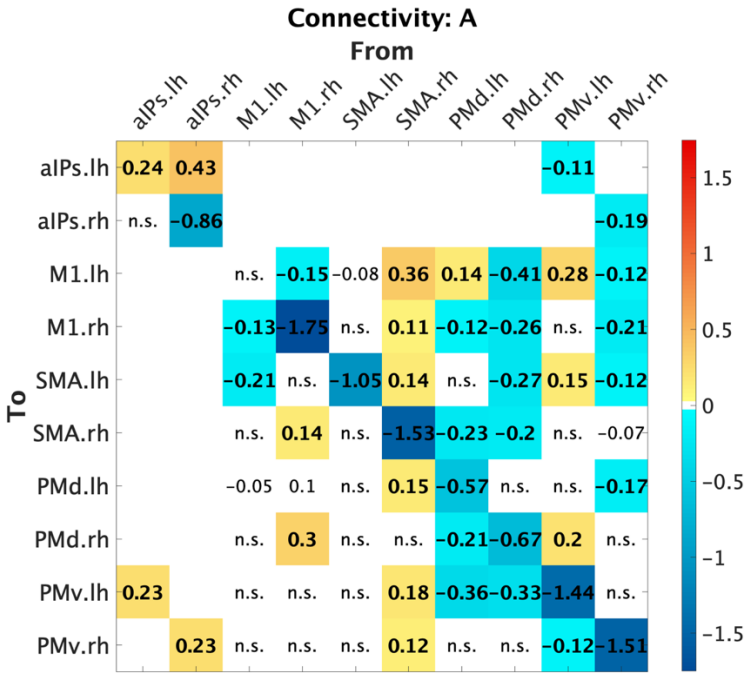

Supplementary Figure 1. *PEB results – A matrix.* Matrix of the effective connectivity of the unmodelled baseline; only suprathreshold parameters posterior probability > 0.95 are shown, whereas subthreshold parameters are marked with "n.s." (i.e., non-suprathreshold), and non-modelled connections, i.e, whose priors are set to 0, are displayed in white. Connection strengths are represented in a scale from yellow to dark red, if excitatory, and from turquoise to dark blue, if inhibitory. Values of connection strengths are also provided.

References

Aberra, A. S., Wang, B., Grill, W. M., & Peterchev, A. V. (2020). Simulation of transcranial magnetic stimulation in head model with morphologically-realistic cortical neurons. Brain Stimulation, 13(1), 175–189. https://doi.org/10.1016/j.brs.2019.10.002

Ahdab, R., Ayache, S. S., Farhat, W. H., Mylius, V., Schmidt, S., Brugières, P., & Lefaucheur, J-P. (2014). Reappraisal of the anatomical landmarks of motor and premotor cortical regions for image-guided brain navigation in TMS practice: Anatomical Landmarks for Motor Cortex Mapping. *Human Brain Mapping, 35*(5), 2435–2447. doi:10.1002/hbm.22339.

Alexander, G. E., & Crutcher, M. D. (1990). Preparation for movement: neural representations of intended direction in three motor areas of the monkey. *Journal of Neurophysiology, 64*(1), 133-150.

Alexander, W. H., & Brown, J. W. (2011). Medial prefrontal cortex as an action-outcome predictor. Nature Neuroscience, 14(10), 1338–1344. https://doi.org/10.1038/nn.2921

Andersen, R. A., & Buneo, C. A. (2002). Intentional Maps in Posterior Parietal Cortex. *Annual Review of Neuroscience, 25*(1), 189–220. doi:10.1146/annurev.neuro.25.112701.142922.

Andersen, R. A., & Cui, H. (2009). Intention, Action Planning, and Decision Making in Parietal-Frontal Circuits. *Neuron, 63*(5), 568–583. doi:10.1016/j.neuron.2009.08.028.

Arbib, M. A., & Mundhenk, T. N. (2005). Schizophrenia and the mirror system: an essay. *Neuropsychologia, 43*(2), 268–280. https://doi.org/10.1016/j.neuropsychologia.2004.11.013.

Archambault, P. S., Ferrari-Toniolo, S., & Battaglia-Mayer, A. (2011). Online Control of Hand Trajectory and Evolution of Motor Intention in the Parietofrontal System. The Journal of Neuroscience, 31(2), 742–752. https://doi.org/10.1523/JNEUROSCI.2623-10.2011

Ashe, J., Taira, M., Smyrnis, N., Pellizzer, G., Georgakopoulos, T., Lurito, J. T., & Georgopoulos, A. P. (1993). Motor cortical activity preceding a memorized movement trajectory with an orthogonal bend. *Experimental Brain Research, 95*(1), 118-130.

Bajaj, S., Butler, A. J., Drake, D., & Dhamala, M. (2015). Brain effective connectivity during motor-imagery and execution following stroke and rehabilitation. *NeuroImage. Clinical, 8*, 572–582. https://doi.org/10.1016/j.nicl.2015.06.006.

Bakola, S., Gamberini, M., Passarelli, L., Fattori, P., & Galletti, C. (2010). Cortical Connections of Parietal Field PEc in the Macaque: Linking Vision and Somatic Sensation for the Control of Limb Action. *Cerebral Cortex, 20*(11), 2592–2604. doi:10.1093/cercor/bhq007.

Bakola, S., Passarelli, L., Gamberini, M., Fattori, P., & Galletti, C. (2013). Cortical Connectivity Suggests a Role in Limb Coordination for Macaque Area PE of the Superior Parietal Cortex. *Journal of Neuroscience, 33*(15), 6648–6658. doi:10.1523/JNEUROSCI.4685-12.2013.

Bakola, S., Passarelli, L., Huynh, T., Impieri, D., Worthy, KH., Fattori, P., Galletti, C., Burman, KJ., & Rosa, MGP. (2017). Cortical Afferents and Myeloarchitecture Distinguish the Medial Intraparietal Area (MIP) from Neighboring Subdivisions of the Macaque Cortex. *eNeuro, 4*(6), ENEURO.0344-17.2017. doi:10.1523/ENEURO.0344-17.2017.

Baliz, Y., Armatas, C., Farrow, M., Hoy, K. E., Fitzgerald, P. B., Bradshaw, J. L., & Georgiou-Karistianis, N. (2005). The influence of attention and age on the occurrence of mirror movements. *Journal of the International Neuropsychological Society, 11*(07). https://doi.org/10.1017/S1355617705051003.

Baltaretu, B. R., Monaco, S., Velji-Ibrahim, J., Luabeya, G. N., & Crawford, J. D. (2020). Parietal Cortex Integrates Saccade and Object Orientation Signals to Update Grasp Plans. The Journal of Neuroscience, 40(23), 4525–4535. https://doi.org/10.1523/JNEUROSCI.0300-20.2020

Batista, A. P., Buneo, C. A., Snyder, LH., & Andersen, RA. (1999). Reach plans in eye-centered coordinates. *Science, 285*(5425), 257–260. doi:10.1126/science.285.5425.257.

Battaglia-Mayer, A., Ferraina, S., Genovesio, A., Marconi, B., Squatrito, S., Molinari, M., Lacquaniti, F., & Caminiti, R. (2001). Eye-hand coordination during reaching. II. An analysis of the relationships between visuomanual signals in parietal cortex and parieto-frontal association projections. *Cerebral Cortex, 11*(6), 528–544. doi:10.1093/cercor/11.6.528.

Begliomini, C., Sartori, L., di Bono, M. G., Budisavljević, S., & Castiello, U. (2018). The neural correlates of grasping in left-handers: When handedness does not matter. *Frontiers in Neuroscience, 12*, 192. https://doi.org/10.3389/fnins.2018.00192.

Begliomini, C., Sartori, L., Miotto, D., Stramare, R., Motta, R., & Castiello, U. (2015). Exploring manual asymmetries during grasping: A dynamic causal modeling approach. *Frontiers in Psychology, 6*. https://doi.org/10.3389/fpsyg.2015.00167.

Begliomini, C., Wall, M. B., Smith, A. T., & Castiello, U. (2007). Differential cortical activity for precision and whole-hand visually guided grasping in humans. *European Journal of Neuroscience, 25*, 1245–1252.

Belmalih, A., Borra, E., Contini, M., Gerbella, M., Rozzi, S., & Luppino, G. (2009). Multimodal architectonic subdivision of the rostral part (area F5) of the macaque ventral premotor cortex. *Journal of Comparative Neurology, 512*(2), 183–217. https://doi.org/10.1002/cne.21892.

Bencivenga, F., Sulpizio, V., Tullo, M. G., & Galati, G. (2021). Assessing the effective connectivity of premotor areas during real vs imagined grasping: A DCM-PEB approach. *NeuroImage, 230*, 117806. https://doi.org/10.1016/j.neuroimage.2021.117806.

Benjamini, Y., & Hochberg, Y. (1995). Controlling the false discovery rate: a practical and.

Bestmann, S., Swayne, O., Blankenburg, F., Ruff, C. C., Haggard, P., Weiskopf, N., Josephs, O., Driver, J., Rothwell, J. C., & Ward, N. S. (2008). Dorsal Premotor Cortex Exerts State-Dependent Causal Influences on Activity in Contralateral Primary Motor and Dorsal Premotor Cortex. *Cerebral Cortex, 18*(6), 1281–1291. https://doi.org/10.1093/cercor/bhm159.

Beurze, S. M., de Lange, F. P., Toni, I., & Medendorp, W. P. (2007). Integration of Target and Effector Information in the Human Brain During Reach Planning. *Journal of Neurophysiology, 97*(1), 188–199. doi:10.1152/jn.00456.2006.

Beurze, S. M., de Lange, F. P., Toni, I., & Medendorp, W. P. (2009). Spatial and Effector Processing in the Human Parietofrontal Network for Reaches and Saccades. *Journal of Neurophysiology, 101*(6), 3053–3062. doi:10.1152/jn.91194.2008.

Bhattacharyya, R., Musallam, S., & Andersen, R. A. (2009). Parietal Reach Region Encodes Reach Depth Using Retinal Disparity and Vergence Angle Signals. *Journal of Neurophysiology, 102*(2), 805–816. doi:10.1152/jn.90359.2008.

Binkofski, F., & Buxbaum, L. J. (2013). Two action systems in the human brain. *Brain and Language, 127*(2), 222–229. https://doi.org/10.1016/j.bandl.2012.07.007.

Binkofski, F., Dohle, C., Posse, S., Stephan, K. M., Hefter, H., Seitz, R. J., and others. (1998). Human anterior intraparietal area subserves prehension: a combined lesion and functional MRI activation study. *Neurology, 50*, 1253–1259.

Blangero, A., Gaveau, V., Luauté, J., Rode, G., Salemme, R., Guinard, M., Boisson, D., Rossetti, Y., & Pisella, L. (2008). A hand and a field effect in on-line motor control in unilateral optic ataxia. Cortex, 44(5), 560–568. https://doi.org/10.1016/j.cortex.2007.09.004

Blatt, G. J., Andersen, R. A., & Stoner, G. R. (1990). Visual receptive field organization and cortico-cortical connections of the lateral intraparietal area (area LIP) in the macaque. *Journal of Comparative Neurology, 299*(4), 421–445. doi:10.1002/cne.902990404.

Blohm, G., & Crawford, J. D. (2007). Computations for geometrically accurate visually guided reaching in 3-D space. *Journal of Vision, 7*(5), 4–4. doi:10.1167/7.5.4.

Blohm, G., Keith, G. P., & Crawford, J. D. (2009). Decoding the Cortical Transformations for Visually Guided Reaching in 3D Space. *Cerebral Cortex, 19*(6), 1372–1393. doi:10.1093/cercor/bhn177.

Bodwell, J. A., Mahurin, R. K., Waddle, S., Price, R., & Cramer, S. C. (2003). Age and Features of Movement Influence Motor Overflow: AGING AND MOTOR OVERFLOW. *Journal of the American Geriatrics Society, 51*(12), 1735–1739. https://doi.org/10.1046/j.1532-5415.2003.51557.x.

Borra, E., Belmalih, A., Calzavara, R., Gerbella, M., Murata, A., Rozzi, S., & Luppino, G. (2008). Cortical connections of the macaque anterior intraparietal (AIP) area. *Cerebral Cortex, 18*(5), 1094–1111. https://doi.org/10.1093/cercor/bhm146.

Borra, E., Belmalih, A., Calzavara, R., Gerbella, M., Murata, A., Rozzi, S., & Luppino, G. (2008). Cortical Connections of the Macaque Anterior Intraparietal (AIP) Area. Cerebral Cortex, 18(5), 1094–1111. https://doi.org/10.1093/cercor/bhm146

Botvinick, M., & Cohen, J. (1998). Rubber hands 'feel' touch that eyes see. Nature, 391(6669), 756–756. https://doi.org/10.1038/35784

Boussaoud, D., Jouffrais, C., Tanné-Gariépy, J., Wannier, T., & Rouiller, E. M. (2005). Callosal connections of dorsal versus ventral premotor areas in the macaque monkey: A multiple retrograde tracing study. *BMC Neuroscience, 6*(1), 67. https://doi.org/10.1186/1471-2202-6-67.

Bozzacchi, C., Giusti, M. A., Pitzalis, S., Spinelli, D., & Di Russo, F. (2012). Similar cerebral motor plans for real and virtual actions. *PLoS ONE, 7*(10), e47783. https://doi.org/10.1371/journal.pone.0047783.

Brandi, M.-L., Wohlschläger, A., Sorg, C., & Hermsdörfer, J. (2014). The Neural Correlates of Planning and Executing Actual Tool Use. The Journal of Neuroscience, 34(39), 13183–13194. https://doi.org/10.1523/JNEUROSCI.0597-14.2014

Breveglieri, R. (2006). Somatosensory Cells in Area PEc of Macaque Posterior Parietal Cortex. *Journal of Neuroscience, 26*(14), 3679–3684. doi:10.1523/JNEUROSCI.4637-05.2006.

Breveglieri, R., Galletti, C., Monaco, S., & Fattori, P. (2008). Visual, somatosensory, and bimodal activities in the macaque parietal area PEc. *Cerebral Cortex, 18*(4), 806–816. doi:10.1093/cercor/bhm127.

Brodoehl, S., Gaser, C., Dahnke, R., Witte, O. W., & Klingner, C. M. (2020). Surface-based analysis increases the specificity of cortical activation patterns and connectivity results. *Scientific Reports, 10*(1), 5737. doi:10.1038/s41598-020-62832-z.

Brookes, J., Warburton, M., Alghadier, M., Mon-Williams, M., & Mushtaq, F. (2020). Studying human behavior with virtual reality: The Unity Experiment Framework. Behavior Research Methods, 52(2), 455–463. https://doi.org/10.3758/s13428-019-01242-0

Bruner, E., & Lozano Ruiz, M. (2014). Extended mind and visuo-spatial integration: three hands for the Neandertal lineage.

Bruner, E., Battaglia-Mayer, A., & Caminiti, R. (2023). The parietal lobe evolution and the emergence of material culture in the human genus. Brain Structure and Function, 228(1), 145-167.

Bruner, E., Spinapolice, E., Burke, A., & Overmann, K. A. (2018). Visuospatial Integration: Paleoanthropological and Archaeological Perspectives. In L. D. Di Paolo, F. Di Vincenzo, & F. De Petrillo (Eds.), Evolution of Primate Social Cognition (Vol. 5, pp. 299–326). Springer International Publishing. https://doi.org/10.1007/978-3-319-93776-2_19

Bufacchi, R. J., & Iannetti, G. D. (2018). An action field theory of peripersonal space. Trends in cognitive sciences, 22(12), 1076-1090.

Bullier, J., Schall, J. D., & Morel, A. (1996). Functional streams in occipito-frontal connections in the monkey. *Behavioral Brain Research, 76*(1–2), 89–97. doi:10.1016/0166-4328(95)00182-4.

Buneo, C. A., & Andersen, R. A. (2006). The posterior parietal cortex: Sensorimotor interface for the planning and online control of visually guided movements. *Neuropsychologia, 44*(13), 2594–2606. doi:10.1016/j.neuropsychologia.2005.10.011.

Buneo, C. A., Jarvis, M. R., Batista, A. P., & Andersen, R. A. (2002). Direct visuomotor transformations for reaching. *Nature, 416*(6881), 632–636. doi:10.1038/416632a.

Burnod, Y., Baraduc, P., Battaglia-Mayer, A., Guigon, E., Koechlin, E., Ferraina, S., Lacquaniti, F., & Caminiti, R. (1999). Parieto-frontal coding of reaching: an integrated framework. *Experimental Brain Research, 129*(3), 325-346. doi:10.1007/s002210050902.

Burstedt, M. K. O., Flanagan, J. R., & Johansson, R. S. (1999). Control of Grasp Stability in Humans Under Different Frictional Conditions During Multidigit Manipulation. Journal of Neurophysiology, 82(5), 2393–2405. https://doi.org/10.1152/jn.1999.82.5.2393

Bursztyn, L. L. C. D., Ganesh, G., Imamizu, H., Kawato, M., & Flanagan, J. R. (2006). Neural Correlates of Internal-Model Loading. *Current Biology, 16*(24), 2440–2445. https://doi.org/10.1016/j.cub.2006.10.051.

Buxton, R. B., Wong, E. C., & Frank, L. R. (1998). Dynamics of blood flow and oxygenation changes during brain activation: the balloon model. *Magnetic Resonance in Medicine, 39*(6), 855-864. https://doi.org/10.1002/mrm.1910390602.

Calton, J. L., Dickinson, A. R., & Snyder, L. H. (2002). Non-spatial, motor-specific activation in posterior parietal cortex. *Nature Neuroscience, 5*(6), 580–588. doi:10.1038/nn0602-862.

Caminiti, R., Genovesio, A., Marconi, B., Mayer, A. B., Onorati, P., Ferraina, S., Mitsuda, T., Giannetti, S., Squatrito, S., Maioli, M. G., et al. (1999). Early coding of reaching: frontal and parietal association connections of parieto-occipital cortex: Reaching: V6A and frontal and parietal association areas. *European Journal of Neuroscience, 11*(9), 3339–3345. doi:10.1046/j.1460-9568.1999.00801.x.

Candidi, M., Sacheli, L. M., Era, V., Canzano, L., Tieri, G., & Aglioti, S. M. (2017). Come together: Human–avatar on-line interactions boost joint-action performance in apraxic patients. Social Cognitive and Affective Neuroscience, 12(11), 1793–1802. https://doi.org/10.1093/scan/nsx114

Cao, Y., Hao, Y., Liao, Y., Xu, K., Wang, Y., Zhang, S., Zhang, Q., Chen, W., & Zheng, X. (2013). Information analysis on neural tuning in dorsal premotor cortex for reaching and grasping. *Computational and Mathematical Methods in Medicine, 2013*. https://doi.org/10.1155/2013/730374.

Carter, C. S., Braver, T. S., Barch, D. M., Botvinick, M. M., Noll, D., & Cohen, J. D. (1998). Anterior Cingulate Cortex, Error Detection, and the Online Monitoring of Performance. Science, 280(5364), 747–749. https://doi.org/10.1126/science.280.5364.747

Casarotto, A., Dolfini, E., Fadiga, L., Koch, G., & D'Ausilio, A. (2023). Cortico-cortical paired associative stimulation conditioning superficial ventral premotor cortex–primary motor cortex connectivity influences motor cortical activity during precision grip. The Journal of Physiology, 601(17), 3945–3960. https://doi.org/10.1113/JP284500

Castiello, U., & Begliomini, C. (2008). The Cortical Control of Visually Guided Grasping. *The Neuroscientist, 14*(2), 157–170. https://doi.org/10.1177/1073858407312080.

Cavina-Pratesi, C., Monaco, S., Fattori, P., Galletti, C., McAdam, T. D., Quinlan, D. J., Goodale, M. A., & Culham, J. C. (2010). Functional Magnetic Resonance Imaging Reveals the Neural Substrates of Arm Transport and Grip Formation in Reach-to-Grasp Actions in Humans. *Journal of Neuroscience, 30*(31), 10306–10323. doi:10.1523/JNEUROSCI.2023-10.2010.

Ceccarini, F., Guerra, S., Peressotti, A., Peressotti, F., Bulgheroni, M., Baccinelli, W., Bonato, B., & Castiello, U. (2020). Speed–accuracy trade-off in plants. Psychonomic Bulletin & Review, 27(5), 966–973. https://doi.org/10.3758/s13423-020-01753-4

Chang, S. W. C., Dickinson, A. R., & Snyder, L. H. (2008). Limb-specific representation for reaching in the posterior parietal cortex. *Journal of Neuroscience, 28*(24), 6128–6140. doi:10.1523/JNEUROSCI.1442-08.2008.

Chang, S. W. C., Papadimitriou, C., & Snyder, L. H. (2009). Using a compound gain field to compute a reach plan. *Neuron, 64*(5), 744–755. doi:10.1016/j.neuron.2009.11.005.

Chaplin, T. A., Yu, H.-H., Soares, J. G. M., Gattass, R., & Rosa, M. G. P. (2013). A Conserved Pattern of Differential Expansion of Cortical Areas in Simian Primates. *Journal of Neuroscience, 33*(38), 15120. doi:10.1523/JNEUROSCI.2909-13.2013.

Chapman, C. S., Gallivan, J. P., Culham, J. C., & Goodale, M. A. (2011). Mental blocks: fMRI reveals top-down modulation of early visual cortex when obstacles interfere with grasp planning. Neuropsychologia, 49(7), 1703–1717. https://doi.org/10.1016/j.neuropsychologia.2011.02.048

Choi, S. H., Na, D. L., Kang, E., Lee, K. M., Lee, S. W., & Na, D. G. (2001). Functional magnetic resonance imaging during pantomiming tool-use gestures. *Experimental Brain Research, 139*(3), 311–317. https://doi.org/10.1007/s002210100777.

Chouinard, P. A., & Paus, T. (2006). The Primary Motor and Premotor Areas of the Human Cerebral Cortex. *Neuroscientist, 12*(2), 143–152. doi:10.1177/1073858405284255.

Chouinard, P. A., Leonard, G., & Paus, T. (2005). Role of the Primary Motor and Dorsal Premotor Cortices in the Anticipation of Forces during Object Lifting. The Journal of Neuroscience, 25(9), 2277–2284. https://doi.org/10.1523/JNEUROSCI.4649-04.2005

Christensen, M. S., Lundbye-Jensen, J., Geertsen, S. S., Petersen, T. H., Paulson, O. B., & Nielsen, J. B. (2007). Premotor cortex modulates somatosensory cortex during voluntary movements without proprioceptive feedback. Nature Neuroscience, 10(4), 417–419. https://doi.org/10.1038/nn1873

Chumbley, J., Worsley, K., Flandin, G., & Friston, K. (2010). Topological FDR for neuroimaging. NeuroImage, 49(4), 3057–3064. https://doi.org/10.1016/j.neuroimage.2009.10.090

Cisek, P., & Hayden, B. Y. (2022). Neuroscience needs evolution. Philosophical Transactions of the Royal Society B: Biological Sciences, 377(1844), 20200518. https://doi.org/10.1098/rstb.2020.0518

Cisek, P., & Kalaska, J. F. (2002). Modest Gaze-Related Discharge Modulation in Monkey Dorsal Premotor Cortex During a Reaching Task Performed With Free Fixation. *Journal of Neurophysiology, 88*(2), 1064–1072. doi:10.1152/jn.00995.2001.

Cisek, P., & Kalaska, J. F. (2005). Neural Correlates of Reaching Decisions in Dorsal Premotor Cortex: Specification of Multiple Direction Choices and Final Selection of Action. *Neuron, 45*(5), 801–814. https://doi.org/10.1016/j.neuron.2005.01.027.

Cisek, P., & Kalaska, J. F. (2010). Neural mechanisms for interacting with a world full of action choices. Annual review of neuroscience, 33, 269-298.

Cona, G., & Semenza, C. (2017). Supplementary motor area as key structure for domain-general sequence processing: A unified account. *Neuroscience and Biobehavioral Reviews, 72*, 28–42. https://doi.org/10.1016/j.neubiorev.2016.10.033.

Connolly, J. D., Andersen, R. A., & Goodale, M. A. (2003). FMRI evidence for a "parietal reach region" in the human brain. *Experimental Brain Research, 153*(2), 140–145. doi:10.1007/s00221-003-1587-1.

Coull, J. T., Charras, P., Donadieu, M., Droit-Volet, S., & Vidal, F. (2015). SMA Selectively Codes the Active Accumulation of Temporal, Not Spatial, Magnitude. *Journal of Cognitive Neuroscience, 27*(11), 2281–2298. https://doi.org/10.1162/jocn_a_00854.

Cui, H., & Andersen, R. A. (2007). Posterior parietal cortex encodes autonomously selected motor plans. *Neuron, 56*(3), 552–559. doi:10.1016/j.neuron.2007.09.031.

Culham, J. (2004). Human brain imaging reveals a parietal area specialized for grasping. In: Duncan J, Kanwisher N, editors. *Attention and performance: functional neuroimaging of visual cognition*. Oxford (UK): Oxford University Press. 417–438.

Culham, J. C., Cavina-Pratesi, C., & Singhal, A. (2006). The role of parietal cortex in visuomotor control: what have we learned from neuroimaging? *Neuropsychologia, 44*(13), 2668–2684. doi:10.1016/j.neuropsychologia.2005.11.003.

Culham, J. C., Danckert, S. L., Souza, J. F. X. D., Gati, J. S., Menon, R. S., & Goodale, M. A. (2003). Visually guided grasping produces fMRI activation in dorsal but not ventral stream brain areas. Experimental Brain Research, 153(2), 180–189. https://doi.org/10.1007/s00221-003-1591-5

Dafotakis, M., Sparing, R., Eickhoff, S. B., Fink, G. R., & Nowak, D. A. (2008). On the role of the ventral premotor cortex and anterior intraparietal area for predictive and reactive scaling of grip force. *Brain Research, 1228*, 73–80. https://doi.org/10.1016/j.brainres.2008.06.027.

Dafotakis, M., Sparing, R., Eickhoff, S. B., Fink, G. R., & Nowak, D. A. (2008). On the role of the ventral premotor cortex and anterior intraparietal area for predictive and reactive scaling of grip force. Brain Research, 1228, 73–80. https://doi.org/10.1016/j.brainres.2008.06.027

Dale, A. M., Fischl, B., & Sereno, M. I. (1999). Cortical surface-based analysis. I. Segmentation and surface reconstruction. *Neuroimage, 9*(2), 179–194. doi:10.1006/nimg.1998.0395.

Dancause, N., Barbay, S., Frost, S. B., Mahnken, J. D., & Nudo, R. J. (2007). Interhemispheric connections of the ventral premotor cortex in a new world primate. *The Journal of Comparative Neurology, 505*(6), 701–715. https://doi.org/10.1002/cne.21531.

Dancause, N., Barbay, S., Frost, S. B., Plautz, E. J., Popescu, M., Dixon, P. M., & others. (2006). Topographically divergent and convergent connectivity between premotor and primary motor cortex. *Cerebral Cortex, 16*(8), 1057-1068.

Dancause, N., Barbay, S., Frost, S. B., Plautz, E. J., Stowe, A. M., Friel, K. M., & Nudo, R. J. (2006). Ipsilateral connections of the ventral premotor cortex in a new world primate. The Journal of Comparative Neurology, 495(4), 374–390. https://doi.org/10.1002/cne.20875

Danielmeier, C., & Ullsperger, M. (2011). Post-Error Adjustments. Frontiers in Psychology, 2. https://doi.org/10.3389/fpsyg.2011.00233

Davare, M. (2006). Dissociating the Role of Ventral and Dorsal Premotor Cortex in Precision Grasping. Journal of Neuroscience, 26(8), 2260–2268. https://doi.org/10.1523/JNEUROSCI.3386-05.2006

Davare, M., Andres, M., Clerget, E., Thonnard, J.-L., & Olivier, E. (2007). Temporal Dissociation between Hand Shaping and Grip Force Scaling in the Anterior Intraparietal Area. Journal of Neuroscience, 27(15), 3974–3980. https://doi.org/10.1523/JNEUROSCI.0426-07.2007

Davare, M., Andres, M., Cosnard, G., Thonnard, J. L., & Olivier, E. (2006). Dissociating the role of ventral and dorsal premotor cortex in precision grasping. *Journal of Neuroscience, 26*(8), 2260–2268. https://doi.org/10.1523/JNEUROSCI.3386-05.2006.

Davare, M., Kraskov, A., Rothwell, J. C., & Lemon, R. N. (2011). Interactions between areas of the cortical grasping network. *Current Opinion in Neurobiology, 21*, 565-70.

Davare, M., Parikh, P. J., & Santello, M. (2019). Sensorimotor uncertainty modulates corticospinal excitability during skilled object manipulation. Journal of Neurophysiology, 121(4), 1162–1170. https://doi.org/10.1152/jn.00800.2018

Davis, M., Wang, Y., Bao, S., Buchanan, J. J., Wright, D. L., & Lei, Y. (2022). The Interactions Between Primary Somatosensory and Motor Cortex during Human Grasping Behaviors. Neuroscience, 485, 1–11. https://doi.org/10.1016/j.neuroscience.2021.11.039

De Luca, M., Smith, S., De Stefano, N., Federico, A., Matthews, P. M. (2005). Blood oxygenation level dependent contrast resting state networks are relevant to functional

activity in the neocortical sensorimotor system. *Experimental Brain Research, 167*(4), 587–594. doi:10.1007/s00221-005-0059-1.

Debener, S., Ullsperger, M., Siegel, M., Fiehler, K., Von Cramon, D. Y., and Engel, A. K. (2005). Trial-by- trial coupling of concurrent elec- troencephalogram and functional magnetic resonance imaging iden- tifies the dynamics of perfor- mance monitoring. J. Neurosci. 25, 11730–11737.

Deits-Lebehn, C., Smith, T. W., Williams, P. G., & Uchino, B. N. (2023). Heart rate variability during social interaction: Effects of valence and emotion regulation. International Journal of Psychophysiology, 190, 20–29. https://doi.org/10.1016/j.ijpsycho.2023.06.004

Desikan, R. S., Ségonne, F., Fischl, B., Quinn, B. T., Dickerson, B. C., Blacker, D., … Killiany, R. J. (2006). An automated labeling system for subdividing the human cerebral cortex on MRI scans into gyral based regions of interest. *NeuroImage, 31*(3), 968–980. https://doi.org/10.1016/j.neuroimage.2006.01.021.

Di Lazzaro, V., & Rothwell, J. C. (2014). Corticospinal activity evoked and modulated by non-invasive stimulation of the intact human motor cortex. The Journal of Physiology, 592(19), 4115–4128. https://doi.org/10.1113/jphysiol.2014.274316

Di Lazzaro, V., Profice, P., Ranieri, F., Capone, F., Dileone, M., Oliviero, A., & Pilato, F. (2012). I-wave origin and modulation. Brain Stimulation, 5(4), 512–525. https://doi.org/10.1016/j.brs.2011.07.008

Di Marco, S., Fattori, P., Galati, G., Galletti, C., Lappe, M., Maltempo, T., Serra, C., Sulpizio, V., Pitzalis, S. (2021). Preference for locomotion-compatible curved paths and forward direction of self-motion in somatomotor and visual areas. *Cortex, 137*, 74–92. doi:10.1016/j.cortex.2020.12.021.

Dijkstra, N., Zeidman, P., Ondobaka, S., van Gerven, M. A. J., & Friston, K. (2017). Distinct Top-down and Bottom-up Brain Connectivity During Visual Perception and Imagery. *Scientific Reports, 7*(1), 5677. https://doi.org/10.1038/s41598-017-05888-8.

Doricchi, F., Lasaponara, S., Pazzaglia, M., & Silvetti, M. (2022). Left and right temporal-parietal junctions (TPJs) as "match/mismatch" hedonic machines: A unifying account of TPJ function. Physics of Life Reviews, 42, 56–92. https://doi.org/10.1016/j.plrev.2022.07.001

Dosenbach, N. U. F., Fair, D. A., Miezin, F. M., Cohen, A. L., Wenger, K. K., Dosenbach, R. A. T., … Raichle, M. E., et al. (2007). Distinct brain networks for adaptive and stable task control in humans. *PNAS Proceedings of the National Academy of Sciences of the United States of America, 104*(26), 11073–11078. doi:10.1073/pnas.0704320104.

Doyon, J., Penhune, V., & Ungerleider, L.G. (2003). Distinct contribution of the corticostriatal and cortico-cerebellar systems to motor skill learning. *Neuropsychologia, 41*, 252–262. https://doi.org/10.1016/S0028-3932(02)00158-6.

Dum, R. P., & Strick, P. L. (2005). Frontal lobe inputs to the digit representations of the motor areas on the lateral surface of the hemisphere. *Journal of Neuroscience, 25*(6), 1375–1386. https://doi.org/10.1523/JNEUROSCI.3902-04.2005.

Duque, J., Hummel, F., Celnik, P., Murase, N., Mazzocchio, R., & Cohen, L. G. (2005). Transcallosal inhibition in chronic subcortical stroke. *NeuroImage, 28*(4), 940–946. https://doi.org/10.1016/j.neuroimage.2005.06.033.

Dutilh, G., Vandekerckhove, J., Forstmann, B. U., Keuleers, E., Brysbaert, M., & Wagenmakers, E.-J. (2012). Testing theories of post-error slowing. Attention, Perception, & Psychophysics, 74(2), 454–465. https://doi.org/10.3758/s13414-011-0243-2

Duvernoy, H., Cabanis, E., & Vannson, J. (1991). *The Human Brain: Surface, Three-dimensional Sectional Anatomy, and MRI*. Springer-Verlag.

Edelman, S., Grill-Spector, K., Kushnir, T., & Malach, R. (1998). Toward direct visualization of the internal shape representation space by fMRI. *Psychobiology, 26*, 309–321.

Eichele, H., Juvodden, H. T., Ullsperger, M., and Eichele, T. (2010). Mal- adaptation of event-related EEG responses preceding performance errors. Front. Hum. Neurosci. 4:65. doi: 10.3389/fnhum.2010.00065

Evarts, E. V., & Tanji, J. (1976). Reflex and intended responses in motor cortex pyramidal tract neurons of monkey. Journal of neurophysiology, 39(5), 1069-1080.

Fabbri, S., Stubbs, K.M., Cusack, R., & Culham, J.C. (2016). Disentangling Representations of Object and Grasp Properties in the Human Brain. *Journal of Neuroscience, 36*, 7648-7662. https://doi.org/10.1523/JNEUROSCI.0313-16.2016.

Fagg, A. H., & Arbib, M. A. (1998). Modeling parietal–premotor interactions in primate control of grasping. *Neural Networks, 11*(7-8), 1277-1303. https://doi.org/10.1016/S0893-6080(98)00047-1.

Faillenot I, Toni I, Decety J, Gregoire MC, Jeannerod M. (1997). Visual pathways for object-oriented action and object recognition: functional anatomy with PET. *Cerebral Cortex, 7*(1), 77-85.

Falkenstein, M., Hohnsbein, J., Hoormann, J., & Blanke, L. (1991). Effects of crossmodal divided attention on late ERP components. II. Error processing in choice reaction tasks. Electroencephalography and clinical neurophysiology, 78(6), 447-455.

Falkenstein, M., Hoormann, J., Christ, S., & Hohnsbein, J. (2000). ERP components on reaction errors and their functional significance: A tutorial. Biological Psychology, 51(2–3), 87–107. https://doi.org/10.1016/S0301-0511(99)00031-9

Farnè, A., & Làdavas, E. (2000). Dynamic size-change of hand peripersonal space following tool use. Neuroreport, 11(8), 1645-1649.

Feinberg, D. A., Moeller, S., Smith, S. M., Auerbach, E., Ramanna, S., Glasser, M. F., Miller, K. L., Ugurbil, K., & Yacoub, E. (2010). Multiplexed Echo Planar Imaging for Sub-Second Whole Brain FMRI and Fast Diffusion Imaging. PLoS ONE, 5(12), e15710. https://doi.org/10.1371/journal.pone.0015710

Ferbert, A., Priori, A., Rothwell, J. C., Day, B. L., Colebatch, J. G., & Marsden, C. D. (1992). Interhemispheric inhibition of the human motor cortex. *The Journal of Physiology, 453*, 525–546. https://doi.org/10.1113/jphysiol.1992.sp019243.

Ferraina S, Battaglia-Mayer A, Genovesio A, Marconi B, Onorati P, Caminiti R. (2001). Early Coding of Visuomanual Coordination During Reaching in Parietal Area PEc. *Journal of Neurophysiology, 85*(1), 462–467. doi:10.1152/jn.2001.85.1.462.

Filimon F, Nelson JD, Hagler DJ, Sereno MI. (2007). Human cortical representations for reaching: mirror neurons for execution, observation, and imagery. *Neuroimage, 37*(4), 1315–1328.

Filimon F, Nelson JD, Huang R-S, Sereno MI. (2009). Multiple Parietal Reach Regions in Humans: Cortical Representations for Visual and Proprioceptive Feedback during On-Line Reaching. *Journal of Neuroscience, 29*(9), 2961–2971. doi:10.1523/JNEUROSCI.3211-08.2009.

Filimon F. (2010). Human Cortical Control of Hand Movements: Parietofrontal Networks for Reaching, Grasping, and Pointing. *Neuroscientist, 16*(4), 388–407. doi:10.1177/1073858410375468.

Fine, J. M., & Hayden, B. Y. (2022). The whole prefrontal cortex is premotor cortex. Philosophical Transactions of the Royal Society B: Biological Sciences, 377(1844), 20200524. https://doi.org/10.1098/rstb.2020.0524

Fischl, B., Sereno, M. I., Tootell, R. B., & Dale, A. M. (1999). High-resolution intersubject averaging and a coordinate system for the cortical surface. *Human Brain Mapping, 8*(4), 272-284. https://doi.org/10.1002/(SICI)1097-0193(1999)8:4<272::AID-HBM10>3.0.CO;2-4.

Fischl, B., Sereno, M.I., & Dale, A. M. (1999). Cortical surface-based analysis: II. Inflation, flattening, and a surface-based coordinate system. *NeuroImage, 9*, 195–207. http://doi.org/10.1006/nimg.1998.0396.

Flanagan, J. R., & Wing, A. M. (1997). The role of internal models in motion planning and control: evidence from grip force adjustments during movements of hand-held

loads. *Journal of Neuroscience, 17*(4), 1519-1528. https://doi.org/10.1523/JNEUROSCI.17-04-01519.1997.

Fogassi, L., Gallese, V., Buccino, G., Craighero, L., Fadiga, L., & Rizzolatti, G. (2001). Cortical mechanism for the visual guidance of hand grasping movements in the monkey: A reversible inactivation study. *Brain, 124*(3), 571-586.

Forte G, Favieri F, Casagrande M (2019). "Heart Rate Variability and Cognitive Function: A Systematic Review". Frontiers in Neuroscience. 13: 710. doi:10.3389/fnins.2019.00710. PMC 6637318. PMID 31354419.

Fox MD, Raichle ME. (2007). Spontaneous fluctuations in brain activity observed with functional magnetic resonance imaging. *Nature Reviews Neuroscience, 8*(9), 700–711. doi:10.1038/nrn2201.

Frey SH, Vinton D, Norlund R, Grafton ST. (2005). Cortical topography of human anterior intraparietal cortex active during visually guided grasping. *Brain Research. Cognitive Brain Research, 23*(2-3), 397-405.

Fries W. (1985). Inputs from motor and premotor cortex to the superior colliculus of the macaque monkey. *Behavioral Brain Research, 18*(2), 95–105. doi:10.1016/0166-4328(85)90066-X.

Friston KJ, Harrison L, Penny W. (2003). Dynamic causal modelling. *NeuroImage, 19*(4), 1273–1302. doi:10.1016/S1053-8119(03)00202-7.

Friston KJ, Litvak V, Oswal A, Razi A, Stephan KE, van Wijk BCM, Ziegler G, Zeidman P. (2016). Bayesian model reduction and empirical Bayes for group (DCM) studies. *NeuroImage, 128*, 413–431. doi:10.1016/j.neuroimage.2015.11.015.

Friston, K. J., Kahan, J., Biswal, B., & Razi, A. (2014). A DCM for resting state fMRI. *NeuroImage, 94*, 396–407. https://doi.org/10.1016/j.neuroimage.2013.12.009.

Friston, K. J., Litvak, V., Oswal, A., Razi, A., Stephan, K. E., van Wijk, B. C. M., Ziegler, G., & Zeidman, P. (2016). Bayesian model reduction and empirical Bayes for group (DCM) studies. *NeuroImage, 128*, 413–431. https://doi.org/10.1016/j.neuroimage.2015.11.015.

Friston, K. J., Mechelli, A., Turner, R., & Price, C. J. (2000). Nonlinear responses in fMRI: the Balloon model, Volterra kernels, and other hemodynamics. *NeuroImage, 12(4), 466-477. https://doi.org/10.1006/nimg.2000.0630.

Friston, K., & Penny, W. (2011). Post hoc Bayesian model selection. *NeuroImage, 56(4), 2089–2099. https://doi.org/10.1016/j.neuroimage.2011.03.062.

Friston, K., Chu, C., Mourão-Miranda, J., Hulme, O., Rees, G., Penny, W., Ashburner, J. (2008). Bayesian decoding of brain images. *NeuroImage, 39*, 181–205.

Friston, K., Mattout, J., Trujillo-Barreto, N., Ashburner, J., & Penny, W. (2007). Variational free energy and the Laplace approximation. *NeuroImage, 34(1), 220–234. https://doi.org/10.1016/j.neuroimage.2006.08.035.

Friston, K., Zeidman, P., & Litvak, V. (2015). Empirical Bayes for DCM: A Group Inversion Scheme. *Frontiers in Systems Neuroscience, 9*. https://doi.org/10.3389/fnsys.2015.00164.

Fu, Q., Zhang, W., & Santello, M. (2010). Anticipatory Planning and Control of Grasp Positions and Forces for Dexterous Two-Digit Manipulation. Journal of Neuroscience, 30(27), 9117–9126. https://doi.org/10.1523/JNEUROSCI.4159-09.2010

Fujii N, Mushiake H, Tanji J. (2000). Rostrocaudal Distinction of the Dorsal Premotor Area Based on Oculomotor Involvement. *Journal of Neurophysiology, 83*(3), 1764–1769. doi:10.1152/jn.2000.83.3.1764.

Gail, A., & Andersen, R. A. (2006). Neural Dynamics in Monkey Parietal Reach Region Reflect Context-Specific Sensorimotor Transformations. *Journal of Neuroscience, 26*(37), 9376. https://doi.org/10.1523/JNEUROSCI.1570-06.2006.

Galati, G., Committeri, G., Pitzalis, S., Pelle, G., Patria, F., Fattori, P., Galletti, C. (2011). Intentional signals during saccadic and reaching delays in the human posterior parietal cortex: Intention-related activity in the human PPC. *European Journal of Neuroscience, 34*(11), 1871–1885. doi:10.1111/j.1460-9568.2011.07885.x.

Galati, G., Committeri, G., Spitoni, G., Aprile, T., Di Russo, F., Pitzalis, S., Pizzamiglio, L. (2008). A selective representation of the meaning of actions in the auditory mirror system. *Neuroimage, 40*, 1274–1286. https://doi.org/10.1016/j.neuroimage.2007.12.044.

Galletti, C., Fattori, P. (2018). The dorsal visual stream revisited: Stable circuits or dynamic pathways? *Cortex, 98*, 203–217. doi:10.1016/j.cortex.2017.01.009.

Gallivan, J. P., McLean, D. A., Flanagan, J. R., Culham, J. C. (2013). Where One Hand Meets the Other: Limb-Specific and Action-Dependent Movement Plans Decoded from Preparatory Signals in Single Human Frontoparietal Brain Areas. *Journal of Neuroscience, 33*(5), 1991–2008. https://doi.org/10.1523/JNEUROSCI.0541-12.2013.

Gallivan, J. P., McLean, D. A., Smith, F. W., Culham, J. C. (2011a). Decoding effector-dependent and effector-independent movement intentions from human parieto-frontal brain activity. *Journal of Neuroscience, 31*(47), 17149–17168. doi:10.1523/JNEUROSCI.1058-11.2011.

Gallivan, J. P., McLean, D. A., Valyear, K. F., Pettypiece, C. E., Culham, J. C. (2011b). Decoding Action Intentions from Preparatory Brain Activity in Human Parieto-Frontal Networks. *Journal of Neuroscience, 31*(26), 9599. doi:10.1523/JNEUROSCI.0080-11.2011.

Gamberini, M., Dal Bò, G., Breveglieri, R., Briganti, S., Passarelli, L., Fattori, P., Galletti, C. (2017). Sensory properties of the caudal aspect of the macaque's superior parietal lobule. *Brain Structure and Function*. doi:10.1007/s00429-017-1593-x.

Gamberini, M., Passarelli, L., Fattori, P., Galletti, C. (2019). Structural connectivity and functional properties of the macaque superior parietal lobule. *Brain Structure and Function, 225*(4), 1349–1367. doi:10.1007/s00429-019-01976-9.

Gamberini, M., Passarelli, L., Fattori, P., Zucchelli, M., Bakola, S., Luppino, G., Galletti, C. (2009). Cortical connections of the visuomotor parietooccipital area V6Ad of the macaque monkey. *Journal of Comparative Neurology, 513*(6), 622–642. doi:10.1002/cne.21980.

Gao, Q., Duan, X., Chen, H. (2011). Evaluation of effective connectivity of motor areas during motor imagery and execution using conditional Granger causality. *Neuroimage, 54(2), 1280-1288.

Gao, Q., Tao, Z., Zhang, M., & Chen, H. (2014). Differential Contribution of Bilateral Supplementary Motor Area to the Effective Connectivity Networks Induced by Task Conditions Using Dynamic Causal Modeling. *Brain Connectivity, 4*(4), 256–264. https://doi.org/10.1089/brain.2013.0194.

Gehring, W. J., Goss, B., Coles, M. G. H., Meyer, D. E., & Donchin, E. (1993). A Neural System for Error Detection and Compensation. Psychological Science, 4(6), 385–390. https://doi.org/10.1111/j.1467-9280.1993.tb00586.x

Gentilucci, M., Toni, I., Chieffi, S., & Pavesi, G. (1994). The role of proprioception in the control of prehension movements: A kinematic study in a peripherally deafferented patient and in normal subjects. Experimental Brain Research, 99(3). https://doi.org/10.1007/BF00228985

Georgopoulos, A. P., & Grillner, S. (1989). Visuomotor coordination in reaching and locomotion. *Science, 245*(4923), 1209-1210.

Gerbella, M., Belmalih, A., Borra, E., Rozzi, S., & Luppino, G. (2011). Cortical connections of the anterior (F5a) subdivision of the macaque ventral premotor area F5. *Brain Structure and Function, 216*(1), 43–65. https://doi.org/10.1007/s00429-010-0293-6.

Gerbella, M., Rozzi, S., & Rizzolatti, G. (2017). The extended object-grasping network. *Experimental Brain Research, 235*(10), 2903–2916. https://doi.org/10.1007/s00221-017-5007-3.

Geyer, S., Matelli, M., Luppino, G., & Zilles, K. (2000). Functional neuroanatomy of the primate isocortical motor system. *Anatomy and Embryology, 202*(6), 443–474. https://doi.org/10.1007/s004290000127.

Ghosh, S., & Gattera, R. (1995). A comparison of the ipsilateral cortical projections to the dorsal and ventral subdivisions of the macaque premotor cortex. *Somatosensory & Motor Research, 12*(3-4), 359-378. https://doi.org/10.3109/08990229509093668.

Ghosh, S., & Porter, R. (1988). Corticocortical synaptic influences on morphologically identified pyramidal neurones in the motor cortex of the monkey. The Journal of Physiology, 400(1), 617–629. https://doi.org/10.1113/jphysiol.1988.sp017139

Glasser, M. F., Sotiropoulos, S. N., Wilson, J. A., Coalson, T. S., Fischl, B., Andersson, J. L., Xu, J., Jbabdi, S., Webster, M., Polimeni, J. R., Van Essen, D. C., & Jenkinson, M. (2013). The minimal preprocessing pipelines for the Human Connectome Project. NeuroImage, 80, 105–124. https://doi.org/10.1016/j.neuroimage.2013.04.127

Glover, S., Wall, M. B., & Smith, A. T. (2012). Distinct cortical networks support the planning and online control of reaching-to-grasp in humans. European Journal of Neuroscience, 35(6), 909-915.

Goldring, A. B., & Krubitzer, L. A. (2020). Evolution of Parietal Cortex in Mammals: From Manipulation to Tool Use. In Evolutionary Neuroscience (pp. 627–656). Elsevier. https://doi.org/10.1016/B978-0-12-820584-6.00026-X

Gordon, A. M., Westling, G., Cole, K. J., & Johansson, R. S. (1993). Memory representations underlying motor commands used during manipulation of common and novel objects. Journal of Neurophysiology, 69(6), 1789–1796. https://doi.org/10.1152/jn.1993.69.6.1789

Graziano, M. (2008). The intelligent movement machine: An ethological perspective on the primate motor system. Oxford University Press.

Gregory, M. D., Kippenhan, J. S., Eisenberg, D. P., Kohn, P. D., Dickinson, D., Mattay, V. S., Chen, Q., Weinberger, D. R., Saad, Z. S., Berman, K. F. (2017). Neanderthal-Derived Genetic Variation Shapes Modern Human Cranium and Brain. *Scientific Reports, 7*(1), 6308. doi:10.1038/s41598-017-06587-0.

Grol, M. J., Majdandžić, J., Stephan, K. E., Verhagen, L., Dijkerman, H. C., Bekkering, H., ... & Toni, I. (2007). Parieto-frontal connectivity during visually guided grasping. *Journal of Neuroscience, 27*(44), 11877–11887. https://doi.org/10.1523/JNEUROSCI.3923-07.2007.

Guerra, S., Bonato, B., Wang, Q., Peressotti, A., Peressotti, F., Baccinelli, W., Bulgheroni, M., & Castiello, U. (2022). Kinematic Evidence of Root-to-Shoot Signaling for the Coding of Support Thickness in Pea Plants. Biology, 11(3), 405. https://doi.org/10.3390/biology11030405

Guerra, S., Peressotti, A., Peressotti, F., Bulgheroni, M., Baccinelli, W., D'Amico, E., Gómez, A., Massaccesi, S., Ceccarini, F., & Castiello, U. (2019). Flexible control of movement in plants. Scientific Reports, 9(1), 16570. https://doi.org/10.1038/s41598-019-53118-0

Gueugneau, N., Bove, M., Avanzino, L., Jacquin, A., Pozzo, T., & Papaxanthis, C. (2013). Interhemispheric Inhibition during Mental Actions of Different Complexity. *PLoS ONE, 8*(2), e56973. https://doi.org/10.1371/journal.pone.0056973.

Guillot, A., Collet, C., Nguyen, V. A., Malouin, F., Richards, C., & Doyon, J. (2009). Brain activity during visual versus kinesthetic imagery: An fMRI study. *Human Brain Mapping, 30*(7), 2157–2172. https://doi.org/10.1002/hbm.20658.

Gutterman, J., Lee-Miller, T., Friel, K. M., Dimitropoulou, K., & Gordon, A. M. (2021). Anticipatory Motor Planning and Control of Grasp in Children with Unilateral Spastic Cerebral Palsy. Brain Sciences, 11(9), 1161. https://doi.org/10.3390/brainsci11091161

Hadjidimitrakis, K., Dal Bo', G., Breveglieri, R., Galletti, C., Fattori, P. (2015). Overlapping representations for reach depth and direction in caudal superior parietal lobule of macaques. *Journal of Neurophysiology, 114*(4), 2340–2352. doi:10.1152/jn.00486.2015.

Hagler, D. J., Riecke, L., Sereno, M. I. (2007). Parietal and superior frontal visuospatial maps activated by pointing and saccades. *NeuroImage, 35*(4), 1562–1577. doi:10.1016/j.neuroimage.2007.01.033.

Haller, S., Chapuis, D., Gassert, R., Burdet, E., & Klarhöfer, M. (2009). Supplementary motor area and anterior intraparietal area integrate fine-graded timing and force control during precision grip. *European Journal of Neuroscience, 30*(12), 2401–2406. https://doi.org/10.1111/j.1460-9568.2009.07003.x.

Halsband, U., Ito, N., Tanji, J., & Freund, H. J. (1993). The role of premotor cortex and the supplementary motor area in the temporal control of movement in man. *Brain, 116*(1), 243-266. https://doi.org/10.1093/brain/116.1.243.

Hamada, M., Galea, J. M., Di Lazzaro, V., Mazzone, P., Ziemann, U., & Rothwell, J. C. (2014). Two Distinct Interneuron Circuits in Human Motor Cortex Are Linked to Different Subsets of Physiological and Behavioral Plasticity. Journal of Neuroscience, 34(38), 12837–12849. https://doi.org/10.1523/JNEUROSCI.1960-14.2014

Hamilton, A. F. D. C., & Grafton, S. T. (2006). Goal representation in human anterior intraparietal sulcus. *Journal of Neuroscience, 26*(4), 1133-1137. https://doi.org/10.1523/JNEUROSCI.4551-05.2006.

Hardwick, R. M., Caspers, S., Eickhoff, S. B., Swinnen, S. P. (2018). Neural correlates of action: Comparing meta-analyses of imagery, observation, and execution. *Neuroscience and Biobehavioral Reviews, 94*, 31–44. https://doi.org/10.1016/j.neubiorev.2018.08.003.

Hartwigsen, G., Bestmann, S., Ward, N. S., Woerbel, S., Mastroeni, C., Granert, O., & Siebner, H. R. (2012). Left Dorsal Premotor Cortex and Supramarginal Gyrus

Complement Each Other during Rapid Action Reprogramming. The Journal of Neuroscience, 32(46), 16162–16171. https://doi.org/10.1523/JNEUROSCI.1010-12.2012

Hashimoto, R., & Rothwell, J. C. (1999). Dynamic changes in corticospinal excitability during motor imagery. *Experimental Brain Research, 125*(1), 75–81. https://doi.org/10.1007/s002210050660.

Haxby, J. V., Gobbini, M. I., Furey, M. L., Ishai, A., Schouten, J. L., Pietrini, P. (2001). Distributed and overlapping representations of faces and objects in ventral temporal cortex. *Science, 293*, 2425–2430.

He, S. Q., Dum, R. P., & Strick, P. L. (1993). Topographic organization of corticospinal projections from the frontal lobe: motor areas on the lateral surface of the hemisphere. *Journal of Neuroscience, 13*(3), 952-980. https://doi.org/10.1523/JNEUROSCI.13-03-00952.1993.

Heed, T., Beurze, S. M., Toni, I., Roder, B., Medendorp, W. P. (2011). Functional Rather than Effector-Specific Organization of Human Posterior Parietal Cortex. *Journal of Neuroscience, 31*(8), 3066–3076. doi:10.1523/JNEUROSCI.4370-10.2011.

Heed, T., Leone, F. T. M., Toni, I., Medendorp, W. P. (2016). Functional versus effector-specific organization of the human posterior parietal cortex: revisited. *Journal of Neurophysiology, 116*(4), 1885–1899. doi:10.1152/jn.00312.2014.

Hensel, L., Lange, F., Tscherpel, C., Viswanathan, S., Freytag, J., Volz, L. J., Eickhoff, S. B., Fink, G. R., & Grefkes, C. (2022). Recovered grasping performance after stroke depends on interhemispheric frontoparietal connectivity. *Brain*, awac157. https://doi.org/10.1093/brain/awac157.

Hermsdörfer, J., Terlinden, G., Mühlau, M., Goldenberg, G., Wohlschläger, A. M. (2007). Neural representations of pantomimed and actual tool use: evidence from an event-related fMRI study. *Neuroimage, 36*, T109-T118.

Hess, A. T., Dylan Tisdall, M., Andronesi, O. C., Meintjes, E. M., & Van Der Kouwe, A. J. W. (2011). Real-time motion and B 0 corrected single voxel spectroscopy using volumetric navigators. Magnetic Resonance in Medicine, 66(2), 314–323. https://doi.org/10.1002/mrm.22805

Hètu, S., Grégoire, M., Saimpont, A., Coll, M. P., Eugène, F., Michon, P. E., & Jackson, P. L. (2013). The neural network of motor imagery: An ALE meta-analysis. *Neuroscience and Biobehavioral Reviews, 37*(5), 930–949. https://doi.org/10.1016/j.neubiorev.2013.03.017.

Hill, J., Inder, T., Neil, J., Dierker, D., Harwell, J., Van Essen, D. (2010). Similar patterns of cortical expansion during human development and evolution. *Proceedings of the National Academy of Sciences, 107*(29), 13135–13140. doi:10.1073/pnas.1001229107.

Hinder, M. R., Fujiyama, H., Summers, J. J. (2012). Premotor-Motor Interhemispheric Inhibition Is Released during Movement Initiation in Older but Not Young Adults. *PLoS ONE, 7*(12), e52573. https://doi.org/10.1371/journal.pone.0052573.

Hinkley, L. B. N., Krubitzer, L. A., Padberg, J., Disbrow, E. A. (2009). Visual-manual exploration and posterior parietal cortex in humans. *Journal of Neurophysiology, 102*(6), 3433–3446. doi:10.1152/jn.90785.2008.

Hirose, S., Hagura, N., Matsumura, M., Naito, E. (2010). Human rostral dorsal premotor cortex mediates graspability judgment of external objects by evaluating hand motor capability. *Brain Research, 1313*, 134–142. doi:10.1016/j.brainres.2009.11.066.

Hoeting, J. A., Madigan, D., Raftery, A. E., Volinsky, C. T. (1999). Bayesian model averaging: A tutorial (with comments by M. Clyde, David Draper and E. I. George, and a rejoinder by the authors. *Statistical Science, 14*(4). https://doi.org/10.1214/ss/1009212519.

Hoshi, E., & Tanji, J. (2007). Distinctions between dorsal and ventral premotor areas: Anatomical connectivity and functional properties. *Current Opinion in Neurobiology, 17*(2), 234–242. https://doi.org/10.1016/j.conb.2007.02.003.

Hoy, K. E., Fitzgerald, P. B., Bradshaw, J. L., Armatas, C. A., & Georgiou-Karistianis, N. (2004). Investigating the cortical origins of motor overflow. *Brain Research Reviews, 46*(3), 315–327. https://doi.org/10.1016/j.brainresrev.2004.07.013.

Huber, L., Handwerker, D. A., Jangraw, D. C., Chen, G., Hall, A., Stuber, C., Gonzalez-Castillo, J., Ivanov, D., Marrett, S., Guidi, M., Uludag, K., Bandettini, P. A., Poser, B. A., & Poser, B. A. (2017). High resolution CBV-fMRI allows mapping of laminar activity and connectivity of cortical input and output in human M1. *Neuron, 96*, 1253–1263.

Huber, L., Ivanov, D., Handwerker, D. A., Marrett, S., Guidi, M., Uludag, K., Bandettini, P. A., and Poser, B. A. (2018). Techniques for blood volume fMRI with VASO: from low-resolution mapping towards sub-millimeter layer-dependent applications. *Neuroimage, 164*, 131–143.

Hutchison, R. M., Gallivan, J. P. (2018). Functional coupling between frontoparietal and occipitotemporal pathways during action and perception. *Cortex, 98*, 8-27. https://doi.org/10.1016/j.cortex.2016.10.020.

Hutto, D. D., & Myin, E. (2014). Neural representations not needed-no more pleas, please. Phenomenology and the Cognitive Sciences, 13, 241-256.

Impieri, D., Gamberini, M., Passarelli, L., Rosa, M.G.P., Galletti, C. (2018). Thalamo-cortical projections to the macaque superior parietal lobule areas PEc and PE. *Journal of Comparative Neurology, 526*(6), 1041–1056. doi:10.1002/cne.24389.

Iriki, A., Tanaka, M., & Iwamura, Y. (1996). Coding of modified body schema during tool use by macaque postcentral neurones. Neuroreport, 7(14), 2325-2330.

Jeannerod, M., Arbib, M.A., Rizzolatti, G., Sakata, H. (1995). Grasping objects: the cortical mechanisms of visuomotor transformation. *Trends in Neurosciences, 18*, 314–320.

Jenny, A. B. (1979). Commissural projections of the cortical hand motor area in monkeys. *The Journal of Comparative Neurology, 188*(1), 137–145. https://doi.org/10.1002/cne.901880111.

Jiang, D., Edwards, M. G., Mullins, P., & Callow, N. (2015). The neural substrates for the different modalities of movement imagery. *Brain and Cognition, 97*, 22-31. https://doi.org/10.1016/j.bandc.2015.04.005.

Jo HJ, Lee JM, Kim JH, Shin Y-W, Kim I-Y, Kwon JS, Kim SI. (2007). Spatial accuracy of fMRI activation influenced by volume- and surface-based spatial smoothing techniques. *NeuroImage, 34*(2), 550–564. doi:10.1016/j.neuroimage.2006.09.047.

Johansson, R. S., & Flanagan, J. R. (2009). Coding and use of tactile signals from the fingertips in object manipulation tasks. Nature Reviews Neuroscience, 10(5), 345–359. https://doi.org/10.1038/nrn2621

Johansson, R. S., & Westling, G. (1984). Roles of glabrous skin receptors and sensorimotor memory in automatic control of precision grip when lifting rougher or more slippery objects. Experimental Brain Research, 56(3). https://doi.org/10.1007/BF00237997

Johansson, R. S., & Westling, G. (1988). Coordinated isometric muscle commands adequately and erroneously programmed for the weight during lifting task with precision grip. *Experimental Brain Research, 71*(1), 59-71. https://doi.org/10.1007/BF00247522.

Johansson, R. S., & Westling, G. (1988). Programmed and triggered actions to rapid load changes during precision grip. Experimental Brain Research, 71(1). https://doi.org/10.1007/BF00247523

Johnasson, R. S., & Cole, K. J. (1992). Sensory-motor coordination during grasping and manipulative actions. Current Biology, 2(12), 648. https://doi.org/10.1016/0960-9822(92)90112-N

Johnson-Frey, S.H., Newman-Norlund, R., and Grafton, S.T. (2005). A distributed left hemisphere network active during planning of everyday tool use skills. *Cerebral Cortex, 15*, 681–695. https://doi.org/10.1093/cercor/bhh169.

Jouffrais C, Boussaoud D. (1999). Neuronal activity related to eye-hand coordination in the primate premotor cortex. *Experimental Brain Research, 128*(1), 205–209. doi:10.1007/s002210050837.

Kaas, J. H., Qi, H.-X., & Stepniewska, I. (2022). Escaping the nocturnal bottleneck, and the evolution of the dorsal and ventral streams of visual processing in primates. Philosophical Transactions of the Royal Society B: Biological Sciences, 377(1844), 20210293. https://doi.org/10.1098/rstb.2021.0293

Kalaska, J. F., & Crammond, D. J. (1992). Cerebral cortical mechanisms of reaching movements. *Science, 255*(5051), 1517-1523.

Karnath, H. O., & Perenin, M. T. (2005). Cortical control of visually guided reaching: evidence from patients with optic ataxia. Cerebral cortex, 15(10), 1561-1569.

Kasess, C. H., Windischberger, C., Cunnington, R., Lanzenberger, R., Pezawas, L., & Moser, E. (2008). The suppressive influence of SMA on M1 in motor imagery revealed by fMRI and dynamic causal modeling. *NeuroImage, 40*(2), 828–837. https://doi.org/10.1016/j.neuroimage.2007.11.040.

Keel, J. C., Smith, M. J., & Wassermann, E. M. (2001). A safety screening questionnaire for transcranial magnetic stimulation. Clinical Neurophysiology, 112(4), 720. https://doi.org/10.1016/S1388-2457(00)00518-6

Kilner, J. M., Friston, K. J., & Frith, C. D. (2007). Predictive coding: An account of the mirror neuron system. Cognitive Processing, 8(3), 159–166. https://doi.org/10.1007/s10339-007-0170-2

Knights, E., Smith, F. W., & Rossit, S. (2022). The role of the anterior temporal cortex in action: Evidence from fMRI multivariate searchlight analysis during real object grasping. Scientific Reports, 12(1), 9042. https://doi.org/10.1038/s41598-022-12174-9

Konen, C. S., Mruczek, R. E. B., Montoya, J. L., & Kastner, S. (2013). Functional organization of human posterior parietal cortex: Grasping- and reaching-related activations relative to topographically organized cortex. Journal of Neurophysiology, 109(12), 2897–2908. https://doi.org/10.1152/jn.00657.2012

Króliczak, G., Cavina-Pratesi, C., Goodman, D. A., & Culham, J. C. (2007). What Does the Brain Do When You Fake It? An fMRI Study of Pantomimed and Real Grasping. Journal of Neurophysiology, 97(3), 2410–2422. https://doi.org/10.1152/jn.00778.2006

Kuhtz-Buschbeck, J. P., Ehrsson, H. H., & Forssberg, H. (2001). Human brain activity in the control of fine static precision grip forces: an fMRI study. *European Journal of Neuroscience, 14*(2), 382–390. https://doi.org/10.1046/j.0953-816X.2001.01639.x.

Kwong KK, Belliveau JW, Chesler DA, Goldberg IE, Weisskoff RM, Poncelet BP, Kennedy DN, Hoppel BE, Cohen MS, Turner R. (1992). Dynamic magnetic resonance imaging of human brain activity during primary sensory stimulation. *Proceedings of the National Academy of Sciences, 89*(12), 5675–5679. doi:10.1073/pnas.89.12.5675.

Lanz, F., Moret, V., Ambett, R., Cappe, C., Rouiller, E. M., & Loquet, G. (2017). Distant heterotopic callosal connections to premotor cortex in non-human primates. *Neuroscience, 344*, 56–66. https://doi.org/10.1016/j.neuroscience.2016.12.035.

Lawrence BM, Snyder LH. (2006). Comparison of effector-specific signals in frontal and parietal cortices. *Journal of Neurophysiology, 96*(3), 1393–1400. doi:10.1152/jn.01368.2005.

Lazzaro, V. D., Oliviero, A., Saturno, E., Pilato, F., Insola, A., Mazzone, P., Profice, P., Tonali, P., & Rothwell, J. (2001). The effect on corticospinal volleys of reversing the direction of current induced in the motor cortex by transcranial magnetic stimulation. Experimental Brain Research, 138(2), 268–273. https://doi.org/10.1007/s002210100722

Lebedev MA, Wise SP. (2001). Tuning for the orientation of spatial attention in dorsal premotor cortex. *European Journal of Neuroscience, 13*(5), 1002–1008. doi:10.1046/j.0953-816x.2001.01457.x.

Lei, Y., Ozdemir, R. A., & Perez, M. A. (2018). Gating of Sensory Input at Subcortical and Cortical Levels during Grasping in Humans. The Journal of Neuroscience, 38(33), 7237–7247. https://doi.org/10.1523/JNEUROSCI.0545-18.2018

Leichnetz, G. R. (1986). Afferent and efferent connections of the dorsolateral precentral gyrus (area 4, hand/arm region) in the macaque monkey, with comparisons to area 8. *The Journal of Comparative Neurology, 254*(4), 460–492. https://doi.org/10.1002/cne.902540403.

Leoné FTM, Heed T, Toni I, Medendorp WP. (2014). Understanding Effector Selectivity in Human Posterior Parietal Cortex by Combining Information Patterns and Activation Measures. *Journal of Neuroscience, 34*(21), 7102. doi:10.1523/JNEUROSCI.5242-13.2014.

Levy I, Schluppeck D, Heeger DJ, Glimcher PW. (2007). Specificity of Human Cortical Areas for Reaches and Saccades. *Journal of Neuroscience, 27*(17), 4687–4696. doi:10.1523/JNEUROSCI.0459-07.2007.

Lewis JW, Van Essen DC. (2000). Corticocortical connections of visual, sensorimotor, and multimodal processing areas in the parietal lobe of the macaque monkey. *Journal of Comparative Neurology, 428*(1), 112–137. doi:10.1002/1096-9861(20001204)428:1<112::aid-cne8>3.0.co;2-9.

Liu Y, Vannuscorps G, Caramazza A, Striem-Amit E. (2020). Evidence for an effector-independent action system from people born without hands. *Proceedings of the National Academy of Sciences USA, 117*(45), 28433. doi:10.1073/pnas.2017789117.

Liuzzi, G., Horniss, V., Zimerman, M., Gerloff, C., & Hummel, F. C. (2011). Coordination of Uncoupled Bimanual Movements by Strictly Timed Interhemispheric Connectivity. *Journal of Neuroscience, 31*(25), 9111–9117. https://doi.org/10.1523/JNEUROSCI.0046-11.2011.

Loh, M. N., Kirsch, L., Rothwell, J. C., Lemon, R. N., & Davare, M. (2010). Information about the Weight of Grasped Objects from Vision and Internal Models Interacts

within the Primary Motor Cortex. The Journal of Neuroscience, 30(20), 6984–6990. https://doi.org/10.1523/JNEUROSCI.6207-09.2010

Lorey, B., Pilgramm, S., Bischoff, M., Stark, R., Vaitl, D., Kindermann, S., Munzert, J., & Zentgraf, K. (2011). Activation of the Parieto-Premotor Network Is Associated with Vivid Motor Imagery—A Parametric fMRI Study. *PLoS ONE, 6*(5), e20368. https://doi.org/10.1371/journal.pone.0020368.

Lukos, J. R., Lee, D., Poizner, H., & Santello, M. (2010). Anticipatory Modulation of Digit Placement for Grasp Control Is Affected by Parkinson's Disease. PLoS ONE, 5(2), e9184. https://doi.org/10.1371/journal.pone.0009184

Luppino, G., Matelli, M., Camarda, R., & Rizzolatti, G. (1993). Corticocortical connections of area F3 (SMA-proper) and area F6 (pre-SMA) in the macaque monkey. *The Journal of Comparative Neurology, 338*(1), 114–140. https://doi.org/10.1002/cne.903380109.

Luppino, G., Murata, A., Govoni, P., & Matelli, M. (1999). Largely segregated parietofrontal connections linking rostral intraparietal cortex (areas AIP and VIP) and the ventral premotor cortex (areas F5 and F4). *Experimental Brain Research, 128*(1–2), 181–187. https://doi.org/10.1007/s002210050833.

Magri, C., Fabbri, S., Caramazza, A., Lingnau, A. (2019). Directional tuning for eye and arm movements in overlapping regions in human posterior parietal cortex. *NeuroImage, 191*, 234–242. doi:10.1016/j.neuroimage.2019.02.029.

Maier, M. A., Armand, J., Kirkwood, P. A., Yang, H. W., Davis, J. N., & Lemon, R. N. (2002). Differences in the corticospinal projection from primary motor cortex and supplementary motor area to macaque upper limb motoneurons: An anatomical and electrophysiological study. *Cerebral Cortex, 12*(3), 281-296. https://doi.org/10.1093/cercor/12.3.281.

Makuuchi, M., Someya, Y., Ogawa, S., & Takayama, Y. (2012). Hand shape selection in pantomimed grasping: Interaction between the dorsal and the ventral visual streams and convergence on the ventral premotor area. *Human Brain Mapping, 33*(8), 1821–1833. https://doi.org/10.1002/hbm.21323.

Malafouris, L. (2013). How things shape the mind. MIT press.

Malouin, F., Richards, C. L., & Durand, A. (2012). Slowing of Motor Imagery after a Right Hemispheric Stroke. *Stroke Research and Treatment, 2012*, 1–10. https://doi.org/10.1155/2012/297217.

Maltempo T, Pitzalis S, Bellagamba M, Di Marco S, Fattori P, Galati G, Galletti C, Sulpizio V. (2021). Lower visual field preference for the visuomotor control of limb movements in the human dorsomedial parietal cortex. *Brain Structure and Function, 226*(9), 2989–3005. doi:10.1007/s00429-021-02254-3.

Mangan, A. P., & Whitaker, R. T. (1999). Partitioning 3D surface meshes using watershed segmentation. *IEEE Transactions on Visualization and Computer Graphics, 5*(4), 308–321. https://doi.org/10.1109/2945.817348.

Mao, T., Kusefoglu, D., Hooks, B. M., Huber, D., Petreanu, L., & Svoboda, K. (2011). Long-Range Neuronal Circuits Underlying the Interaction between Sensory and Motor Cortex. Neuron, 72(1), 111–123. https://doi.org/10.1016/j.neuron.2011.07.029

Maravita, A., & Iriki, A. (2004). Tools for the body (schema). Trends in cognitive sciences, 8(2), 79-86.

Maravita, A., & Romano, D. (2018). The parietal lobe and tool use. Handbook of clinical neurology, 151, 481-498.

Marconi, B., Genovesio, A., Battaglia-Mayer, A., Ferraina, S., Squatrito, S., Molinari, M., ... & Caminiti, R. (2001). Eye–hand coordination during reaching. I. Anatomical relationships between parietal and frontal cortex. *Cerebral Cortex, 11*(6), 513-527. https://doi.org/10.1093/cercor/11.6.513.

Marconi, B., Genovesio, A., Giannetti, S., Molinari, M., & Caminiti, R. (2003). Callosal connections of dorso-lateral premotor cortex. *European Journal of Neuroscience, 18*(4), 775–788. https://doi.org/10.1046/j.1460-9568.2003.02807.x.

Marneweck, M., & Grafton, S. T. (2020). Representational Neural Mapping of Dexterous Grasping Before Lifting in Humans. The Journal of Neuroscience, 40(13), 2708–2716. https://doi.org/10.1523/JNEUROSCI.2791-19.2020

Marneweck, M., Barany, D. A., Santello, M., & Grafton, S. T. (2018). Neural Representations of Sensorimotor Memory- and Digit Position-Based Load Force Adjustments Before the Onset of Dexterous Object Manipulation. The Journal of Neuroscience, 38(20), 4724–4737. https://doi.org/10.1523/JNEUROSCI.2588-17.2018

Marneweck, M., Lee-Miller, T., Santello, M., & Gordon, A. M. (2016). Digit Position and Forces Covary during Anticipatory Control of Whole-Hand Manipulation. Frontiers in Human Neuroscience, 10. https://doi.org/10.3389/fnhum.2016.00461

Martino, A. M., & Strick, P. L. (1987). Corticospinal projections originate from the arcuate premotor area. *Brain Research, 404*(1-2), 307-312. https://doi.org/10.1016/0006-8993(87)91384-9.

Matelli M, Govoni P, Galletti C, Kutz DF, Luppino G. (1998). Superior area 6 afferents from the superior parietal lobule in the macaque monkey. *Journal of Comparative Neurology, 402*(3), 327–352.

Matelli, M., Camarda, R., Glickstein, M., & Rizzolatti, G. (1986). Afferent and efferent projections of the inferior area 6 in the macaque monkey. *The Journal of Comparative Neurology, 251*(3), 281–298. https://doi.org/10.1002/cne.902510302.

Mayka MA, Corcos DM, Leurgans SE, Vaillancourt DE. (2006). Three-dimensional locations and boundaries of motor and premotor cortices as defined by functional brain imaging: A meta-analysis. *NeuroImage, 31*(4), 1453–1474. doi:10.1016/j.neuroimage.2006.02.004.

Mayston, M. J., Harrison, L. M., & Stephens, J. A. (1999). A neurophysiological study of mirror movements in adults and children. *Annals of Neurology, 45*(5), 583–594. https://doi.org/10.1002/1531-8249(199905)45:5<583::aid-ana6>3.0.co;2-w.

McGuire, B. A., Gilbert, C. D., Rivlin, P. K., & Wiesel, T. N. (1991). Targets of horizontal connections in macaque primary visual cortex. *The Journal of Comparative Neurology, 305*(3), 370–392. https://doi.org/10.1002/cne.903050303.

Medendorp, W. P., & Heed, T. (2019). State estimation in posterior parietal cortex: Distinct poles of environmental and bodily states. Progress in Neurobiology, 183, 101691. https://doi.org/10.1016/j.pneurobio.2019.101691

Miall, R. C., & Wolpert, D. M. (1996). Forward Models for Physiological Motor Control. Neural Networks, 9(8), 1265–1279. https://doi.org/10.1016/S0893-6080(96)00035-4

Miller, L. E., Montroni, L., Koun, E., Salemme, R., Hayward, V., & Farnè, A. (2018). Sensing with tools extends somatosensory processing beyond the body. Nature, 561(7722), 239-242.

Mochizuki, H., Huang, Y.-Z., & Rothwell, J. C. (2004). Interhemispheric interaction between human dorsal premotor and contralateral primary motor cortex: Interhemispheric interaction of dorsal premotor area. *The Journal of Physiology, 561*(1), 331–338. https://doi.org/10.1113/jphysiol.2004.072843.

Moeller, S., Yacoub, E., Olman, C. A., Auerbach, E., Strupp, J., Harel, N., & Uğurbil, K. (2010). Multiband multislice GE-EPI at 7 tesla, with 16-fold acceleration using partial parallel imaging with application to high spatial and temporal whole-brain fMRI. Magnetic Resonance in Medicine, 63(5), 1144–1153. https://doi.org/10.1002/mrm.22361

Mojtahedi, K., Fu, Q., & Santello, M. (2015). Extraction of Time and Frequency Features From Grip Force Rates During Dexterous Manipulation. IEEE Transactions on Biomedical Engineering, 62(5), 1363–1375. https://doi.org/10.1109/TBME.2015.2388592

Monaco, S., Malfatti, G., Culham, J. C., Cattaneo, L., & Turella, L. (2020). Decoding motor imagery and action planning in the early visual cortex: Overlapping but distinct neural mechanisms. *NeuroImage, 218*, 116981. https://doi.org/10.1016/j.neuroimage.2020.116981.

Monaco, S., Sedda, A., Cavina-Pratesi, C., & Culham, J. C. (2015). Neural correlates of object size and object location during grasping actions. *European Journal of Neuroscience, 41*(4), 454–465. https://doi.org/10.1111/ejn.12786.

Moreau, Q., Candidi, M., Era, V., Tieri, G., & Aglioti, S. M. (2020). Midline frontal and occipito-temporal activity during error monitoring in dyadic motor interactions. Cortex, 127, 131–149. https://doi.org/10.1016/j.cortex.2020.01.020

Muakkassa KF, Strick PL. (1979). Frontal lobe inputs to primate motor cortex: evidence for four somatotopically organized 'premotor' areas. *Brain Research, 177*, 176–82.

Mullette-Gillman OA, Cohen YE, Groh JM. (2005). Eye-Centered, Head-Centered, and Complex Coding of Visual and Auditory Targets in the Intraparietal Sulcus. *Journal of Neurophysiology, 94*(4), 2331–2352. doi:10.1152/jn.00021.2005.

Mullette-Gillman OA, Cohen YE, Groh JM. (2009). Motor-Related Signals in the Intraparietal Cortex Encode Locations in a Hybrid, rather than Eye-Centered Reference Frame. *Cerebral Cortex, 19*(8), 1761–1775. doi:10.1093/cercor/bhn207.

Munzert, J., Lorey, B., & Zentgraf, K. (2009). Cognitive motor processes: The role of motor imagery in the study of motor representations. *Brain Research Reviews, 60*(2), 306–326. https://doi.org/10.1016/j.brainresrev.2008.12.024.

Murase, N., Duque, J., Mazzocchio, R., & Cohen, L. G. (2004). Influence of interhemispheric interactions on motor function in chronic stroke. *Annals of Neurology, 55*(3), 400–409. https://doi.org/10.1002/ana.10848.

Murata, A., Gallese, V., Luppino, G., Kaseda, M., & Sakata, H. (2000). Selectivity for the shape, size, and orientation of objects for grasping in neurons of monkey parietal area AIP. *Journal of Neurophysiology, 83*(5), 2580-2601.

Nashed, J. Y., Crevecoeur, F., & Scott, S. H. (2014). Rapid online selection between multiple motor plans. Journal of Neuroscience, 34(5), 1769-1780.

Ni, Z., Charab, S., Gunraj, C., Nelson, A. J., Udupa, K., Yeh, I.-J., & Chen, R. (2011). Transcranial Magnetic Stimulation in Different Current Directions Activates Separate Cortical Circuits. Journal of Neurophysiology, 105(2), 749–756. https://doi.org/10.1152/jn.00640.2010

Ni, Z., Gunraj, C., Nelson, A. J., Yeh, I.-J., Castillo, G., Hoque, T., & Chen, R. (2009). Two Phases of Interhemispheric Inhibition between Motor Related Cortical Areas and the Primary Motor Cortex in Human. *Cerebral Cortex, 19*(7), 1654–1665. https://doi.org/10.1093/cercor/bhn201.

Notebaert, W., Houtman, F., Opstal, F. V., Gevers, W., Fias, W., & Verguts, T. (2009). Post-error slowing: An orienting account. Cognition, 111(2), 275–279. https://doi.org/10.1016/j.cognition.2009.02.002

Novembre, G., & Iannetti, G. D. (2021). Towards a unified neural mechanism for reactive adaptive behaviour. Progress in Neurobiology, 204, 102115. https://doi.org/10.1016/j.pneurobio.2021.102115

Nowak, D. A. (2004). How predictive is grip force control in the complete absence of somatosensory feedback? Brain, 127(1), 182–192. https://doi.org/10.1093/brain/awh016

Nowak, D. A., Berner, J., Herrnberger, B., Kammer, T., Grön, G., & Schönfeldt-Lecuona, C. (2009). Continuous theta-burst stimulation over the dorsal premotor cortex interferes with associative learning during object lifting. *Cortex; a Journal Devoted to the Study of the Nervous System and Behavior, 45*(4), 473–482. https://doi.org/10.1016/j.cortex.2007.11.010.

Nowik, A. M., Styrkowiec, P. P., & Kroliczak, G. (2019). Manual Grasparatus: A nifty tool for presenting real objects in fMRI research. MethodsX, 6, 1353–1359. https://doi.org/10.1016/j.mex.2019.06.003

Nyberg, L., Eriksson, J., Larsson, A., Marklund, P. (2006). Learning by doing versus learning by thinking: an fMRI study of motor and mental training. *Neuropsychologia, 44*, 711–717. https://doi.org/10.1016/j.neuropsychologia.2005.08.006.

Ohbayashi, M., Ohki, K., & Miyashita, Y. (2003). Conversion of working memory to motor sequence in the monkey premotor cortex. *Science, 301*(5630), 233–236. doi:10.1126/science.1084884.

Oldfield, R. C. (1971). The assessment and analysis of handedness: The Edinburgh inventory. *Neuropsychologia, 9*(1), 97–113. doi:10.1016/0028-3932(71)90067-4.

Olivier, E., Davare, M., Andres, M., & Fadiga, L. (2007). Precision grasping in humans: from motor control to cognition. *Current Opinion in Neurobiology, 17*, 644–648. https://doi.org/10.1016/j.conb.2008.01.008.

Oosterhof, N. N., Wiestler, T., Downing, P. E., & Diedrichsen, J. (2011). A comparison of volume-based and surface-based multi-voxel pattern analysis. *NeuroImage, 56*(2), 593–600. doi:10.1016/j.neuroimage.2010.04.270.

Orban, G. A. (2016). Functional definitions of parietal areas in human and non-human primates. *Proceedings of the Royal Society B, 283*(1828), 20160118. doi:10.1098/rspb.2016.0118.

Orgogozo, J. M., & Larsen, B. (1979). Activation of the supplementary motor area during voluntary movement in man suggests it works as a supramotor area. *Science, 206*(4420), 847-850. DOI: 10.1126/science.493986.

Page, S. J., Levine, P., & Leonard, A. (2007). Mental practice in chronic stroke: Results of a randomized, placebo-controlled trial. *Stroke, 38*, 1293–1297. https://doi.org/10.1161/01.STR.0000260205.67348.2b.

Papitto, G., Friederici, A. D., & Zaccarella, E. (2020). The topographical organization of motor processing: An ALE meta-analysis on six action domains and the relevance of Broca's region. *NeuroImage, 206*, 116321. https://doi.org/10.1016/j.neuroimage.2019.116321.

Paré, M., & Wurtz, R. H. (2001). Progression in neuronal processing for saccadic eye movements from parietal cortex area LIP to superior colliculus. *Journal of Neurophysiology, 85*(6), 2545–2562. doi:10.1152/jn.2001.85.6.2545.

Parikh, P. J., Fine, J. M., & Santello, M. (2020). Dexterous Object Manipulation Requires Context-Dependent Sensorimotor Cortical Interactions in Humans. Cerebral Cortex, 30(5), 3087–3101. https://doi.org/10.1093/cercor/bhz296

Parise, A. G., Gagliano, M., & Souza, G. M. (2020). Extended cognition in plants: Is it possible? Plant Signaling & Behavior, 15(2), 1710661. https://doi.org/10.1080/15592324.2019.1710661

Park, C. H., Chang, W. H., Lee, M., Kwon, G. H., Kim, L., Kim, S. T., & Kim, Y. H. (2015). Which motor cortical region best predicts imagined movement?. *Neuroimage, 113*, 101-110.

Paulignan, Y., Jeannerod, M., MacKenzie, C., & Marteniuk, R. (n.d.). Selective perturbation of visual input during prehension movements.

Penny, W., Mattout, J., & Trujillo-Barreto, N. (2006). Bayesian model selection and averaging. In *Statistical Parametric Mapping: The analysis of functional brain images*. London: Elsevier.

Perenin, M. T. (1997). Optic ataxia and unilateral neglect: clinical evidence for dissociable spatial functions in posterior parietal cortex. Experimental Brain Research Series, 25, 289-308.

Persichetti, A. S., Avery, J. A., Huber, L., Merriam, E. P., & Martin, A. (2020). Layer-Specific Contributions to Imagined and Executed Hand Movements in Human Primary Motor Cortex. *Current Biology, 30*, 1721-1725.e3. https://doi.org/10.1016/j.cub.2020.02.046.

Pesaran, B., Nelson, M. J., & Andersen, R. A. (2006). Dorsal Premotor Neurons Encode the Relative Position of the Hand, Eye, and Goal during Reach Planning. *Neuron, 51*(1), 125–134. doi:10.1016/j.neuron.2006.05.025.

Pesaran, B., Nelson, M. J., & Andersen, R. A. (2010). A Relative Position Code for Saccades in Dorsal Premotor Cortex. *Journal of Neuroscience, 30*(19), 6527. doi:10.1523/JNEUROSCI.1625-09.2010.

Picard, N., & Strick, P. L. (2001). Imaging the premotor areas. *Current Opinion in Neurobiology, 11*(6), 663–672. doi:10.1016/s0959-4388(01)00266-5.

Picard, N., & Strick, P. L. (2003). Activation of the supplementary motor area (SMA) during performance of visually guided movements. *Cerebral Cortex, 13*(9), 977-986. https://doi.org/10.1093/cercor/13.9.977.

Pilgramm, S., de Haas, B., Helm, F., Zentgraf, K., Stark, R., Munzert, J., & Krüger, B. (2016). Motor imagery of hand actions: Decoding the content of motor imagery from brain activity in frontal and parietal motor areas. *Human Brain Mapping, 37*, 81-93. https://doi.org/10.1002/hbm.23015.

Pinotsis, D. A., Perry, G., Litvak, V., Singh, K. D., & Friston, K. J. (2016). Intersubject variability and induced gamma in the visual cortex: DCM with empirical Bayes and neural fields. *Human Brain Mapping, 37*(12), 4597–4614. https://doi.org/10.1002/hbm.23331.

Piserchia, V., Breveglieri, R., Hadjidimitrakis, K., Bertozzi, F., Galletti, C., Fattori, P. (2016). Mixed Body/Hand Reference Frame for Reaching in 3D Space in Macaque Parietal Area PEc. *Cerebral Cortex*. doi:10.1093/cercor/bhw039.

Pitzalis, S., Serra, C., Sulpizio, V., Committeri, G., de Pasquale, F., Fattori, P., Galletti, C., Sepe, R., Galati, G. (2020). Neural bases of self- and object-motion in a naturalistic vision. *Human Brain Mapping, 41*(4), 1084–1111. doi:10.1002/hbm.24862.

Pitzalis, S., Serra, C., Sulpizio, V., Di Marco, S., Fattori, P., Galati, G., Galletti, C. (2019). A putative human homologue of the macaque area PEc. *NeuroImage, 202*, 116092. doi:10.1016/j.neuroimage.2019.116092.

Power, J. D., Barnes, K. A., Snyder, A. Z., Schlaggar, B. L., & Petersen, S. E. (2012). Spurious but systematic correlations in functional connectivity MRI networks arise from subject motion. NeuroImage, 59(3), 2142–2154. https://doi.org/10.1016/j.neuroimage.2011.10.018

Pruszynski, J. A., & Scott, S. H. (2012). Optimal feedback control and the long-latency stretch response. Experimental Brain Research, 218(3), 341–359. https://doi.org/10.1007/s00221-012-3041-8

Przybylski, Ł., & Króliczak, G. (2017). Planning Functional Grasps of Simple Tools Invokes the Hand-independent Praxis Representation Network: An fMRI Study. Journal of the International Neuropsychological Society, 23(2), 108–120. https://doi.org/10.1017/S1355617716001120

Quilodran, R., Rothé, M., & Procyk, E. (2008). Behavioral Shifts and Action Valuation in the Anterior Cingulate Cortex. Neuron, 57(2), 314–325. https://doi.org/10.1016/j.neuron.2007.11.031

Rabbitt, P. M. (1966). Errors and error correction in choice-response tasks. J. Exp. Psychol. 71, 264–272.

Raffi, M., Carrozzini, C., Maioli, M. G., & Squatrito, S. (2010). Multimodal representation of optic flow in area PEc of macaque monkey. *Neuroscience, 171*(4), 1241–1255. doi:10.1016/j.neuroscience.2010.09.026.

Raffi, M., Maioli, M. G., & Squatrito, S. (2011). Optic flow direction coding in area PEc of the behaving monkey. *Neuroscience, 194*, 136–149.

Raffi, M., Persiani, M., Piras, A., & Squatrito, S. (2014). Optic flow neurons in area PEc integrate eye and head position signals. *Neuroscience Letters, 568*, 23–28.

Raffi, M., Squatrito, S., & Maioli, M. G. (2002). Neuronal Responses to Optic Flow in the Monkey Parietal Area PEc. *Cerebral Cortex, 12*(6), 639–646. doi:10.1093/cercor/12.6.639.

Raos, V., Umiltà, M. A., Gallese, V., & Fogassi, L. (2004). Functional properties of grasping-related neurons in the dorsal premotor area F2 of the macaque monkey. *Journal of Neurophysiology, 92*(4), 1990–2002. https://doi.org/10.1152/jn.00154.2004.

Razi, A., Seghier, M. L., Zhou, Y., McColgan, P., Zeidman, P., Park, H.-J., Sporns, O., Rees, G., & Friston, K. J. (2017). Large-scale DCMs for resting-state fMRI. *Network Neuroscience (Cambridge, Mass.), 1*(3), 222–241. https://doi.org/10.1162/NETN_a_00015.

Rice, N. J., Tunik, E., & Grafton, S. T. (2006). The Anterior Intraparietal Sulcus Mediates Grasp Execution, Independent of Requirement to Update: New Insights from Transcranial Magnetic Stimulation. The Journal of Neuroscience, 26(31), 8176–8182. https://doi.org/10.1523/JNEUROSCI.1641-06.2006

Rizzolatti, G., & Craighero, L. (2004). THE MIRROR-NEURON SYSTEM. Annual Review of Neuroscience, 27(1), 169–192. https://doi.org/10.1146/annurev.neuro.27.070203.144230

Roland, P. E., Larsen, B., Lassen, N. A., & Skinhoj, E. (1980). Supplementary motor area and other cortical areas in the organization of voluntary movements in man. *Journal of Neurophysiology, 43*(1), 118-136. https://doi.org/10.1152/jn.1980.43.1.118.

Rosa, M. J., Friston, K., & Penny, W. (2012). Post-hoc selection of dynamic causal models. *Journal of Neuroscience Methods, 208*(1), 66–78. https://doi.org/10.1016/j.jneumeth.2012.04.013.

Rossi, S., Hallett, M., Rossini, P. M., & Pascual-Leone, A. (2009). Safety, ethical considerations, and application guidelines for the use of transcranial magnetic stimulation in clinical practice and research. Clinical Neurophysiology, 120(12), 2008–2039. https://doi.org/10.1016/j.clinph.2009.08.016

Rouiller, E. M., Babalian, A., Kazennikov, O., Moret, V., Yu, X.-H., & Wiesendanger, M. (1994). Transcallosal connections of the distal forelimb representations of the primary and supplementary motor cortical areas in macaque monkeys. *Experimental Brain Research, 102*(2). https://doi.org/10.1007/BF00227511.

Ruddy, K. L., Leemans, A., & Carson, R. G. (2017). Transcallosal connectivity of the human cortical motor network. *Brain Structure and Function, 222*(3), 1243–1252. https://doi.org/10.1007/s00429-016-1274-1.

Rushworth, M. F. S., Ellison, A., & Walsh, V. (2001). Complementary localization and lateralization of orienting and motor attention. Nature Neuroscience, 4(6), 656–661. https://doi.org/10.1038/88492

Rushworth, M. F., Nixon, P. D., Wade, D. T., Renowden, S., & Passingham, R. E. (1998). The left hemisphere and the selection of learned actions. *Neuropsychologia, 36*(1), 11-24. https://doi.org/10.1016/S0028-3932(97)00101-2.

Sacheli, L. M., Candidi, M., Era, V., & Aglioti, S. M. (2015). Causative role of left aIPS in coding shared goals during human–avatar complementary joint actions. Nature Communications, 6(1), 7544. https://doi.org/10.1038/ncomms8544

Sacheli, L. M., Candidi, M., Pavone, E. F., Tidoni, E., & Aglioti, S. M. (2012). And Yet They Act Together: Interpersonal Perception Modulates Visuo-Motor Interference and Mutual Adjustments during a Joint-Grasping Task. PLoS ONE, 7(11), e50223. https://doi.org/10.1371/journal.pone.0050223

Sakata, H., Taira, M., Murata, A., & Mine, S. (1995). Neural mechanisms of visual guidance of hand action in the parietal cortex of the monkey. *Cerebral Cortex, 5*(5), 429-438.

Salimi, I., Hollender, I., Frazier, W., & Gordon, A. M. (2000). Specificity of Internal Representations Underlying Grasping. Journal of Neurophysiology, 84(5), 2390–2397. https://doi.org/10.1152/jn.2000.84.5.2390

Schaffelhofer, S., & Scherberger, H. (2016). Object vision to hand action in macaque parietal, premotor, and motor cortices. *Elife, 5*, e15278. doi: 10.7554/eLife.15278.001.

Schluppeck D, Glimcher P, Heeger DJ. (2005). Topographic Organization for Delayed Saccades in Human Posterior Parietal Cortex. *Journal of Neurophysiology, 94*(2), 1372–1384. doi: 10.1152/jn.01290.2004.

Scott, S. H. (2012). The computational and neural basis of voluntary motor control and planning. Trends in Cognitive Sciences, 16(11), 541–549. https://doi.org/10.1016/j.tics.2012.09.008

Sebanz, N., Bekkering, H., & Knoblich, G. (2006). Joint Action: bodies and minds moving together. Trends in Cognitive Sciences, 10(2), 70-76.

Seidler, R. D., Kwak, Y., Fling, B. W., & Bernard, J. A. (2013). Neurocognitive Mechanisms of Error-Based Motor Learning. In M. J. Richardson, M. A. Riley, & K. Shockley (Eds.), Progress in Motor Control (Vol. 782, pp. 39–60). Springer New York. https://doi.org/10.1007/978-1-4614-5465-6_3

Seitz, R. J., Kleiser, R., Bütefisch, C. M., Jörgens, S., Neuhaus, O., Hartung, H.-P., Wittsack, H.-J., Sturm, V., & Hermann, M. M. (2004). Bimanual recoupling by visual cueing in callosal disconnection. *Neurocase, 10*(4), 316–325. doi: 10.1080/13554790490505373.

Seki K, Fetz EE. (2012). Gating of sensory input at spinal and cortical levels during preparation and execution of voluntary movement. *Journal of Neuroscience, 32*, 890–902.

Selen, L. P., Shadlen, M. N., & Wolpert, D. M. (2012). Deliberation in the motor system: reflex gains track evolving evidence leading to a decision. Journal of Neuroscience, 32(7), 2276-2286.

Sereno MI, Pitzalis S, Martinez A. (2001). Mapping of contralateral space in retinotopic coordinates by a parietal cortical area in humans. *Science, 294*(5545), 1350–1354. doi: 10.1126/science.1063695.

Sharma, S., Mantini, D., Vanduffel, W., & Nelissen, K. (2019). Functional specialization of macaque premotor F5 subfields with respect to hand and mouth movements: A comparison of task and resting-state fMRI. *NeuroImage, 191*, 441–456. doi: 10.1016/j.neuroimage.2019.02.045.

Shikata, E., Hamzei, F., Glauche, V., Koch, M., Weiller, C., Binkofski, F., & Buchel, C. (2003). Functional properties and interaction of the anterior and posterior intraparietal areas in humans. *European Journal of Neuroscience, 17*, 1105–1110. doi: 10.1046/j.1460-9568.2003.02540.x.

Shimazu, H., Maier, M. A., Cerri, G., Kirkwood, P. A., & Lemon, R. N. (2004). Macaque ventral premotor cortex exerts powerful facilitation of motor cortex outputs to upper limb motoneurons. *Journal of Neuroscience, 24*(5), 1200–1211. doi: 10.1523/JNEUROSCI.4731-03.2004.

Simon, O., Mangin, J. F., Cohen, L., Le Bihan, D., Dehaene, S. (2002). Topographical layout of hand, eye, calculation, and language-related areas in the human parietal lobe. *Neuron, 33*, 475–487.

Smith, A. M., Bourbonnais, D., & Blanchette, G. (1981). Interaction between forced grasping and a learned precision grip after ablation of the supplementary motor area. *Brain Research, 222*(2), 395–400. doi: 10.1016/0006-8993(81)91043-X.

Smyser, C. D., Snyder, A. Z., & Neil, J. J. (2011). Functional connectivity MRI in infants: Exploration of the functional organization of the developing brain. NeuroImage, 56(3), 1437–1452. https://doi.org/10.1016/j.neuroimage.2011.02.073

Snyder LH, Batista AP, Andersen RA. (1997). Coding of intention in the posterior parietal cortex. *Nature, 386*(6621), 167–170. doi: 10.1038/386167a0.

Snyder LH, Batista AP, Andersen RA. (1998). Change in Motor Plan, Without a Change in the Spatial Locus of Attention, Modulates Activity in Posterior Parietal Cortex. *Journal of Neurophysiology, 79*(5), 2814–2819. doi: 10.1152/jn.1998.79.5.2814.

Snyder LH, Batista AP, Andersen RA. (2000). Saccade-related activity in the parietal reach region. *Journal of Neurophysiology, 83*(2), 1099–1102. doi: 10.1152/jn.2000.83.2.1099.

Solodkin A, Hlustik P, Chen EE, Small SL. (2004). Fine modulation in network activation during motor execution and motor imagery. *Cerebral Cortex, 14*, 1246-1255.

Sommer, M., Norden, C., Schmack, L., Rothkegel, H., Lang, N., & Paulus, W. (2013). Opposite Optimal Current Flow Directions for Induction of Neuroplasticity and Excitation Threshold in the Human Motor Cortex. Brain Stimulation, 6(3), 363–370. https://doi.org/10.1016/j.brs.2012.07.003

Spampinato, D. A., Celnik, P. A., & Rothwell, J. C. (2020). Cerebellar–Motor Cortex Connectivity: One or Two Different Networks? The Journal of Neuroscience, 40(21), 4230–4239. https://doi.org/10.1523/JNEUROSCI.2397-19.2020

Squatrito S, Raffi M, Maioli MG, Battaglia-Mayer A. (2001). Visual motion responses of neurons in the caudal area PE of macaque monkeys. *Journal of Neuroscience, 21*(4), RC130. doi: 10.1523/JNEUROSCI.21-04-j0002.2001.

Stancak, A. (2003). Desynchronization of cortical rhythms following cutaneous stimulation: Effects of stimulus repetition and intensity, and of the size of corpus callosum. *Clinical Neurophysiology, 114*(10), 1936–1947. doi: 10.1016/S1388-2457(03)00201-3.

Stanton GB, Bruce CJ, Goldberg ME. (1995). Topography of projections to posterior cortical areas from the macaque frontal eye fields. *Journal of Comparative Neurology, 353*(2), 291–305. doi: 10.1002/cne.903530210.

Stephan, K. E., Penny, W. D., Moran, R. J., den Ouden, H. E., Daunizeau, J., & Friston, K. J. (2010). Ten simple rules for dynamic causal modeling. *NeuroImage, 49*(4), 3099-3109.

Stepniewska, I., Preuss, T. M., & Kaas, J. H. (1993). Architectionis, somatotopic organization, and ipsilateral cortical connections of the primary motor area (M1) of owl monkeys. *The Journal of Comparative Neurology, 330*(2), 238–271. doi: 10.1002/cne.903300207.

Sulpizio, V., Neri, A., Fattori, P., Galletti, C., Pitzalis, S., & Galati, G. (2020). Real and Imagined Grasping Movements Differently Activate the Human Dorsomedial Parietal Cortex. Neuroscience, 434, 22–34. https://doi.org/10.1016/j.neuroscience.2020.03.019

Sun, H., Blakely, T. M., Darvas, F., Wander, J. D., Johnson, L. A., Su, D. K., … Ojemann, J. G. (2015). Sequential activation of premotor, primary somatosensory and primary motor areas in humans during cued finger movements. *Clinical Neurophysiology, 126*(11), 2150–2161. doi: 10.1016/j.clinph.2015.01.005.

Taira, M., Mine, S., Georgopoulos, A. P., Murata, A., & Sakata, H. (1990). Parietal cortex neurons of the monkey related to the visual guidance of hand movement. *Experimental brain research, 83*(1), 29-36. doi: 10.1007/BF00232190.

Tak, Y. W., Knights, E., Henson, R., & Zeidman, P. (2021). Ageing and the ipsilateral M1 BOLD response: A connectivity study. Preprint. Neuroscience. doi: 10.1101/2021.07.29.454012.

Tanji, J. U. N., & Evarts, E. V. (1976). Anticipatory activity of motor cortex neurons in relation to direction of an intended movement. Journal of neurophysiology, 39(5), 1062-1068.

Tarvainen, M. P., Niskanen, J. P., Lipponen, J. A., Ranta-Aho, P. O., & Karjalainen, P. A. (2014). Kubios HRV–heart rate variability analysis software. Computer methods and programs in biomedicine, 113(1), 210-220.

Task Force of the European Society of Cardiology. (1996). Heart rate variability: standards of measurement, physiological interpretation and clinical use. circulation, 93, 1043-1065.

Thayer, J. F., & Lane, R. D. (2000). A model of neurovisceral integration in emotion regulation and dysregulation. Journal of Affective Disorders, 61(3), 201–216. https://doi.org/10.1016/S0165-0327(00)00338-4

Thura D, Hadj-Bouziane F, Meunier M, Boussaoud D. (2008). Hand position modulates saccadic activity in the frontal eye field. *Behavioural Brain Research, 186*(1), 148–153. doi: 10.1016/j.bbr.2007.07.035.

Tieri, G., Tidoni, E., Pavone, E. F., & Aglioti, S. M. (2015). Mere observation of body discontinuity affects perceived ownership and vicarious agency over a virtual hand. Experimental Brain Research, 233(4), 1247–1259. https://doi.org/10.1007/s00221-015-4202-3

Tisdall, M. D., Hess, A. T., Reuter, M., Meintjes, E. M., Fischl, B., & Van Der Kouwe, A. J. W. (2012). Volumetric navigators for prospective motion correction and selective reacquisition in neuroanatomical MRI. Magnetic Resonance in Medicine, 68(2), 389–399. https://doi.org/10.1002/mrm.23228

Todorov, E. (2004). Optimality principles in sensorimotor control. Nature Neuroscience, 7(9), 907–915. https://doi.org/10.1038/nn1309

Tokimura, H., Di Lazzaro, V., Tokimura, Y., Oliviero, A., Profice, P., Insola, A., ... & Rothwell, J. (2000). Short latency inhibition of human hand motor cortex by somatosensory input from the hand. The Journal of Physiology, 523(Pt 2), 503.

Tosoni A, Galati G, Romani GL, Corbetta M. (2008). Sensory-motor mechanisms in human parietal cortex underlie arbitrary visual decisions. *Nature Neuroscience, 11*(12), 1446–1453. doi: 10.1038/nn.2221.

Tosoni A, Pitzalis S, Committeri G, Fattori P, Galletti C, Galati G. (2015). Resting-state connectivity and functional specialization in human medial parieto-occipital cortex. *Brain Structure and Function, 220*(6), 3307–3321. doi: 10.1007/s00429-014-0858-x.

Trampel, R., Bazin, P. L., Pine, K., & Weiskopf, N. (2019). In-vivo magnetic resonance imaging (MRI) of laminae in the human cortex. *NeuroImage, 197*, 707-715.

Tunik E, Rice NJ, Hamilton A, & Grafton ST. (2007). Beyond grasping: representation of action in the human anterior intraparietal sulcus. *Neuroimage, 36*, T77-T86. doi: 10.1016/j.neuroimage.2007.03.026.

Tunik, E., Frey, S. H., & Grafton, S. T. (2005). Virtual lesions of the anterior intraparietal area disrupt goal-dependent on-line adjustments of grasp. Nature Neuroscience, 8(4), 505–511. https://doi.org/10.1038/nn1430

Turella, L., Rumiati, R., & Lingnau, A. (2020). Hierarchical Action Encoding Within the Human Brain. *Cerebral Cortex, 30*(5), 2924–2938. doi: 10.1093/cercor/bhz284.

Turner, R. (2016). Uses, misuses, new uses and fundamental limitations of magnetic resonance imaging in cognitive science. *Philosophical Transactions of the Royal Society B: Biological Sciences, 371*, 20150349.

Umeda, T., Isa, T., & Nishimura, Y. (2019). The somatosensory cortex receives information about motor output. Science Advances, 5(7), eaaw5388. https://doi.org/10.1126/sciadv.aaw5388

Valk, S. L., Xu, T., Margulies, D. S., Masouleh, S. K., Paquola, C., Goulas, A., ... & Eickhoff, S. B. (2020). Shaping brain structure: Genetic and phylogenetic axes of macroscale organization of cortical thickness. Science Advances, 6(39), eabb3417.

van den Heuvel MP, Hulshoff Pol HE. (2010). Exploring the brain network: A review on resting-state fMRI functional connectivity. *European Neuropsychopharmacology, 20*(8), 519–534. doi: 10.1016/j.euroneuro.2010.03.008.

Van Essen DC, Drury HA, Joshi S, Miller MI. (1998). Functional and structural mapping of human cerebral cortex: Solutions are in the surfaces. *Proceedings of the National Academy of Sciences of the United States of America, 95*(3), 788. doi: 10.1073/pnas.95.3.788.

Van Essen, D. C., Glasser, M. F., Dierker, D. L., Harwell, J., & Coalson, T. (2012). Parcellations and Hemispheric Asymmetries of Human Cerebral Cortex Analyzed on Surface-Based Atlases. *Cerebral Cortex, 22*(10), 2241–2262. doi: 10.1093/cercor/bhr291.

Verguts, T., Notebaert, W., Kunde, W., & Wühr, P. (2011). Post-conflict slowing: Cognitive adaptation after conflict processing. Psychonomic Bulletin & Review, 18(1), 76–82. https://doi.org/10.3758/s13423-010-0016-2

Vernet M, Quentin R, Chanes L, Mitsumasu A, Valero-Cabré A. (2014). Frontal eye field, where art thou? Anatomy, function, and non-invasive manipulation of frontal regions involved in eye movements and associated cognitive operations. *Frontiers in Integrative Neuroscience, 8*, 66–66. doi: 10.3389/fnint.2014.00066.

Verstynen, T., & Ivry, R. B. (2011). Network Dynamics Mediating Ipsilateral Motor Cortex Activity during Unimanual Actions. *Journal of Cognitive Neuroscience, 23*(9), 2468–2480. doi: 10.1162/jocn.2011.21612.

Verstynen, T., Diedrichsen, J., Albert, N., Aparicio, P., & Ivry, R. B. (2005). Ipsilateral Motor Cortex Activity During Unimanual Hand Movements Relates to Task Complexity. *Journal of Neurophysiology, 93*(3), 1209–1222. doi: 10.1152/jn.00720.2004.

Vesia M, Crawford JD. (2012). Specialization of reach function in human posterior parietal cortex. *Experimental Brain Research, 221*(1), 1–18. doi: 10.1007/s00221-012-3158-9.

Vesia M, Prime SL, Yan X, Sergio LE, Crawford JD. (2010). Specificity of Human Parietal Saccade and Reach Regions during Transcranial Magnetic Stimulation. *Journal of Neuroscience, 30*(39), 13053. doi: 10.1523/JNEUROSCI.1644-10.2010.

Vesper, C., Abramova, E., Bütepage, J., Ciardo, F., Crossey, B., Effenberg, A., Hristova, D., Karlinsky, A., McEllin, L., Nijssen, S. R. R., Schmitz, L., & Wahn, B. (2017). Joint Action: Mental Representations, Shared Information and General Mechanisms for Coordinating with Others. Frontiers in Psychology, 07. https://doi.org/10.3389/fpsyg.2016.02039

Vincent JL, Snyder AZ, Fox MD, Shannon BJ, Andrews JR, Raichle ME, Buckner RL. (2006). Coherent spontaneous activity identifies a hippocampal-parietal memory network. *Journal of Neurophysiology, 96*(6), 3517–3531. doi: 10.1152/jn.00048.2006.

Volz, L. J., Hamada, M., Rothwell, J. C., & Grefkes, C. (2015). What Makes the Muscle Twitch: Motor System Connectivity and TMS-Induced Activity. Cerebral Cortex, 25(9), 2346–2353. https://doi.org/10.1093/cercor/bhu032

Weidenreich, F. (1941). The brain and its role in the phylogenetic transformation of the human skull. Transactions of the American Philosophical Society, 320-442.

Weiler, N., Wood, L., Yu, J., Solla, S.A., and Shepherd, G.M. (2008). Topdown laminar organization of the excitatory network in motor cortex. *Nature Neuroscience, 11*, 360–366.

Westling, G., & Johansson, R. S. (1984). Factors influencing the force control during precision grip. Experimental Brain Research, 53(2). https://doi.org/10.1007/BF00238156

White, O., Davare, M., Andres, M., & Olivier, E. (2013). The Role of Left Supplementary Motor Area in Grip Force Scaling. *PLoS ONE, 8*(12), e83812. doi: 10.1371/journal.pone.0083812.

Wilterson, A. I., & Graziano, M. S. A. (2021). The attention schema theory in a neural network agent: Controlling visuospatial attention using a descriptive model of attention. Proceedings of the National Academy of Sciences, 118(33), e2102421118. https://doi.org/10.1073/pnas.2102421118

Wise SP, Boussaoud D, Johnson PB, Caminiti R. (1997). PREMOTOR AND PARIETAL CORTEX: Corticocortical Connectivity and Combinatorial Computations. *Annual Review of Neuroscience, 20*(1), 25–42. doi: 10.1146/annurev.neuro.20.1.25.

Xia M, Wang J, He Y. (2013). BrainNet Viewer: a network visualization tool for human brain connectomics. *PLOS One, 8*(7), e68910. doi: 10.1371/journal.pone.0068910.

Yarosh, C. A., Hoffman, D. S., & Strick, P. L. (2004). Deficits in movements of the wrist ipsilateral to a stroke in hemiparetic subjects. *Journal of Neurophysiology, 92*(6), 3276–3285. doi: 10.1152/jn.00549.2004.

Yousry, T. A., Schmid, U. D., Alkadhi, H., Schmidt, D., Peraud, A., Buettner, A., & Winkler, P. (1997). Localization of the motor hand area to a knob on the precentral gyrus. A new landmark. *Brain: a journal of neurology, 120*(1), 141-157. doi: 10.1093/brain/120.1.141.

Zabicki, A., de Haas, B., Zentgraf, K., Stark, R., Munzert, J., & Krüger, B. (2016). Imagined and Executed Actions in the Human Motor System: Testing Neural Similarity Between Execution and Imagery of Actions with a Multivariate Approach. *Cerebral Cortex*, cercor;bhw257v1. doi: 10.1093/cercor/bhw257.

Zarei, M., Johansen-Berg, H., Smith, S., Ciccarelli, O., Thompson, A. J., & Matthews, P. M. (2006). Functional anatomy of interhemispheric cortical connections in the human brain. *Journal of Anatomy, 209*(3), 311–320. doi: 10.1111/j.1469-7580.2006.00615.x.

Zeidman, P., Jafarian, A., Corbin, N., Seghier, M. L., Razi, A., Price, C. J., & Friston, K. J. (2019a). A guide to group effective connectivity analysis, part 1: First level analysis with DCM for fMRI. *NeuroImage, 200*, 174–190. doi: 10.1016/j.neuroimage.2019.06.031.

Zeidman, P., Jafarian, A., Seghier, M. L., Litvak, V., Cagnan, H., Price, C. J., & Friston, K. J. (2019b). A guide to group effective connectivity analysis, part 2: Second level analysis with PEB. *NeuroImage, 200*, 12–25. doi: 10.1016/j.neuroimage.2019.06.032.